Gro Sagli

Model uncertainty and simplified estimates of long term extremes of hull girder loads in ships

NTNU Trondheim
Norges teknisk-naturvitenskapelige universitet

Doktor ingeniøravhandling 2000:15
Institutt for marine konstruksjoner

MTA-rapport 2000:138

Model uncertainty and simplified estimates of long term extremes of hull girder loads in ships

A thesis submitted in partial fulfillment of the
requirements for the degree of
doktor ingeniør
by

Gro Sagli

Trondheim, January 20, 2000

Department of Marine Structures
Faculty of Marine Technology
Norwegian University of Science and Technology

To Inger Johanne & Herloff Gunnar Sagli

for teaching me the joy of creation

&

for your endless support and encouragement
over the years

It is our duty as human to do our best. Not to gain something or get something back, but because the journey itself is important. The real journey is self discovery, exploring your own possibilities.

David Kring

Acknowledgements

I want to express my gratitude towards my supervisor professor Torgeir Moan at the Department of Marine Structures, NTNU. His guidance and support have been invaluable. Thanks a lot for pushing me forward when the hills were steep and top was out of sight.

Dr. Sverre Haver should have been devoted a chapter of his own. I am very grateful for his guidance, support and for being a good friend. Not to forget, the meetings you arranged and the other employees at Exploration & Production Technology, Statoil, have been inspiring. Thanks a lot for introducing me to professor Steven Winterstein, Stanford University, who has offered valuable help.

I also want to thank MingKang Wu, Ole Hermundstad and Jan R. Hoff at MARINTEK for answering infinitely many questions regarding hydrodynamics and use of the simulation programs. Their help was shamelessly appreciated.

My thanks to my colleagues at Department of Marine Structures and Marine Hydrodynamics. In particular, I had entertaining evenings playing board games into late hours of the night together with Guttorm Grytøyr, Catrine T. Grytøyr, Olav Rognebakke, Pål Lader and Helen Tislevoll. And thanks to Elin Marita Hermundstad,- an allied and running partner. Lihua Wang has carefully read the draft of the thesis. Our discussions have been fruitful and the kayak trips have been joyful and wet. Anne Gunn G. Berge has been my very best friend through thick and thin.

My beloved, Rolf J. Baarholm, brought harmony into my life. He has always been very supportive and encouraging. It is amazing what some sardonic humour can do to a tired soul. Without you, these years would have been poorer.

This work was financially supported through the ShipR3D program, Kværner ASA. In addition support was given by Norges Forskningsråd and Faculty of Marine Technology, NTNU. Lundby,- what would I do without you. Thank you. MARINTEK and in particular K. Holden have been very helpful and supportive.

Abstract

The work consists of two parts. The first part is a study of the model uncertainty of different hydrodynamic models used to estimate global loads on mono hull vessels. The applied hydrodynamic models are the linear strip theory as presented by Salvesen et al. (1970) and a quasi-nonlinear code developed at the Department of Marine Structures, Wu (1996).

The physical and numerical hydrodynamic models are simplifications of the reality. The first mentioned theory assumes linearity. The second theory takes into account some effects which are assumed to represent the major part of nonlinear contribution in an approximate manner. A method to estimate the model uncertainty is therefore presented. For linear response, the model uncertainty is given as the ratio between the estimated and experimental design value for a given return period, D, as ψ_D. The model uncertainty of the nonlinear theory is expressed as the ratio between the experimental and theoretical response amplitude in a regular wave, χ.

A linear relation is detected between ψ_D and the discrepancy between the predicted and measured value of the transfer function at a frequency corresponding to a decomposed wave length equal to the ship length. An estimate of the model error for a given heading angle is expressed by mean value and standard deviation. It is concluded that the long term vertical bending moment is highly influenced by the model error and that it varies somewhat with the heading.

In this work there is not found any general trend indicating that the nonlinear model uncertainty, χ, is a function of the wave steepness, degree of nonlinearity or wave length. A relation between the model error and the block coefficient are also examined, but the number of cases are too small to ascertain a trend. However, the study confirms that in most cases the sagging and hogging responses are over- and underestimated respectively. The nonlinear model error herein is determined for each vessel and might be used for similar vessel types.

For new ship types and other theoretical models, uncertainty measures found in this work will not necessarily be applicable.

The second part is concerned with estimating the long term extreme value for a given return period, let say $D = 100$ years. In principle, this response needs to be obtained by combining the response in all the sea states. The response for a given sea state, specified by the significant

wave height, H_s, and the peak period, T_p, can be obtained in the frequency domain for the linear response. Time domain simulation is required to obtain the nonlinear response, and long time series is required to limit the statistical uncertainty. Especially in the latter case, it is crucial to introduce ways to improve the efficiency in the calculation. In this work it is shown that the long term extremes can be estimated by considering only a few short term sea states. The key issue in this approach is to identify a *contour* curve corresponding to an iso-density curve of the short term sea state parameters, H_s & T_p. These contours are structure independent and therefore an useful tool for the designer since they can be handed contour curves for a given return period and further conduct the necessary analysis. And, as shown in this thesis, the number of necessary short term analysis is limited to a few sea states.

The contour curves are established by using inverse First Order Reliability Method, IFORM. In general, the design value established using the contour curve corresponding to a return period, say D years, will be defined as the largest short term characteristic along the contour line.

The contour line approach is validated by complete long term analysis. As long as the response is linear, the parameters in the weighted short term distribution are found using the appropriate transfer functions. However, nonlinear response simulations are in the time domain. Therefore, the long term analysis become rather complicated and time consuming. A long term analysis based on identifying the most important sea state, defined by the coefficient of contribution, using linear analysis is applied. An iteration procedure is thereafter used to find the nonlinear long term extreme values. It is concluded that only a limited number of sea states is necessary to get an acceptable estimate of the nonlinear D-year response as long as the most important sea states are included, *i.e.* the sea state with maximum coefficient of contribution.

The extreme value obtained by using long term analysis are then compared to the value of the short term characteristic. The short term characteristic is accepted when the ratio between the two values are approximately equal to one.

It is concluded that the design extreme value defined by the parameters in the short term distribution and an appropriate fractile, is suitable for estimating the long term extreme value. The necessary fractile can be determined using linear response analysis at zero forward speed and head sea waves. This fractile is also applicable for the corresponding nonlinear analysis, *i.e.* sagging and hogging.

Wave loads depend upon the routing and manoeuvring and speed limitation to reduce the effects of heavy weather. Account of manoeuvring and speed limitation is made in a simple way in this thesis. It is shown that the contour line approach is applicable for these events. However, in some cases a three dimensional contour surface must be established if the effect of speed limitation should be properly treated.

wave height, H_s, and the peak period, T_p, can be obtained in the frequency domain for the linear response. Time domain simulation is required to obtain the nonlinear response, and long time series is required to limit the statistical uncertainty. Especially in the latter case, it is crucial to introduce ways to improve the efficiency in the calculation. In this work it is shown that the long term extremes can be estimated by considering only a few short term sea states. The key issue in this approach is to identify a *contour* curve corresponding to an iso-density curve of the short term sea state parameters, H_s & T_p. These contours are structure independent and therefore an useful tool for the designer since they can be handed contour curves for a given return period and further conduct the necessary analysis. And, as shown in this thesis, the number of necessary short term analysis is limited to a few sea states.

The contour curves are established by using inverse First Order Reliability Method, IFORM. In general, the design value established using the contour curve corresponding to a return period, say D years, will be defined as the largest short term characteristic along the contour line.

The contour line approach is validated by complete long term analysis. As long as the response is linear, the parameters in the weighted short term distribution are found using the appropriate transfer functions. However, nonlinear response simulations are in the time domain. Therefore, the long term analysis become rather complicated and time consuming. A long term analysis based on identifying the most important sea state, defined by the coefficient of contribution, using linear analysis is applied. An iteration procedure is thereafter used to find the nonlinear long term extreme values. It is concluded that only a limited number of sea states is necessary to get an acceptable estimate of the nonlinear D-year response as long as the most important sea states are included, *i.e.* the sea state with maximum coefficient of contribution.

The extreme value obtained by using long term analysis are then compared to the value of the short term characteristic. The short term characteristic is accepted when the ratio between the two values are approximately equal to one.

It is concluded that the design extreme value defined by the parameters in the short term distribution and an appropriate fractile, is suitable for estimating the long term extreme value. The necessary fractile can be determined using linear response analysis at zero forward speed and head sea waves. This fractile is also applicable for the corresponding nonlinear analysis, *i.e.* sagging and hogging.

Wave loads depend upon the routing and manoeuvring and speed limitation to reduce the effects of heavy weather. Account of manoeuvring and speed limitation is made in a simple way in this thesis. It is shown that the contour line approach is applicable for these events. However, in some cases a three dimensional contour surface must be established if the effect of speed limitation should be properly treated.

Nomenclature

General Rules

- Only the most used symbols are declared in this chapter
- Symbols are generally defined where they appear in the text for the first time
- Matrices and vectors are represented by bold characters
- Overdots signify differentiation with respect to time

Subscripts

$cubic$	Cubic splines
$linear$	Linear splines
Gen	Generalised Gamma distribution
Her	Hermite distribution
hog	Hogging
LT	Long term
max	Maxima
R	Related to random variable R
sag	Sagging

Superscripts

l	Linear
nl	Nonlinear

Roman Letters

A	Wave amplitude
A_{jk}	Added mass force in direction j due to η_k
$\boldsymbol{A}$	Added mass matrix

B_{jk}	Damping force in direction j due to η_k
$\boldsymbol{B}$	Damping matrix
$\boldsymbol{C}$	Damping matrix
C_b	Block coefficient
$C_R(si)$	Coefficient of contribution
D	Return period in years
$D(\theta)$	Spreading function
E	Energy Content
$E[\cdot]$	Expected value
$f(\cdot)$	Probability density distribution
$F(\cdot)$	Cumulative distribution
$\boldsymbol{F}$	Wave exciting forces and moments
g	Gravitational acceleration
g_1, g_{1R}	Estimate of skewness, estimate of the skewness of R
g_2, g_{2R}	Estimate of kurtosis, estimate of the kurtosis of R
H	Wave height
$H(\omega)$	Calculated transfer function
$\hat{H}(\omega)$	Measured transfer function
H_s	Significant wave height
H_s^{lim}	Limiting significant wave height
$H_{\eta\zeta}(\cdot)$	Transfer function
$H_{\eta\zeta}(\cdot)^*$	Complex conjugate of $H_{\eta\zeta}(\cdot)$
j_{max}	Number of peak periods, T_p
k, $k(\omega)$	Wave number
k_{max}	Number of significant wave heights, H_s
$\boldsymbol{k}$	Wave number vector
$\boldsymbol{K}$	Hydrostatic restoring force
L_{pp}	Length between the perpendiculars
m	Parameter in the Generalised Gamma distribution
m_0	Varians
m_n	Spectral moments
$\hat{m}_n$	Spectral moments using $\hat{H}(\omega)$
M	Scale parameter in the Rayleigh distribution
$\boldsymbol{M}$	Mass matrix
M_5	Midship vertical, bending moment
$\boldsymbol{n}$	Normal vector
n_{tot}	Number of peaks in all sea states within D years
n_{si}	Number of peaks in sea state si within D years
$\boldsymbol{n}$	Normal vector
N	Number of regular components

N	Number of maxima
N_D	Number of peaks during D years
N_{si}	Number of sea states
p	Random number
p_a	Atmospheric pressure
$\boldsymbol{p}$	Generalised coordinate matrix
$\boldsymbol{p}_l$	Generalised coordinate matrix due to linear forces
$\boldsymbol{p}_n$	Generalised coordinate matrix due to nonlinear forces
$Q(\cdot)$	Probability of being above, *i.e.* $1 - P(\cdot)$
r_p	Probable extreme value of the random variable R
$r_{\alpha,design}$	Design extreme value of the random variable R
R	Random variable
$R(\cdot)$	Auto-correlation function
$R(t)$	Parent response
R_{jk}	Restoring force in direction j due to η_k
$\boldsymbol{R}$	Restoring matrix
$R_0(t)$	Normalised response
R_D	Response with return period D years
$R_{D,N_{si}}$	Response with return period D years when N_{si} sea states are included
si	Sea state with $(H_s, T_P)_i$
s^2, s_R^2	Estimate of variance, estimate of the variance of R
$S_\zeta(\cdot)$	Wave energy spectrum
$S_{\eta\zeta}(\cdot)$	Response energy spectrum
t	Time
T	Period
T_1	Mean wave period
T_p	Peak period
T_p^{lim}	Limiting peak period
T_z	Zero up-crossing period
$\bar{T}_z$	Average zero up-crossing period
U	Forward speed
$U_0(t)$	Standard Gaussian process
$Var[\cdot]$	Variance
$\boldsymbol{V}(\boldsymbol{x}, t)$	Fluid, velocity vector
$\boldsymbol{V}_s(\boldsymbol{x}, t)$	Fluid, velocity vector on the point $\boldsymbol{x}$ on the body
$\boldsymbol{w}$	Eigenmode matrix
$\boldsymbol{x}$	Position vector
$x(t)$	Realization
y	Simulated response amplitude midship for a given wave length and wave height
$\hat{y}$	Measured response amplitude midship for a given wave length and wave height

Greek Letters

α_N	Scale parameter in the Gumbel distribution
$\hat{\alpha}$	Probability of exceedance
α	Probability of being below, *i.e.* $1 - \hat{\alpha}$
α_{design}	Design fractile
β	Scale parameter in the Weibull distribution
β	Wave heading
γ	Peakedness parameter
γ	Shape parameter in the Weibull and Generalised Gamma distribution
γ_1, γ_{1R}	Skewness, skewness of R
γ_2, γ_{2R}	Kurtosis, kurtosis of R
$\Gamma()$	Gamma function
$\delta(\cdot)$	Dirac delta function
δ	Location parameter in the Weibull distribution
ε	Phase difference between the real and imaginary part of $H_{\eta\zeta}(\cdot)$
ε	Bandwidth of the process
ζ, $\zeta(t)$	Wave elevation
η, $\eta(t)$	Response
η	Shift parameter
$\ddot{\boldsymbol{\eta}}$, $\dot{\boldsymbol{\eta}}$ and $\boldsymbol{\eta}$	Acceleration, the velocity and displacement matrices
$\ddot{\eta}$, $\dot{\eta}$ and $\boldsymbol{\eta}$	Acceleration, the velocity and displacement in degree of freedom k
$\eta_n(t)$	Response due to nonlinear forces
$\eta_{tot}(t)$	Total response
κ	Correction factor
$\kappa_{E[R^l_{max}]}$	Correction factor for expected largest value
$\kappa_{E[R^l_{max}],design}$	Design correction factor for expected largest value
$\kappa_{r^l_p}$	Correction factor for the most probable extreme value
$\kappa_{r^l_{p,design}}$	Design correction factor for the most probable extreme value
λ	Scale parameter in the Generalised Gamma distribution
λ	Wave length
μ, μ_R	Mean value, mean value of R
μ_N	Location parameter in the Gumbel distribution
σ	Standard deviation
σ^2, σ^2_R	Estimate of variance, variance of R
ρ	Density of water
$\phi(\omega)$	Relative model error
$\bar{\phi}(\omega)$	Additive model error
$\phi''(\omega)$	Nondimensional additive model error, *i.e.* $\phi''(\omega) = 1 + \frac{\bar{\phi}(\omega)}{H(\omega)}$

ϕ_0	Undisturbed potential due to incoming waves
$\phi^{1,..,n}$	n'th order, unsteady potential
$\phi_{1,..,6}$	First order potential due motion η_k
ϕ_D	Diffraction potential
ϕ_s	Steady state potential
Φ	Fluid velocity potential
χ	Ratio between measured and simulated response amplitude midship for a given wave length and wave height , *i.e.* $\hat{y}/y$
$\bar{\chi}$	Ratio between measured and simulated response for a given wave length
ψ	Arbitrary phase angle
ψ	Ratio between $\frac{\hat{R}_D^I}{R_D^I}$
ω	Wave frequency
$\bar{\omega}$	Weighting function
ω_e	Encounter frequency
ω_p	Peak frequency

Abbreviations

AP	Aft perpendicular
DASS	Dynamic Analysis System and Support project
DNV	Det Norske Veritas
FORM	First Order Reliability Method
Fn	Froude number, *i.e.* $\frac{U}{\sqrt{gL_{pp}}}$
FP	Fore perpendicular
IACS	International Association of Classification Societies
IFORM	inverse First Order Reliability Method
ITTC	International Towing Tank Conference
LAMP	Large Amplitude Motion Program
LANWIL	Linear And Nonlinear Wave Induced Loads program
LRNM	Linear Response Nonlinear Maxima
MIT	Massachusetts Institute of Technology
NKK	Nippon Kokan Co., Ltd.
NV1418	Norske Veritas program number 1418
SHI	Sumitomo Heavy Industries
SORM	Second Order Reliability Method
SRI	Ship Research Institute
SWAN	Ship Wave ANalysis program
TiMIT	TIme domain analysis program, MIT
VERES	VEssel RESponse program

Contents

CHAPTER 1

Introduction

1.1 Background

Accurate prediction of wave-induced ship motions, hydrodynamic loads and the resulting structural response is of crucial importance in ship design. The severe motion can limit operability, affect serviceability as well as safety. The extreme loads may cause structural failure due to fatigue and fracture, *e.g.* Watanabe and Ohtsubo (1998). Furthermore, the importance of accurate prediction of the motions, loads and structural response become increasingly important with the advent of novel ship design and more demanding operational requirements.

Safety requirements to ship hulls are specified in Ship Rules issued by Classification Societies who harmonise their rules through the International Association of Classification Societies, IACS, *e.g.* Nitta et al. (1992). Traditionally, the *rule book* approach is applied in the design of ships. The rule book approach meet well the busy designers' need and preference for rules which are simple to use. They do not yet provide means, for example, to quantify the effect of a proposed design change on the subsequent safety on that design. In addition, as new designs are entering the arena, the ship rules may become out-of-date since the formulae are based on data for various ship types and would not generally be optimal for a given vessel. The variation and complexity of novel hull concepts, see Fig. 1.1 & 1.2, the possible influence of structural dynamics as well as nonlinear load effect, suggest that *direct calculation* of the hull girder load effects are preferable in such cases.

The most common way to establish design loads by direct calculations is by means of long term description of the response. This require that a wide range of sea states must be analysed and that the final distribution is obtained as a weighted sum of these sea states. In addition, information about routes and operational profiles must be obtained. If linear response analysis are conducted, the response in a given sea state is defined by the transfer function, while time domain simulations are in general required to obtain the nonlinear response. This leads to time

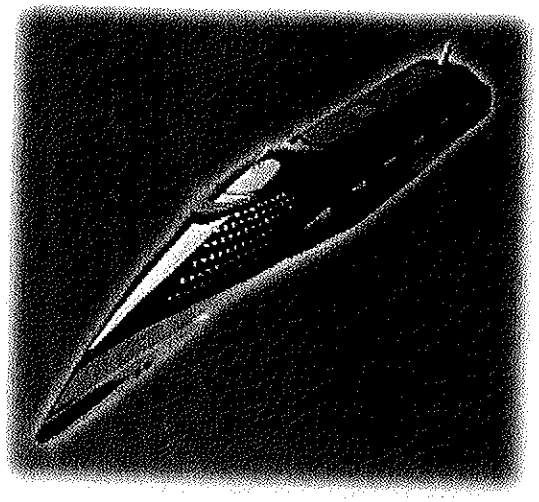

Figure 1.1: *Super liner for 1500 passengers. (The illustration is down loaded from the Kværner web server at www.kvaerner.com/ship/masa-yards/.)*

consuming analysis. The long term analysis become rather impractical from the designers point of view, since a large number of long, time domain simulation must be conducted to estimate the nonlinear design loads. A more efficient and practical feasible method to estimate the long term design values is therefore wanted. But first, suitable ship motion and loads theories to be implemented into simulation programs must be evaluated. The final choice should be based on a set of defined criteria, *e.g.* accuracy, computer capacity and economy and level-of-learning.

For the past two decades, significant effort have been devoted to study the nonlinear hydrodynamics. Three-dimensional time-domain theory have been implemented, *e.g.* Lin et al. (1994), Kring et al. (1996), into the program packages SWAN, Vada and Helmers (1992) and LAMP, Lin et al. (1996), respectively. Both ship motions and incident waves are assumed to be large and the free surface condition have been satisfied on the incident wave surface. However, the three dimensional theory do not enjoy the same success as the linear strip theory. This is partly due to the difficulties in the theory and the implementation. The main reason is the requirement of tremendous computer power. The LAMP system mentioned in Lin et al. (1994), offer an opportunity to use simpler codes as a filtering mechanism for more accurate and power demanding theories.

Simplified approaches has emerged at the expense of accuracy, *e.g.* Børresen and Tellsgård (1980), Wu and Moan (1996), Wu et al. (1996). These theories use a combination of linear strip theory and a nonlinear modification of the hydrodynamic forces. That is they are quasi-nonlinear theories. Simulation programs applying the fore mentioned theories are *i.e.* NV1418, Appendix A.1.3, and LANWIL, Appendix A.1.2, respectively.

The ship-wave problem was traditionally formulated in the frequency domain assuming small ship motions and waves. VERES, mentioned in Fathi (1997), is a simulation program based

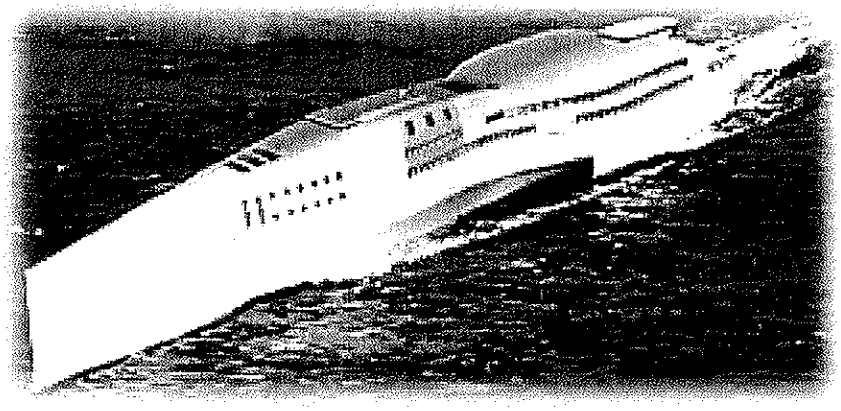

Figure 1.2: *Fast cargo trimaran. (The illustration is down loaded from the Kværner web server at www.kvaerner.com/ship/masa-yards/.)*

on linear, strip theory formulations. Two different theories are implemented,- namely the conventional strip theory and the high-speed strip theory, Salvesen et al. (1970), Faltinsen and Zhao (1991). The linear frequency domain programs have been successful in many ways, *i.e.* in estimating the wave induced loads for conventional ships. However, the linearity assumptions of small ship motions relative to the wave surface is violated at the fore quarter of the ship even in moderate sea states. In addition, the flare will introduce significant nonlinear effects in the region. Even though heave and pitch may be well predicted by linear theory, the hull girder loads will be affected by the nonlinear effects. An overview of existing nonlinear hydrodynamic theories is presented in Beck and Faltinsen (1999).

The choice of the hydrodynamic theory to be used in direct calculation of design loads, will naturally depend on the the designers' level of learning, the wanted accuracy, available computer capacity and of course, the economy plays an important role. The needed simulation time may be reduced by a factor 5 by using a supercomputer instead of a work station, Lin et al. (1994). In addition the simulation time will depend on the complexity of the theoretical formulation. Roughly, the time requirement is proportional to N_{3D}^2, where N_{3D} is total number of elements, for a 3-dimensional theory. The time is proportional to $N_{2D}^2 * S$ for a 2-dimensional theory, where N_{2D} is the number of elements for each strip and S is the number of strips. A $2\frac{1}{2}$-dimensional theory will require time somewhere in between the two fore mentioned formulations. In the time domain, the required time will be proportional to the number of time steps, Hoff (1999). In Lin et al. (1994) it is pointed out that a fully nonlinear formulation require as much as 6000 longer time to simulate a realization of one minute compared to a linear, strip theory analysis in frequency domain.

For most practical purposes, it is in general not feasible to apply the most complex theoretical formulations in direct calculation of design loads. This is based on that use require a certain level of knowledge, and that the simulation programs themselves are expensive. In addition, extensive investments must be made to install the powerful computers needed to be able to

conduct the simulations within reasonable time. Therefore, the more simpler theoretical formulations are in general applied, *i.e.* linear and nonlinear strip theories. These are easy to use and reasonably fast with personal computer.

The hydrodynamic theory applied to estimate the design loads are all burdened with a certain degree of uncertainty. The uncertainty is of less importance when different ship design are to be compared. However, in order to obtain an optimal design it is important to quantify the uncertainty related to the design process. Roughly, the contributing error sources can be related to

- theoretical limitations
- modelling of seas

21th ITTC (1996) presents an overview of studies on uncertainty analysis and validation of numerical sea keeping methods. A systematic work has been conducted throughout the years by C. Guedes Soares starting with Soares (1984) where he studied the model uncertainty of standard methods for predicting the wave induced loads both in connection with short- and long term statistics. In Soares (1986) modelling of the wave environment was treated and later he also studied the uncertainty in wave climatology and the effect on ship responses in Soares and Moan (1987), Soares and Viana (1988). Soares (1991) treated the transfer function uncertainty and its effect on short term responses. The effect of wave climate modelling on long term response was studied in Soares and Moan (1991), Soares and Trovão (1991). Faltinsen and Svensen (1990) studied the uncertainty in linear, strip theory related to human, numerical and physical errors. They were concentrating on heave and pitch motion.

1.2 Objective

A purpose of this thesis is to achieve an overview of existing hydrodynamic theories used to estimate global loads on monohull vessels. Theories which are incorporated in numerical codes should be chosen for the this work. The chosen hydrodynamic theories are validated against a significant amount of laboratory tests. The model uncertainty will be estimated by comparing loads predicted with the relevant theories and experimental values that were taken to be true values.

It is further the aim of this thesis to contribute to develop an accurate as well as simplified method for calculating design loads on modern ships, *i.e.* global loads on monohull vessels. The simplified method should account for the long term variation of the sea and use *direct calculation* based of the chosen hydrodynamic theories. Refined methods will be used for validating the simplified method to be used in practical design. The simplified method should account for probabilistic as well as nonlinear character of the load effect.

An important aspect is that the simplified method should be practical feasible and simple to use. This will also affect the choice of the theoretical formulation of the ship-wave problem. Determination of the hydrodynamic loads will be based on state-of-the-art methods, however

the computer code should be easy to use, reasonably fast and inexpensive (relatively). The final choice will naturally be a golden middle course of the mentioned criteria.

Some cases studies applying the simplified method in particular cases will be presented.

1.3 Organisation of the Thesis

A brief discussion of ship motion and load theories are given in Ch. 2. A linear and -nonlinear strip theory implemented in simulation programs chosen for the further study, are discussed. Other possible simulation programs are presented in Appendix A.

Ch. 3 contains the applied probabilistic theory. Basic theory is briefly discussed. Short term and extreme value statistics are presented. Particular attention has been paid to long term statistics. Operational restrictions is briefly touched.

In Ch. 4 the model uncertainty problem is treated. Theoretical limitations, Chap. 4.2, and experimental errors, Sect. 4.7, have been under discussion. Model uncertainty of the linear strip theory is given in Sect. 4.3 - 4.5, whereas model uncertainty regarding the nonlinear model is treated in Sect. 4.6.

A simplified method used to find the long term extreme values for the vertical bending moment midship, based on the contour line concept is fully described and discussed in Chap. 5. Both the linear and nonlinear ship motion and load theories have been used in the analysis, see Chap. 5.3 and 5.4.

Two case studies are conducted using the results in Ch. 5. The studies are given in Ch. 6 and 7. Finally, main conclusions and suggestions for further work are presented in Ch. 8.

1.4 Contributions of the Thesis

There are two main contributions in this thesis. The first is a study on the model uncertainty of different hydrodynamic theories. A new formulation of the model error of the transfer function is presented. The model error is further investigated and applied to find the uncertainty of the estimated hundred year vertical midship bending moment on monohull vessels. The trends of the model uncertainty of nonlinear theory are investigated in order to look for particular behaviour with regard to wave steepness, wave length, degree of nonlinearity in the response and block coefficient.

The second contribution is a simplified method to estimate the design loads, *i.e.* global loads on monohull vessels. The simplified method is based on the contour line concept, which previously has been applied on floating offshore structures. However, in this work the method has been tested on vessels with forward speed, and suitable short term characteristics to be used with the contour line have been found. Its applicability has also been tested for varying forward speed,

and when operability restriction is considered.

The simplified method has been verified with refined methods, *i.e.* long term analysis. The long term response is obtained by combining the response in all sea states. This is rather straightforward for linear response, since the analysis can be conducted in the frequency domain. However, time domain analysis is required to obtain the nonlinear response. It is therefore crucial to improve the efficiency in the calculation. In this thesis, it is demonstrated that the long term extremes can be obtained by considering only a few short term sea states.

The main contributions of the thesis are found in the following chapters:

- Sect. 4.3.2 contains a new formulation of the model error of the transfer function as a function of the frequency.
- Sect. 4.4.2 contains sensitivity analysis of the model error. Influence of the difference frequency areas is investigated.
- Sect. 4.4.1 and 4.4.3 contain different analysis using the model error.
- Sect. 4.5.1 contains generalisation of the model error. A relation between the uncertainty in the hundred year value of the vertical midship bending moment and the dimensionless model error is established.
- Sect. 4.6.2 - 4.6.3 contain investigation of the trends of the model error of nonlinear response given as the ratio of the experimental and predicted value of a regular wave.
- Sect. 5.3.1 - 5.3.4 contain verification of the applicability of the contour line approach on monohull vessels with forward speed and different wave headings. Appropriate short term characteristics are tested and suitable design fractiles and correction factors are found and presented.
- Sect. 5.3.5 contains a theory about relation between the trend of the correction factor/fractile and the location of the maximum coefficient of contribution to the exceedance probability.
- Sect. 5.4.5 - 5.4.6 contain a procedure used to improve the efficiency of long term analysis of nonlinear load response analysis. The procedure is based on using a combination of linear frequency domain analysis and nonlinear time domain analysis.
- Sect. 5.4.7 contains calculation of long term nonlinear extremes using the simplified methods, *i.e.* contour line concept and the short term extreme characteristic, design extreme value.
- Ch. 6 contains a case study on the use of the contour line approach on a monohull vessel with varying forward speed. Only linear load analysis is performed. The results are also presented in Haver et al. (1998a) , Haver et al. (1998b) .

- Ch. 7 contains a case study on the use of the contour lines on a monohull vessel when operational restrictions is taken into account and the forward speed is kept constant. Both linear and nonlinear load response analysis are conducted.

Chapter 2

Ship Motion and Load Theories

2.1 Introduction

Accurate prediction of the wave-induced ship motions, hydrodynamic loads and the resulting structural response is of crucial importance in ship design. Severe motion can limit operability, affect serviceability as well as safety. Extreme loads may cause structural failure due to buckling, collapse and fracture.

The advances in computational ship hydrodynamics over the last decade have resulted in increasingly accurate methods for predicting ship motions, loads and structural response. Especially the use of the codes has been improved over the last years due to the development of the modern computers. As a result of these developments, a new level of computational capability is emerging for prediction of the wave-induced ship motions, hydrodynamic loads and structural responses.

In traditional ship design the ship motions, the hydrodynamic forces and the structural response are evaluated in the frequency domain using some sort of potential theory formulation. There are both two and three dimensional theories. A two and a half dimensional theory, *i.e.* two dimensional body boundary conditions and three dimensional free surface conditions, has also been developed. Among these, it is the 2D theory which has gained most popularity as it offers an efficient tool for solving the ship wave problem. In particular the conventional strip theory, also known as the linear strip theory once presented by Salvesen et al. (1970) back in the 1970's, has attained a unique reputation. The linear strip theory has been widely used the past few decades due to its simplicity and accurate prediction of wave induced ship motions and global loads.

The following is an introduction to the theories applied in this thesis. First, the fully, nonlinear problem will be defined. The assumptions leading to the simplified linear, strip theory

will be pointed out. The basic assumptions and hydrodynamic theory given in Salvesen et al. (1970) will be presented. The theory is implemented in the program VERES, Fathi (1997). In addition, simplified nonlinear corrections, Wu and Moan (1996), as extension to the linear theory are described. The nonlinear corrections are implemented in the nonlinear, strip theory code LANWIL, Wu and Moan (1996).

The software packages VERES, Fathi (1997), and LANWIL, Wu and Moan (1996), will be used in this work. The theoretical background will be presented in the following chapters.

2.2 Complete Hydrodynamic Problem

2.2.1 Coordinate system

Let (x, y, z) be a right-handed coordinate system with respect to the mean position of the ship with the z-axis pointing vertically upwards through the centre of gravity of the ship. x is pointing towards the stern. The body is moving with a constant velocity, U, in the negative x-direction with heading, β. The other coordinate system, (x_0, y_0, z_0), is fixed in space. Let the translatory and rotational displacement in the x,y and z-direction be η_1,η_2,η_3,η_4,η_5 and η_6 respectively. The coordinate system and the definition of the translatory and the rotational displacement are given in figure 2.1.

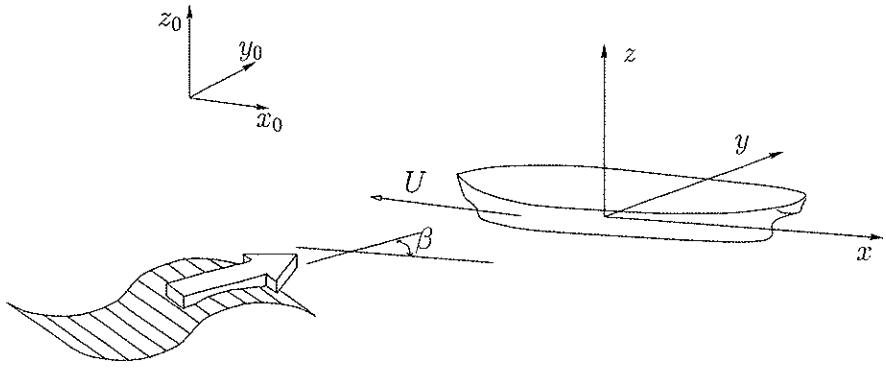

Figure 2.1: *Sign conventions and definitions of coordinate axis.*

2.2.2 Fluid Velocity Potential

Let the fluid velocity potential be defined as

$$\Phi = Ux + \phi_S(\boldsymbol{x}) + \phi^1(\boldsymbol{x}, t) + \phi^2(\boldsymbol{x}, t) + .. + \phi^n(\boldsymbol{x}, t) \tag{2.1}$$

where Ux and ϕ_S is the steady state solution describing the steady flow and, the steady flow pattern created around the ship respectively. ϕ^1 is the first order unsteady potential containing the first order velocity potential ϕ_0 due to the incoming, undisturbed wave and other first order, unsteady potentials. ϕ^2...ϕ^n are the second,..,n'th order unsteady potentials.

2.2.3 Ideal Fluid

The fluid is assumed to be irrotational, inviscid and incompressible. The fluid velocity vector, $\boldsymbol{V}(\boldsymbol{x},t)$, can be described by the fluid potential, Φ, at time, t, and the point, (x,y,z), as

$$\boldsymbol{V}(\boldsymbol{x},t) = \nabla\Phi(\boldsymbol{x},t) \tag{2.2}$$

The fluid is irrotational when $\nabla \times \boldsymbol{V} = 0$, in the fluid domain. The incompressibility, $\nabla \cdot \boldsymbol{V} = 0$, requires that the velocity potential is the fluid has to be a solution of the Laplace equation

$$\nabla^2\Phi = 0 \tag{2.3}$$

2.2.4 Pressure in the Fluid

From the Bernoulli's equation, one may find the pressure as, *e.g.* Newman (1977);

$$p = -\rho(\frac{\partial\Phi}{\partial t} + \frac{1}{2}\nabla\Phi\cdot\nabla\Phi + gz) + p_a \tag{2.4}$$

when the atmospheric pressure is assumed to be independent of the position on the free surface.

2.2.5 Free Surface Condition

The exact free surface condition is applied on the surface, $z = \zeta$, is given as, *e.g.* Newman (1977);

$$\frac{\partial^2\Phi}{\partial t^2} + g\frac{\partial\Phi}{\partial z} + 2\nabla\Phi\cdot\nabla\frac{\partial\Phi}{\partial t} + \frac{1}{2}\nabla\Phi\cdot\nabla(\nabla\Phi\cdot\nabla\Phi) = 0 \tag{2.5}$$

This conditions is achieved by requiring that the substantial derivative of the pressure, $\frac{D(p-p_a)}{Dt}$, is zero on the surface, *i.e.* from the dynamic condition. The expression for the free surface, ζ is obtained from Eq. 2.4 giving

$$\zeta = -\frac{1}{g}\left(\frac{\partial\Phi}{\partial t} + \frac{1}{2}\nabla\Phi\cdot\nabla\Phi\right) \tag{2.6}$$

2.2.6 Additional Condition

The body boundary condition on the wetted surface of the body is given as, *e.g.* Faltinsen (1990);

$$\boldsymbol{n}\cdot\nabla\Phi = \boldsymbol{V_s}\cdot\boldsymbol{n} \text{ on } S_b(t) \tag{2.7}$$

where $S_b(t)$ is the exact position on the ship surface pointing out in the fluid domain and $\boldsymbol{V_s}(\boldsymbol{x},t)$ is the fluid velocity at the point $\boldsymbol{x}$ on the body. In addition to the body boundary condition, the fluid motion caused by the body will go to zero far away from the body. That means the fluid motions in the far field will tend to those of the free stream and the undisturbed incident wave;

$$\nabla\Phi = U\boldsymbol{i} + \nabla\phi_0(\boldsymbol{x},t) \text{ for } |\boldsymbol{x}| \to -\infty, t \leq \infty \tag{2.8}$$

2.3 Linear strip theory

2.3.1 Linearization

In order to make progress towards a linear solution, both the free surface condition, the body boundary condition and the Bernoulli equation will be linearized. The total velocity potential in the ship fixed reference frame, $\boldsymbol{x}$, is given as

$$\Phi = Ux + \phi_S(\boldsymbol{x}) + \phi^1(\boldsymbol{x}, t) \tag{2.9}$$

That is only the steady state solution, $Ux + \phi_S(\boldsymbol{x})$, and the first order unsteady potential including the first order velocity potential ϕ_0 due to the incoming, undisturbed wave are taken into account. In addition it is assumed that the hull geometry is slender so that the steady perturbation potential ϕ_S is small. Assuming that the unsteady motion is small implies that also ϕ^1 and its derivatives will be small, Sect. 2.3.4. Thus, higher-order term of ϕ_S and ϕ^1 and cross products of the two will be neglected. Physically this mean that there is no interaction between the steady and unsteady wave systems. And that the free surface waves created by the steady potential has no effect on the motions and wave loads.

In order to reduce the problem from three to two dimensions it is necessary to assume that the frequency is relatively high, Sect. 2.3.3. This implies that the classical free surface condition with forward speed, see Eq. 97 page 364 Newman (1977), is simplified to Eq. 2.10. An approximation of the three dimensional result may be obtained by solving the hydrodynamic problem at each strip and integrating along the length of the hull to get the three dimensional solution, see Fig. 2.2 for an illustration. Then the two dimensional, unsteady problem that must be solved at each strip is given by the two dimensional Laplace equation, the linearized body boundary condition and the free surface condition, see Salvesen et al. (1970) for details.

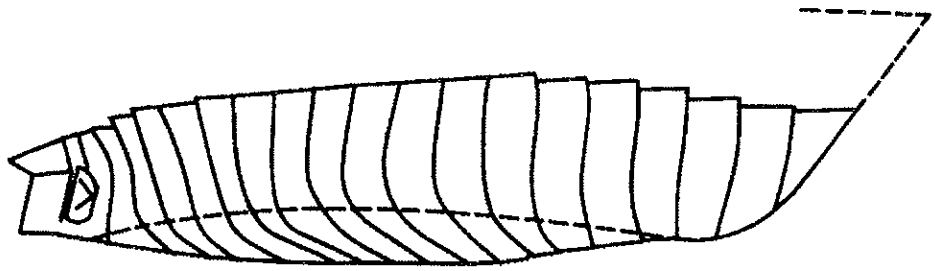

Figure 2.2: *Splitting up the vessel for strip theory calculation.*

The free surface condition is given as

$$\left[\left(\frac{\partial}{\partial t}\right)^2 + g\frac{\partial}{\partial z}\right]\phi^1(\boldsymbol{x}, t) = 0 \text{ on } z = 0 \tag{2.10}$$

The linearized pressure is given as

$$p = -\rho(\frac{\partial}{\partial t} + U\frac{\partial}{\partial x})\phi^1(\boldsymbol{x}, t) \tag{2.11}$$

In the following three chapters, the consequences of the three basic assumptions in the linear, strip theory will be pointed out and discussed in view of other theories.

2.3.2 Ideal Fluid

It is assumed that the fluid is homogeneous, irrotational, non-viscous and incompressible. Since the viscous effects are neglected it means that the only damping considered is the hydrodynamic damping due to energy loss when free surface-waves are generated, *i.e.* wave radition. This assumption is justified for vertical motions, heave and pitch, where the viscous damping is very small. On the other hand, the roll motion is significantly affected by the viscous damping. The amplitude of the roll motion can only be reasonable computed in the resonance area if one take into consideration the viscous damping. In general, the viscous roll damping is taken into account using empirical formulas.

In the strip theory program VERES, Fathi (1997), three different components of the viscous damping, *i.e.* frictional roll damping, eddy damping and bilge keel damping are taken into account. Fig. 2.3 shows the theoretical and experimental data for the roll amplitude of a cylinder with rectangular cross sectionwhen both wave and viscous damping and only wave damping are included. One may notice that the viscous effect significantly affects the roll amplitude at resonance.

Other contributions to damping are structural damping and hydrodynamic damping due to forward speed. None of these contribution to the damping will be important as long as the dynamic amplification of the hull is not taken into account, *i.e.* the hull is rigid. In Wu and Moan (1996) an example is presented to show the effect of the hydrodynamic damping due to forward speed for an elastic ship, structural damping is omitted, relative to a static analysis (rigid ship), see Fig. 2.4. One may notice that the damping due to wave radiation dies out very quickly for high frequencies, but the damping due to forward speed is not reduced.

2.3.3 High Frequency

In order to reduce the problem from three to two dimensions, it is assumed that the frequency is relatively high. In addition, one has to assume that the variation of the flow in the cross-sectional direction is much larger than in the longitudinal direction. One result of this simplification is that the method is more applicable in head than following seas.

The 16th International Towing Tank Conference, ITTC, reports that there is substantial disagreement between experimental and calculated results for the vertical wave loads in following seas (ITTC container ship ship S-175). This is may be due to the low encounter frequency. Another result is that the generated unsteady waves are propagating in directions perpendicular to the center plane of the vessel. The real wave picture is far more complex. At high Froude

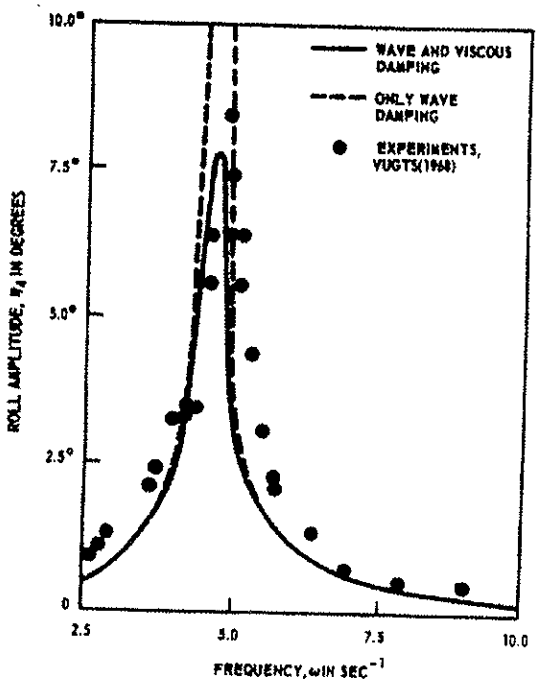

Figure 2.3: *Theoretical and experimental roll amplitude for rectangular cylinder in beam waves, Salvesen et al. (1970)*

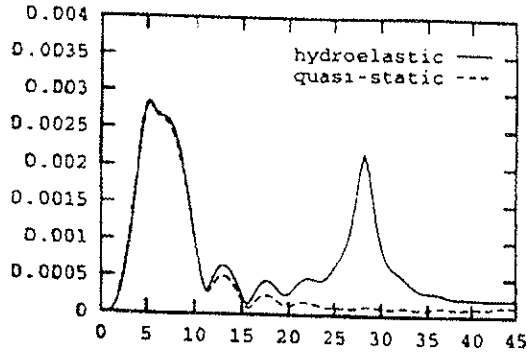

Figure 2.4: *Transfer function of the midship bending moment at* $Fn = 0.52$*, with structural damping omitted. All values are made dimensionless by the ship length,* L_{pp}*, the mass density of water,* ρ*, and the acceleration of gravity,* g*. Abscissa:* $\omega_e/\sqrt{\frac{g}{L_{pp}}}$*; ordinate:*$M_5/(\rho g L_{pp}^3 \zeta)$*, Wu and Moan (1996).*

numbers divergent wave systems occur. This indicates that the strip theory is a low Froude number theory. The forward speed limitation is the most severe restriction for naval applications.

Salvesen (1981) presents comparisons between strip theory and a three dimensional theory developed by Chang (1977). He solves the complete three dimensional hydrodynamic problem by distributing Green's function over the wetted surface of the body, and satisfies correctly all forward speeds. Some computations of the added mass and damping coefficients for the Series 60 model with with block coefficient $C_b = 0.70$, are presented. Chang's method agree well with the experimental data throughout the frequency range while the strip theory agree well in the high frequency area.

Fig. 2.5 shows a comparison between strip theory, three dimensional theory and experimental data for the vertical midship bending moment for the Series 60 model, with $C_B = 0.70$. There are some differences between the results in the low frequency area, but in the high frequency area there is quite good agreement for both experimental results and numerical simulations. The numerical three dimensional simulation is conducted with the program system Lamp, Lin et al. (1996) and see Appendix A.2.4.

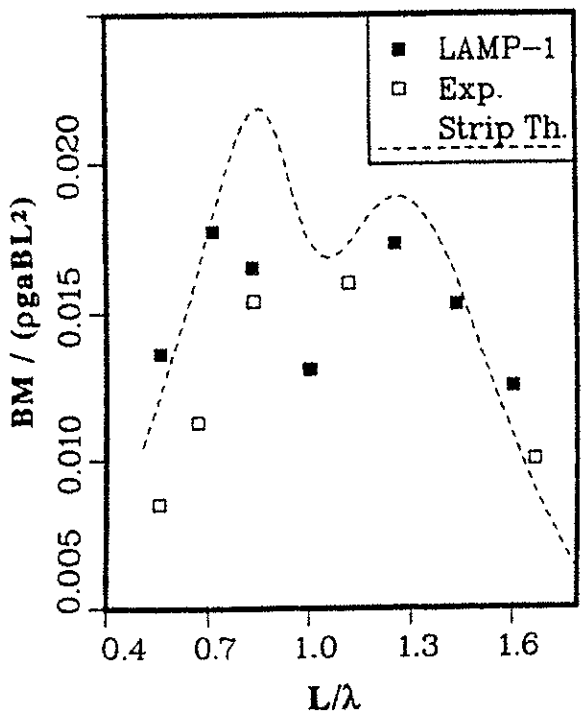

Figure 2.5: *Vertical bending moment midship for the Series 60 model, $C_b = 0.70$. Comparisons of linear theories and experimental results, Lin et al. (1994). BM is the vertical bending moment midship, a is the wave amplitude and $L = L_{pp}$. The experiments are condcuted with a wave steepness $2a/\lambda = 1/50$.*

Faltinsen and Zhao (1991) presented a method to analyse any type of slender, high-speed vessel

in waves. This is a modification of the strip theory which accounts for the interaction upstream. It is therefore denoted as a $2\frac{1}{2}$ dimensional theory, *i.e.* two dimensional body boundary conditions and three dimensional free surface conditions. The problem is solved by a stepping procedure starting at the bow. The diverging waves, which is not included in the strip theory, is now taken care of with only a small increase in the computational costs. Total forces are obtained by integrating the cross-sectional, two-dimensional forces over the ship length.

2.3.4 Small Waves

The basic assumption of linear theory is that the wave-amplitudes are assumed to be small relative to some characteristic dimension of the vessel, *i.e.* draft. The unsteady responses are then equivalently small. Due to the linearity assumption there are only hydrodynamic effects of the hull under the mean free surface. Therefore, the strip theory does not distinguish between alternative hull forms above the mean free surface. Consequently, the above-water hull form should be wall sided to get optimal results.

The linearity assumption of small ship motions relative to the wave surface is violated at the fore quarter of the ship even in moderate sea states. This can be seen in Fig. 2.6 which illustrates the bow motion of a destroyer in a sinusoidal wave with $\lambda = 1.20L_{pp}$ and $\frac{H}{\lambda} = 0.013$. The flare will introduce significant nonlinear effects in the bow region, even though heave and pitch may be well predicted by linear theory. This presides that the calculated results are violated in high sea states where slamming and green water on deck occur, Wu and Moan (1996), Wu et al. (1996), Sagli et al. (1997). The second order effects will affect the sagging and hogging moment in both frequency and amplitude.

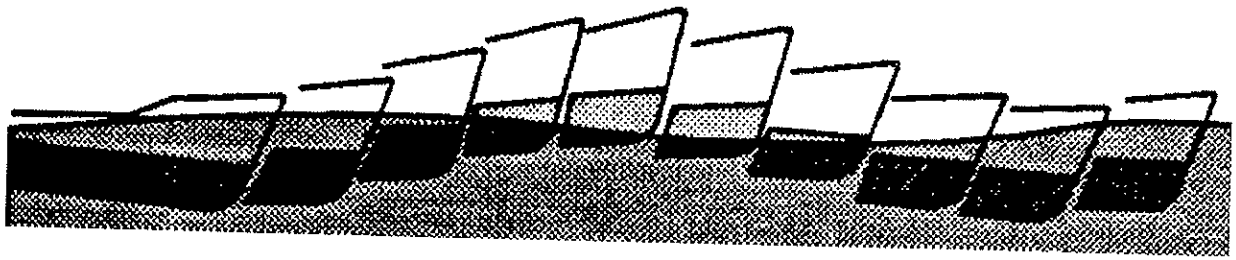

Figure 2.6: *Destroyer hull in sinusoidal wave,* $\lambda = 1.20L$ *and* $\frac{H}{\lambda} = 0.013$. *Salvesen (1981)*

The effect due to nonlinearity is exemplified in Fig. 2.7 showing comparisons of linear and nonlinear vertical bending moment midship for the reefer vessel. The numerical results are obtained using the three dimensional program SWAN with nonlinear correction for the hydrostatics and the Froude-Krylov forces, see Appendix A.2.3. Simplified nonlinear results are found by using the nonlinear strip theories implemented in the simulation program NV1418, Børresen and Tellsgård (1980) & Appendix A.1.3, and Lanwil, Wu and Moan (1996) & Appendix A.1.2. Included are also some experimental results, Korbijn (1991), and results from ordinary strip theory are shown

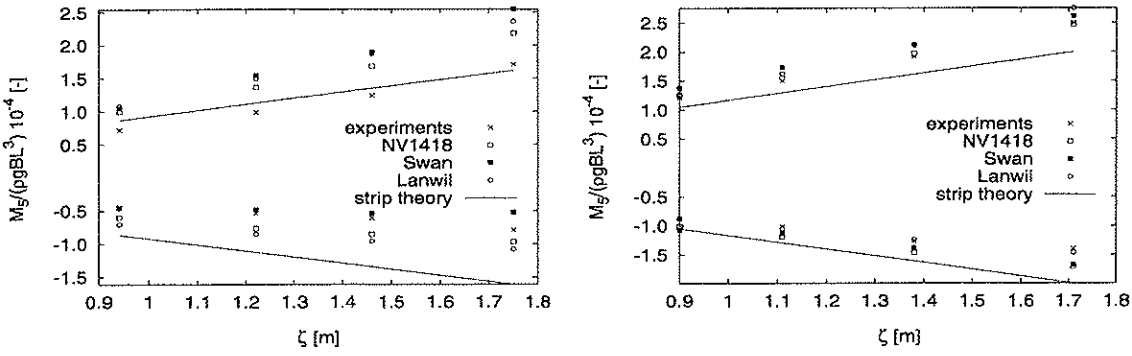

(a) 8.0m draft

(b) 11.4m draft

Figure 2.7: *Midship bending moment for the reefer vessel versus the wave amplitude for* $\lambda/L_{pp} = 1.0$ *at drafts* $8.0m$ *and* $11.4m$. *Both linear and nonlinear simulations results are included.*

by continuous lines. Numerical results from SWAN and NV1418 are taken from Kring et al. (1996). The figure shows that there are relatively large nonlinear effects for the sagging- and hogging moments.

2.4 Equation of motion

Assuming that the unsteady responses are small one may, as already mentioned, linearise the problem. The governing equation of the unsteady ship wave problem can be written as

$$(\mathbf{M} + \mathbf{A})\ddot{\boldsymbol{\eta}} + \mathbf{B}\dot{\boldsymbol{\eta}} + \mathbf{R}\boldsymbol{\eta} = \mathbf{F} \tag{2.12}$$

where $\mathbf{M}$ is the mass matrix. $\mathbf{A}$, $\mathbf{B}$ and $\mathbf{R}$ are the added mass, the linear damping and the hydrostatic restoring matrix respectively. $\mathbf{F}$ are the complex amplitudes of the wave exciting forces and moments. $\ddot{\boldsymbol{\eta}}$, $\dot{\boldsymbol{\eta}}$ and $\boldsymbol{\eta}$ are the acceleration, the velocity and displacement matrices.

The degree of complexity in the structural analysis depends mainly on whether it is necessary to include a dynamic hull response analysis or not. The next question is if it is necessary to include this as a part of the ship motion analysis.

Most existing theories treat the ship as rigid. Since, the dynamic analysis can be performed separately after the ship motion analysis is conducted, it is in general sufficient to assume the ship to be rigid. However, there are two main instances where the ship should be modelled as a flexible beam and the ship structural loads should be an integrated part of the ship motion analysis, *i.e.*

- if the encounter frequencies synchronise with the lowest natural modes of frequencies of the ship hull, the phenomenon of flexible hull vibration known as springing may occur
- if the response due to slamming is to be examined and the ship is so small that the motions are significantly affected by slamming

Wu and Moan (1996) presents a hydroelastic strip theory for both low- and high speed vessels. The work is a modification of the conventional strip theory and the high-speed theory, Salvesen et al. (1970) and (Faltinsen and Zhao 1991) respectively. The flexibility of the ship is taken into account by applying a number of dry-eigenmodes in addition to the six-rigid body modes, see Sect. 2.5. Hermundstad (1995), Hermundstad et al. (1999) established a similar approach to include the flexibility of catamarans in the high-speed code.

If the natural frequency coincides with the wave frequency, hydroelasticity will have a remarkable effect on the transfer function, Fig. 2.4. However, it does not mean that the same effect will be found in the response spectrum. This is due to the energy distribution in the wave spectrum. In general, the vessel's eigenfrequency is larger than the wave frequency. Increased hydroelasticity reduces the eigenfrequency and may cause springing. The hydroelasticity will first be of importance for moderate waves and may contribute to fatigue.

2.4.1 Added mass, damping and restoring forces and moments.

The added mass and damping forces are steady-state hydrodynamic forces caused by forced motions of the vessel when there are no incident waves. The forced motions generate outgoing waves and dynamic pressure on the hull. When the pressure is integrated over the wetted surface of the vessel, hydrodynamic forces which are proportional to the acceleration and velocity are obtained.

The added mass, damping and restoring forces and moments can be formally written as

$$F_{hydrodynamic,j} = -A_{jk}\ddot{\eta}_k - B_{jk}\dot{\eta}_k - R_{jk}\eta_k \tag{2.13}$$

where the added mass and damping coefficients are given as

$$A_{jk} = -\frac{\rho}{\omega^2}\Re\left\{\int\int_S \left(i\omega + U\frac{\partial}{\partial x}\right)\phi_k n_j ds\right\} \tag{2.14}$$

$$B_{jk} = \frac{\rho}{\omega}\Im\left\{\int\int_S \left(i\omega + U\frac{\partial}{\partial x}\right)\phi_k n_j ds\right\} \tag{2.15}$$

The added mass and damping coefficients are found by solving the 2D boundary value problem for each section along the ship and integrating the results over the length, Salvesen et al. (1970). As already mentioned, the applicability of the strip theory approach is dependent on relatively high frequencies and a high length to beam ratio. The strip theory neglects the interaction between the sections. An example on the influence of the three dimensional effects can be found in Faltinsen (1979). For instance, when the length to beam ratio of a spheroid in infinite fluid is 5, the three dimensional added mass in heave is 90% of the two dimensional result. The added moment in pitch or yaw is found to be 70% of the two dimensional results.

There are different ways to compute these two dimensional hydrodynamic quantities. For very simple cross sections, *i.e.* circular cylinder, analytical solution exist. For more arbitrary cross sections, numerical techniques must be used. The most common numerical techniques are, see Fig. 2.8;

- Frank close-fit source distribution method
- Lewis-form method

In the first method the section is represented by a number of straight segments. The potential is obtained by distributing pulsating source singularities with constant strength over each segment (2D sink and source method). The Frank close-fit method is time-consuming and in addition the method breaks down at an infinite number of discrete frequencies (irregular frequencies). However, this is a mathematical problem and may be circumvented by using different techniques. The advantage of this method is that it can be applied to any cross-sectional shape. Using the Lewis form method, the geometrical shape is mathematically represented by the Lewis form with the same beam, draft and area as the given section, but not necessarily the actual shape of the given section. This method is fast and quite accurate for common ship section, but can not be used on sections with large bulb or with a very small sectional area. The advantage is that it is a very fast method relative to the Frank close-fit method.

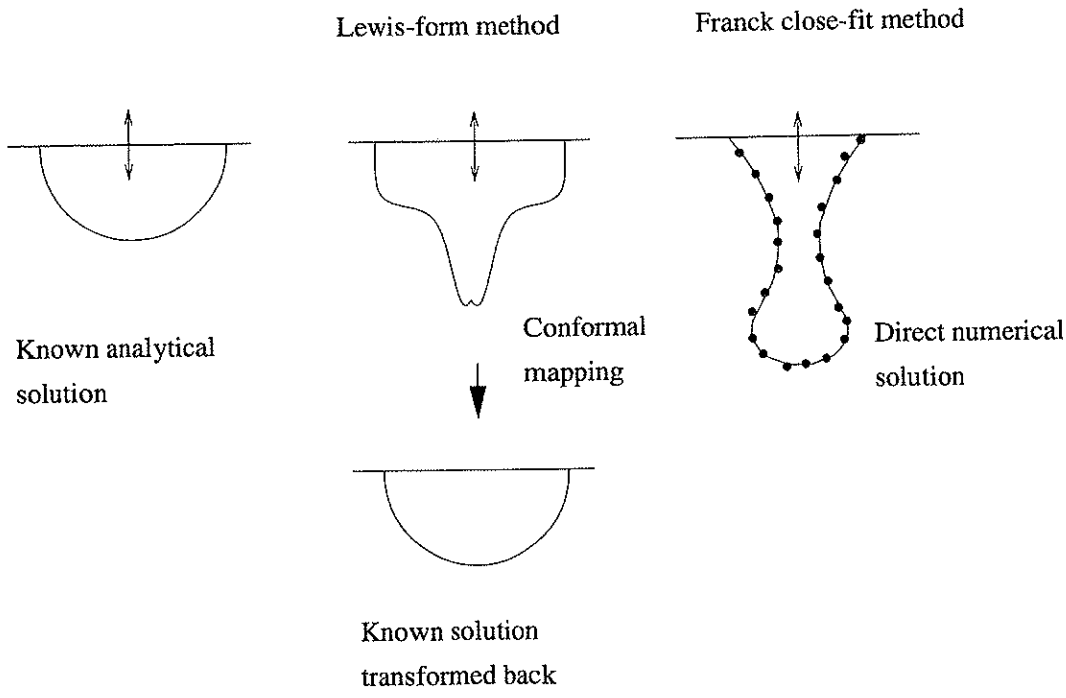

Figure 2.8: *Calculation methods for two dimensional ship sections.*

As already mentioned, the linear strip theory does not distinguish between alternative hull form above the mean free surface. In the case of large waves and motion, nonlinearities are introduced in the problem. Lin et al. (1994) and Kring et al. (1996) took into account the nonlinearities in the hydrodynamic forces by satisfying the body boundary condition on the instantaneous position and integrating the pressure below the undisturbed incident free surface. Since their methods are fully nonlinear one can not find the added mass and damping separately, since it is solved as one large problem.

However, there are several approximate methods. Jensen and Pedersen (1979) and Wu and Moan (1996) took into account second order modifications of the added mass and damping. Wu and Moan (1996) did the corrections for the added mass at high frequency ($\phi \rightarrow 0$), see Sect. 2.5. In Jensen and Pedersen (1979) the added mass and damping is Taylor expanded about $\bar{z} = 0$, where $\bar{z}$ is the relative displacement, to the first order ($m(\bar{z}, t) = m(0, x) + \bar{z}\frac{\partial m}{\partial \bar{z}}|_{\bar{z}=0}$).

In most cases, the nonlinear corrections tend to increase sagging moments and decrease the hogging moment. However, the nonlinear modification of the added mass and its derivative may in some cases give the opposite results, *i.e.* the sagging moment is reduced and whereas the hogging moment increases, Sagli et al. (1997). One should remember that the nonlinear hydrodynamic force is a function of the total relative displacement, velocity and acceleration. Therefore the nonlinear response to all those components does not equal the superposition of the nonlinear response by applying the components individually.

The restoring forces are independent of the velocity potential and the only influencing factors are the geometry and the mass distribution. The restoring forces follow directly from hydrostatic considerations.

2.4.2 Exciting forces and moments

The exciting forces and moments are the forces and moments acting upon the vessel when the vessel is restrained from moving and there are incident waves present. The exciting forces and moments can be divided into two groups:

1. The forces and moments due to the undisturbed waves causing the undisturbed pressure field is called Froude-Krylov forces.

2. The presence of the vessel cause a disturbance in the pressure field. The forces due to this disturbed pressure field are called diffraction forces. The forces are found in a similar way as the added mass and damping forces; i.e to solve a 2D boundary value problem for each section and integrate the results over the wetted length of the body.

Formally the exciting forces can be written as

$$F_{exciting,j} = \rho \int \int_S \left(i\omega + U\frac{\partial}{\partial x} \right) (\phi_0 + \phi_D) ds \tag{2.16}$$

where ϕ_0 is the undisturbed wave potential and ϕ_D is the potential due to the diffracted waves.

The nonlinearity in the exciting forces and moments can be included in similar ways as for the added mass and damping mentioned above. The Froude-Krylov force is always exactly included, since this force is caused by the undisturbed pressure field. In Jensen and Pedersen (1979) the nonlinearity of the free surface are taken into account by using a perturbation method. The hydrodynamic pressure due to the incoming waves is integrated to the free surface. Wu and Moan (1996) also introduce nonlinear modification of the Froude-Krylov forces at high frequency.

Using fully nonlinear methods, both Froude-Krylov and the diffraction forces may be included is a consistent manner. However, the nonlinear Froude-Krylov and restoring forces are in some cases included as an extension of the linear method. This is done *i.e.* in the LAMP Code, Lin et al. (1994) and Appendix A.2.4. $LAMP-2$, see Table 2.1, is based on three dimensional linear hydrodynamic, but nonlinear restoring and Froude-Krylov forces are included. The reason for developing this simplified code is that it drastically reduces the need for computer resources.

2.5 Extension to a simplified nonlinear, strip theory

An efficient method to determine the hull girder wave response in head sea waves considering both nonlinear hydrodynamic and possible structural dynamic effects are presented in Wu and Moan (1996). The total response is decomposed into linear and nonlinear parts. The linear part is evaluated by using linear, strip theory as presented in Sect. 2.3. The nonlinear part comes from the convolution of the impulse response function of the linear ship-fluid system and the nonlinear modifications of added mass, damping, restoring and wave forces. The global dynamics are taken into account by using modal analysis. The method for for both high and slow speed vessels are described in Wu and Moan (1996). Validation based on a model test is presented in Wu et al. (1996). A short overview will be presented in the following.

The method is based on the following assumptions

- The nonlinearity comes from the large ship motions in heave and pitch while the structural deformation remains small.
- The incident waves can be described sufficiently by linear wave theory.
- The influence of ship motion on the incident wave elevation is negligible

The theory is implemented in the nonlinear, strip theory program LANWIL, see Appendix A.1.2.

2.5.1 Equation of motion

The equation of motion of the ship structure in the vertical direction per unit length can be written as

$$m(x)\ddot{w}(x,t) + c(x)\dot{w}(x,t) + k(x)w(x,t) = F(x,t) \tag{2.17}$$

where $m(x)$, $c(x)$ and $k(x)$ are the structural mass, the structural damping and the structural stiffness respectively. $F(t)$ is the external nonlinear forces, acting on the ship and $w(x,t)$ is the

unknown vertical displacement.

The vertical displacements may be approximated by an aggregate of the s lowest dry eigenmodes, $w_k(x)$ $k = 1, .., s$ including heave and pitch which are the dominant parts. $w(x,t)$ is given as

$$w(x,t) = \sum_{k=1}^{s} w_k(x) p_k(t) = \mathbf{w}^T \mathbf{p} \tag{2.18}$$

in which $p_k(t)$ are the unknown generalised coordinates.

The vertical force per unit length exerted by the fluid on the ship hull at position x can be written as, *e.g.* Faltinsen (1990);

$$F(x,t) = -\frac{D}{Dt}\left[\tilde{m}(x,t)\frac{D\xi(x,t)}{Dt}\right] + f(x,t) \tag{2.19}$$

where $\tilde{m}(x,t)$ is the double-body added mass (or high-frequency added mass) of the submerged cross section. $f(x,t)$ consists of the Froude-Krylov force and the hydrostatic restoring force per unit length on the instantaneous wetted surface. D/Dt represents the total derivative with respect to time, t;

$$\frac{D}{Dt} = \frac{\partial}{\partial t} + U\frac{\partial}{\partial x} \tag{2.20}$$

and $\xi(x,t) = w(x,t) - \zeta(x,t)$ is the vertical displacement of the ship hull relative to wave surface.

2.5.2 Matrix Formulation

Inserting Eq. 2.18 into Eq. 2.17 gives

$$m(x)\mathbf{w}^T\ddot{\mathbf{p}} + c(x)\mathbf{w}^T\dot{\mathbf{p}} + k(x)\mathbf{w}^T\mathbf{p} = F(x,t) \tag{2.21}$$

Multiplying Eq. 2.21 by the eigenmode matrix ,$\mathbf{w}$, and integrating over the length of the hull, Langen and Sigbjörnsen (1979), gives

$$(\mathbf{M} + \mathbf{A_0})\ddot{\mathbf{p}}(t) + (\mathbf{C} + \mathbf{B_0})\dot{\mathbf{p}}(t) + (\mathbf{K} + \mathbf{R}_0)\mathbf{p}(t) = \mathbf{F}(t) \tag{2.22}$$

$\mathbf{M}$, $\mathbf{C}$ and $\mathbf{K}$ are the generalised structural mass, damping and stiffness matrices of the ship hull. $\mathbf{A}_0$, $\mathbf{B}_0$ and $\mathbf{R}_0$ are the generalised linear fluid added mass, damping and restoring matrices. $\mathbf{F}(t)$ is the generalised wave force vector. The wave forces are separated into a linear and nonlinear part, *i.e.*

$$\mathbf{F}(t) = \mathbf{F}_l(t) + \mathbf{F}_n(t) \tag{2.23}$$

where $\mathbf{F}_l(t)$ is the linear excitation forces. The terms in the nonlinear component $\mathbf{F}_n(t)$ will be described in the following.

2.5.3 Nonlinear Forces

The nonlinear effect has been put into the generalized force vector $\mathbf{F_n(t)}$ which contains the following terms

$$F_k(t) = F_{1k}(t) + F_{2k}(t) + F_{3k}(t) + F_{4k}(t) \; k = 1, 2, .., s \tag{2.24}$$

where

$$F_{1k}(t) = -\int_L w_k(x) \frac{\partial \tilde{m}(x,t)}{\partial t} \frac{D\xi(x,t)}{Dt} dx \tag{2.25}$$

is the slamming force. The hydrodynamic forces due to the nonlinear modifications of the two dimensional added mass and its derivatives with respect to x is given as

$$F_{2k}(t) = -\int_L w_k(x) \left[\tilde{m}(x,t) - \tilde{m}_0(x,t)\right] \frac{D^2\xi(x,t)}{Dt^2} dx \tag{2.26}$$

$$F_{3k}(t) = -U \int_L w_k(x) \frac{\partial \left[\tilde{m}(x,t) - \tilde{m}_0(x,t)\right]}{\partial x} \frac{D\xi(x,t)}{Dt} dx \tag{2.27}$$

$$F_{4k}(t) = -\int_L w_k(x) \left[Q(x,t) - Q_0(x,t) + b_0(x)\xi(x,t)\right] dx \tag{2.28}$$

They reflect to some extent the nonlinear effects in the fluid added mass, damping and diffraction force. The last element in Eq. 2.24, $F_{4k}(t)$, is the nonlinear modification of the Froude-Krylov force and the hydrostatic restoring force. $\tilde{m}_0(x)$ is the double-body added mass of the mean submerged cross section $Q_0(x,t)$. $Q(x,t)$ is the area of the instantaneous submerged cross section, and $b_0(x)$ is the beam at mean draft.

Decomposing the total generalized response, $\mathbf{p}(t)$, into a linear part and part which is the response due to the nonlinear corrections gives

$$\mathbf{p}(t) = \mathbf{p}_l(t) + \mathbf{p}_n(t) \tag{2.29}$$

Eq. 2.22 can be rearranged as

$$(\mathbf{M} + \mathbf{A_0})\ddot{\mathbf{p}}_l(t) + (\mathbf{C} + \mathbf{B}_0)\dot{\mathbf{p}}_l(t) + (\mathbf{K} + \mathbf{R}_0)\mathbf{p}_l(t) = \mathbf{F}_l(t) \tag{2.30}$$

$$(\mathbf{M} + \mathbf{A_0})\ddot{\mathbf{p}}_n(t) + (\mathbf{C} + \mathbf{B}_0)\dot{\mathbf{p}}_n(t) + (\mathbf{K} + \mathbf{R}_0)\mathbf{p}_n(t) = \mathbf{F}_n(t) \tag{2.31}$$

In order to take into account the memory effect of the free surface, $\mathbf{A}_0$, $\mathbf{B}_0$, $\mathbf{R}_0$ and $\mathbf{F}_l$ are replaced with the frequency dependent mass $\mathbf{A}$, damping $\mathbf{B}$, restoring matrix $\mathbf{R}$ and the frequency dependent Froude-Krylov and diffraction force, $\mathbf{F}_{FK} + \mathbf{F}_D$, derived in linear theory, respectively, Wu and Moan (1996). The linear and nonlinear responses, which are the solution of these equations, are found by applying convolution integration

$$\mathbf{p}_l(t) = \int_{-\infty}^{t} \mathbf{h}(t-\tau)\left[\mathbf{F}_{FK}(\tau) + \mathbf{F}_D(\tau)\right] d\tau \tag{2.32}$$

$$\mathbf{p}_n(t) = \int_{-\infty}^{t} \mathbf{h}(t-\tau)\mathbf{F}_n(\tau) \tag{2.33}$$

where

$$\mathbf{h}(t) = \frac{1}{2\pi}\int_{-\infty}^{\infty}\left[-\omega_e^2(\mathbf{M}+\mathbf{A}) + i\omega_e(\mathbf{C}+\mathbf{B}) + (\mathbf{K}+\mathbf{R})\right]^{-1} e^{i\omega_e t} d\omega_e \tag{2.34}$$

is the impulse response function matrix.

Unlike most existing nonlinear analysis procedures, this method is not confined to conventional strip theory. The impulse response function, $\mathbf{h}(t)$, can be solved by employing different linear potential-flow theories. The way the nonlinear hydrodynamic force is dealt with, implies that although large amplitude relative motion is introduced, the memory effect of the free surface is still treated in a linear manner, Wu and Moan (1996).

2.5.4 Rigid body

If the ship is treated as a rigid body, only the two first dry eigenmodes in Eq. 2.18 will be included, *i.e.* heave and pitch. Therefore the linear part of the theory will be equivalent to the solution of Eq. 2.12. That is the solution of the ordinary linear strip theory as discussed in Sect. 2.3. The nonlinear contribution comes from the solution of Eq. 2.33.

When the simulation program LANWIL, Appendix A.1.2, was applied in this work, numerical problems were encountered. The nonlinear contribution from slamming, Eq. 2.25, turned out to be sensitive to the discretization of the hull. When response in extreme, irregular sea states was simulated, high frequent oscillations were encountered when bottom slamming occurred. In particular this was a problem, when bottom slamming was located in the midship region causing large hogging responses. This could be dealt with by increasing the number of sections along the hull. This can bee seen in Fig. 2.9, showing pieces of the time domain simulations in irregular seas for the vertical bending moment midship on the S-175 container ship. For this specific vessel, the result was converging as the number of sections was increased to $N = 126$. Increasing the number of sections, did not influence the peak values of the sagging response significantly.

Naturally, the number of sections needed to get convergent results will depend on the hull form, the length between the perpendiculars and also forward speed. Simulations conducted with a tanker did not show any problems as indicated above. The vessel was large, $L_{pp} = 270m$, and the motions were small. Response histories for a destroyer had equivalent numerical problems as for the S-175 container ship. However, the deadrise angle is larger for the destroyer than the S-175 container ship. The S-175 container ship has a deadrise angle approximately equal to zero and one believes that this flat bottom is a part of the problem.

How this particular numerical instability can be dealt with in stochastic analysis is discussed in detail in Sect. 5.4.2.

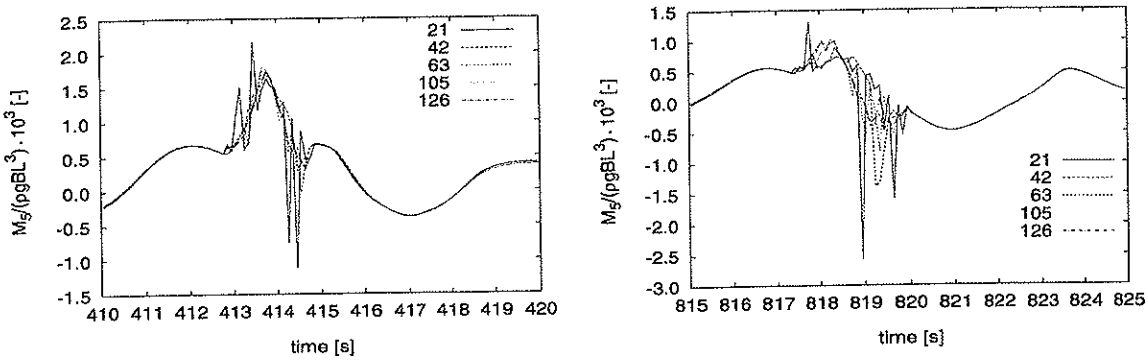

(a) $H_s = 14.5m$ & $T_p = 15.9s$

(b) $H_s = 13.56m$ & $T_p = 13.76s$

Figure 2.9: *Vertical bending moment midship for the S-175 container ship in head sea, irregular waves.* $Fn = 0.275$

2.6 Summary

The strip theory has been presented. Its limitations have been pointed out and commented versus other existing theories for ship motions and loads. In addition a simplified nonlinear theory have been introduced.

The ordinary strip theory is implemented in the simulation program VERES, Fathi (1997), and the nonlinear strip theory implemented in the simulation program LANWIL, Wu and Moan (1996). These two programs will be used throughout this work.

Other existing programs for calculation of ship motions and loads have been mentioned. More information can be found in Appendix A. An overview of some features of existing simulation programs is shown in Table 2.1.

Table 2.1: *Programs for calculation of ship motions and loads ($\mathcal{Z} = 0$ and $\mathcal{F}(t)$ are still water surface and incident wave surface respectively)*

Method:	Hydrodynamic, Restoring and Froude-Krylov Forces	Domain	Hydroelasticity
VERES	Free Surface Boundary Conditions on $\mathcal{Z} = 0$ $2\frac{1}{2}$-D Linear Hydrodynamics 2D Linear Hydrodynamics Linear Restoring and Froude-Krylov	frequency	no
LANWIL	Free Surface Boundary Conditions on $\mathcal{Z} = 0$ 2D Large-Amplitude Hydrodynamics Nonlinear Restoring and Froude-Krylov	time & frq	yes
NV1418	Free Surface Boundary Conditions on $\mathcal{Z} = 0$ 2D Large-Amplitude Hydrodynamics Nonlinear Restoring and Froude-Krylov	time	no
SWAN-1	Free Surface Boundary Conditions on $\mathcal{Z} = 0$ 3D Linear Hydrodynamics Linear Restoring and Froude-Krylov	frequency	no
SWAN-2	Free Surface Boundary Conditions on $\mathcal{F}(t)$ 3-D Large-Amplitude Hydrodynamics Nonlinear Restoring and Froude-Krylov	time	no
LAMP - 4	Free Surface Boundary Conditions on $\mathcal{F}(t)$ 3-D Large-Amplitude Hydrodynamics Nonlinear Restoring and Froude-Krylov	time	yes
LAMP - 3	Free Surface Boundary Conditions on $\mathcal{F}(t)$ $2\frac{1}{2}$-D Large-Amplitude Hydrodynamics Nonlinear Restoring and Froude-Krylov	time	no
LAMP - 2	Free Surface Boundary Conditions on $\mathcal{Z} = 0$ 3-D Linear Hydrodynamics Nonlinear Restoring and Froude-Krylov	time	no
LAMP - 1	Free Surface Boundary Conditions on $\mathcal{Z} = 0$ 3-D Linear Hydrodynamics Linear Restoring and Froude-Krylov	time	no

Chapter 3

Probabilistic Theory

3.1 Introduction

As mentioned, in the previous chapter, two different formulations are available for numerical solution of the ship response due to stochastic wave loads, *i.e.*

- frequency domain solution
- time domain solution

The frequency domain solution is significantly quicker than the time domain solution of any useful length. For Gaussian processes the energy spectrum will give a complete description of the statistical properties of the process. This means that all statistical values, *i.e.* variation, zero-up-crossing frequency, distribution of maxima and extremes, can be found without any statistical uncertainty.

In a time domain solution, the response is given as a time record of limited length, *i.e.* a realization of the process. The record represents values of the underlying process at discrete time increments and is called a time series. If a realization of the response due to a wave process with constant parameters are divided into two halves, one will have two realizations of the response process. The two realizations will be different and so will the statistical parameters. Therefore, none of them can be taken as true values. The statistical uncertainty can be dealt with by making the time series sufficiently long. Time domain analysis will require estimation of statistical parameters, and also the ability to find uncertainties related to such estimates.

In the following sections probabilistic methods to describe the above mentioned stochastic processes will be introduced. Some basic concepts are given. In addition short term and extreme value statistics will be briefly mentioned. Classical long term statistic is described together with an approximate long term method. The former includes all sea states in the scatter diagram.

While the latter method uses coefficients of contribution in order to select a part of the scatter diagram to be used in the long term analysis. This will save computing time and man-hours if time domain solutions are applied.

3.2 Basic Concepts

In general the wind generated sea waves is a nonlinear random process. The nonlinearity is more prominent in severe sea states. This is seen in many observation showing a large excess of high crest to shallow troughs. Lounguet-Higgins (1963) presented the nonlinear random process as

$$\zeta = \sum \alpha_i \epsilon_i + \sum \alpha_{ij} \epsilon_i \epsilon_j + \sum \alpha_{ijk} \epsilon_i \epsilon_j \epsilon_k \tag{3.1}$$

where α are constants and ϵ are independent, regular components. Neglecting the higher order terms one is left with the a linear representation of the sea surface, *i.e.*

$$\zeta = \sum \alpha_i \epsilon_i \tag{3.2}$$

It is known that in linear theory of wind generated sea waves, the statistical distribution of wave elevation, ζ, is normally described by the Gaussian distribution with zero mean value and variance m_0. Effects like skewness and kurtosis will therefore not be modelled. It is assumed that the wave process is stationary within a short period of time (normally 20 minutes to 3 hours) and ergodic, *i.e.* ensemble average is equal to the temporal average.

The long term, *i.e.* monthly to years, variation of the sea, is simply described by a sequence of stationary, short term sea states. If sequence effects are of no importance, the long term variation is normally presented in a scatter diagram showing the joint frequency of the wave spectral parameters that completely describe each short term Gaussian process. This includes the significant wave heights and peak periods over a period of time ranging from months to many years.

The wave elevation can be characterised in the frequency domain by the wave spectrum. For long-crested sea states, *i.e.* no spreading, the spectrum is a function of the wave frequency given as $S_\zeta(\omega)$. For short crested sea state, *i.e.* waves are spread about the dominant wave direction, the spectrum is given as a function of the wave frequency, ω, and wave heading, β, as $S_\zeta(\omega, \beta)$ and called a directional spectrum.

The wave spectrum can be estimated directly from the time series by mean of the auto-correlation function, $R(\tau)$, *e.g.* Newland (1984). For long-crested waves this relationship is given by

$$S_\zeta(\omega) = \frac{1}{2\pi} \int_{-\infty}^{\infty} R(\tau) \exp^{-i\omega\tau} \, d\tau \tag{3.3}$$

where the auto-correlation function is given as $R(\tau) = E[\zeta(t)\zeta(t+\tau)]$. For short-crested sea states the expression is given as, *e.g.* Myrhaug (1993),

$$S_\zeta(\omega, \boldsymbol{k}) = \frac{1}{(2\pi)^3} \int_{\boldsymbol{\xi}} \int_{-\infty}^{\infty} R(\tau, \boldsymbol{\xi}) \exp^{-i(\omega\tau - \boldsymbol{k}\boldsymbol{\xi})} \, d\tau d\boldsymbol{\xi} \tag{3.4}$$

where $\boldsymbol{k}$ is the wave number vector given as $\boldsymbol{k} = [k\cos\beta, k\sin\beta]$. The auto-correlation function is now given as $R(\boldsymbol{\xi}, \tau) = E[\zeta(\boldsymbol{x}, t)\zeta(\boldsymbol{x} + \boldsymbol{\xi}, t + \tau)]$. Where $\boldsymbol{x}$ is the position vector and $\boldsymbol{\xi}$ is the vectorial distance between the two actual points in the horizontal plane. It can be shown, *e.g.* Myrhaug (1993), that the spectrum $S_\zeta(\omega, \boldsymbol{k})$ can be given as

$$S_\zeta(\omega, k, \beta) = S_\zeta(\omega, \beta)\delta[k - sign(\omega)k(\omega)] \tag{3.5}$$

which means that irregular short-crested waves are described by adding linear waves with wave frequencies, ω, wave number, $k(\omega)$, and wave heading, β. Generally, standardised spectra are used in statistical analysis, see Sect. 3.3.

The relation between the wave spectrum and the wave amplitude can be found in many text-books, see *e.g.* Faltinsen (1990), Myrhaug (1992), as

$$A_j = \sqrt{2S_\zeta(\omega_j)\Delta\omega_j} \tag{3.6}$$

$$A_{ij} = \sqrt{2S_\zeta(\omega_j)\Delta\omega_j\Delta\beta_i} \tag{3.7}$$

where the expression represents the energy content in wave component number j and ij. The total energy is given by a summation of the wave components, see Eq. 3.25 and 3.26. $\Delta\omega_j$ and $\Delta\beta_i$ are the difference between two successive frequencies and wave headings respectively. This leads to the next topic treating irregular wave elevation and response.

3.3 Standardised Wave Elevation Spectrum

Wave measurements indicate that the scatter diagram may be divided into three parts as shown in Fig. 3.1, Torsethaugen (1987). Part one and three consist of swell and wind sea generated waves, where the third part is dominated by swell. Part 2 consists purely of wind sea generated waves and can be described by the one peaked Jonswap spectrum or the the Pierson Moskowitz spectra which is a special case of Jonswap spectrum. The Torsethaugen spectrum, Torsethaugen (1993), is a two-peak formulation, which includes both swell and wind generated waves. Only the formulations of the Jonswap and Pierson Moskowitz spectrum are presented in this work.

3.3.1 The Jonswap Spectrum

The Jonswap spectrum is used to represent sea states which are fully and not fully developed. The spectrum has a peakedness parameter, γ, which determines the energy concentration around the peak frequency, T_p. The higher value of γ the more energy around the peak frequency ω_p, Bishop and Price (1979).

The Jonswap spectrum is given on the form

$$S_\zeta(\omega) = \frac{\alpha g^2}{\omega^5}\exp\left[-\beta(\frac{\omega_p}{\omega})^4\right]\gamma^{\exp\left[-\frac{(\frac{\omega}{\omega_p}-1)^2}{2\sigma^2}\right]} \tag{3.8}$$

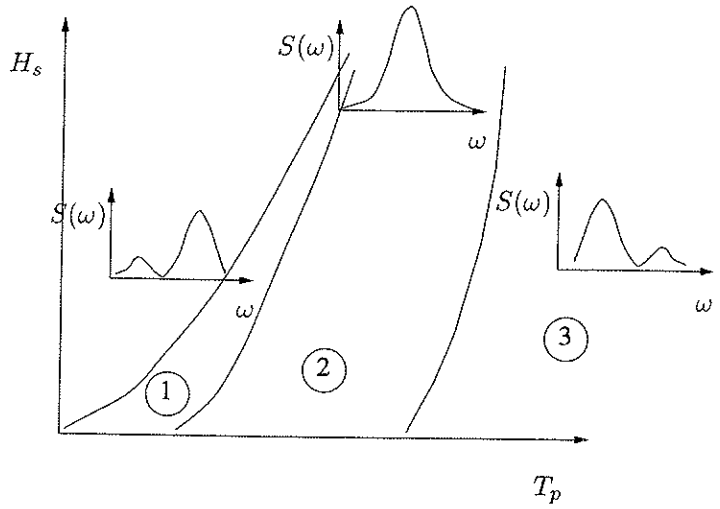

Figure 3.1: *Different sea types in the scatter diagram.*

where

α	spectral parameter	
ω_p	peak frequency	
γ	peakedness parameter	
β	spectral parameter,$\beta = 1.25$	
σ	spectral parameter,$\sigma =$	$\begin{cases} 0.07 & \text{if } \omega < \omega_p \\ 0.09 & \text{if } \omega > \omega_p \end{cases}$

The relation between the spectral parameter, α, and the significant wave height, H_s, the peak period, T_p, and the peakedness parameter, γ, is given as, *e.g.* Fathi (1997);

$$\alpha = 5.061 \frac{H_s^2}{T_p^2}(1 - 0.287 \ln \gamma) \tag{3.9}$$

where the value of the peakedness parameter can be found as

$$\gamma = \exp\left[3.848\left(1 - \frac{0.1975\delta T_p^4}{H_s^2}\right)\right] \text{ where } \delta = 0.036 - \frac{0.0056 T_p}{\sqrt{H_s}} \tag{3.10}$$

and the limiting values for the peakedness parameter is set to

$$1.0 \leq \gamma \leq 7.0 \tag{3.11}$$

The ratio between the peak period, T_p, and the zero-up crossing period is given as

$$\frac{T_p}{T_z} = -0.01698\gamma + 1.30301 + \frac{0.12102}{\gamma} \tag{3.12}$$

The Pierson Moskowitz spectrum is a special case of the Jonswap spectrum with $\gamma = 1.0$.

3.3.2 Pierson Moskowitz Spectrum

The Pierson Moskowitz spectrum is given as

$$S_\zeta(\omega) = \frac{H_s^2 T_z}{8\pi}(\frac{\omega T_z}{2\pi})^{-5} \exp\left[-\frac{1}{\pi}(\frac{\omega T_z}{2\pi})^{-4}\right] \tag{3.13}$$

where H_s is the significant wave height and T_z is the zero up-crossing period. The significant wave height is defined as the average of the one third highest waves. The zero-up crossing period and the mean wave period is given as

$$T_z = 2\pi\sqrt{\frac{m_0}{m_2}} \tag{3.14}$$

$$T_1 = 2\pi\frac{m_0}{m_1} \tag{3.15}$$

where m_0, m_1 and m_2 are spectral moments given as

$$m_n = \int_0^\infty \omega^n S_\zeta(\omega) d\omega,\ n = 0, 1, 2, 3, .. \tag{3.16}$$

For this particular wave spectrum, the following relations exist between the mean wave period, the peak period, T_p, and the zero-up crossing period, T_z

$$T_1 = 1.086 T_z \tag{3.17}$$

$$T_p = 1.408 T_z \tag{3.18}$$

The Pierson Moskowitz spectrum is suitable for a fully developed sea state, *e.g.* Bishop and Price (1979). For a given peak period and significant wave height, the Pierson Moskowitz spectrum is identical to the Bretschneider, ISSC and ITTC spectrum models.

3.3.3 Direction Spectrum

In short-crested waves where the waves tend to spread about the dominant wind direction, one has to take into account the heading angle. This can be done by introducing a spreading function, $D(\beta)$. The direction spectrum is given as

$$S_\zeta(\omega, \beta) = S_\zeta(\omega) D(\beta) \tag{3.19}$$

Different functions has been proposed for the spreading function, but a common one is a cosine type function, *e.g.* Bishop and Price (1979);

$$D(\beta) = A_n \cos^n \beta \tag{3.20}$$

where β is $-\pi/2 \leq \beta \leq \pi/2$. A_n is given as

$$A_n = (\int_{-\pi/2}^{\pi/2} \cos^n \beta d\beta)^{-1} = \frac{2^{n-1}}{\pi}\frac{\Gamma(\frac{n}{2})\Gamma(\frac{n}{2}+1)}{\Gamma(n)} \tag{3.21}$$

where $\Gamma()$ is the gamma function.

3.4 Response Spectrum

The response spectrum is given as a function of the frequency of encounter and wave heading by

$$S_{\eta\zeta}(\omega_e,\beta) = H_{\eta\zeta}(\omega_e,\beta)H^*_{\eta\zeta}(\omega_e,\beta)S_\zeta(\omega_e,\beta) \tag{3.22}$$

where $H_{\eta\zeta}(\omega_e,\beta)$ is the the transfer function for a given speed and heading. $S_\zeta(\omega_e,\beta)$ is the wave direction spectrum as a function of the frequency of encounter and wave heading. η indicates the response and ζ the wave elevation. The star denotes the complex conjugate. The frequency of encounter is given as a function of the heading angle, the wave frequency and forward speed, U, as

$$\omega_e = \omega + \frac{\omega^2 U}{g}\cos\beta \tag{3.23}$$

It can be shown that the moments of the response spectrum in short-crested waves for directions between head to following sea can be written as, Hoff (1994),Tikka (1989);

$$m_n = \int_0^\infty \int_\beta |\omega_e|^n H_{\eta\zeta}(\omega,\beta)H^*_{\eta\zeta}(\omega,\beta)S_\zeta(\omega,\beta)d\beta d\omega \tag{3.24}$$

as opposed to Eq. 3.16 where the spectrum is multiplied with the wave frequency. For long crested waves Eq. 3.24 is somewhat modified, *i.e.* the heading is dropped as a variable in the analysis.

3.5 Generation of Time Series

A realization of limited length, can be written as a large sum of regular components, *i.e.*

$$x(t) = \sum_{j=1}^{N} c_j \sin(\omega_j t - \psi_j) \tag{3.25}$$

where c_j is the amplitude determined from the energy spectrum, ω_j is a discrete frequency and ψ_j an arbitrary phase angle.

Different methods can be applied to generate time records, *e.g.* Langen and Sigbjörnsen (1979), Langen (1981). Tucker et al. (1984) has also treated this problem. The results from the different methods will have different statistical properties. Some alternatives are

1. deterministic amplitude and stochastic phase
2. stochastic amplitude and phase
3. stochastic frequency and phase

The third method above is implemented into the simulation program used in this work, Wu and Moan (1996).

The stochastic frequency is found by drawing a random number p from an even distribution in the interval $[0,1]$. The random frequency in the interval $[\omega_{lower,j}, \omega_{upper,j}]$ is then given as $w_j = \omega_{lower,j} + p \times \Delta\omega_j$. An equivalent procedure can be used in order to establish a random wave heading β_i, *i.e.* $\beta_i = \beta_{lower,i} + p \times \Delta\beta_i$ when the time series for the response is wanted, see Eq. 3.27. Thus the amplitude for long crested waves can be found as $A_j = \sqrt{2S_\zeta(\omega_j)\Delta\omega_j}$ or as $A_{ij} = \sqrt{2S_\zeta(\omega_j)\Delta\omega_j\Delta\beta_i}$ for short crested waves, Wu and Moan (1996).

The stochastic phase is distributed randomly in an interval between 0 and 2π.

3.5.1 Description of Irregular Wave Elevation

Linear superposition of short crested wave components, gives the total wave elevation as the sum of N regular wave components and I headings as

$$\zeta(x,y,t) = \sum_{i=1}^{I}\sum_{j=1}^{N} A_{ij}\sin(\omega_j t - \boldsymbol{k}_j\cdot\boldsymbol{x} + \psi_{ij}) \tag{3.26}$$

where the wave amplitude A_{ij} is given in Eq. 3.7. ψ_{ij} is the random phase angle. The phase angle is a stochastic variable uniformly distributed between 0 and 2π. The wave number vector $\boldsymbol{k}$ is a function of the wave heading β and the wave number, k. The wave frequency and the wave number is related by the dispersion relation which is given as $\omega_j^2 = k_j g$ for deep water waves.

3.5.2 Description of Irregular Response

If one wants to calculate the linear response, $\eta(t)$, due to the wave, $\zeta(t)$, this will be a sum of the responses due to each single wave component. Given that the response is linear, this can be written as

$$\eta(t) = \sum_{i=1}^{I}\sum_{j=1}^{N} |H_{\eta\zeta}(\omega_{ej},\beta_i)|A_{ij}\sin(\omega_{ej}t - \boldsymbol{k}_j\cdot\boldsymbol{x} + \psi_{ij} + \varepsilon_{ij}) \tag{3.27}$$

where $H_{\eta\zeta}(\omega_{ej},\beta_i)$ is the complex transfer function for between the response and wave at frequency ω_j and heading β_i. ω_{ej} is the encounter frequency given i Eq. 3.23. $\boldsymbol{k}$ is the wave number vector. ψ_{ij} is the random phase angle and ε_{ij} is the phase difference between the real and imaginary part of $H_{\eta\zeta}(\omega_{ej},\beta_i)$.

If the response is nonlinear, a superposition can not be used. If a fully nonlinear theory is applied to solve the hydrodynamics, one has to create the irregular wave, *i.e.* Eq. 3.26, and solve the hydrodynamic problem for each time step.

The nonlinear theory applied herein is valid only for head seas and uses a combination of Eq. 3.26

and Eq. 3.27, modified to long crested waves. As mentioned in Sect. 2.5, the hydrodynamic problem is solved in two steps, *i.e.*

- linear response in the frequency domain
- response due to nonlinear forces in the time domain

The linear response time series are found by by combining the transfer functions and the irregular wave elevation analogous to Eq. 3.27. Next, the corresponding wave elevation is used to find the response due to the nonlinear forces, Eq. 2.25 - 2.28 at each time step in the time domain giving $\eta^{nl}(t)$. The nonlinear corrections are calculated on basis of the linear motions. Finally, the total response is found by adding linear and nonlinear parts in the time domain, *i.e.*

$$\eta_{tot}(t) = \sum_{j=1}^{N} |H_{\eta\zeta}(\omega_{ej})| A_j \sin(\omega_{ej} t + \psi_j + \varepsilon_j) + \eta^{nl}(t) \text{ where } \omega_{ej} = \omega_j + \omega_j^2 \frac{U}{g} \tag{3.28}$$

3.6 Short Term Statistics

In the following four different probability density distributions used to describe the maxima are presented. The Rayleigh distribution is the exact distribution for a narrow banded process. The Rayleigh distribution is a special case of the Weibull distribution which has shown to be useful to describe processes which are nonlinear in nature. The Generalised Gamma distribution cover a wide range of distribution, including the ones mentioned here. Due to the large number of parameters the distribution is very flexible and care should be shown applying the distribution. Fig. 3.2 shows various probability functions for specific values of γ and m. In addition the Hermite distribution, Winterstein (1988), is described.

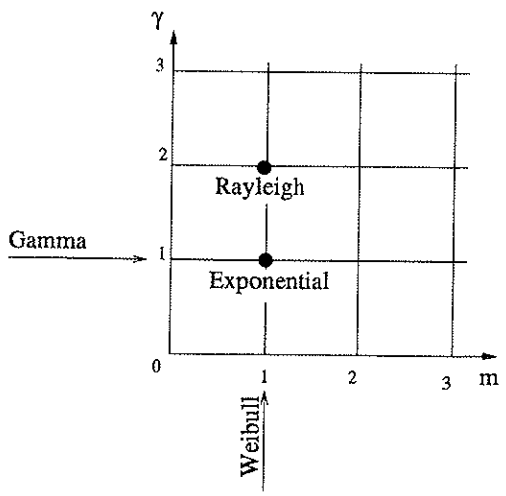

Figure 3.2: *Probability distributions for various values of the parameters m and γ of the generalised Gamma distribution.*

3.6.1 The Rayleigh Distribution

The Rayleigh probability density distribution is given as, Ochi (1990);

$$f_R(r) = \frac{2r}{M} \exp\left\{-\left(\frac{r^2}{M}\right)\right\} \quad r \geq 0 \; ; \; M > 0 \tag{3.29}$$

and the cumulative distribution is given as

$$F_R(r) = 1 - \exp\left\{-\left(\frac{r^2}{M}\right)\right\} \tag{3.30}$$

where

$$M = \begin{cases} 2\sigma_R^2 = 2m_0 & \text{for amplitude} \\ 8\sigma_R^2 = 8m_0 & \text{for height (crest-to-trough)} \end{cases} \tag{3.31}$$

where m_0 is the zeroth spectral moment.

The mean value and the standard deviation is given by

$$\mu_R = \frac{\sqrt{M\pi}}{2} \tag{3.32}$$

$$\sigma_R = \frac{\sqrt{M(4-\pi)}}{2} \tag{3.33}$$

3.6.2 The Weibull Distribution

The three parameter Weibull probability density distribution is given as, *e.g.* Ochi (1990);

$$f_R(r) = \frac{\gamma}{\beta}\left(\frac{r-\delta}{\beta}\right)^{\gamma-1} \exp^{\left[-\left(\frac{r-\delta}{\beta}\right)^{\gamma}\right]} \text{ where } \delta \leq r < \infty \tag{3.34}$$

and the cumulative as

$$F_R(r) = 1 - \exp^{\left[-\left(\frac{r-\delta}{\beta}\right)^{\gamma}\right]} \text{ where } \delta \leq r < \infty \tag{3.35}$$

where δ is the location parameter, β is the scale parameter and γ is the shape parameter. The Rayleigh distribution in Eq. 3.29 is a special case of the Weibull distribution, *i.e.* $\gamma = 2.0$, $\delta = 0.0$ and $\beta = \sqrt{M}$. β and γ are both positive values. The mean value and the standard deviation of R is given by

$$\mu_R = \delta + \beta\Gamma\left(1 + \frac{1}{\gamma}\right) \tag{3.36}$$

$$\sigma_R = \beta\sqrt{\Gamma\left(1 + \frac{2}{\gamma}\right) - \Gamma^2\left(1 + \frac{1}{\gamma}\right)} \tag{3.37}$$

3.6.3 The Generalised Gamma Distribution

The generalised Gamma probability distribution is given as, Ochi (1978);

$$f_R(r) = \frac{\gamma}{\Gamma(m)} \lambda^{\gamma m} r^{\gamma m - 1} \exp^{-(\lambda r)^\gamma} \quad 0 \leq r < \infty \tag{3.38}$$

where $\Gamma(m)$ is the gamma function, γ, m and λ are constants that may be estimated through certain moments of the histogram Stacy and Mihram (1965), or by weighted curve-fitting. The latter is advantageous, because $f_R(r)$ can be made much closer to the histogram in the important high-value region, by proper choice of the weighting function. The Rayleigh distribution represents a special case of Eq. 3.38 with $\gamma = 2$ and $m = 1$.

The cumulative distribution of $F_R(r)$ is obtained as the incomplete gamma function with argument $(\lambda r)^\gamma$, *i.e.*

$$F_R(r) = \int_0^r f_R(r) dr = \frac{1}{\Gamma(m)} \int_0^{(\lambda r)^\gamma} u^{m-1} \exp^{-u} du = \frac{\Gamma_{(\lambda r)^\gamma}(m)}{\Gamma(m)} \tag{3.39}$$

The n'th moment is given as, Ochi (1978);

$$m_n = \frac{1}{\lambda^n} \frac{\Gamma(m + \frac{n}{\gamma})}{\Gamma(m)} \tag{3.40}$$

The mean value and the standard deviation of R are given respectively as

$$\mu_R = m_1 \tag{3.41}$$

$$\sigma_R = \sqrt{m_2 - m_1^2} \tag{3.42}$$

3.6.4 The Hermite Distribution

Alternatively, one may adopt the approach suggested by Winterstein (1988) where the resulting process is replaced by an Hermite expansion of a standard Gaussian process, $U_0(t)$. The coefficients in the expansion are determined such that the lowest moments, *i.e.* the mean value, variance, skewness, and kurtosis, equal the target values.

Including the first four terms in the Hermite expansion, the transformation of the standard Gaussian process is given as

$$R_0(t) = \frac{R(t) - \mu_R}{\sigma_R} = g(U_0(t)) \tag{3.43}$$

where

$$R_0(t) = K[U_0(t) + h_3(U_0^2(t) - 1) + h_4(U_0^3(t) - 3U_0(t))] \tag{3.44}$$

and $R_0(t)$ is the normalised response, μ_R the mean value of the parent response $R(t)$ and σ_R is the standard deviation of $R(t)$. γ_{1R} and γ_{2R} is the skewness and kurtosis of the parent response respectively. The other parameters are given by, Winterstein (1988),

$$h_3 = \frac{\gamma_{1R}}{6(1+6h_4)} \tag{3.45}$$

$$h_4 = \frac{\sqrt{1+1.5(\gamma_{2R}-3)}-1}{18} \tag{3.46}$$

$$K = (1+2h_3^{-2}+6h_4^{-2})^{-0.5} \tag{3.47}$$

This approximation is valid for $\gamma_{2R} > 3$ and $h_3^2 < 3h_4(1-3h_4)$. Petersen (1992) presents an approach to find the exact values of the parameters. According to Sødahl (1991) the probability density distribution of the R-maxima can be expressed as

$$f_R(r) = \frac{1}{\sigma_R}\left[cu_0\Phi\left(\frac{cu_0}{\varepsilon}\right)\exp[-\frac{u_0^2}{2}] + \varepsilon\phi\left(\frac{u_0}{\varepsilon}\right)\right]\frac{du_0}{dr_0} \tag{3.48}$$

and the cumulative distribution is given as

$$F_R(r) = 1 - c\Phi\left(\frac{cu_0}{\varepsilon}\right)\exp[-\frac{u_0^2}{2}] - \Phi\left(-\frac{u_0}{\varepsilon}\right) \tag{3.49}$$

where

$$c = \sqrt{1-\varepsilon^2} \tag{3.50}$$

$$\frac{du_0}{dr_0} = \{K[1+2h_3u_0+3h_4(u_0^2-1)]\}^{-1} \tag{3.51}$$

where ε is the bandwidth of the R process.

If the response is narrow banded and Gaussian, the response is characterised by $\gamma_{1R} = 0.0$ and $\gamma_{2R} = 3.0$. Eq. 3.48 & 3.49 is then reduced to the Rayleigh probability density and cumulative distribution respectively.

The Hermite model has not been verified for nonlinear response in this work. However, it has been used in order to compare results from classical linear, longterm analysis result from using the IFORM-technique, Kumar and Winterstein (1997). This is shown in Sect. 5.2.3. A few comparisons of nonlinear longterm analysis are also given, see Sect. 5.4.5.

3.7 Extreme Value Statistics

The largest value of a random variable that is expected to occur during a period of time or a certain number of observations is called the extreme value. It is defined as

$$R_{max} = \max[R^1\ R^2....R^N] \tag{3.52}$$

Then, the extreme value distribution of the N independent and identically distributed maxima is given as

$$F_{R_{max}}(r) = [F_R(r)]^N \tag{3.53}$$

where N is the number of maxima and $F_R(r)$ is the initial distribution. The probability density distribution becomes

$$f_{R_{max}}(r) = \frac{d[F_R(r)]^N}{dr} = NF_R(r)^{(N-1)} f_R(r) \tag{3.54}$$

Depending on the tail behaviour of the distribution of maxima, the extreme distribution converges towards one of three asymptotic distribution. These were studied by Gumbel (1958) and systematized as Type I, II & III asymptotic distributions. The Type I asymptotic distribution is frequently used and arises from distributions with exponentially decaying tail. This is the case for the distributions mentioned in Sect. 3.6.

The Type I asymptotic distribution, called the Gumbel distribution, is given as *e.g.* Ochi (1990);

$$F_{R_{max}}(r) = \exp\{-\exp[-\alpha_N(r-\mu_N)]\} \text{ where } -\infty < r < \infty \tag{3.55}$$

where α_N is the scale parameter and μ_N the location parameter.

If the initial distribution of the maxima is known, Eq. 3.53 gives the exact extreme distribution of the N maxima. The initial distribution, $F_R(r)$, could be any of the distributions mentioned in Sect. 3.6. The choice will be dependent on the nature of the random process.

The Rayleigh Distribution

Let F_R be the Rayleigh distribution given as Eq. 3.29. The expected largest value, the probable extreme value (characteristic extreme value) and the design extreme value can be found in many textbooks, *e.g.* Ochi (1990);

$$E[R_{max}] = \sqrt{2m_0}\left\{\sqrt{\ln N} + \frac{0.2886}{\sqrt{\ln N}}\right\} \tag{3.56}$$

$$r_p = \sqrt{2m_0 \ln N} \tag{3.57}$$

$$r_{\alpha,design} = \sqrt{2m_0 \ln \frac{N}{\hat{\alpha}}} \text{ where } \hat{\alpha} = 1 - \alpha \tag{3.58}$$

where $r_{\alpha,design}$ is the extreme value corresponding to a probability of $\hat{\alpha}$ of being exceeded or a probability of α of being below. The probable extreme value is the value where the density function peaks and the expected extreme value is the "center of gravity" in the probability density distribution.

The Weibull Distribution

If the initial maxima distribution $P_R(r)$ is given by the Weibull distribution, Eq. 3.35, the expected largest value, the probable extreme value and design extreme value will be equal to, *i.e.* Ochi (1978), Farnes (1990);

$$E[R_{max}] = \delta + \beta \left\{ (\ln N)^{\frac{1}{\gamma}} + \frac{0.57722...(\ln n)^{\frac{1-\gamma}{\gamma}}}{\gamma} \right\} \tag{3.59}$$

$$r_p = \beta\{\ln(N)\}^{1/\gamma} + \delta \tag{3.60}$$

$$r_{\alpha,design} = \beta\{\ln(\frac{N}{\hat{\alpha}})\}^{1/\gamma} + \delta \tag{3.61}$$

The Generalized Gamma Distribution

The design extreme value, $r_{\alpha,design}$, for which the probability of being exceeded is a specified value, $\hat{\alpha} = (1 - \alpha)$, can be evaluated as the solution of the following equation, Ochi (1978),

$$\frac{\Gamma_{(\lambda r_{\alpha,design})^\gamma}(m)}{\Gamma(m)} = (1 - \hat{\alpha})^{1/N} \tag{3.62}$$

where n is the number of peaks. For a large number of peaks N and a small probability of being exceeded $\hat{\alpha}$ an asymptotic solution of Eq. 3.62 is obtained as

$$(\lambda r_{\alpha,design})^{\gamma(m-1)} \exp^{-(\lambda r_{\alpha,design})^\gamma} = \Gamma(m)\frac{\hat{\alpha}}{N} \tag{3.63}$$

Solving the above equation for $(\lambda r_{\alpha,design})^\gamma$ for given m, γ, λ and $\hat{\alpha}$ the desired extreme value $r_{\alpha,design}$ can be determined. The most probable extreme value can be found by solving

$$(\lambda r_p)^{\gamma(m-1)} \exp^{-(\lambda r_p)^\gamma} = \Gamma(m)\frac{1}{N} \tag{3.64}$$

3.8 Long Term Statistics

3.8.1 Long Term Response

In order to estimate the lifetime extreme value for ship response, a long term analysis has to be performed. The long term peak distribution of maxima is obtained by summation of short term probabilities of exceedance in all possible combinations of mean wave periods, significant wave heights, heading angles and speeds,

$$F_{LT}(r) = \int_{H_S}\int_{T_p}\int_{U}\int_{\beta} F_R(r|h,t,\beta,u) f_{H_s,T_p}(h,t) f(u,\beta|h,t) \bar{w}_{h,t,u,\beta} dh dt du d\beta \tag{3.65}$$

where β and U is the heading angle and forward speed respectively. $\bar{w}_{h,t,u,\beta}$ is a weighting factor which expresses the relative rate of response peaks within each sea state. $f(u,\beta|h,t)$ accounts for the effect of manoeuvring in heavy weather with respect to sailing speed and heading into

the waves. $f_{H_s,T_p}(h,t)$ is the long term joint probability distribution of significant wave height and peak periods. $F_R(r|h,t,\beta,u)$ is the short term cumulative probability distribution. If the response process is Gaussian the short term cumulative probability distribution may be described by the Rayleigh distribution, Eq. 3.30. If the process deviates too much from the Gaussian process, the Weibull distribution may be used, Eq. 3.34, and one should possibly use empirical expressions for the zero-up-crossing frequency of the process.

Assuming that the velocity and heading angle are independent variables, the long term distribution is given as

$$F_{LT}(r) = \int_{H_S}\int_{T_p}\int_{U}\int_{\beta} F_R(r|h,t,\beta,u) f_{H_s,T_p}(h,t) f(u|h,t) f(\beta|h,t) \bar{w}_{h,t,u,\beta} dh dt du d\beta \tag{3.66}$$

If the effect of peak period on heavy weather manoeuvring is negligible, Eq. 3.66 can be written as

$$F_{LT}(r) = \int_{H_S}\int_{T_p}\int_{U}\int_{\beta} F_R(r|h,t,\beta,u) f_{H_s,T_p}(h,t) f(u|h) f(\beta|h) \bar{w}_{h,t,u,\beta} dh dt du d\beta \tag{3.67}$$

The conditional distribution of speed and direction can further be simplified by assuming $f(\beta|h) = \delta(\beta_0)$ and $f(u|h) = \delta(c(h))$, where $\delta()$ is the Dirac delta function. The simplification means that only one heading is considered, and a deterministic relation between the significant wave height and the forward speed is assumed.

The probability of excedance, *i.e.* the probability that R will be larger than r, is given as

$$Q_{LT}(r) = 1 - F_{LT}(r) \tag{3.68}$$

If in addition only consider one forward speed is considered, *i.e.* $f(u|h) = \delta(u_0)$, Eq. 3.67 is reduced to

$$F_{LT}(r) = \int_{H_S}\int_{T_p} F_R(r|h,t,\beta_0,u_0) f_{H_s,T_p}(h,t) \bar{w}_{h,t,u,\beta} dh dt \tag{3.69}$$

The above equations may be discretized. Defining by a mesh of $k_{max} = no.of H_s$ by $j_{max} = no.of T_p$, see Fig. 3.3(a), Eq. 3.69 can approximated by

$$F_{LT}(r) = \sum_{k=1}^{k_{max}}\sum_{j=1}^{j_{max}} F_R(r|h_k,t_j,\beta_0,u_0) f_{H_s,T_p}(h_k,t_j) \bar{w}_{h_k,t_j,u,\beta} \Delta h \Delta t \tag{3.70}$$

where Δh and Δt are the grid size in the H_s and T_p ranges respectively. According to Fig. 3.3(b) Eq. 3.70 can further be rewritten as

$$F_{LT}(r) = \sum_{i=1}^{N_{si}} F_R(r|si,\beta_0,u_0) f_{H_s,T_p}(h_{si},t_{si}) \bar{w}_{h_{si},t_{si},u,\beta} \Delta h \Delta t \tag{3.71}$$

where N_{si} is the number of sea states, *i.e.* for a square mesh $N_{si} = k_{max} \times j_{max}$.

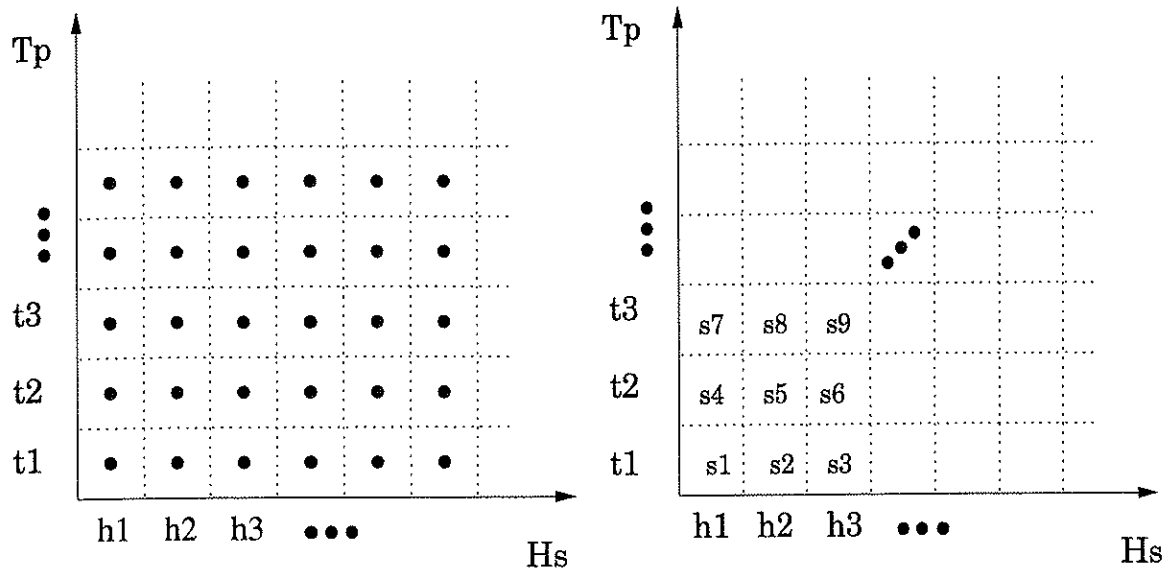

Figure 3.3: *Discretization of the scatter diagram into single sea states.*

The weight function which expresses the relative rate of response peaks in each sea state is defined by the zero-up-crossing wave period, T_z for the sea state si and the average zero-up-crossing wave period wave period, $\bar{T}_z$, as

$$\bar{\omega}_{si} = \frac{\bar{T}_z}{T_{z,si}} \tag{3.72}$$

The long term value r_D for a given return period of D years is given by

$$F_{LT}(r_D) = 1 - \frac{1}{N_D} \qquad \text{where } N_D = \frac{D \cdot 365 \cdot 24 \cdot 3600}{\bar{T}_z} \tag{3.73}$$

N_D is the number of peaks during D years.

The probability that the long term value R will be larger than r_D is given by

$$Q_{LT}(r_D) = 1 - F_{LT}(r_D) = \frac{1}{N_D} \tag{3.74}$$

where

$$1 - F_{LT}(r_D) = \sum_{i=1}^{N_{si}} Q_R(R > r_D | si, \beta_0, u_0) f_{H_s,T_p}(h_{si}, t_{si}) \bar{w}_{h_{si},t_{si},u,\beta} \Delta h_i \Delta t_i \tag{3.75}$$

The contribution to the probability of exceedance $Q_{LT}(r_D)$ from a sea state si is given as, *e.g.* Farnes and Passano (1989), Larsen and Passano (1990), Videiro (1998),

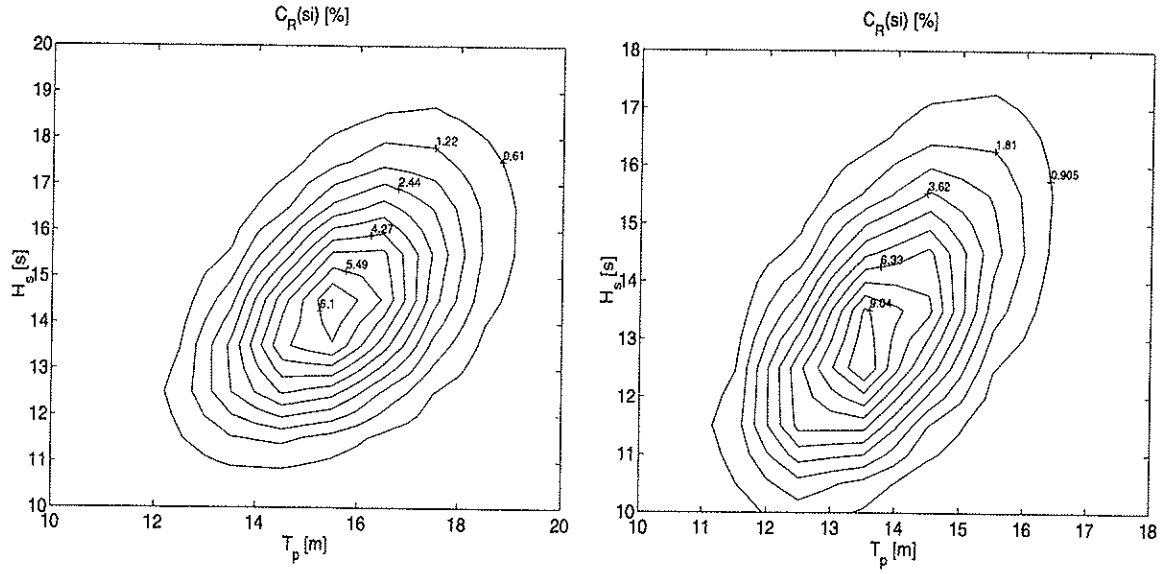

(a) (b)

Figure 3.4: *Contour plot of the coefficient of contribution,$C_R(si)$, for wave heights , Fig. 3.4(a), and vertical bending moment midship at Fn=0.275 for the S-175 container ship, Fig. 3.4(b), in the Northern North Sea.*

$$C_R(si) = \frac{Q_R(R > r_D|si, \beta_0, u_0) f_{H_s,T_p}(h_{si}, t_{si}) \bar{w}_{h_{si},t_{si},u,\beta}}{Q_{LT}(r_D)} \tag{3.76}$$

Fig. 3.4 presents a typical example of the contour curves of the coefficient of contribution, $C_R(si)$, for the long term response of wave heights and ship response in the Northern North Sea. As can seen, there is a limited area of the scatter diagram which contributes to the long term response. Most parts of the scatter diagram have $C_R(si)$-values close to zero. Keeping this in mind, the scatter diagram can be divided into two regions, *i.e.*

- a region $\tilde{s}$ which contributes to the long term response
- a region outside $\tilde{s}$ which does not contribute to the long term response

The contributing areas could be selected by choosing the areas where $C_R(si) > a$. Thus Eq. 3.75 can be rewritten as

$$Q_{LT}(r_D) = \sum_{i=1}^{N_{si}|C_R(si)>a} Q_R(R > r_D|si, \beta_0, u_0) f_{H_s,T_p}(h_{si}, t_{si}) \bar{w}_{h_{si},t_{si},u,\beta} \Delta h_i \Delta t_i + \sum_{others} \ldots \tag{3.77}$$

where $N_{si}|C_R(si) > a$ is the number of discrete, contributing sea states within $\tilde{s}$. The last term in Eq. 3.77 is approximately equal to zero, giving

$$Q_{LT}(r_D) = \sum_{i=1}^{N_{si}|C_R(si)>a} Q_R(R > r_D|si, \beta_0, u_0) f_{H_s,T_p}(h_{si}, t_{si}) \bar{w}_{h_{si},t_{si},u,\beta} \Delta h_i \Delta t_i \tag{3.78}$$

The weight function $\bar{w}_{h_{si},t_{si},u,\beta}$ has to be recalculated for the sea states within $\tilde{s}$ since the average zero-up-crossing wave period $\bar{T}_z$ is changed.

Eq. 3.78 will reduce computational cost when doing long term analysis for time domain simulations since only a limited number of simulations will be necessary to predict the long term response. Naturally, one will need to locate the contributing part of the scatter diagram. This can be done by using frequency domain analysis to establish $C_R(si)$-contours. The $C_R(si)$-coefficients might be used to locate important sea states, and further selected regions of the scatter diagram to be included in the nonlinear long term analysis. The contributing part for linear response will not necessarily coincide with the contributing part for nonlinear time domain simulations. However, it will give a good indication about its location.

Next, time domain simulations might be conducted in the selected areas of the scatter diagram. A suitable short term distribution, $Q_R(R > r|si, \beta_0, u_0)$, must be found and the corresponding statistical parameters must be estimated for the sea state, si.

In this work, the above mentioned procedure is applied. Linear frequency domain analysis will be used to establish the $C_R(si)$-values for the vertical bending moment midship. The most important sea states for the response can then be located. Next, nonlinear time domain analysis are conducted in chosen areas of the scatter diagram. The nonlinear long term response is thus found by solving Eq. 3.78, rewritten as

$$Q_{LT}(r_D) = \sum_{i=1}^{N_{si}|C_R(si)>a} Q_R(R > r_D|si, \beta_0, u_0) \frac{n_{si}}{n_{tot}} \tag{3.79}$$

where n_{si} is the number of peaks in sea state si. n_{tot} is the total number of peaks for all sea states, *i.e.* $n_{tot} = \sum_{i=1}^{N_{si}|C_R(si)>a} n_{si}$, within D years. Even if the computation time is reduced by using this method, it will still be rather time consuming since the number of sea states needed to predict the long term response within a certain accuracy is not known beforehand.

It can easily be shown for linear frequency domain response that the number of sea states needed to predict the long term response within an accuracy of 5%, is small as long as the sea state with max $C_R(si)$ is included. An example is presented in Fig. 3.5. Fig. 3.5(a) shows the $C_R(si)$-coefficient for the linear, vertical bending moment midship for the S-175 container ship obtained by conducting a complete long term analysis giving r_D^l where $D = 100$ years. Also shown are four smaller, selected areas of the scatter diagram named $A1$, $A2$, $A3$ and $A4$. $A1$ contains only one sea state, the one with max $C_R(si)$. Using this four small areas, the long term responses $r_{D,N_{si}}^l$ are obtained. The ratios $r_{D,N_{si}}^l/r_D^l$ versus the sum of the included $C_R(si)$-values in the original scatter diagram are shown in Fig. 3.5(b). In addition, several other ratios are shown. One may notice that by including only $A1$, the long term response is reduced by approximately 10% even if the $C_R(si)$-value for this sea state is only $9 - 10\%$. $A2$ which contains

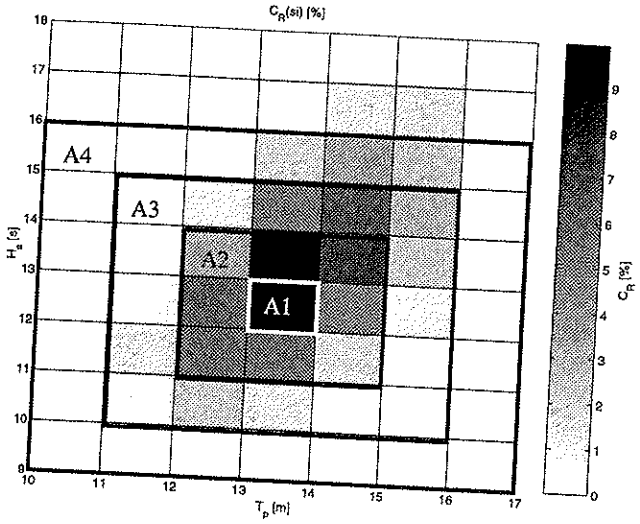

(a)

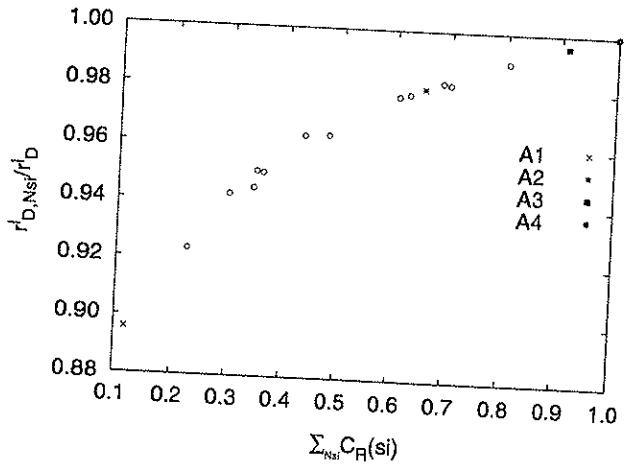

(b)

Figure 3.5: *Coefficient of contribution,$C_R(si)$, for vertical bending moment midship for the S-175 container ship at $Fn = 0.275$ in head sea waves at the top. Importance of different areas of the scatter digram at the bottom. Sea area is Northern North Sea. Return period $D = 100$ years.*

only 9 sea states, gives a reduction of 2%. 50% of the $C_R(si)$ will give a reduction of only 5%.

This observation is important, since it hints on that the number of sea states needed to get an estimate of the long term response is limited. This knowledge is applied in Sect. 5.4.

3.8.2 Long Term Wave Climate

The North Atlantic has often been used as a reference climatology for prediction of design values of wave induced load effects. For this area Walden (1967) and Hogben and Lumb (1967) collected data by visual observation and from passing ships respectively. Hogben et al. (1986) contains statistics of the ocean wave climate for the whole globe. An extensive amount of data is also collected in the vicinity of the numerous offshore installations along the Norwegian coast. These data will be applied in this work.

The long term wave climate can be described by the simultaneous probability distribution for the significant wave height, H_s, and the peak period, T_p, given as

$$f_{H_s,T_p}(h,t) = f_{H_s}(h) f_{T_p|H_s}(t|h) \tag{3.80}$$

The probability distribution function is estimated by fitting the probability distribution for the significant wave height, H_s, and the conditional distribution for the peak period, T_p, to observations separately. $f_{H_s}(h)$ is modelled by a log-normal distribution for $H_s \leq \eta$ and as a Weibull distribution for $H_s > \eta$, Haver (1980),

$$f_{H_s}(h) = \begin{cases} \frac{1}{\sqrt{2\pi}\sigma_{\ln H_s} h} \exp(-0.5\frac{(\ln h - \mu_{\ln H_s})^2}{\sigma^2_{\ln H_s}}) & ; h \leq \eta \\ \gamma \frac{h^{\gamma-1}}{\beta^\gamma} \exp(-(\frac{h}{\beta})^\gamma) & ; h > \eta \end{cases} \tag{3.81}$$

where $\mu_{\ln H_s}$ and $\sigma^2_{\ln H_s}$ are the mean and the variance of the of the variable $\ln H_s$ respectively. The parameters in the Weibull distribution are estimated by requiring continuity at $h = \eta$ for both $f_{H_s}(h)$ and $F_{H_s}(h)$. This requirement gives us two additional equations which can be solved to give us γ and β. The value of η is chosen in order to get an optimal fit. For the Northern North Sea the values are found to be $\eta = 3.27m$, $\mu_{\ln H_s} = 0.836$, $\sigma^2_{\ln H_s} = 0.376$, $\beta = 2.822$ and $\gamma = 1.547$, Haver and Nyhus (1986). The conditional distribution of the peak period , T_p, given H_s is given by the log-normal distribution is, Haver (1980),

$$f_{T_p|H_s}(t|h) = \frac{1}{\sqrt{2\pi}\sigma_{\ln T_p} t} \exp\left(-0.5\frac{(\ln t - \mu_{\ln T_p})^2}{\sigma^2_{\ln T_p}}\right) \tag{3.82}$$

where $\mu_{\ln T_p} = E[\ln T_p]$ and $\sigma^2_{\ln T_p} = Var[\ln T_p]$ are the mean value and variance respectively. The mean value and the variance are further fitted for each class of significant wave height which has a sufficient number of observations. These are again used to establish estimates for the most extreme sea states, see Haver and Nyhus (1986). The estimated mean value and variance are given below,

$$\mu_{\ln T_p} = a_1 + a_2 \ln(h + a_3) \tag{3.83}$$

or

$$\mu_{\ln T_p} = a_1 + a_2 h^{a_3} \tag{3.84}$$

and for all areas

$$\sigma^2_{\ln T_p} = b_1 + b_2 \exp(-b_3 h^{b_4}) \tag{3.85}$$

The conditional mean peak period is given as, Bury (1975)

$$T_p|H_s = \exp(\mu_{\ln T_p} + \frac{1}{2}\sigma^2_{\ln T_p}) \tag{3.86}$$

It is believed that the scatter diagram for the Northern North Sea is representative for a large group of sea areas. Data for different sea areas for the parameters in Eq. 3.81 - 3.85 are given in Table 3.1. The Troms I data in Andersen et al. (1987a) and Andersen et al. (1987b) has the Statfjord/Brent data. The Sleipner and Ekofisk zone II-VI data in Bjerke et al. (1991) and the Aasgard data can be found in Andersen et al. (1996). Data from Ekofisk are given Haver (1993). The simultaneous probability distribution, $f_{H_s,T_p}(h,t)$, for the Northern North Sea is presented in Fig. 3.6.

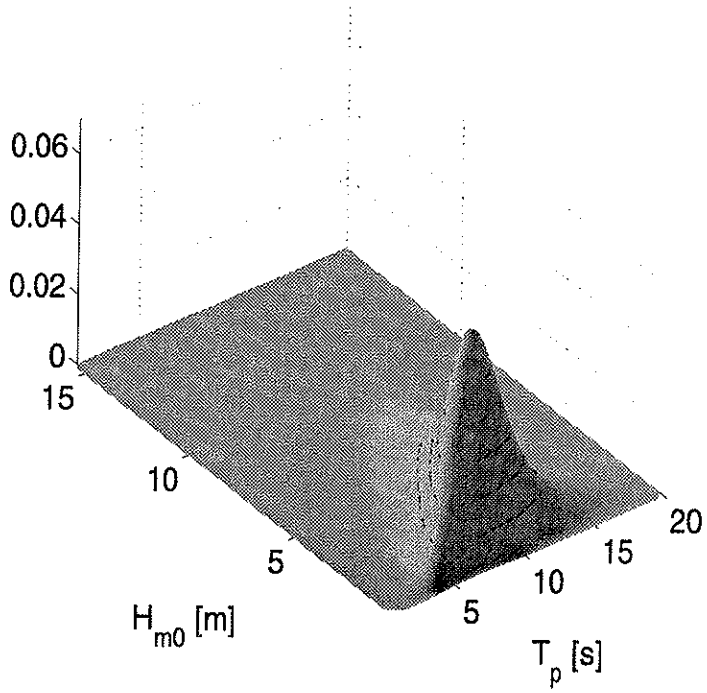

Figure 3.6: *The simultaneous probability distribution $f_{H_s,T_p}(h,t)$ for the Northern North Sea*

3.9 Operational Restrictions

A ship master will in general tend to avoid severe sea states and conditions by for instance reducing speed and change of heading, or a combination of the two. Actions will be based on for instance observation of waves and the ships response and will in general be a results of the ship masters experience.

Table 3.1: *Parameters in the description of the long term description of the wave climate.*

Area	γ	η	β	$\mu_{\ln H_s}$	$\sigma_{\ln H_s}$	a_1	a_2	a_3	b_1	b_2	b_3	b_4
Northern North Sea[a]	1.547	3.27	2.82	0.84	0.61	1.59	0.42	2.0	0.005	0.09	0.13	1.34
Aasgard	1.45	3.95	2.73	0.84	0.59	1.72	0.34	0.46	0.005	0.10	0.29	-
Sleipner	1.44	3.0	2.38	0.69	0.60	0.23	1.69	0.15	0.005	0.12	0.40	-
Troms I	1.36	4.25	2.26	0.72	0.56	1.35	0.61	0.34	0.005	0.12	0.36	-
Stafjord/Brent	1.55	3.27	2.82	0.84	0.61	0.40	1.59	0.15	0.005	0.12	0.34	-
Ekofisk	1.37	2.65	2.08	0.52	0.67	1.0	0.90	0.25	0.005	0.10	0.44	-
Ekofisk Zone II	1.37	2.7	2.12	0.54	0.67	0.03	1.81	0.15	0.005	0.16	0.58	-
Ekofisk Zone III	1.55	2.15	2.05	0.50	0.65	0.03	1.81	0.15	0.005	0.16	0.58	-
Ekofisk Zone IV	1.46	2.0	1.56	0.25	0.62	1.41	0.38	0.54	0.010	0.08	0.41	-
Ekofisk Zone VI	1.42	1.25	1.18	0.07	0.70	0.0	1.72	0.15	0.010	0.14	1.0	-

[a]Eq. 3.83 is used to caluculate the mean value μ.

In this work, the effect of voluntary speed loss and manoevring to avoid severe sea states will be studied. Voluntary speed loss means that the ship master reduces the speed due for instance to slamming, green water on deck and large vertical accelerations. The two former features will induce large loads on most ships. The slamming load affects the global load. Green water on deck will mainly induce large loads on the superstructure. The influence on the global loads are found to be minor. The reason is mainly that green water load is out of phase with the peak values of the bending moments, (Wang et al. 1998). The latter operability limitation will affect the ability to perform work effectively, NORDFORSK (1987).

The operability limiting boundaries are obtained from short term statistics combined with the sea keeping criteria. The limiting curves can be presented as envelope curves as a function of the limiting significant wave height, $H_s^{lim}(T_p)$, and the corresponding peak period, T_p.

The limiting significant wave height, is in the following defined by three chosen limiting sea keeping characteristics. An example of the limiting wave heights boundaries are shown in Fig. 3.7.

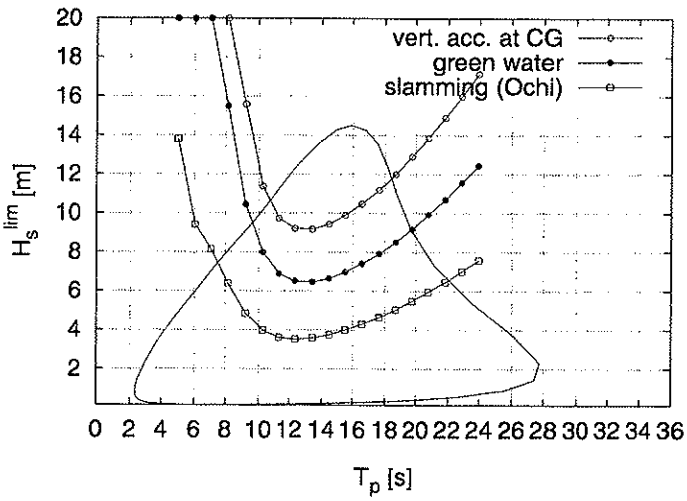

Figure 3.7: *Limiting operability limiting curves for the S-175 container ship at a forward speed of 22 knots, $Fn = 0.275$. The 100-year contour lines for the Northern North sea is shown by the continuous lines.*

3.9.1 Slamming

In Ochi (1964), where theoretical results are compared to experiments, the limiting significant wave height due to the slamming criteria is given as

$$H_s^{lim}(T_p) = \sqrt{-\frac{1}{2\ln P_{slam}}\left(\frac{d^2}{\sigma_r^2} + \frac{V_{crit}^2}{\sigma_{rv}^2}\right)} \tag{3.87}$$

where V_{crit} is the critical re-entry velocity, d, σ_r and σ_{rv} is the local draft, standard deviation of relative motion and velocity for a unit significant wave height respectively. P_{slam} is the probability of slam. According to Ochi (1964) a bottom impact is called a slam if the fore ship, *i.e.* at $0.15L_{pp}$ behind FP, emerges from water and the re-entry velocity at the station exceeds the critical value

$$V_{crit} = 0.093\sqrt{gL_{pp}} \tag{3.88}$$

If one is looking for the limiting significant wave height due to bow flare slamming, an option is to use a criteria based on a critical pressure, Faltinsen (1990). The probability of slam is defined as

$$P(impact\ pressure > p) = \exp\left[-\left(\frac{p}{\rho k \sigma_{rv}^2} + \frac{d^2}{2\sigma_r^2}\right)\right] \tag{3.89}$$

where k is the pressure coefficient which can for instance be found in Zhao et al. (1996). In addition it is necessary to define how large the pressure is at slamming. A possibility is to use a fraction of the hydrostatic pressure $\rho g d$. However, there is no clear answer to that problem.

NORDFORSK (1987) suggests that a probability of slam $P_{slam} = 0.03$ is suitable .

3.9.2 Green water on deck

The limiting significant wave height due to the green water on deck criteria is given as, Ochi (1964),

$$H_s^{lim}(T_p) = \frac{F}{g_r(T_p)\sqrt{-2\ln P_{gw}}} \tag{3.90}$$

where P_{gw} is the probability of green water on deck and $g_r(T_p)$ is the standard deviation of the relative vertical motion at a chosen position. F is the height of the free board. NORDFORSK (1987) suggests a permissible probability for green water of 7%.

3.9.3 Vertical Acceleration

The limiting significant wave height due to the acceleration criteria is given as, Fathi (1997),

$$H_s^{lim}(T_p) = \frac{\sigma_{\ddot{\eta}}^{lim}}{\sigma_{\ddot{\eta}}(Tp)} \tag{3.91}$$

where $\sigma_{\ddot{\eta}}^{lim}$ and $\sigma_{\ddot{\eta}}(tp)$ are the limiting vertical acceleration defined by the designer and standard deviation of the vertical acceleration for a unit wave height respectively. In NORDFORSK (1987) values for $\sigma_{\ddot{\eta}}^{lim}$ are suggested allowing for different levels of activity. For instance $\sigma_{\ddot{\eta}}^{lim} = 0.15$ at the bridge is suggested for merchant ships. This will allow for heavy manual work.

3.9.4 Effect of Operability Restrictions on Long Term Responses

Wave induced loads, being sensitive to the relative heading of the ship and the forward speed, will be affected by the manoevring in heavy seas. Furthermore, the long term responses are highly influenced by the large sea states. Thus, it will be important to account for this effect in the prediction of the extreme values of the wave induced loads.

The effect of manoevring may be taken directly into account into the long term analysis. For a given condition, *i.e.* heading and forward speed, the the operability criteria must be checked. If the criteria is not fulfilled, the condition must be changed until the criteria is met. If this is not possible, one may assume that the situation does not occur at all or occurs with a certain probability. Finally, the long term distribution must be found.

Alternatively, simplified methods may be used to study the effect of manoevring on long term extreme values. The effect of voluntary speed loss might be studied by creating velocity and heading profiles based on the limiting sea keeping criteria. Looking at Fig. 3.7 it is clear that the profiles are functions of the sea state parameters, H_s and T_p. In addition, the velocity and heading profiles are burdened with some randomness, *i.e.* the operability criteria for a given sea state is met with a certain probability partly depending on the ship master attitude. If there exist instructions on board regarding the sea keeping, one would expect that the operability criteria would be met with a larger probability than if no such instructions exist and manoevring is performed according to the ship master interpretation of the severity of the sea state and ship response.

The profiles can be modelled as functions of both the significant wave height and the peak period. A somewhat simplified approach is to assume that the profiles are independent of the peak period, *i.e.* the limiting significant wave height is constant and taken as the minimum value along the limiting operability curve, see Fig. 3.7. Smooth surfaces and "staircase" profiles may be used to describe the speed and heading variation as H_s and T_p changes. Both a smoothed and staircase profile are applied in Ch. 6 to study the effect of varying forward speed on estimation of the long term extreme values.

Inclusion of the operability limitation into the long term analysis, implies that the probability distributions $f(u|h,t)$ and $f(\beta|h,t)$ must be established if the profiles are functions of the two sea state parameters. Accordingly, the distributions $f(u|h)$ and $f(\beta|h)$ must be established if the profiles are independent on the peak period. Naturally one may assume that there is a deterministic relation between the sea state parameters and the forward speed and heading, as commented on page 40. In Ch. 6 the relation between the significant wave height and forward speed is modelled as deterministic and stochastic.

Heavy weather may also be avoided by

- Keep the vessel anchored in the harbor until the weather has calmed down
- Manoeuvre the vessel into calmer sea areas

The former can for instance be taken into account in the long term analysis by a slightly modification of Eq. 3.66. That is the operational restrictions will give the upper limit of the significant wave height to be used in the analysis. That is

$$F_{LT}(r) = \int_{H_s}^{H_s^{lim}(T_p)} \int_{T_p} \int_U \int_\beta F_R(r|h,t,\beta,u) f_{H_s,T_p}(h,t) f(u|h,t) f(\beta|h,t) \bar{w}_{h,t,u,\beta} dh dt du d\beta \quad (3.92)$$

$H_s^{lim}(T_p)$ is the limiting significant wave height given by the operability limiting boundaries. Alternatively, the limiting significant wave height can taken as the minimum value along the limiting operability curve, see Fig. 3.7. Since only parts of the scatter diagram is included in the analysis the other part corresponds to the time spent in the harbour. However, if the ship master instead manoeuvre into calmer seas, this may be modelled by using a scatter diagram representing this situation or by modifying an existing scatter diagram. That is

$$F_{LT}(r) = \int_{H_s} \int_{T_p} \int_U \int_\beta F_R(r|h,t,\beta,u) \hat{f}_{H_s,T_p}(h,t) f(u|h,t) f(\beta|h,t) \bar{w}_{h,t,u,\beta} dh dt du d\beta \quad (3.93)$$

where $\hat{f}_{H_s,T_p}$ is the scatter diagram accounting for operability restrictions. This will be studied in Ch. 7 where three different modification of the scatter diagram is presented.

Chapter 4

Uncertainty Analysis

4.1 Introduction

Prediction of wave induced loads and motions is an important part of the design process. Estimated design loads shall ensure that structural safety is obtained, both regarding safety for crew, environment and property. Such requirements encourage the designer to choose conservative design loads. On the other hand, too conservative design may be so expensive that the vessel is no longer economically feasible.

In order to obtain optimal design, it is important to quantify and account for the uncertainties related to the design process. Sources of error contributing to the uncertainty in loads are for instance

- wave data (scatter diagram and spectral shape uncertainty)
- model accuracy and weight distribution
- theoretical limitations
- ship operation

(21th ITTC 1996) presents a review of studies on uncertainty analysis for physical model testing and validation of numerical sea keeping methods. Soares has presented a large extent of work regarding uncertainty analysis. In one of his earliest work, Soares (1984), he studied the model uncertainty of standard methods for prediction the wave induced loads both in connection with long- and short term statistics. In Kaplan et al. (1984) different uncertainties associated with ship longitudinal strength and loading are reviewed. Uncertainties in stress analysis of marine structures are studied in Nikolaides and Kaplan (1991). Faltinsen and Svensen (1990) studied the uncertainty, among other topics, in linear strip theory. They concentrated on heave and

pitch ship motions. The effect on long term response due to uncertainty in the wave climate modelling is studied in Soares and Moan (1991), Soares and Trovão (1991), while the effect of transfer function uncertainty on short term ship responses are discussed in Soares (1991). The uncertainty involved in modelling the directionality in waves are discussed in Soares (1995). Schellin et al. (1996) studied the uncertainty of existing theoretical models by comparing two dimensional and three dimensional theories.

In this work the uncertainty regarding the theoretical model will be studied. In addition, the effect of the wave spectrum on the theoretical uncertainty is also touched on. This will be referred to as *model uncertainty* in the following chapters. The aim with uncertainty analysis, is that the estimated design load should represent the real world. Information about the uncertainty of the theoretical model is needed in reliability analysis. In addition, detection of systematic errors may imply weakness of the theoretical method and be basis for improvement of the theoretical model. The model uncertainty gives a measure on the difference between the *true* and the predicted loads expressed as

$$\text{model uncertainty} = \frac{\text{true value}}{\text{predicted value}} \tag{4.1}$$

A convenient way to assess the uncertainty of the transfer function is by calculating the corresponding long term distributions and quantifying the uncertainty on the characteristic values, Soares and Trovão (1991), if sufficiently data is available. A possibility is to compare true and predicted response in regular waves. The model error will be a stochastic variable describing the uncertainty in a specific theoretical model. The model error can be described by its probability density distribution. In general, the available information about the model error is limited and the distribution can not be established. A possibility is to present the model by its mean value, μ with standard deviation σ. In this work these two parameters will be used to describe the model error. The values parameters are quantified Sect. 4.5.1 and 4.6.2 as an estimate of the uncertainty in the linear, long term extreme value and the uncertainty in nonlinear response in regular waves.

If the model uncertainty is estimated by using a *wave-by-wave* approach, the estimated, true probability distribution is not necessarily completely correct, Haver (1995), Jonathan and Taylor (1996). A method which can be used in order to get correct the predicted probability density distribution are given in Winterstein and Sweetman (1999). However, a large amount of data is needed for these analysis. In general, this is not the case and simplifications must be done to estimate the uncertainty in the design loads.

In this work, the uncertainty in linear- and a quasi-nonlinear strip theory, Ch. 2, will be studied, but first of all theoretical limitations will be briefly discussed.

4.2 Theoretical Limitations

The validity of strip theory is previously discussed in Ch. 2. The nonlinear theory applied herein, will of course have some of the defects as in the linear strip theory. Therefore, most of the men-

tioned defects of the linear strip theory, will also be limitations for the nonlinear formulation. However, one would expect smaller uncertainties, relative to physical reality, when nonlinear theory is applied since nonlinear effects due the waves are taken into account as slamming and modification of the Froude-Krylov force and the hydrostatics. However, different nonlinear theoretical models exist and there is uncertainty connected to the modelling of nonlinear effects.

It is known that the strip theory is not valid for low frequencies, Salvesen et al. (1970). This is due to that the added mass and damping are not correctly predicted at low frequencies, see Sect. 2.3, which again is resulting in incorrect radiation forces. However, at low frequencies the vertical motions and loads are dominated by the hydrostatics, meaning that the errors in the added mass and damping should not influence the final result. Therefore, one should not expect to get more uncertain results in following and quartering sea than in head and bow seas when dealing with vertical loads and motions. In addition transom stern effects are not taken into account and the behaviour of the fluid aft of the ship is therefore neglected. However, for the vessels applied in this study only one has transom stern and it is located above the free surface. It is therefore expected that the transom stern effect is not large.

The theories applied herein do not include the steady state contribution, *i.e.* the component caused by a moving ship in still water. The steady state component may give hogging or sagging moment depending on the hull form, Ueno and Watanabe (1987). As a result, caution should be taken when experimental and simulated results are compared. However, in a private conversation Wang (1999) states that the steady state contribution to the vertical bending moment midship is in the range of $5 \sim 10\%$ for the ITTC container ship S-175.

The assumption of linear and small waves of the strip theory, implies that the responses are proportional to wave height and that the there is no difference in value between hogging and sagging moments. Generally, nonlinear effects results in difference between sagging and hogging response. Experiments described in Korbijn (1992) indicate that there is a difference between sagging and hogging response for the reefer vessel vessel. The same experimental data are used in order to compare a three dimensional theory and the simplified nonlinear theory, NV1418, Børresen and Tellsgård (1980), with experimental data, Kring et al. (1996). Jensen and Pedersen (1979) presented nonlinear calculations on the SL-7 container ship. Also here, a clear difference was found between sagging and hogging. Fig. 4.1 shows the transfer function for the midship bending moment for the tanker at $Fn = 0.13$ and in head sea waves. The experimental data points for maximum response in regular waves at increasing wave height are also included. They are presented as response value divided on the regular wave amplitude. If the response was linear, these data points would coincide in the figure. The observed scatter is probably due to nonlinearity in the response and randomness in the experimental data. In addition, one may notice that for this particular vessel it seems that the nonlinearity reduces both sagging and hogging response.

A section which causes a large change in water area as the ship is moving is likely to give nonlinear effects. This is for sections in the bow and stern. If the stern is flared or the stern is transom or very shallow, nonlinearities will occur. Some examples of hull forms can be seen on Fig. F.1 in Appendix F. One would expect that ships with a small block coefficient will be exposed to

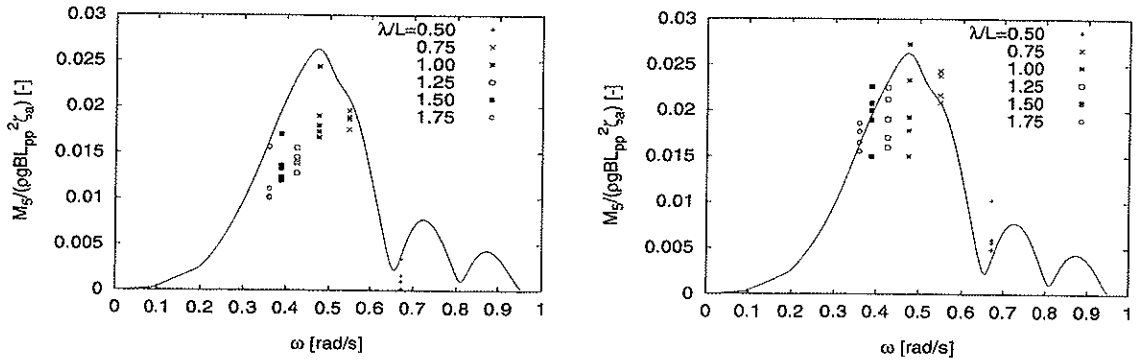

(a) Sagging

(b) Hogging

Figure 4.1: *Predicted transfer function for the vertical bending moment midship for the tanker at* $Fn = 0.13$ *in head sea (continuous line). Experimental response data in regular waves for different wave lengths,* λ/L_{pp}*, and wave heights are also included.*

more nonlinearity than ships with a large block coefficients. This is because the non vertical ship sides are more accentuated for small coefficients. Since wave induced structural loads are obtained by integration over a portion of the ship hull, nonlinearities due to the end sections play a much more important role than in the predictions of the ship motions, *e.g.* Fujino and Yoon (1986).

As mentioned earlier, the linearity assumption requires vertical ship sides. The nonlinear code uses a momentum von Karman solution in order to estimate the slamming force, von Kármán and Wattendorf (1929). This means that the pile-up of water is not taken into account. A comparison of the Wagner, Wagner (1932), which take pile-up into account, and the von Karman solution for a cylinder shows that the slamming coefficient is twice as large when the pile up is considered, Faltinsen (1990). Zhao et al. (1996) states that the von Karman and conservation of momentum gives too low maximum force and thus the time history of the force will be underestimated.

In addition, there will be three dimensional slamming effects which are not taken into account by the simplified nonlinear strip theory. The three dimensional effects will reduce the slamming force, Zhao et al. (1996). Other effects which tend to reduce the slamming force is the possible presence of air bubbles. However, this will probably not be a problem in the bow as the bow section would not trap the air. It could be a problem at aft if there is a transom stern with a rather flat bottom.

The nonlinear effect due to green water is taken into account in a simplified manner. When the wave elevation exceeds the main deck, the extra force due to green water is equal the hydrostatic pressure of a water column equal to the breadth of the ship and the exceeding wave height. The water formation when the wave elevation exceeds the main deck might look dif-

ferently, *i.e.* flow separation. Wang et al. (1998) presents an improved method to include the green water on deck. However, their results showed that for the S-175 container ship with rigid hull, the the inclusion of the green water load seems to have a negligible effect on the global loads.

The slamming force has the same value both for water entry and exit. It always acts upward regardless of the direction of motion. In the nonlinear code, the force due to slamming is set equal to zero at water exit according to general agreement. In reality, the force at water exit is not zero and will probably contribute to the loads. The water exit problem is little studied. The water exit problem for a cylinder was studied in Greenhow and Lin (1983) where some experimental results are presented. Comparisons of experiments and numerical results are given in Greenhow (1988).

Yet, it is hard to say whether the deviation between measured and predicted data are due to errors during the measuring of data or if the physical assumptions in the theory are wrong. It is most likely that the deviations are due to many factors and combination of these.

4.3 Modelling of Transfer Function Uncertainty

The aim is to randomise the model error of linear strip theory based on the ratio between the true and predicted long term extreme values. In order to that, the transfer function uncertainty must be modelled.

The model error of the transfer function can either be expressed by the ratio or difference between the measured and calculated transfer function. The former can be written as

$$\hat{H}(\omega) = \phi(\omega)H(\omega) \tag{4.2}$$

and the latter as

$$\hat{H}(\omega) = H(\omega) + \bar{\phi}(\omega) \tag{4.3}$$

where $\hat{H}(\omega)$ represents the measured transfer function. $H(\omega)$ is the calculated transfer function. $\phi(\omega)$ and $\bar{\phi}(\omega)$ represent the different modelling errors. In Soares (1984) the former formulation is used in the assessment of uncertainty for the midship bending moment. Faltinsen and Svensen (1990) used the latter formulation on order to to study the uncertainty in heave and pitch transfer functions. In this work both formulation will be tested.

The drawback of using the difference between the measured and predicted value, is that the model error is not dimensionless. This is of inconvenient, if one wish to generate a general formulation to be used on other ships. Eq. 4.3 can be rewritten to a dimensionless form as;

$$\hat{H}(\omega) = H(\omega) + \bar{\phi}(\omega) = H(\omega)\left(1 + \frac{\bar{\phi}(\omega)}{H(\omega)}\right) \tag{4.4}$$

Rewriting the above expression even more, gives

$$\hat{H}(\omega) = H(\omega)(1 + \phi^{'}(\omega)) = H(\omega)\phi^{''}(\omega) \tag{4.5}$$

where $\phi^{'}(\omega) = \frac{\bar{\phi}(\omega)}{H(\omega)}$ and $\phi^{''}(\omega) = 1 + \phi^{'}(\omega)$. This is the common way to express dimensionless model error. The above expression can be utilised keeping in mind that the basis for the modelling error is the difference between the experimental and predicted data as in Eq. 4.3. In the following, no distinction will be made between $\bar{\phi}(\omega)$ and $\phi^{"}(\omega)$. It will be clear from the context which formulation that is applied.

Herein, the discrete values of the model error was obtained by using the following procedure

- Predict transfer function by using the relevant theory, $H(\omega)$
- Find the ratio or difference between experimental value $\hat{H}(\omega_i)$ versus $H(w_i)$ at ω_i for $i = 1, .., n$ giving $\phi(\omega_i)$ and $\bar{\phi}(\omega_i)$, *i.e.*
  - $\phi(\omega_i) = \frac{\hat{H}(\omega_i)}{H(\omega_i)}$
  - $\bar{\phi}(\omega_i) = \hat{H}(\omega_i) - H(\omega_i)$
- This discrete data sets, $[\phi(\omega_1), \phi(\omega_2), .., \phi(\omega_n)]$ and $[\bar{\phi}(\omega_1), \bar{\phi}(\omega_2), .., \bar{\phi}(\omega_n)]$, will be used to find a functional form of the model errors, $\phi(\omega)$ and $\bar{\phi}(\omega)$

4.3.1 Polynomial Representation of Model Error

The most general representation of the model error can be given as

$$\phi(\omega) = \sum_{i=0}^{n} a_i \omega^i = a_0 + a_1\omega + a_2\omega^2 + ... + a_n\omega^n \tag{4.6}$$

The simplest formulation of the model error is obtained is $n = 0$ which means that $\phi(\omega)$ is set equal to a constant value, *i.e.* independent of ω. Soares (1984) defined the model error $\phi(\omega)$ as given by Eq. 4.2. The function $\phi(\omega)$ can be of the general form

$$\phi(\omega) = a + b\omega + c\omega^2 \tag{4.7}$$

In Soares (1984) the model error is given as a constant value, *i.e.* $\phi(\omega) = a$. The value of a can be estimated by means of the method of least mean square values, giving

$$\hat{a} = \frac{\sum_i \hat{H}_i H_i}{\sum_i H_i^2} \tag{4.8}$$

where $\hat{H}_i$ and H_i is the experimental and simulated response value at frequency i. This implies that the uncertainty at frequencies which are not relevant for maximum response, may have a large influence on the model error.

A disadvantage of setting $\phi(\omega) = a$ is that it is difficult to provide an adequate description of the measured transfer function, $\hat{H}(\omega)$, in cases where the experimental data deviate from

simulated results in peak frequency of the transfer function. On the other hand, it is rather easy to generate a frequency independent model valid for a range of speeds, headings and block coefficients using regression analysis. A model error which is a function of the above mentioned variables can be written as, Soares (1984);

$$\phi(\theta, U, C_b) = a(\theta, U, C_b) = A\theta + BU + CC_b + D \tag{4.9}$$

where θ is the heading angle, U the forward speed and C_b is the block coefficient. A, B, C and D are constants.

The accuracy of the model error will be improved by introducing additional frequency dependent terms. A linear model is obtained if $n = 1$ and a quadratic model is created when $n = 2$ and so on. The improved accuracy is dependent on the number of data points available and of course the method used to fit the model error, $\phi(w)$. Of course, the parameters, $a_0, a_1, ..., a_n$, can be estimated by using the least square method as applied in Eq. 4.8. Larger number of parameters will on the other hand demand increasing size of the data sets to get reliable estimates. Unfortunately, the experimental data sets are in general not that comprehensive. However, one may circumvent the problem with lack of data points. By using another fitting procedure, a frequency dependent polynomial representation of the model error may be established. This can be done by using splines.

4.3.2 Spline Representation of Model Error

In order to study the influence of the frequency on the modelling error, $\phi(\omega)$ and $\bar{\phi}(\omega)$, splines were chosen in this work. The advantage is that only a limited number of experimental data is needed to establish the modelling error. As mentioned above, it is rather difficult to establish a model error based on regression analysis, but using splines one is able to take into account the frequency dependence. For more details, see Appendix C.

One of the disadvantages with the spline representation may turn up when data points are located very close to each other. This may cause radically changes in the value of $\phi(\omega)$ and $\bar{\phi}(\omega)$ from one point to another because the derivative, $d\phi(\omega)/dx$ and $d\bar{\phi}(\omega)/dx$, is so large. This problem can be solved by substituting a group of data points in a small region by a single data point prior to the curve fitting. This is done by calculating the average value of the n measured transfer function points, $\hat{H}(\omega_i)$, as

$$\bar{\hat{H}}(\bar{\omega}) = \frac{1}{n}\sum_{i=1}^{n}\hat{H}(\omega_i) \text{ where } \bar{\omega} = \frac{1}{n}\sum_{i=1}^{n}\omega_i \tag{4.10}$$

The problem is caused by random measurement error. This was in particular a problem for the model error, $\phi(\omega)$, defined by the ratio between the measured and predicted value given by Eq. 4.2, and when cubic splines were used in order to fit a function through the points. In order to circumvent the problem, the modelling error was also fitted by using linear splines for both formulations of the model error.

The procedure was as follows

- Fit the function $\phi(w)$ and $\bar{\phi}(\omega_i)$ using linear or cubic splines to the the data sets $[\phi(\omega_1), \phi(\omega_2), .., \phi(\omega_n)]$ and $[\bar{\phi}(\omega_1), \bar{\phi}(\omega_2), .., \bar{\phi}(\omega_n)]$ respectively
- The value of $\phi(w)$ and $\bar{\phi}(w)$ can now be calculated at arbitrary point along the interval $[\omega_1, ..., \omega_n]$

Using the procedure above, gives totally four different combinations by using Eq. 4.2 - 4.3 for linear and cubic splines.

4.4 Uncertainty in the Long Term Response

Long term characteristic values may be found for both the measured, $\hat{H}(\omega)$, and predicted, $H(\omega)$, transfer functions by using the appropriate spectral moment in the Rayleigh distribution, *i.e.* $\hat{m}_n$ and m_n respectively. Assuming that the waves are long-crested, it is only necessary to change $H(\omega)$ with $\hat{H}(\omega)$ in Eq. 3.24 and modify the equation to represent long crested waves. The result is

$$\hat{m}_n = \int_0^\infty |\omega_e|^n |\hat{H}(\omega)|^2 S_\zeta(\omega) d\omega \tag{4.11}$$

where ω is the wave frequency and ω_e is the frequency of encounter.Using this spectral moment in the Rayleigh distribution, Eq. 3.29, it is easy to calculate the long term characteristic values by using Eq. 3.69.

The uncertainty in the long term extreme vale can be quantified by the ratio between the long term extreme value estimated using $\hat{H}(\omega)$ and $H(\omega)$ respectively.

4.4.1 Influence of the Return Period

Characteristic load effects for design of marine structures are typically referred to return periods of 100, 50 or 20 years. Classification Societies refer to the probability level 10^{-8}, normally meant to correspond to an operating life of 20 years in the North Atlantic. The effects of speed reduction due to heavy weather are allowed for and a uniform probability is normally assumed for the occurrence of different ship to wave headings, DNV (1995). On the other hand, for offshore structures in *e.g.* Norway and US the reference period is 100 years, while 50 years is used in UK.

To study the effect of return period, the 100, 50 and 20 year characteristic values were calculated using Eq. 3.69. Since only the linear response is considered, the Rayleigh distribution was assumed to be suitable to describe the short term probability in a single sea state. The needed spectral moments were found by calculation of the response spectrum using both the predicted transfer function and the corrected transfer function, *w.r.t.* model data as mentioned above. Thereafter, the response moments were found according to Eq. 3.24 modified to long crested waves. The number of response peaks can easily be found by using standard equations, Eq. 3.14.

In the further context, the scatter diagram for the Northern North Sea will be applied in the calculations. The smoothing of the scatter diagram is described in Sect. 3.8.2. Both the Pierson

Moskowitz and the Jonswap spectra are applied.

To identify the response amplitude r_D^l, the following equation is solved by iteration.

$$Q_{LT}(R > r_D^l) = \frac{1}{N_D} \tag{4.12}$$

where N_D is the number of response zero-up-crossings during D-years in all sea states. The superscript l indicates linear response, see Sect. 3.8.1.

The D-years long term extreme values are established for both predicted, $H(\omega)$, and measured transfer functions, $\hat{H}(\omega)$, *i.e.* r_D^l and $\hat{r}_D^l$ respectively. The relative value of the D-year value of the wave induced bending moment obtained by the corrected transfer function normalised by the respective value of the uncorrected transfer function, is given as

$$\psi_D = \frac{\hat{r}_D^l}{r_D^l} \tag{4.13}$$

This number will indicate the uncertainty in the D-year response using linear strip theory. While the the ratios of r_{100}^l to r_{50}^l and r_{100}^l to r_{20}^l are approximately 0.96 and 0.92, see Appendix E, the difference between the uncertainty in the D-year value is not sensitive to the return period. That is, for all practical purposes

$$\psi_{100} \approx \psi_{50} \approx \psi_{20} \tag{4.14}$$

See Table 4.1 - 4.4 where these values were calculated for 100, 50 and 20 years return periods giving ψ_{100}, ψ_{50} and ψ_{20} for ITTC ship S-175 at six different headings. The results are presented as the ratios $\frac{\psi_{50}}{\psi_{100}}$ and $\frac{\psi_{20}}{\psi_{100}}$. Both the Pierson Moskowitz and the Jonswap spectrum, with peakedness parameter as given in Eq. 3.10, are used in the analysis. This ship was chosen since it has been the object of comprehensive study for many years. The data used in this study was provided by several institutions to the ITTC in order to identify differences in the various strip theories and computer programs, 15th & 16th ITTC Seakeeping Committee (1983). The contributing institutions were Nippon Kokan Co., Ltd., Sumitomo Heavy Industries and Ship Research Institute, indicated by NKK, SHI and SRI respectively. The hull form is shown in Appendix F and the mass distribution is reproduced from 15th & 16th ITTC Seakeeping Committee (1983) in Appendix G.

As can be seen, the tables are not complete as the numerical correction fail to work in some parts of the transfer function. In some cases the model error based on Eq. 4.2 and cubic splines is highly oscillating. In other cases the model error based on Eq. 4.3 causes negative transfer function values at lower and upper bound frequencies. How to deal with this matter will be discussed in Sect. 4.4.2.

In what follows, the 100-year return period will be applied in order to quantify the transfer function uncertainty.

Table 4.1: *The ratio of the relative values ψ_{50} and ψ_{100} for the S-175 container ship, $Fn = 0.275$. The Pierson Mosckowitz spectrum is used in the analysis.*

Heading	0		30		60	120	150		180	
	SHI	SRI	SHI	SRI	SRI	SRI	SHI	SRI	SHI	NKK
$H(\omega)$	1.0	1.0	1.0	1.0	1.0	1.0	1.0	1.0	1.0	1.0
$H(\omega)\phi_{cubic}(\omega)$	1.002	–	1.001	0.999	1.0	1.0	0.999	0.999	1.0	0.998
$H(\omega) + \bar{\phi}(\omega)_{cubic}$	1.002	–	1.001	–	0.997	0.999	–	–	–	–
$H(\omega)\phi(\omega)_{linear}$	1.002	–	1.001	1.0	1.0	0.999	1.0	0.999	1.0	0.998
$H(\omega) + \bar{\phi}(\omega)_{linear}$	1.002	–	1.001	–	0.999	0.999	–	–	–	–
$H(\omega)\frac{\sum_i \hat{H}_i H_i}{\sum_i H_i^2}$	1.0	1.0	1.0	1.0	1.0	1.0	1.0	1.0	1.0	1.0

Table 4.2: *The ratio of the relative values ψ_{20} and ψ_{100} for the S-175 container ship, $Fn = 0.275$. The Pierson Mosckowitz spectrum is used in the analysis.*

Heading	0		30		60	120	150		180	
	SHI	SRI	SHI	SRI	SRI	SRI	SHI	SRI	SHI	NKK
$H(\omega)$	1.0	1.0	1.0	1.0	1.0	1.0	1.0	1.0	1.0	1.0
$H(\omega)\phi_{cubic}(\omega)$	1.004	–	1.002	0.999	0.999	0.999	0.997	0.996	0.999	0.996
$H(\omega) + \bar{\phi}(\omega)_{cubic}$	1.003	–	1.001	–	0.994	0.999	–	–	–	–
$H(\omega)\phi(\omega)_{linear}$	1.003	–	1.001	1.0	0.999	0.999	1.0	0.997	0.999	0.996
$H(\omega) + \bar{\phi}(\omega)_{linear}$	1.003	–	1.0	–	0.997	0.999	–	–	–	–
$H(\omega)\frac{\sum_i \hat{H}_i H_i}{\sum_i H_i^2}$	1.0	1.0	1.0	1.0	1.0	1.0	1.0	1.0	1.0	1.0

Table 4.3: *The ratio of the relative values ψ_{50} and ψ_{100} for the S-175 container ship, $Fn = 0.275$. The Jonswap spectrum is used in the analysis.*

Heading	0		30		60	120	150		180	
	SHI	SRI	SHI	SRI	SRI	SRI	SHI	SRI	SHI	NKK
$H(\omega)$	1.0	1.0	1.0	1.0	1.0	1.0	1.0	1.0	1.0	1.0
$H(\omega)\phi_{cubic}(\omega)$	1.003	–	1.001	1.001	1.001	1.001	0.996	0.997	1.0	0.998
$H(\omega) + \bar{\phi}(\omega)_{cubic}$	1.002	–	1.002	–	0.998	1.002	–	–	–	–
$H(\omega)\phi(\omega)_{linear}$	1.002	–	1.001	1.0	1.002	1.002	0.997	0.997	1.0	0.998
$H(\omega) + \bar{\phi}(\omega)_{linear}$	1.001	–	1.001	–	1.002	1.002	–	–	–	–
$H(\omega)\frac{\sum_i \hat{H}_i H_i}{\sum_i H_i^2}$	1.0	1.0	1.0	1.0	1.0	1.0	1.0	1.0	1.0	1.0

Table 4.4: *The ratio of the relative values ψ_{20} and ψ_{100} for the S-175 container ship, $Fn = 0.275$. The Jonswap spectrum is used in the analysis.*

Heading	0		30		60	120	150		180	
	SHI	SRI	SHI	SRI	SRI	SRI	SHI	SRI	SHI	NKK
$H(\omega)$	1.0	1.0	1.0	1.0	1.0	1.0	1.0	1.0	1.0	1.0
$H(\omega)\phi_{cubic}(\omega)$	1.007	–	1.002	1.001	1.003	1.005	0.996	0.993	0.999	0.995
$H(\omega) + \bar{\phi}(\omega)_{cubic}$	1.004	–	1.002	–	0.995	1.006	–	–	–	–
$H(\omega)\phi(\omega)_{linear}$	1.004	–	1.002	1.001	1.004	1.006	0.997	0.994	0.999	0.995
$H(\omega) + \bar{\phi}(\omega)_{linear}$	1.003	–	1.002	–	1.004	1.005	–	–	–	–
$H(\omega)\frac{\sum_i \hat{H}_i Y_i}{\sum_i H_i^2}$	1.0	1.0	1.0	1.0	1.0	1.0	1.0	1.0	1.0	1.0

4.4.2 Sensitivity Analysis

As mentioned in Sect. 4.3.2, many types of curve fittings have been tried in order to model the uncertainty of the transfer function. The final choice should be based on accuracy and simplicity. It was found that the frequency dependent error modelled using Eq. 4.2, *i.e.* the ratio between experimental and predicted values of the transfer function, when the complete frequency range was applied was not well behaved. The random nature of the experimental data caused large oscillations in areas where the ratio between neighboring experimental and predicted data were distinct in value. This was not only a problem at low or high frequencies, but it also occasionally happened at frequencies close to the dominant peak of the transfer function.

The most well behaved modelling error was based on the difference between the measured and predicted transfer function value, Eq. 4.3. Cubic splines were used to fit the curve. The reason why cubic splines are preferred to linear splines is that the corrected transfer function, $\hat{H}(\omega)$, and modelling error, $\bar{\phi}(\omega)$, in general looks smoother using the cubic splines. However, at low and high frequencies negative values of the corrected transfer function, $\hat{H}(\omega)$ occurred. Fortunately, this can be dealt with in an easy manner. Since mainly area close to the peak value of the transfer function will contribute to characteristic values, a simplified approach may be used to model the part of the transfer function which contains less energy. Some areas might in fact be skipped completely as the contribution is rather small and in most cases negligible. This will be shown later in this section.

An example on the above mentioned problems are presented in Fig. 4.2. The figure illustrates the transfer function of vertical bending moment midship for the S-175 container ship at $Fn = 0.275$, and the effect of using the different ways to model the transfer function uncertainty. It clearly indicates that the model error based on relative error causes large oscillations. The model error based on Eq. 4.3 causes negative values of the transfer function.

Unfortunately, it is not possible to generate a simple formulation of the uncertainty in the transfer function using splines. The optimal solution to the problem would of course be some kind of black box solution similar to the constant model error used by Soares (1984). However, it is

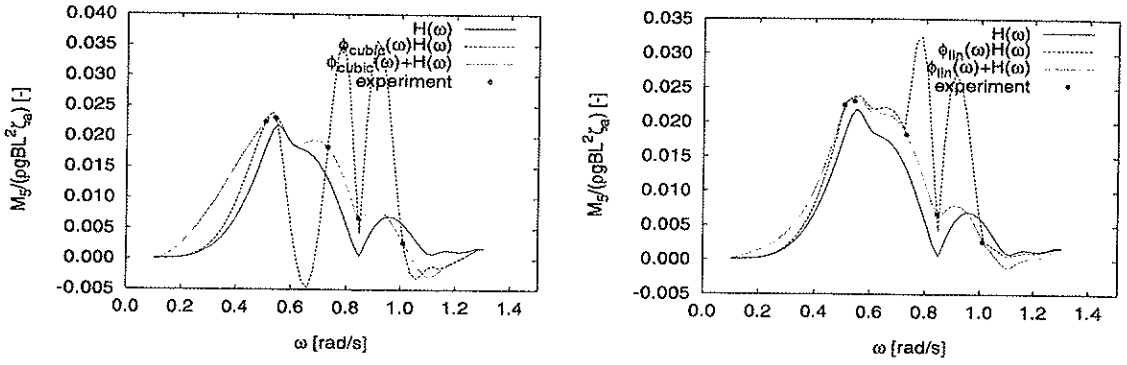

(a) (b)

Figure 4.2: *Transfer functions for the vertical bending moment midship for the S-175 ship at head sea with Fn = 0.275. The different model errors are illustrated. Experimental data from SRI, 15th & 16th ITTC Seakeeping Committee (1983).*

not possible to model a frequency dependent error using regression analysis unless the number of experimental data points is rather large. In this work, the most adequate and simple formulation was found to be the dimensionless error based on the difference between the experimental and predicted values of the transfer function given as $\phi^{"}(\omega) = 1 + \frac{\tilde{\phi}(\omega)}{H(\omega)}$. The model error of the transfer function will be used to quantify the uncertainty in the long term extreme values. Finally, the model uncertainty may be randomised by the uncertainty in the long term extreme value, ψ_{100}. That is, the uncertainty is given as a mean value with a standard deviation, μ, see Sect. 4.5.1.

In order to verify the importance of the different frequency areas of the transfer function, the 100-year value for the vertical bending moment midship was calculated for the ITTC ship S-175, see 15th & 16th ITTC Seakeeping Committee (1983). The transfer function was predicted by using linear, strip theory and the resulting transfer functions are shown in Fig. 4.3. The transfer function is plotted against $\alpha = \frac{\lambda}{L_{pp}\cos\beta}$. That is the expression is the ratio between the decomposed wave- and the ship length, where β is the heading angle and λ is the wave length. One would therefore expect, that the peak value of the transfer function would be close to $\alpha = 1.0$ since this corresponds to a decomposed wave length equal to the ship length, L_{pp}.

To study the influence of the frequency areas, the transfer functions were modified in the sense that the areas above $\alpha = 1.5, 2.0, 3.0, 4.0, 5.0$ and 6.0 were removed, see Fig. 4.4. Further, the 100-year value for using both non modified and modified transfer function was calculated to see when the r^l_{100} "converged".

The results are presented in Fig. 4.5, showing the error, *i.e.* change in the r^l_{100} value due to the removal of frequency areas, as a function of the heading angle.

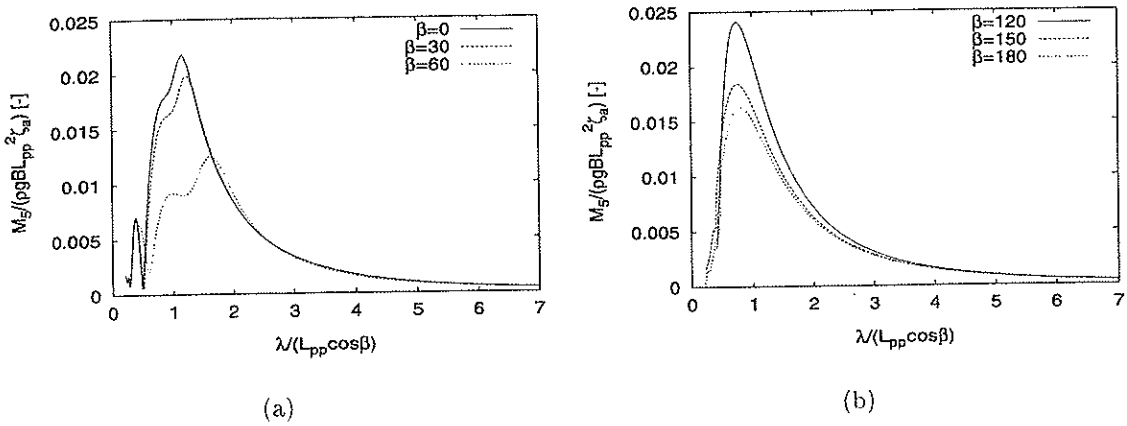

Figure 4.3: *Transfer function for the vertical bending moment midship for the S-175 ship.* $Fn = 0.275$.

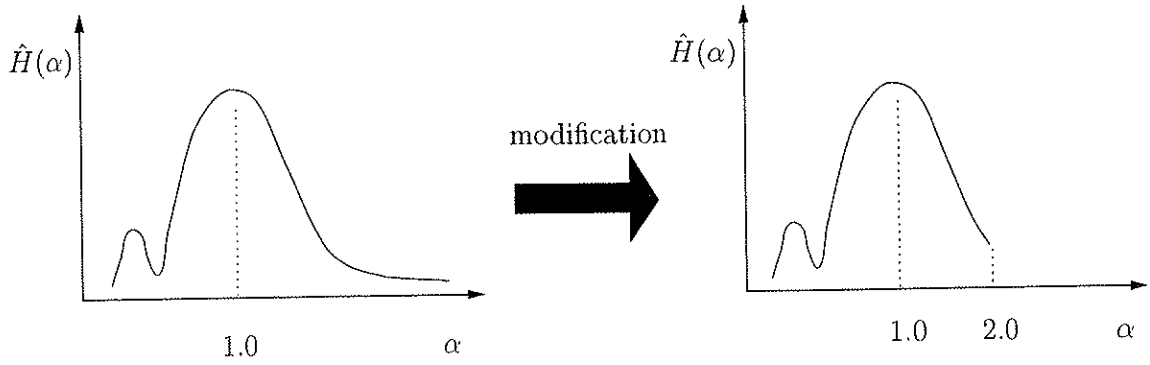

Figure 4.4: *Illustration of the modification of the transfer function by removing areas above* $\alpha = \frac{\lambda}{L_{pp}\cos\beta} = 2.0$

In addition, part of $H(\omega)$ below the cancellation frequency was removed, see illustration in Fig. 4.6. These smaller peaks are caused by ship wave interaction, and the contribution to the 100-year value is rather small. However, if the response is hydroelastic these peaks may contribute to fatigue and the removal of these frequency areas may not be justified. The limit of α is not fixed, as the value changes from transfer function to transfer function. For the S-175 container ship the cancellation frequency is located at $\alpha \approx 0.5$. The results are given in Table 4.5, where the error indicates the change in the 100-year value for the vertical bending moment midship when only the "main" peak is kept. Only three headings, namely 0, 30, and 60, are included as the headings 120, 150 and 180, did not have any prominent cancellation frequency in the frequency range included.

Fig. 4.5 shows that the alteration in the r^l_{100} value decreases as the α-value increases. Another

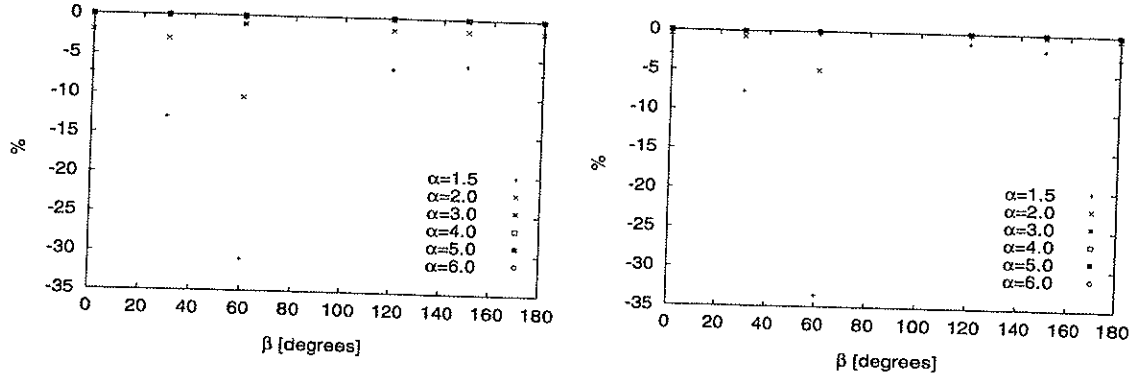

(a) Pierson Moskowitz

(b) Jonswap

Figure 4.5: *The error due to change in the 100-year value, r^{l}_{100}, by removing the frequency areas above α. Vertical bending moment midship for the S-175 ship. $Fn = 0.275$.*

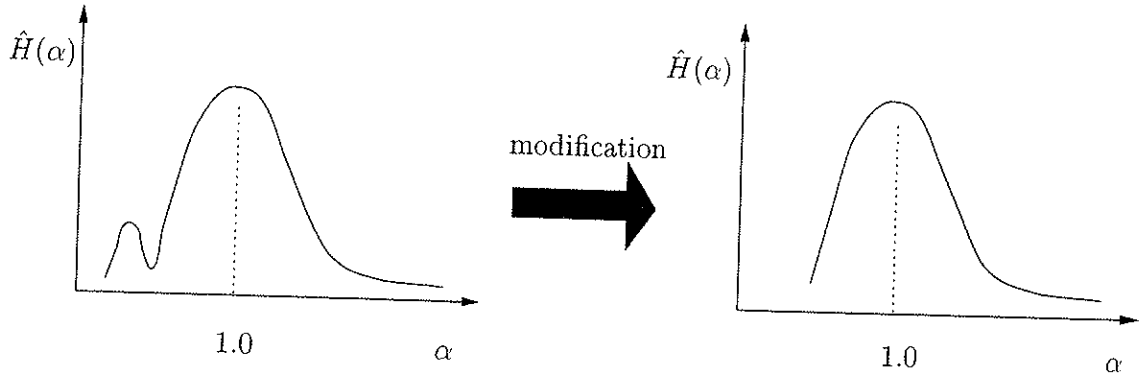

Figure 4.6: *Illustration of the modification of the transfer function by removing areas below the cancellation frequency.*

Table 4.5: *Percentage change in the 100 year vertical bending moment mid ship on the S-175 ship due to removal of frequencies below the cancellation, see Fig. 4.6*

Heading	Pierson Moskowitz [%]	Jonswap [%]
0	−0.49	−0.29
30	−0.55	−0.33
60	−0.81	−0.46

feature for both spectra, is that by skipping the area above $\alpha = 3.0$ the 100-year value is changed by less than 2.5%. Compared to the uncertainties in experimental data, this error is negligible. This result indicates that frequencies above $\alpha = 3.0$ is less important in the calculation of long term extremes for the vertical bending moment midship. The explanation is that, the sea states which are most influent on the 100-year value are concentrated in the vicinity of $\alpha = 1.0$

where the transfer function has it maximum value. Therefore, as long the energy content of the response spectra, *i.e.* $S(\omega)H(w)^2$, is maintained to a certain degree, the 100-year value will have a minimal change in value. The same explanation is, of course valid for the removal of the peaks below the dominant peak of the transfer function, *i.e.* below $\alpha \approx 0.5$.

4.4.3 Hundred Year Values and Sensitivity to Sea States Based on Linear Theory

In order to find the 100 year value, $\hat{r}^l_{100}$, for the fitted transfer function, $\hat{H}(\omega)$, of the vertical bending moment midship, the method presented in the preceding section, Sect. 4.4.2, was employed. Calculations were conducted on five different ship, namely the container ships SL-7 and S-175, a reefer vessel and two cargo ship the Wolverine State and the California Bear, where the latter belongs to the Mariner class. The Mariners are represented with two load distributions, which is indicated as full and light load for the Wolverine State and eastbound and westbound route for the California Bear. The eastbound route has the smallest displacement. Geometrical data, mass distribution and experimental data can be found in Gie (1972), 15th & 16th ITTC Seakeeping Committee (1983), (Korbijn 1992), Chicco and Numata (1969) and Numata and Yonkers (1969). The hull forms are shown in Appendix F and the mass distribution are reproduced in Appendix G. An overview over the applied transfer functions is given in Appendix H.

The procedure was as follows

- Predict transfer functions using linear, strip theory, $H(\omega)$
- Digitalize experimental data points
- Calculate the error $\bar{\phi}(\omega_i) = \hat{H}(\omega_i) - H(\omega_i)$ $i = 1..n$
- Use cubic splines to fit $\bar{\phi}(\omega)$ to the data points $[\bar{\phi}(\omega_1), \bar{\phi}(\omega_2), .., \bar{\phi}(\omega_n)]$
- Calculate the dimensionless model error $\phi''(\omega)$ and find the corrected transfer function $\hat{H}(\omega)$
- Remove high and low frequency region according to Sect. 4.4.2.
- Calculate the 100-year value for the smoothed, extended and measured transfer function giving $\hat{r}^l_{100}$

The results are presented in Table 4.6 - 4.15. Both the Pierson Moskowitz and the Jonswap spectrum is used in the analysis. The peakedness parameter in the Jonswap spectrum is given by Eq. 3.10. Scatter diagram from the Northern North Sea is applied in all analysis, see Sect. 3.8.2.

The relative heading between ship and waves is probably the most important factor with respect to wave induced loads. The estimated 100-year value of the vertical bending moment reaches its maximum at head to bow seas, increasing in magnitude towards head sea. This can be seen in the Table 4.6 - 4.15, where the 100-year measured vertical bending moments are presented. The vertical bending moment is less sensitive to increase in speed, but a slight increase with speed

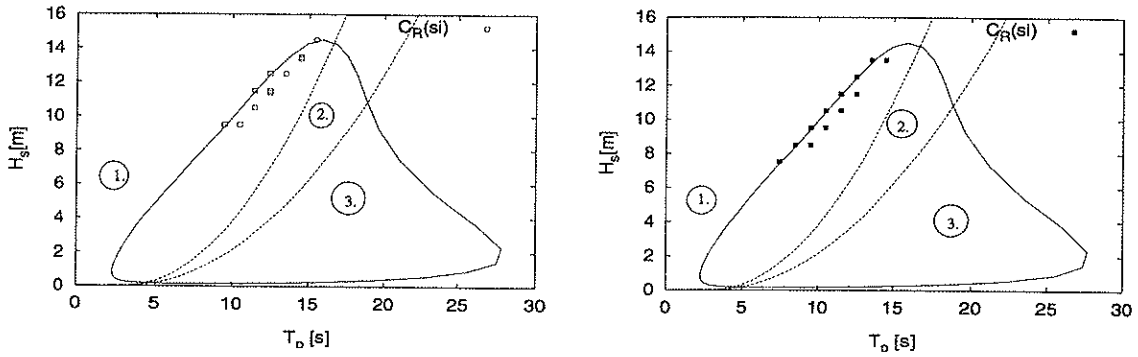

(a) Pierson Moskowitz

(b) Jonswap

Figure 4.7: *100-year contour line of the Northern North Sea and the locality of the maximum coefficient of contribution,* $\max C_R(si)$*, indicated by the dots.*

is detected, see Table 4.6 - 4.8.

In addition to the 100-year values, $\hat{r}^l_{100}$, also the most important sea state is presented. By most important sea state is meant the individual sea state, $si = (H_s, T_p)_i$, which has the largest coefficient of contribution, *i.e.* $\max C_R(si)_i$, see Sect. 3.8.

One may notice that maximum $C_R(si)$-values occur at $H_s \sim 8 - 14$m and with peak periods where the corresponding wave length is approximately equal to the ship length. This indicates that only sea states surrounding $si = (H_s, T_p)_i$ are necessary to consider when estimating $\hat{r}^l_{100}$ by long term statistics. It also explains why removal of high and low frequencies in the transfer functions $\hat{H}(\omega)$, see Sect. 4.4.2, have only minor effect on the 100-year value.

As mentioned in Sect. 3.3, the scatter diagram may be divided into three different regions. Part 1 and 3 consist of windsea and swell, while part 2 is purely windsea dominated. Part 2 can be modelled by a onepeaked spectrum like Jonswap or Pierson Moskowitz which is applied in this work. The borders between the three zones, Torsethaugen (1987), are shown in Fig. 4.7 together with the coefficient of contribution which and the 100-year contour line in the Northern North Sea. The coefficient of contribution may give an indication on which spectrum should be used, *i.e.* one- or twopeaked spectrum. Even if the figure indicates that the two peaked spectrum should be used, a one peaked spectrum will give conservative results for the responses studied in this work and is therefore applied herein.

The $\max C_R(si)$ using the Jonswap spectrum is larger than the corresponding value using the Pierson Moskowitz spectrum in most cases. This could indicate that fewer sea states are necessary to estimate the r^l_{100}-value using Jonswap spectrum. Use of the coefficient of contribution in long term analysis will be studied in more in Sect. 5.4.5.

Table 4.6: *100 year characteristic values, $\hat{r}^l_{100}$, for the vertical bending moment midship for the SL-7 container ship. All $\hat{r}^l_{100}$ are made dimensionless w.r.t. $L^3_{pp}B\rho g$. $Fn = 0.220$.*

	Pierson Moskowitz				Jonswap			
		Most Important Sea State				Most Important Sea State		
Heading	$\hat{r}^l_{100}[10^3]$	H_s	T_p	C_R [%]	$\hat{r}^l_{100}[10^3]$	H_s	T_p	C_R [%]
0	1.111	14.5	15.5	8.25	1.118	13.5	13.5	10.87
45	0.904	12.5	13.5	9.58	0.944	12.5	12.5	15.87

Table 4.7: *100 year characteristic values, $\hat{r}^l_{100}$, for the vertical bending moment midship for the SL-7 container ship. All $\hat{r}^l_{100}$ are made dimensionless w.r.t. $L^3_{pp}B\rho g$. $Fn = 0.245$.*

	Pierson Moskowitz				Jonswap			
		Most Important Sea State				Most Important Sea State		
Heading	$\hat{r}^l_{100}[10^3]$	H_s	T_p	C_R [%]	$\hat{r}^l_{100}[10^3]$	H_s	T_p	C_R [%]
0	1.152	14.5	15.5	8.22	1.211	13.5	13.5	10.62
25	1.059	13.5	14.5	8.86	1.111	13.5	13.5	11.34
45	0.944	12.5	13.5	9.44	0.989	12.5	12.5	17.89
65	0.656	11.5	12.5	9.84	0.648	10.5	11.5	20.79
115	0.574	11.5	12.5	9.05	0.544	8.5	9.5	12.97
135	0.730	12.5	13.5	9.36	0.748	11.5	12.5	8.10
155	0.822	13.5	14.5	9.63	0.922	12.5	12.5	16.00

Table 4.8: *100 year characteristic values, $\hat{r}^l_{100}$, for the vertical bending moment midship for the SL-7 container ship. All $\hat{r}^l_{100}$ are made dimensionless w.r.t. $L^3_{pp}B\rho g$. $Fn = 0.270$.*

	Pierson Moskowitz				Jonswap			
		Most Important Sea State				Most Important Sea State		
Heading	$\hat{r}^l_{100}[10^3]$	H_s	T_p	C_R [%]	$\hat{r}^l_{100}[10^3]$	H_s	T_p	C_R [%]
0	1.196	13.5	14.5	8.30	1.278	13.5	13.5	11.97
45	1.033	12.5	13.5	9.31	1.089	12.5	12.5	20.23

Table 4.9: *100 year characteristic values, $\hat{r}^l_{100}$, for the vertical bending moment midship for the S-175 container ship. All $\hat{r}^l_{100}$ are made dimensionless w.r.t. $L^3_{pp}B\rho g$. $Fn = 0.275$.*

Heading		Pierson Moskowitz				Jonswap			
			Most Important Sea State				Most Important Sea State		
		$\hat{r}^l_{100}[10^3]$	H_s	T_p	C_R [%]	$\hat{r}^l_{100}[10^3]$	H_s	T_p	C_R [%]
0	SHI	1.131	12.5	13.5	9.14	1.154	10.5	11.5	18.69
	SRI	1.480	13.5	14.5	8.85	1.571	13.5	13.5	9.32
30	SHI	1.057	11.5	12.5	9.60	1.097	10.5	11.5	22.90
	SRI	1.366	12.5	13.5	8.23	1.377	11.5	11.5	10.33
60	SRI	1.069	13.5	14.5	7.42	1.040	13.5	14.5	8.52
120	SRI	0.777	10.5	11.5	8.83	0.726	8.5	8.5	17.72
150	SHI	0.880	12.5	13.5	9.41	0.903	9.5	9.5	14.36
	SRI	0.954	13.5	14.5	8.40	0.966	11.5	12.5	8.34
180	SHI	0.657	12.5	13.5	9.74	0.669	11.5	12.5	11.23
	NKK	0.846	12.5	13.5	8.30	0.874	11.5	12.5	12.69

Table 4.10: *100 year characteristic values, $\hat{r}^l_{100}$, for the vertical bending moment midship for the reefer vessel. All $\hat{r}^l_{100}$ are made dimensionless w.r.t. $L^3_{pp}B\rho g$. $Fn = 0.0$.*

Heading		Pierson Moskowitz				Jonswap			
			Most Important Sea State				Most Important Sea State		
		$\hat{r}^l_{100}[10^3]$	H_s	T_p	C_R [%]	$\hat{r}^l_{100}[10^3]$	H_s	T_p	C_R [%]
0	fore	0.763	11.5	12.5	10.53	0.802	9.5	10.5	22.89
	aft	0.809	11.5	12.5	10.65	0.829	9.5	10.5	20.87

Table 4.11: *100 year characteristic values, $\hat{r}^l_{100}$, for the vertical bending moment midship for the reefer vessel. All $\hat{r}^l_{100}$ are made dimensionless w.r.t. $L^3_{pp}B\rho g$. $Fn = 0.145$.*

Heading		Pierson Moskowitz				Jonswap			
			Most Important Sea State				Most Important Sea State		
		$\hat{r}^l_{100}[10^3]$	H_s	T_p	C_R [%]	$\hat{r}^l_{100}[10^3]$	H_s	T_p	C_R [%]
0	fore	0.919	11.5	12.5	9.41	0.950	10.5	11.5	15.13
	aft	0.988	11.5	12.5	9.82	1.031	9.5	10.5	17.77

Table 4.12: *100 year characteristic values, $\hat{r}^l_{100}$, for the vertical bending moment midship for the cargo ship Wolverine State, full loading condition. All $\hat{r}^l_{100}$ are made dimensionless w.r.t. $L^3_{pp}B\rho g$. $Fn = 0.214$.*

	Pierson Moskowitz				Jonswap			
		Most Important Sea State				Most Important Sea State		
Heading	$\hat{r}^l_{100}[10^3]$	H_s	T_p	C_R [%]	$\hat{r}^l_{100}[10^3]$	H_s	T_p	C_R [%]
0	1.138	12.5	13.5	9.18	1.177	10.5	11.5	20.94
30	1.001	11.5	12.5	10.21	1.078	9.5	10.5	31.96
60	0.642	11.5	11.5	10.55	0.655	8.5	9.5	33.93
120	0.820	9.5	9.5	12.30	0.774	7.5	7.5	26.23
150	0.893	11.5	12.5	10.14	0.906	8.5	9.5	19.75
180	0.807	12.5	13.5	8.98	0.807	10.5	11.5	10.99

Table 4.13: *100 year characteristic values, $\hat{r}^l_{100}$, for the vertical bending moment midship for the cargo ship Wolverine State, light loading condition. All $\hat{r}^l_{100}$ are made dimensionless w.r.t. $L^3_{pp}B\rho g$. $Fn = 0.214$.*

	Pierson Moskowitz				Jonswap			
		Most Important Sea State				Most Important Sea State		
Heading	$\hat{r}^l_{100}[10^3]$	H_s	T_p	C_R [%]	$\hat{r}^l_{100}[10^3]$	H_s	T_p	C_R [%]
0	1.171	11.5	11.5	10.04	1.243	9.5	10.5	19.79
30	1.025	11.5	11.5	10.89	1.052	9.5	9.5	26.40
60	0.622	9.5	9.5	14.34	0.628	7.5	7.5	30.28
120	0.549	9.5	9.5	12.63	0.522	7.5	7.5	31.22
150	0.893	11.5	12.5	10.14	0.906	8.5	9.5	19.75
180	0.787	10.5	11.5	10.46	0.787	9.5	10.5	17.77

Table 4.14: *100 year characteristic values, $\hat{r}^l_{100}$, for the vertical bending moment midship for the Mariner Class cargo ship California Bear, westbound loading condition. All $\hat{r}^l_{100}$ are made dimensionless w.r.t. $L^3_{pp}B\rho g$. $Fn = 0.258$.*

	Pierson Moskowitz				Jonswap			
		Most Important Sea State				Most Important Sea State		
Heading	$\hat{r}^l_{100}[10^3]$	H_s	T_p	C_R [%]	$\hat{r}^l_{100}[10^3]$	H_s	T_p	C_R [%]
0	1.088	12.5	12.5	8.98	1.094	10.5	10.5	15.44
30	1.032	11.5	12.5	10.24	1.063	9.5	10.5	25.06
60	0.758	9.5	9.5	11.43	0.709	8.5	8.5	22.79
120	0.752	9.5	9.5	11.00	0.709	7.5	7.5	30.17
150	0.945	11.5	12.5	10.90	0.963	9.5	10.5	20.30
180	0.864	11.5	12.5	10.02	0.895	9.5	10.5	25.01

Table 4.15: *100 year characteristic values, $\hat{r}^l_{100}$, for the vertical bending moment midship for the Mariner Class cargo ship California Bear, eastbound loading condition. All $\hat{r}^l_{100}$ are made dimensionless by $L^3_{pp}B\rho g$. $Fn = 0.258$.*

	Pierson Moskowitz				Jonswap			
		Most Important Sea State				Most Important Sea State		
Heading	$\hat{r}^l_{100}[10^3]$	H_s	T_p	C_R [%]	$\hat{r}^l_{100}[10^3]$	H_s	T_p	C_R [%]
0	0.951	11.5	12.5	10.06	0.970	9.5	10.5	20.48
30	0.839	11.5	11.5	10.40	0.870	9.5	9.5	18.63
60	0.609	9.5	9.5	13.48	0.597	7.5	7.5	34.17
120	0.646	9.5	10.5	11.00	0.622	7.5	7.5	25.07
150	0.783	11.5	12.5	10.65	0.796	9.5	10.5	20.11
180	0.702	11.5	12.5	10.55	0.709	9.5	10.5	19.15

To assess the uncertainty in the transfer function, the uncertainty in the long term extreme value was quantified. That is the ratio between measured and predicted long term extreme value, ψ_{100}, was calculated for the vertical bending moment midship. A value is denoted as *measured* when the transfer function is corrected using the model error of the transfer function and as *predicted* if the transfer function is uncorrected. The results for all ships are presented in Table 4.16 - 4.19.

The ratio shows that in most cases the estimated hundred year value, r^l_{100}, is overestimated, *i.e.* $\psi_{100} < 1.0$. The r^l_{100} is overpredicted by as much as 40% for the Wolverine State in light loaded condition in following sea. The results for the S-175 and the SL-7 container ship state the contrary for head to beams seas. That is the r^l_{100}-values are underpredicted. However, the results for beam to following seas could indicate overprediction is a general trend. The results for these two container ships might indicate that systematic error is present in the theory, *i.e.* a shift from underprediction to overprediction at beam sea, when the loads for this vessel type is estimated.

Looking at the ψ_{100}-values for the SL-7 and the reefer, the values increase as the forward speed increases for the two heading angles applied in this work. Comparing the ratios for the other vessel, the same behaviour is not observed. However, only one forward speed case is available for the other vessels. The increase of the ratio might only be observed when comparing results for a given vessel as the forward speed increases.

Experimental data obtained by different organisations for a given model, should give results with similar tendencies. This was not the case for the S-175 container ship. In most cases the the experimental data from different test programs showed large scatter. Consequently, this will emerge in the estimated $\hat{r}^l_{100}$ and the corresponding ψ_{100}.

The data from SRI, SHI and NKK lead to significantly different results. The largest deviation between the submitted data groups[1] was as large as 36% in the worst case, *i.e.* in head sea.

[1] Collection of data points for a given test case

Since the experimental data show a large scatter, one may suspect that something in incorrect with the data and one could be tempted to neglect data from some of the contributing organisations. However, to neglect data groups, the corresponding result must differ from all other data groups. This is not the case for the S-175 container ship. Whereas the results for the SRI are in the same order of magnitude as the ψ_{100} values for the SL-7 vessel, the SHI and NKK data are resembling the result for the reefer vessel, California Bear and Wolverine State. In addition, the SRI-value at 60-degrees is substantially larger than the results for the mentioned three vessels. However, the tendency is similar as for the SL-7 container ship. Instead of neglecting the data for the S-175, the above comments should be kept in mind.

Table 4.16: *Ratio between predicted and measured 100 year value for the vertical bending moment midship,* $\psi_{100} = \frac{\hat{r}^l_{100}}{r^l_{100}}$. *The Jonswap spectrum is applied in the calculations.*

Heading			0	30	60	120	150	180
S-175	Fn=0.275	SRI	1.237	1.232	1.717	0.840	1.084	-
		SHI	0.909	0.982	-	-	1.012	0.781
		NKK	-	-	-	-	-	1.021
reefer vessel	Fn=0.0	fore	0.928	-	-	-	-	-
		aft	0.959	-	-	-	-	-
	Fn=0.145	fore	0.970	-	-	-	-	-
		aft	1.053	-	-	-	-	-
California Bear	Fn=0.258	west	0.749	0.815	0.927	0.804	1.032	0.976
		east	0.739	0.744	0.876	0.730	0.874	0.796
Wolverine State	Fn=0.214	light	0.946	0.881	0.832	0.678	0.883	0.588
		full	0.912	0.954	1.055	0.925	0.969	0.830

Table 4.17: *Ratio between predicted and measured 100 year value for the vertical bending moment midship,* $\psi_{100} = \frac{\hat{r}^l_{100}}{r^l_{100}}$. *Results for the SL-7 container ship is presented. The Jonswap spectrum is applied in the calculations.*

Heading		0	25	45	65	115	135	155
SL-7	$Fn = 0.220$	1.197	-	1.245	-	-	-	-
	$Fn = 0.245$	1.204	1.178	1.273	1.482	0.768	0.921	1.129
	$Fn = 0.270$	1.238	-	1.367	-	-	-	-

Table 4.18: *Ratio between predicted and measured 100 year value for the vertical bending moment midship,* $\psi_{100} = \frac{\hat{r}^l_{100}}{r^l_{100}}$. *The Pierson Moskowitz spectrum is applied in the calculations.*

Heading			0	30	60	120	150	180
S-175	Fn=0.275	SRI	1.242	1.288	1.829	0.871	1.048	-
		SHI	0.957	0.997	-	-	0.967	0.772
		NKK	-	-	-	-	-	0.995
reefer vessel	Fn=0.0	fore	0.890	-	-	-	-	-
		aft	0.944	-	-	-	-	-
	Fn=0.145	fore	0.971	-	-	-	-	-
		aft	1.045	-	-	-	-	-
California Bear	Fn=0.258	west	0.789	0.834	1.031	0.825	0.989	0.989
		east	0.938	0.746	0.916	0.735	0.735	0.837
Wolverine State	Fn=0.214	light	0.938	0.908	0.857	0.692	0.866	0.585
		full	0.935	0.939	1.099	0.944	0.935	0.833

Table 4.19: *Ratio between predicted and measured 100 year value for the vertical bending moment midship,* $\psi_{100} = \frac{\hat{r}^l_{100}}{r^l_{100}}$. *Results for the SL-7 container ship is presented. The Pierson Moskowitz spectrum is applied in the calculations.*

Heading		0	25	45	65	115	135	155
SL-7	$Fn = 0.220$	1.224	-	1.252	-	-	-	-
	$Fn = 0.245$	1.238	1.203	1.281	1.546	0.791	0.920	1.068
	$Fn = 0.270$	1.261	-	1.374	-	-	-	-

4.5 Dimensionless Model Error for Linear Theory

A procedure to estimate the dimensionless model error for the vertical bending moment midship for seven ships is presented. A method based on cubic splines and model error as in Eq. 4.3. The transfer function uncertainty is given as a function of ω and the model uncertainty is quantified by the ratio between the measured and predicted 100-year value for the vertical bending moment midship, ψ_{100}. One may notice that there is a large discrepancy between the measured and predicted data. There is not only large difference on the ratio for one heading, but there is also noticeable difference between the measured data for one ship when experimental measurements are conducted by different organisation, see data for the S-175 container ship. In addition, the data from one organisation always tends to either overestimate or underestimate the 100 year value, *i.e.* $\psi_{100} \leq 1.0$ or $\psi_{100} \geq 1.0$.

In this section, a general measure of the uncertainty in the linear, strip theory will be presented as the uncertainty in the long term extreme value and the corresponding standard deviation based on the results in Sect. 4.4.3

4.5.1 Generalisation of the Dimensionless Model Error

In the previous chapters, some errors that may contribute to the deviation between predicted and measured data for the transfer function are pointed out. Another uncertainty is the actual mathematical formulation of the model error. During the experimental testing, one is mainly concerned about collecting data in the vicinity of $\lambda/L_{pp} = 1.0$ in order to capture the dominant peak of the transfer function. Therefore, one is normally in lack of experimental data. One should therefore keep in mind that the dimensionless model error, $\phi''(\omega)$, is only an indication of the uncertainty of the theory relative to experimental testing. It can be used in order to get an idea about uncertainty in the calculation when one is performing long term statistics. A direct use of the model error in short term statistics is not recommended. Especially not for sea states where the peak period is far off the peak period of the transfer function. This is due to the uncertainty in the modelling in those areas.

The model error for all ships are collectively presented in Fig. 4.8 for the headings 0, 30, 60, 120, 150 and 180 degrees. Results for the SL-7 container ship are only included for head sea, since data are not available for the other headings. There is not made any distinction for the separate ships since one is aiming at a general measure of the model uncertainty, ψ_{100}. Hand-drawn continuous lines are included to emphasize the spread of the results. Looking at the figure, one may see that the model errors have a large scatter at small and large wave lengths, *i.e.* high and low frequencies. In the area where the $\frac{\lambda}{L_{pp}\cos\beta}$ is close to unity the scatter seems to narrow. But, even in this area the values can vary as much as $0.6 \sim 2.0$. An interesting observation is that the upper limits are in all cases results of analysis with the S-175 container ship. In particular, large deviation can be observed for the headings $\beta = 30$, 60 & 120 degrees. As mentioned in Sect. 4.4.3, the ratio, ψ_{100}, at $\beta = 60$ degrees was suspiciously large for this vessel. This is also reflected in Fig. 4.8(c) where the dimensionless error, $\phi''(\frac{\lambda}{L_{pp}\cos\beta} = 1.0)$ is approximately 2.0. This may confirm that the the experimental data from SRI is questionable. However, one may say that the uncertainty in the transfer function for all wave lengths seems to be in a scatter band which is drawn on the figures as continuous, thick lines.

In order to find a method to get an estimate of the uncertainty in the long term extreme value expressed by the ratio ψ_{100}, a relationship between the the ratio ψ_{100} and the model error of the transfer function, $\phi''()$, at either $\frac{\omega}{\omega_o} = 1.0$ or $\frac{\lambda}{L_{pp}\cos\beta} = 1.0$ was searched for (ω is the wave frequency and ω_o is the frequency where the corresponding wave length is equal to the ship length). The model error of the transfer function can be expressed by the ratio between the measured and predicted transfer function at this point. Or else one may find the difference between the measured and predicted transfer function and normalise the value as shown in Eq. 4.4 - 4.5.

For every transfer function the value of the model error ϕ'' at $\frac{\omega}{\omega_o} = 1.0$ or $\frac{\lambda}{L_{pp}\cos\beta} = 1.0$ was selected and plotted against the ratio ψ_{100} obtained by long term statistics of the corresponding transfer function. The final results are presented in Fig. 4.9. The results using the value of the model error at $\frac{\omega}{\omega_o} = 1.0$ versus ψ_{100} are shown in Fig. 4.9(a) and Fig. 4.9(c). The other two figures, 4.9(b) and 4.9(d) show the results picking out the value of the model error at $\frac{\lambda}{L_{pp}\cos\beta} = 1.0$. Both the Pierson Moskowitz and the Jonswap spectrum are presented. In the figures there is

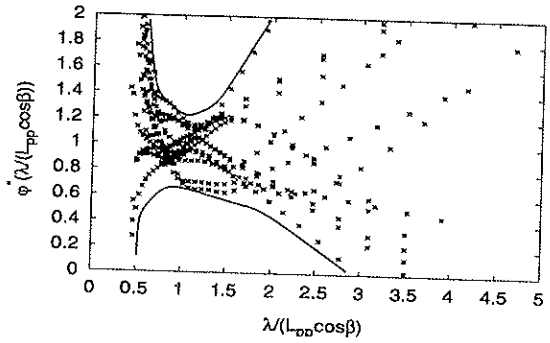

(a) $\beta = 0$ degrees

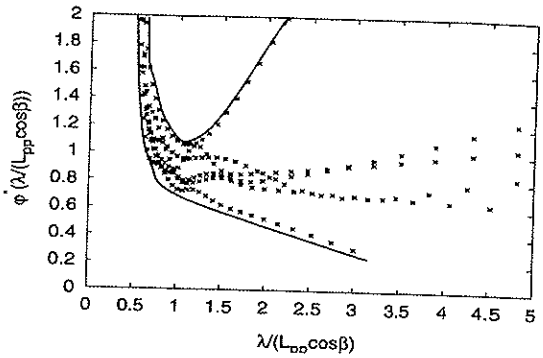

(b) $\beta = 30$ degrees

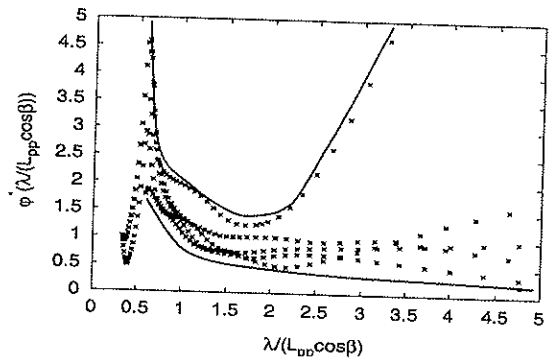

(c) $\beta = 60$ degrees

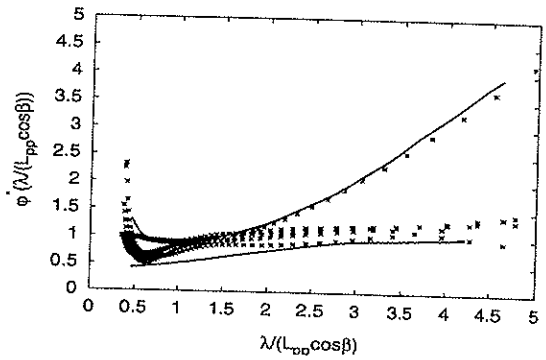

(d) $\beta = 120$ degrees

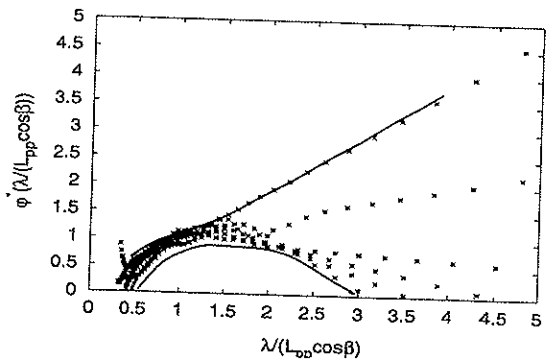

(e) $\beta = 150$ degrees

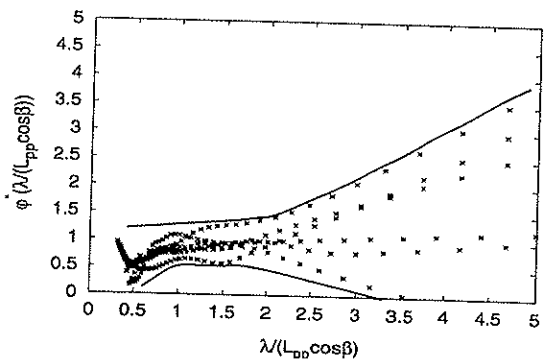

(f) $\beta = 180$ degrees

Figure 4.8: *Model error of the transfer function, ϕ"(ω), for all ships and headings. The continuous lines are hand-drawn envelope curves.*

also a straight line which is calculated using linear regression analysis;

$$y = ax + b \tag{4.15}$$

The coefficients are found by using the least square method given as

$$\hat{a} = \frac{\sum_{j=1}^{n}(y_j x_j) - n\bar{x}\bar{y}}{\sum_{j=1}^{n}(x_j^2) - n\bar{x}^2} \quad \text{and } \hat{b} = \bar{y} - a\bar{x} \tag{4.16}$$

Table 4.20: *Values of the estimated parameters, Eq. 4.15, for the various curves used to estimate the model uncertainty by the ratio ψ_{100}. Also given are the standard deviation, $\hat{\sigma}$, and the correlation coefficient, $\hat{\rho}$.*

	Spectrum	a	b	$\hat{\sigma}$	$\hat{\rho}$
$\psi_{100} = \mathcal{F}(\phi''(\frac{w}{\omega_o} = 1.0))$	PM	0.813	0.195	0.171	0.69
	Jonswap	0.800	0.195	0.155	0.72
$\psi_{100} = \mathcal{F}\{\phi''(\frac{\lambda}{L_{pp}\cos\theta} = 1.0)\}$	PM	0.722	0.262	0.128	0.84
	Jonswap	0.658	0.316	0.131	0.81

where the $\bar{x}$ and $\bar{y}$ are the average values. The values of the estimated parameters, the standard deviation and correlation coefficient are given i Table 4.20. In Fig. 4.9 also a straight obtained using regression anlysis with head sea data are shown. It is a prominent linear relationship between the ψ_{100} and ϕ'' using only head sea data. However, due to the limited number of data points available for a given heading, it is chosen not distinct between the headings in the this work.

One may notice that by plotting the value of the model error $\phi''()$ at $\frac{\lambda}{L_{pp}\cos\beta} = 1.0$ versus ψ_{100}, the data points seem to gather closer to the straight line. Using the value of the model error ϕ'' at $\frac{\omega}{\omega_o} = 1.0$ versus ψ_{100} this tendency is not so strong, indicating that there is a stronger correlation between the model error $\phi''(\frac{\lambda}{L_{pp}\cos\beta} = 1.0)$ and ψ_{100}. Even though the spread is large in either of the cases, the correlation coefficients are largest for the former cases. That is, the correlation coefficients are 0.81 and 0.84 in Fig. 4.9(b) and 4.9(d) respectively, whereas they are 0.69 and 0.72 in Fig. 4.9(a) and 4.9(c). One may also notice that the standard deviation is smaller in the former than the latter case.

This discovery leads to a simplified method to obtain an estimate of the uncertainty of the 100 year value of the vertical bending moment midships. For a given heading angle, the band for the model error at $\frac{\lambda}{L_{pp}\cos\beta} = 1.0$ can be found on Fig. 4.8. The range for the ratio, ψ_{100}, can thus be found by returning to Fig. 4.9(b) and 4.9(d). This is exemplified in Fig. 4.10. For every heading, the mean value, $\phi''(\frac{\lambda}{L_{pp}\cos\beta} = 1.0)$, and the standard deviation, σ, of $\phi''(\frac{\lambda}{L_{pp}\cos\beta} = 1.0)$ is found. The parameters for the linear regression in Table 4.20 is used in order to find an estimate for ψ_{100} and the lower and upper limit, see range on Fig. 4.10. The upper and lower limit is found by using $(\phi''(\frac{\lambda}{L_{pp}\cos\beta} = 1.0) \pm \sigma)$ and the linear relationship to ψ_{100} giving $[\psi_{100}^{lower}, \psi_{100}^{upper}]$.

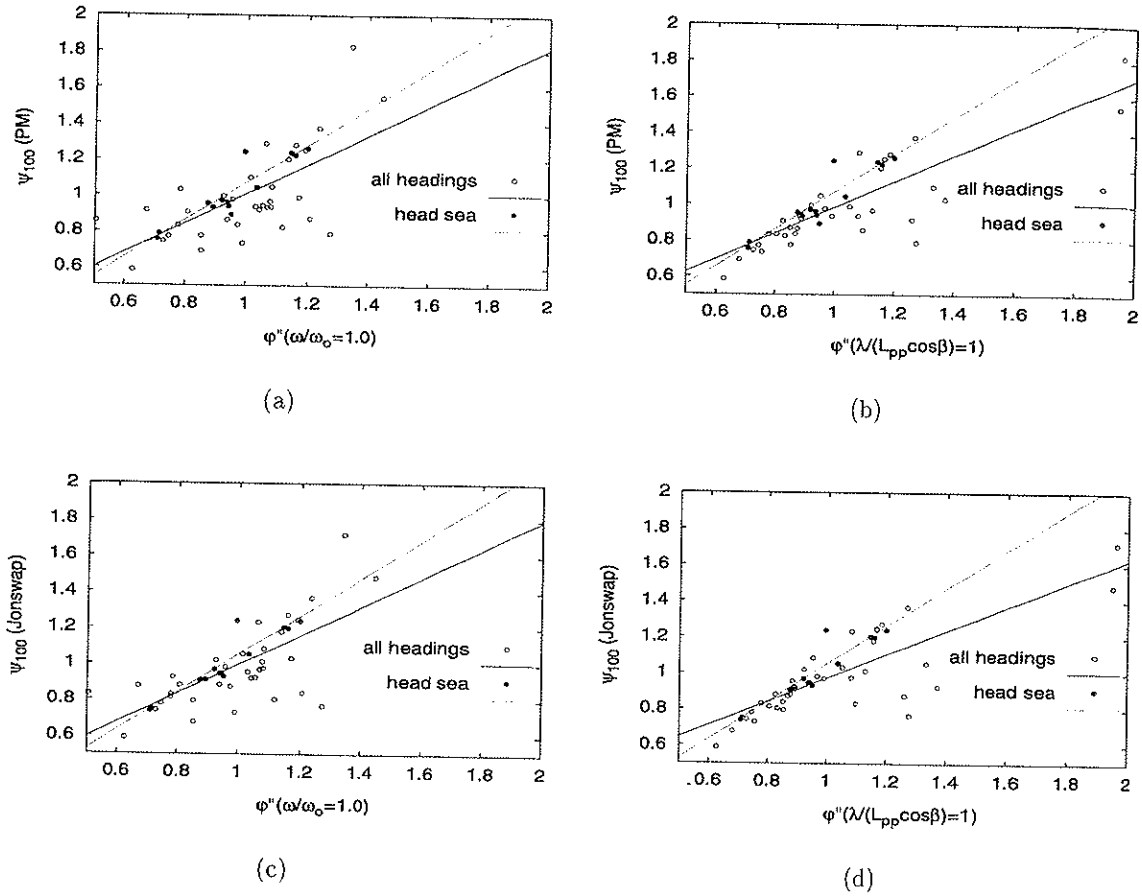

Figure 4.9: *Correlation between the uncertainty in the long term extreme value, ψ_{100}, versus the ratio between the measured and predicted transfer function at $\omega/w_o = 1.0$ and $\lambda/(L_{pp}\cos\beta) = 1.0$. Represented data are the vertical bending moment midship for all ships, speeds and headings.*

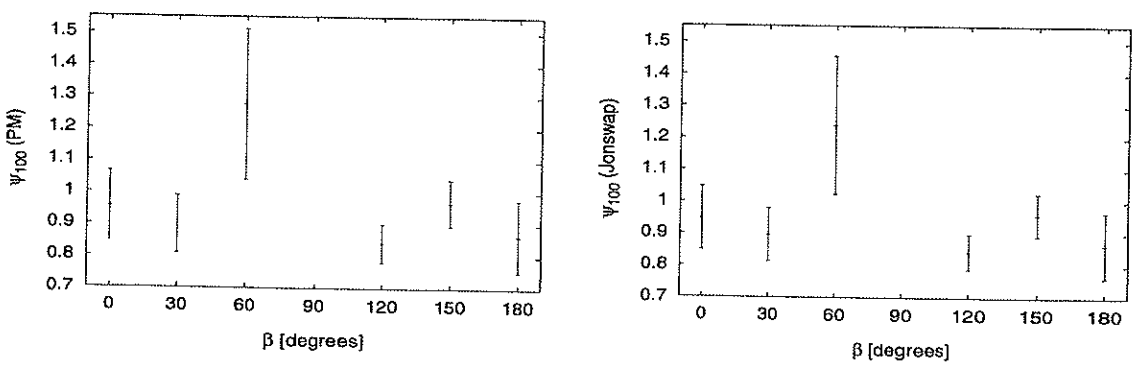

Figure 4.10: *Model uncertainty expressed by ψ_{100} for linear, strip theory. Northern North Sea.*

4.6 Model Uncertainty of Nonlinear, Strip Theory

To asses the model uncertainty of nonlinear hydrodynamics, different methods can be applied. In general, the possible methods will be restricted due to the experimental data. Experimental investigation of nonlinear response is normally conducted in regular waves. It is not common to do experiments to measure nonlinear, irregular response.

The simplest model would be to find a constant value in a format similar to that of the IACS'rules, Nitta et al. (1992).

Another possibility is to use a nonlinear model uncertainty based on a regular wave correction. That is for a given wave defined by its wave height, H, and its period, T, one can find the ratio between the measured amplitudes for sagging and hogging and the corresponding simulated values.

$$\hat{y}_{sag\ or\ hog} = \chi(H,T) y_{sag\ or\ hog} \tag{4.17}$$

An option is of course to do a time domain simulation for a given significant wave height, H_s, and peak period, T_p. The corresponding time series could be created in an experiment. Further, stochastic analysis to find extreme values could be carried out. An estimate of the model uncertainty is based on the ratio of simulated, $y(t)$, and measured extreme values, $\hat{y}(t)$. The equivalent procedure could be carried out to find other measures as for instance ratios between individual peaks in the simulated time series and the corresponding measured series in order to correct the simulated time series, *i.e.*

$$\hat{y}(t) = g(H_s, T_p) y(t) \tag{4.18}$$

In order to reduce the length of the time series, a similar method to that presented in Torhaug (1996), could be used. Torhaug located " critical wave episodes" which were expected to give the largest nonlinear response. The critical wave episodes were located by means of linear analysis. In order to find the extreme, nonlinear responses, only short time series were needed. This idea was also initiating the development of the quasi-nonlinear code in Wu and Moan (1996). A similar method could be used in experiments in order to reduce length and cost of creating long time series.

To assess the nonlinear model uncertainty, a simplified nonlinear theory was applied. The total response is decomposed into linear and nonlinear parts. The linear part is evaluated by using the ordinary strip theory discussed in Sect. 2.3. The nonlinear part comes from the convolution of the impulse response function of the ship-fluid system and the nonlinear modification of the hydrodynamic forces. The method for high and slow speed vessel are described in Wu and Moan (1996). Validation based on a model test is presented in Wu et al. (1996).

The nonlinear components taken into account are due to slamming and modifications of the Froude-Krylov and hydrostatic restoring force. In order to evaluate to slamming force, an asymptotic solution is used for the added mass. For details, see Sect. 2.5.

4.6.1 Regular Waves

The model uncertainty of the nonlinear, strip theory was associated with the model error expressed as the ratio between experimental and predicted amplitudes of the vertical midship bending moments responses due to a regular wave. That is the true response maxima is given as

$$\hat{y}_{sag\ or\ hog} = \chi y_{sag\ or\ hog} \tag{4.19}$$

$\hat{y}$ and y represents the measured and predicted maximum values respectively, for the sagging or hogging. χ is the ratio between the two. One can imagine that χ is a function of different parameters such as wave height, wave periods, hull form, loading conditions and also the measuring method is a parameter contributing to the uncertainty. In order to find a trend for the relative difference, a large amount of experimental data were used and a number of simulations were carried out.

The uncertainty in linear strip theory was characterised by the ratio between the true and the predicted long term extreme value. The aim is to establish a similar approach for correction of the predicted nonlinear, long term extreme value, *i.e.*

$$\hat{r}_D^{nl} = correction\ factor\ \cdot r_D^{nl} \tag{4.20}$$

where $\hat{r}_D^{nl}$ and r_D^{nl} is the true and predicted sagging or hogging response respectively.

However, due to the limited amount of experimental data for the nonlinear case, the correction factor is near to impossible to establish for the nonlinear response using a technique as in Sect. 4.4.3. One has to be content with a simplified approach based on the available experimental measurements in regular waves. It will be shown in Sect. 5.4.5 that there is mainly one sea state which does contribute to the long term extreme value. The long term extreme value can be estimated within an error of 15% using this specific sea states for the response cases applied herein. There is therefore no need to perform uncertainty analysis with a wide range of sea states to obtain a reasonable estimate of the correction factor. In addition, the vessel will have its maximum response for a given set of wave heights and periods depending on the the degree on nonlinearity. These responses will contribute most to the extreme responses. An estimate of the uncertainty in the long term extreme value can be based on uncertainty analysis of the response in a set of regular waves. The correction factor may be given as a function of χ, *i.e.*

$$\hat{r}_D^{nl} = f(\chi) \cdot r_D^{nl} \tag{4.21}$$

In the following, a measure of the uncertainty in nonlinear strip theory will be established on bases of response in regular waves.

Unfortunately, limited data exist in the open literature. They quite often lack details which render impossible any further use. In the following, the reports which have been applied, found or read in this study will be listed in the hope that others do not have to waste their time by searching for experimental data.

Experimental data are collected for different ships ranging from 100-300 meters full scale. Results for a tanker and a destroyer are found in Dalzell (1964a) and Dalzell (1962a). A large amount of data for a mariner type of vessel and three variants are given in Dalzell (1964b) and Dalzell (1962b) and Dalzell (1962c). The mariner models are named 2251A-V1, 2251A-V2, 2251A-V3 and 2251B. The original mariner hull was designated as 2251A. The designation V1 refers to the design weight distribution. V2 and V3 represent variation of the weight distribution within the model, namely cargo at the ends and at midship respectively. Results for the model 2251A-V3 are not included as the weight distribution is somewhat unusual. The model tests were merely included in the report in order to study the change of the radius of gyration. The last model 2251B is equivalent to the 2251A-V1 with increased freebord.

A reefer vessel is described in Korbijn (1992). This vessel is also used in this work in order to study the model uncertainty for the linear strip theory. The experimental data for the reefer vessel is determined by measuring strains at different localities on a backbone frame. The sagging and hogging values midship are found by solving a set of equations and integrating from aft and front. Ideally, the two values should be equal. However, the strain gauges has limited accuracy and the inaccuracies adds up differently starting from aft or front. This may lead to large deviations between the two values. The results for the reefer vessel are therefore indicated by *aft* and *front* to separate the cases.

The experiments have been carried out for a constant wave length λ and increasing wave height h and a constant forward speed U. Calculations were conducted with the wave length, wave height and speed as in the experiments scaled to full scale. For every regular wave, the ratio between the experimental and simulated value for the sagging and hogging value midship were found. The value of the hogging response is in the following designated *negative* sign. Fig. 4.11 is an example of a comparison between the experimental values and simulations carried out for the destroyer vessel at two different speeds and equal wave length.

The hull forms are shown in Appendix F and the mass distributions are reproduced in Appendix G.

Lloyd et al. (1980) presents a rather large amount of experimental data and details so that the data can be used of independent workers in order to verify their own theories. However, there are limited data for the midship bending moment. Detailed information are also given in Nethercote (1981). A limited amount of comparisons of experimental data and nonlinear calculations are presented by Fujino and Yoon (1986), Petersen (1992), Xia et al. (1995) based on different nonlinear theories. Kring et al. (1996) presents comparisons of measured data for the above mentioned reefer vessel and different nonlinear theories, *i.e.* nonlinear strip and 3D theories. The experimental data can be found in Korbijn (1991). However, Korbijn (1998) suggested that these data were not reliable and should not be used.

4.6.2 Trends

In order to find a more general expression for the model error, χ, the dependence of the error on relevant parameters has been investigated. The motivation is that if no such trend is detected,

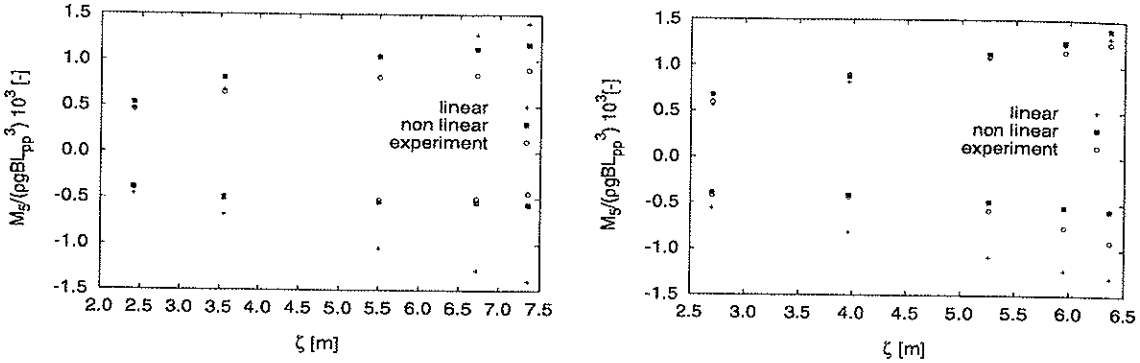

(a) $Fn = 0.0$ (b) $Fn = 0.13$

Figure 4.11: *Midship bending moment for the destroyer vessel versus the wave amplitude for* $\lambda/L_{pp} = 1.0$. *Both linear and nonlinear simulations results are included.*

this may justify that an average value may used to describe the model error for a given vessel.

Firstly, the relation between the model error χ and the wave steepness H/λ is investigated. Secondly, the influence of the degree of nonlinearity is studied. Also the dependence of χ on wave length will be commented.

The model uncertainty for the mariner vessels 2251A-V1 and 2251A-V2 as a function of the wave steepness are presented in Fig. 4.12 and 4.13. One might suspect that the model uncertainty would increase as the wave steepness increases as a result of large nonlinear effects which the quasi-nonlinear theory applied in this work, will be unable to predict accurate. Fig. 4.12(a) and 4.13(a) show the model error χ versus the wave steepness H/λ for wave lengths ranging from $\lambda/L_{pp} = 0.75 - 1.75$. The results for the 2251A-V1 vessel indicate that the model error is more or less in the same range for sagging and hogging. However, for the 2251A-V2 vessel the model uncertainty for sagging is clearly concentrated below 1.0 and for hogging the results are larger than 1.0. For the latter vessel, the tendency is also that the model uncertainty decreases and increases for increasing wave steepness for the sagging and hogging response, respectively. The trend was not so clear for the 2251A-V1 vessel. This is more easily seen in Fig.4.12(b) and 4.13(a). The lines are connecting the model uncertainty for constant wave lengths λ/L_{pp} versus the wave steepness. As already mentioned, the χ for the mariner 2251A-V1 does not have so strong tendency to increase or decrease when H/λ increase. The value of χ seems to depend on the type of response. That is sagging is overestimated and hogging underestimated. The results for the 2251A-V2 are emphasising what is already mentioned above. One should notice that the hull form for the 2251A-V1 and 2251A-V2 vessels are identical. The only difference between the vessels is the distribution of the mass along the length of the hull. The deviation of the behaviour of the model uncertainty is therefore somewhat unexpected.

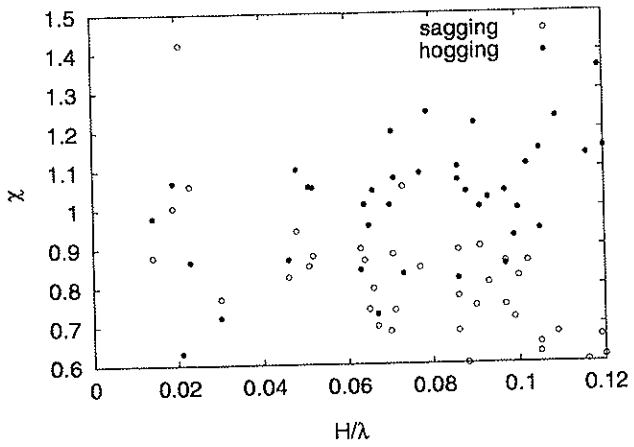

(a) No distinction between the different λ/L_{pp}-ratios

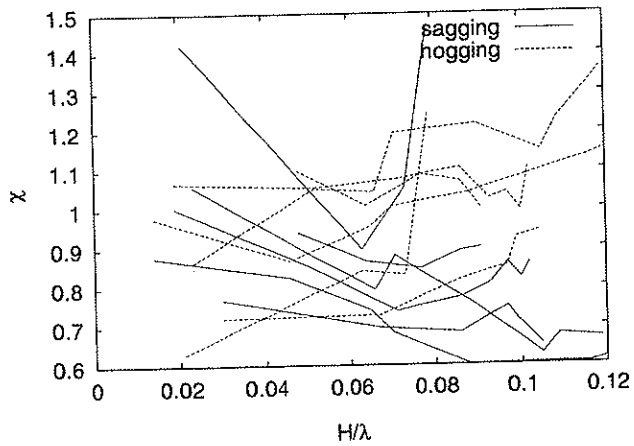

(b) Lines connecting the model uncertainty for constant λ/L_{pp}-ratios

Figure 4.12: *Model uncertainty χ versus the wave steepness H/λ for the mariner 2251A-V1 in regular head sea waves. $Fn = 0.0$.*

A correlation between the model uncertainty and the degree of nonlinearity in the response, *i.e.* the ratio between the nonlinear response amplitude for the sagging and hogging moment midship and the equivalent linear value, is expected and was therefore investigated. The degree on nonlinearity is indicated by *nonlin/lin*. The results for the tanker at two different forward speeds, $Fn = 0.0$ and $Fn = 0.13$, are shown in Fig. 4.14. It seems that the model uncertainty is independent of the degree on nonlinearity in the response, even if at some wave lengths there is a indication that χ is decreasing as *nonlin/lin* is increasing. It also seems like the mariner

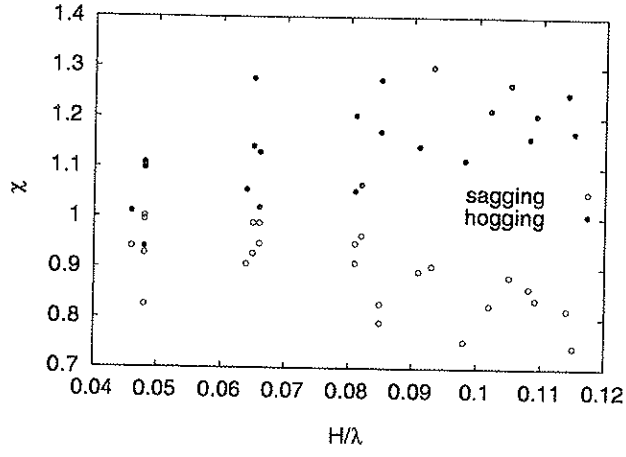

(a) No distinction between the different λ/L_{pp}-ratios

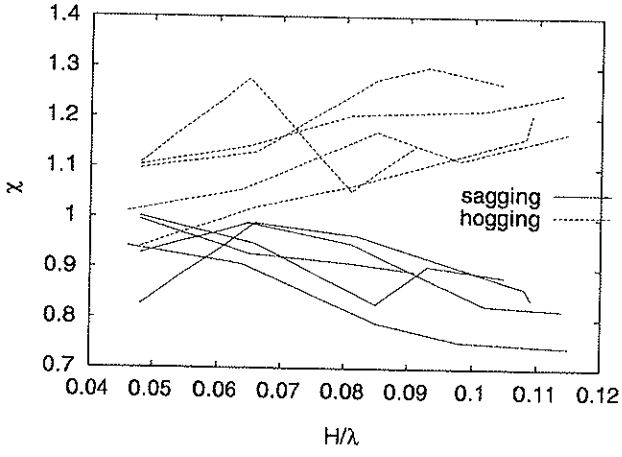

(b) Lines connecting the model uncertainty for constant λ/L_{pp}-ratios

Figure 4.13: *Model uncertainty χ versus the wave steepness H/λ for the mariner 2251A-V2 in regular head sea waves.* $Fn = 0.0$.

2251A-V2 is somewhat sensitive to the degree of nonlinearity for some wave lengths, especially at zero forward speed. However, this is not a general trend but an occasional happening. The results seem to be evenly distributed around a constant value. Since the model error of the nonlinear, strip theory seems to be independent of wave steepness and degree of nonlinearity, this implies that the theory is able to account for even large nonlinearities. This leads us to the next concept, where an average value is calculated for each wave length, *i.e.*

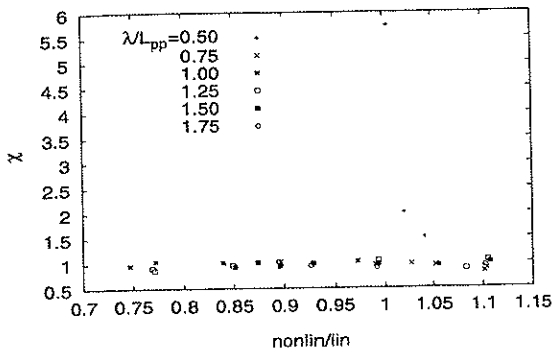

(a) Sagging. $Fn = 0.0$

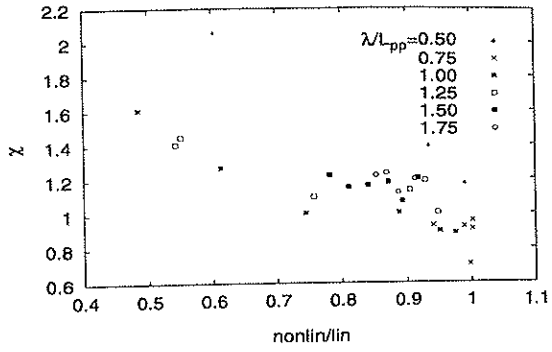

(b) Hogging. $Fn = 0.0$

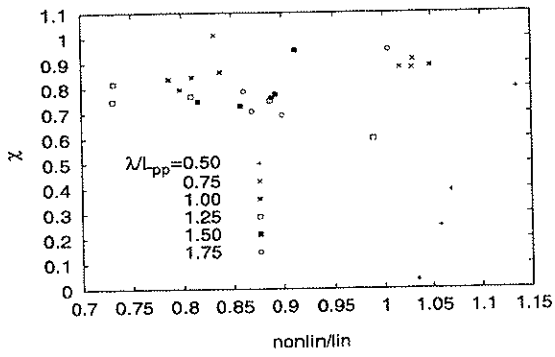

(c) Sagging. $Fn = 0.13$

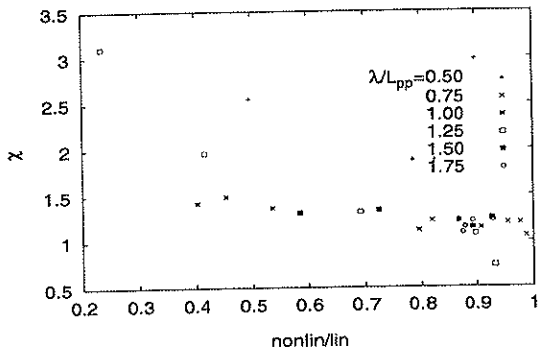

(d) Hogging. $Fn = 0.13$

Figure 4.14: *Model error χ as a function of the ratio between the nonlinear and linear response amplitude of a tanker in regular head sea waves.*

$$\bar{\chi} = \frac{1}{k}\sum_{i=1}^{k}(\chi)_i \tag{4.22}$$

where k is the number of experiments/simulations for a given wavelength λ_j. The value of $\bar{\chi}$ is calculated for each vessel, with and without forward speed, and presented in Fig. 4.15. In the forward speed cases, 4.15(c) and 4.15(d), two different Froude numbers are included *i.e.* $Fn = 0.13$ and $Fn = 0.145$. It is not expected any significant differences in the results for $\bar{\chi}$ at these two Froude numbers. Therefore they are not treated separately.

Again the value of $\bar{\chi}$ does not seem to depend on the parameter along the abscissa. The tendency is once more that the value of $\bar{\chi}$ vary around a mean value, except for some significant deviations at low wave lengths in sagging for the tanker.

Table 4.21: *The average value, μ, for the tanker both including and excluding the data points at $\lambda/L_{pp} = 0.5$. All λ/L_{pp} and H/λ included.*

	Fn	$\lambda/L_{pp} = 0.5$	Average Value, μ	Variance, σ^2	Standard Deviation, σ
sagging	0.0	incl.	1.314	0.7494	0.866
		excl.	0.960	0.0001	0.011
	0.13	incl.	0.741	0.0374	0.193
		excl.	0.816	0.0049	0.070
hogging	0.0	incl.	1.186	0.0445	0.211
		excl.	1.116	0.0181	0.134
	0.13	incl.	1.476	0.2016	0.449
		excl.	1.307	0.0380	0.194

A generalisation of the model uncertainty is pursued. The most striking idea is to link the value of $\bar{\chi}$ to a parameter which is individual for each vessel. One is therefore suggesting to use an average value for each of the response cases. For a given vessel and forward speed the average value is given as

$$\mu = \frac{1}{l}\sum_{j=1}^{l} \bar{\chi}_j \tag{4.23}$$

and with variance

$$\sigma^2 = \frac{\sum_{j=1}^{l}(\bar{\chi}_j - \mu)^2}{l-1} \tag{4.24}$$

where μ is the average model error $\bar{\chi}_j$ for all wavelengths λ_j and l is the number of wave lengths.

Fig. 4.15 shows that the value $\bar{\chi}$ for the tanker at $\lambda/L_{pp} = 0.5$ deviates strongly from the other $\bar{\chi}$-values. Looking back on Fig. 4.14 showing the model error, χ, for the tanker, the values of χ at λ/L_{pp} is substantially larger or smaller than χ-values at other λ/L_{pp} ratios. One may suspect that there is something wrong with the measurements and one is tempted to neglect the data at $\lambda/L_{pp} = 0.5$. This is also supported by the fact that the measurement were conducted at very low wave heights, *i.e.* 2-3cm. The smaller the wave heights are, the more difficult it will be to produce them physically. The average value, μ, for the tanker is calculated and presented in Table 4.21 both including and excluding the data at $\lambda/L_{pp} = 0.5$. Also presented are the variance σ^2 and the standard deviation σ. By excluding the data points belonging to $\lambda/L_{pp} = 0.5$ the standard deviations are reduced very much. In the following the values of μ, excluding data points at $\lambda/L_{pp} = 0.5$, will be used.

The average values, μ, variance, σ^2 , and standard deviation, σ, for all vessel are given in Table 4.22 - 4.25. The mean value, $\bar{\mu}$, variance, $\bar{\sigma}^2$, and standard deviation, $\bar{\sigma}$, of the of mean values, μ, for all ships are given in the last row in the tables. An estimate of the model error of the nonlinear hydrodynamic theory may be obtained by using the average value for a given vessel. One may notice that in most cases, the sagging values are conservative. That is the

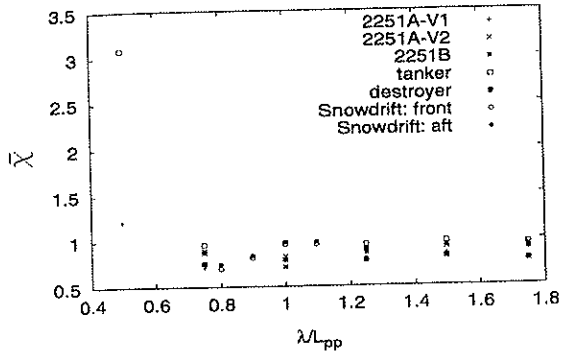

(a) Sagging. $Fn = 0.0$

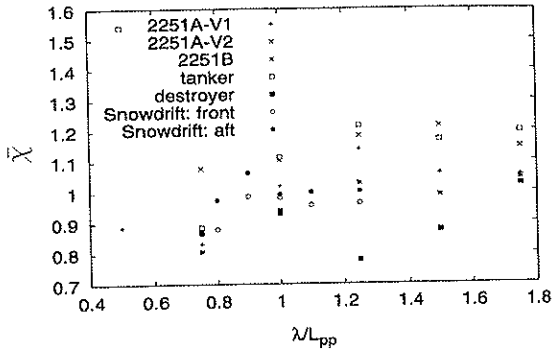

(b) Hogging. $Fn = 0.0$

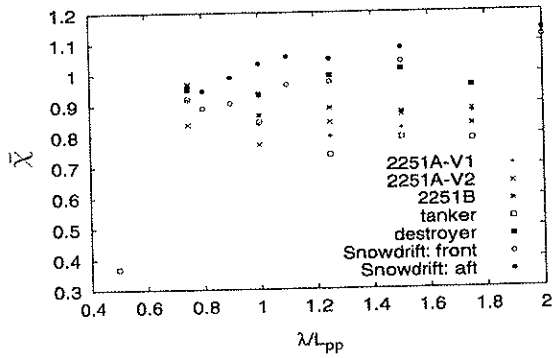

(c) Sagging. $Fn = 0.13$ & 0.145

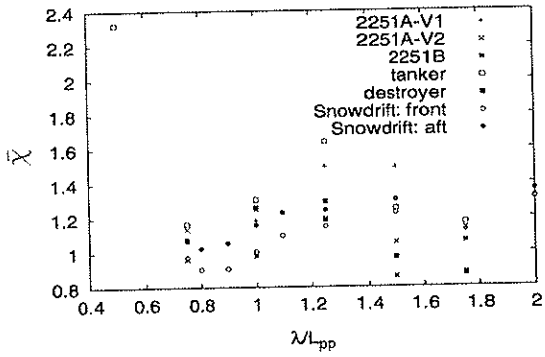

(d) Hogging. $Fn = 0.13$ & 0.145

Figure 4.15: *Model error $\bar{\chi}$ as a function of the ratio λ/L_{pp}.*

simulated values are larger than the experimental results. In general, the model error, χ, for the hogging response is larger than one, meaning that the experimental values are larger than the simulated response.

Sufficient experimental data were available for the reefer vessel to perform uncertainty analysis for both linear and nonlinear strip theory. This enable comparison of the ratio, ψ_{100}, characterising the model uncertainty in linear, strip theory and the average value, μ, for this specific vessel. One may notice that the model error, μ, for sagging response, see Table 4.22 and 4.24, is in general smaller than ψ_{100}, see Tab. 4.16 and 4.18. The model error for hogging, see Table 4.23 and 4.25 is larger than ψ_{100}. This implies that the predicted sagging response using nonlinear, strip theory is more conservative than the prediction by linear, strip theory. The contrary is the result for the hogging predictions.

A more general approach would be if one is able to find a connection between the model error

and some characteristic of the vessel. This may make the model error more applicable for other vessels. On the other hand, there will be additional uncertainty connected to the model errors if applied on other vessel then those presented herein. This will be discussed in Sect. 4.6.3.

Table 4.22: *Average values of the ratios of measured and simulated values of the sagging response midships in regular head sea waves. $Fn = 0.0$. All λ/L_{pp} and H/λ included.*

		C_b	Average Value, μ	Variance, σ^2	Standard Deviation, σ
2251A-V1		0.61	0.856	0.0346	0.186
2251A-V2		0.61	0.893	0.0016	0.040
2251B		0.61	0.853	0.0071	0.084
Tanker		0.80	0.960	0.0001	0.011
Destroyer		0.55	0.781	0.0005	0.022
reefer vessel	fore	0.57	0.862	0.0102	0.101
	aft		0.886	0.0102	0.101
All ships			$\bar{\mu} = 0.871$	$\bar{\sigma}^2 = 0.0029$	$\bar{\sigma} = 0.054$

Table 4.23: *Average values of the ratios of measured and simulated values of the hogging response midships in regular head sea waves. $Fn = 0.0$. All λ/L_{pp} and H/λ included.*

		C_b	Average Value, μ	Variance, σ^2	Standard Deviation, σ
2251A-V1		0.61	0.998	0.0134	0.116
2251A-V2		0.61	1.145	0.0030	0.055
2251B		0.61	0.961	0.0090	0.095
Tanker		0.80	1.116	0.0181	0.134
Destroyer		0.55	0.895	0.0082	0.090
reefer vessel	fore	0.57	0.953	0.0019	0.043
	aft		1.006	0.0011	0.033
All ships			$\bar{\mu} = 1.010$	$\bar{\sigma}^2 = 0.0081$	$\bar{\sigma} = 0.089$

4.6.3 Generalisation of the Model Error

A relation between the model uncertainty and for instance the block coefficient might be established. If an equation is fitted to the average values for the model error, $\bar{\chi}$, estimates of χ can be obtained for the intermediate block coefficients.

A function on the form

$$y = aC_b + bC_b^n = f(C_b) \qquad \text{where } n = 0, 2, 3, 4 \tag{4.25}$$

was chosen for the purpose. The constants a and b can be estimated by using the method of least mean square values, Appendix D, giving

Table 4.24: *Average values of the ratios of measured and simulated values of the sagging response midships in regular head sea waves. $Fn = 0.13$ & 0.145. All λ/L_{pp} and H/λ included.*

		C_b	Average Value, μ	Variance, σ^2	Standard Deviation, σ
2251A-V1		0.61	0.849	0.0023	0.048
2251A-V2		0.61	0.839	0.0018	0.043
2251B		0.61	0.886	0.0025	0.050
Tanker		0.80	0.816	0.0062	0.079
Destroyer		0.55	0.971	0.0011	0.033
reefer vessel	fore	0.57	0.975	0.0064	0.080
	aft		1.042	0.0039	0.063
All ships			$\bar{\mu} = 0.911$	$\bar{\sigma}^2 = 0.007$	$\bar{\sigma} = 0.085$

Table 4.25: *Average values of the ratios of measured and simulated values of the hogging response midships in regular head sea waves. $Fn = 0.13$ & 0.145. All λ/L_{pp} and H/λ included.*

		C_b	Average Value, μ	Variance, σ^2	Standard Deviation, σ
2251A-V1		0.61	1.255	0.0530	0.230
2251A-V2		0.61	1.156	0.0053	0.073
2251B		0.61	1.010	0.0150	0.122
Tanker		0.80	1.307	0.0380	0.194
Destroyer		0.55	1.095	0.0326	0.181
reefer vessel	fore	0.57	1.087	0.0244	0.156
	aft		1.197	0.0153	0.124
All ships			$\bar{\mu} = 1.158$	$\bar{\sigma}^2 = 0.0107$	$\bar{\sigma} = 0.103$

$$\hat{a} = \frac{\sum_{i=1}^{m} yC_b \sum_{i=1}^{m} C_b^{2n} - \sum_{i=1}^{m} C_b^{n+1} \sum_{i=1}^{m} yC_b^n}{\sum_{i=1}^{m} C_b^2 \sum_{i=1}^{m} C_b^{2n} - (\sum_{i=1}^{m} C_b^{n+1})^2} \tag{4.26}$$

$$\hat{b} = \frac{\sum_{i=1}^{m} yC_b^n - a \sum_{i=1}^{m} C_b^{n+1}}{\sum_{i=1}^{m} C_b^{2n}} \tag{4.27}$$

If $n = 0$ the estimates of a and b is equivalent to the estimates for a straight line given as

$$\hat{a} = \frac{\sum_{i=1}^{m} yC_b - \sum_{i=1}^{m} C_b \sum_{i=1}^{m} y}{\sum_{i=1}^{m} C_b^2 - (\sum_{i=1}^{m} C_b)^2} \tag{4.28}$$

$$\hat{b} = \frac{\sum_{i=1}^{m} y - a \sum_{i=1}^{m} C_b}{m} \tag{4.29}$$

where m is the number of data points.

Eq. 4.25 was fitted to each of the data groups of average values of the model uncertainty χ

versus the block coefficient C_b. Four equations, one for each value of n, was fitted to the data and the best fit were chosen on the basis of least residual mean square deviation from the data. The resulting values for the coefficients a and b is presented in Table 4.26 together with the values of n that is minimising the mean square deviation. In addition the variance and standard deviation is presented for each case. The variance and standard deviation are calculated by using

$$\hat{\sigma}^2 = \left[\frac{\sum_{i=1}^{m}(y - f(C_b))^2}{m-1}\right] \tag{4.30}$$

where m is the number of ships (for the reefer vessel aft and $front$ counts two). By fitting an equation to the data points instead of using the average value will reduce the interval for the model uncertainty, *i.e.* $y(C_b) \pm \hat{\sigma}$ will be smaller than $\bar{\mu} \pm \bar{\sigma}$ ($\bar{\mu}$ and $\bar{\sigma}$ refers to the average values and standard deviation for all ships). This is because the deviation between the Eq. 4.25 and the data points is minimised by using the method of least mean squares.

Table 4.26: *Values of the estimated parameters, Eq. 4.26, for the various curves used to estimate the model uncertainty χ.*

	Fn	n	a	b	Variance, $\hat{\sigma}^2$	Standard Deviation, $\hat{\sigma}$
Sagging	0.0	4	1.631	−0.844	0.0009	0.030
	0.13 & 0.145	0	−0.694	1.334	0.0038	0.062
Hogging	0.0	4	1.882	−0.935	0.0040	0.063
	0.13 & 0.145	0	0.786	0.673	0.0063	0.079

The resulting equations for the model error for the sagging and hogging response midship in regular waves are presented in Fig. 4.16 together with the average values given in Table 4.22 - 4.25.

Looking at Fig. 4.16 one may notice that there is a small difference between the linear, $n = 0$, and the three other nonlinear curves, except for sagging at forward speed. Based on this observation, the model error, $\chi = f(C_b)$, can be approximated by a linear function. The values of the estimated parameters a and b for $n = 0$ and the corresponding variance and standard deviation are given in Table 4.27.

In three cases the, model error increases, as C_b increases. The opposite trend is observed for sagging response with forward speed decreases as the value of C_b increases. Even if a proportional tendency is observed, it is believed that the number of data is too small to state that this as a general trend. If more data where available, one could naturally studied more carefully.

4.7 Experimental Errors

Calibration of the measuring instruments may introduce errors from one test to another even if the experiments are conducted in the same towing tank. If equivalent experiments are conducted

Table 4.27: *Values of the estimated parameters, Eq. 4.26, for the various curves used to estimate the model uncertainty χ.*

	Fn	n	a	b	Variance, $\hat{\sigma}^2$	Standard Deviation, $\hat{\sigma}$
Sagging	0.0	0	0.521	0.549	0.0010	0.031
	0.13 & 0.145	0	−0.694	1.334	0.0038	0.062
Hogging	0.0	0	0.692	0.583	0.0047	0.068
	0.13 & 0.145	0	0.786	0.673	0.0063	0.079

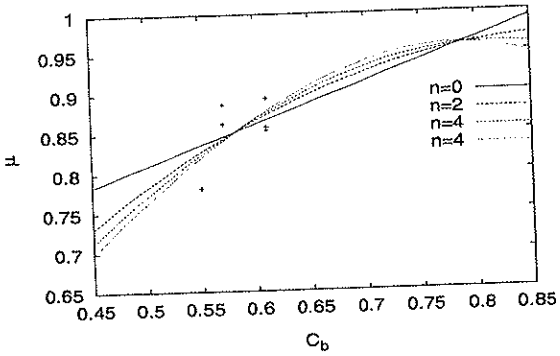

(a) Sagging. $Fn = 0.0$

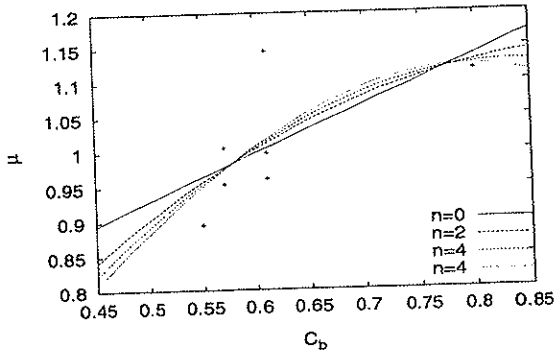

(b) Hogging. $Fn = 0.0$

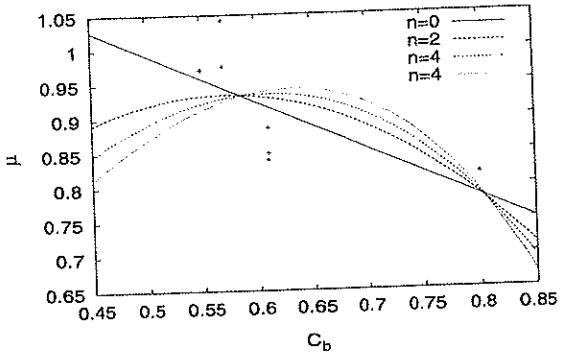

(c) Sagging. $Fn = 0.13$ & 0.145

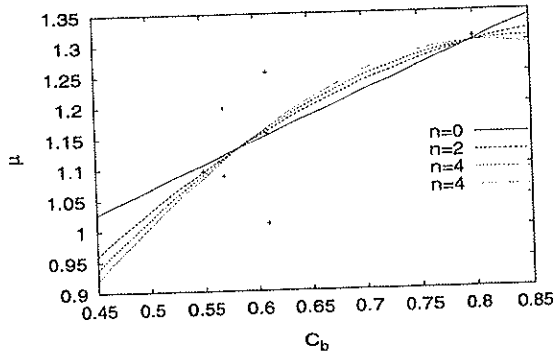

(d) Hogging. $Fn = 0.13$ & 0.145

Figure 4.16: *Model error μ as a function of the block coefficient C_b together with the data points used in the fitting procedure.*

in different towing tanks, there is most likely introduced systematic deviations. Looking at the ratio ψ_{100}, *i.e.* the uncertainty in the long term extreme value, for the S-175 container ship this is quite evident. The difference between the ratios are maximum 36% and minimum 7% where two different institutions have submitted experimental data.

In order to measure the loads, one need specific information about the load distribution along the hull and the locality of the centre of gravity. Exact knowledge of these data will only be known after the ship is built. If the mass distribution is known approximately, this will cause trouble when one wants to do simulations for further verification of the model tests.

Uncertainties in the encounter frequency is another source of error. Since the physics of the boat is dependent on this number, it is important to generate the encounter frequency correctly. The encounter frequency, ω_e, is given as

$$\omega_e = \omega_e(\omega, \beta, U) = \omega + \frac{\omega^2 U cos\beta}{g} \tag{4.31}$$

where the ω is the wave frequency, U is the forward speed, β the heading angle and g is the acceleration of gravity. One would expect that the wave frequency is quite accurately determined, but reflection from sides of the tank/ocean basin and distortion can be another source to uncertainty. Another important parameter is the heading angle. If the test model is towed, one would expect that the heading angle is less uncertain as the model is normally fixed to a carriage. On the other hand, if the model is towed it can be be restricted from moving in a natural way. Most likely, the error due to uncertainty in the heading angle is small in a towing tank. In the case where the model is moving freely in an ocean basin, this uncertainty is larger. At bow or aft sea, the rudder will be used quite actively in order to keep the heading. It is probable that the model will tend to oscillate somewhat from side to side, even though the change from its average position will be small.

Since the encounter frequency goes as $\sim \cos\beta$ the change in ω_e due to change in the heading angle β, $\partial\omega_e/\partial\beta \sim \sin\beta$. That means that the encounter frequency is most sensitive to inaccuracies in the heading angle at bow or quartering seas. As an example a change of the heading angle of $\Delta = 0.2$ degrees cause a variation for the encounter frequency between $[0.62 - 0.64]$ at sixty degrees, whereas the same change cause a negligible difference at head sea.

Another important parameter that concerns the frequency of encounter is the forward speed. If the model is towed this will not be a problem as the carriage will run at constant speed. However, for a free running model added resistance will reduce the speed and thus influence the final encounter frequency.

Naturally, the deviation in the encounter frequency will not be so conspicuous when one is looking at a figure showing both measured and predicted data. But when one is trying to quantify the uncertainty by some kind of mathematical methods, this uncertainty can aggravate the results. In the case where the measured data points are located in the very steep areas of the transfer function it is rather obvious that accurate knowledge of the position of the data point is quite important. And that uncertainties in the wave frequency, the heading angle, the forward the speed are sources of error. This may explain why the model error is very large at high and low frequencies, *i.e.* large and small waves. One may notice that in the region where $\alpha \approx 1.0$ the model errors are ranging from $0.5 \sim 1.0 - 2.0$ in all cases, whereas at large and small waves the error, in most cases, increases.

Among the models, only the SL-7 and the S-175 container ships which are free running models steered by an autopilot. For the three boats, Wolverine State, California Bear and the reefer vessel, the experimental data has been found by towing tests. The tanker, destroyer and the mariner vessels 2251A-V1, -V2, 2251B have been towed in the same towing tank.

Chapter 5

Simplified Estimates of Long Term Extreme Response

5.1 Introduction

In the design of ship, two approaches are applied to obtain the design loads, *i.e.*

- Ship Rules
- direct calculations

Traditionally extreme wave loads are obtained from Ship Rule formulae. Such formulae are based on data for various ship types and would not generally be optimal for a given vessel. This is particularly the case for novel vessels, and direct calculation of the hull girder loads is therefore preferable in such cases.

The most used method is a complete long term description of the response itself. This means that many wave conditions must be analysed and that the long term description is obtained as a weighted sum of the short term descriptions, see Sect. 3.8, considering various wave headings, velocities, routes and operational restrictions, i.e. velocity and heading profiles. The response in a given sea state, defined by the parameters significant wave height, H_s, and peak period, T_p, can be obtained in the frequency domain for the linear response, while time domain simulation is, in general, required to obtain nonlinear response. Consequently the number of load cases to be analysed become almost impractical from a designers point of view. Therefore, a simplified method is necessary to improve the efficiency in the calculation for the nonlinear long term extreme values. This may be done in different ways, but some possible methods are

- regular design waves

- design storm
- set of sea states

The first approach is based on a deterministic wave description. The wave height and period are determined from wave statistics or physical considerations calibrated by more accurate methods. The method is attractive as it is rather simple. No stochastic analysis is needed when the method is calibrated. On the other hand, if a system is sensitive to the period, *i.e.* dynamic system or a highly nonlinear system, information is omitted and the method becomes questionable depending on the calibration. For offshore platform a critical wave length and corresponding wave height is applied, while for fixed platforms, which have negligible dynamic effects, the extreme responses occur for the highest waves, NORSOK STANDARD (1999). Ships have been designed by calculating the response from a wave with length equal to the ship length. The wave height can be found from the breaking wave criterion, *e.g.* Olufsen et al. (1991) applied this for flexible risers and Adegeest et al. (1998) for ships. However, the method is not commonly used for hull girder load calculations in ships, but in the DNV (1987) there are given guidelines on design wave parameters to be used for analysis of semi submersible platforms.

The second approach is to use a design storm. This is a stochastic analysis of a response in one specific area defined by its energy spectrum. In this case the lifetime extreme can be recognised as the most probable or the expected value during the storm. Using this approach, a long term analysis is not necessary, but large uncertainties are seen in connection with the design storm parameters which is the significant wave height, H_s, peak period, T_p, and storm duration. In addition, the chosen parameters are often based on experience and different methods are applied.

The third method, is a tool giving the designer a set of sea states to be used in the design analysis, *i.e.* some chosen sea states or sea states defined by the contour lines. The contour lines (contour curves) are simultaneous values of significant wave height and period corresponding to a certain probability of occurrence, Haver (1987), Winterstein et al. (1993). In this thesis, it will be shown how these kind of curves can be established and utilised.

5.2 The Contour Line Approach

The contour line concept is mainly suggested as a method for predicting load- and response-maxima corresponding to a prescribed return period without having to carry out a full long term analysis. The advantage with this concept is that the environmental and response analysis is decoupled. Meaning that the structural analyst can be handed contour curves for a given return period and a chosen sea area from an environmental analyst. This also opens for different interpretations of the contour line itself which could all be equally valid when seen in view of the procedure established for selecting a characteristic short term extreme value, but the simplified method must be calibrated by full long term analysis.

In general, the design extreme value established using the contour line approach will be defined as

$$X_D = \max \hat{X}_D \text{ along} (H_s, T_p)_D \text{ contour} \tag{5.1}$$

where D is the return period of interest and $\hat{X}_D$ is the short term characteristic used to estimate the design extreme value X_D. A suitable short term extreme characteristic, $\hat{X}_D$, must be determined trough thorough analysis with sufficient number of response problems using long term analysis and contour line solutions.

Initially, the contour lines were proposed to follow lines of constant probability density of the joint density function going to *e.g.* $(H_s)_{100year}$, $(T_p)_{mean}$, Haver et al. (1980). The estimate of the largest response was chosen as the most probable extreme value. However, this short term characteristic was not able to predict the D-year value properly. The actual location of the contour lines was therefore determined such that the largest most probable extreme wave crest during 6 hours along the contour line, did equal the 100-year crest height, Haver (1996). Consequently, the significant wave height along the contour line exceeds the marginal 100-year value for a certain range around the conditional mean spectral peak period. The reason for this is that in addition to the variability in the slowly varying parameters, *e.g.* the significant wave height and the peak period, there is also an inherent randomness associated with the largest maximum crest height within the stationary sea state, Haver (1996).

This may be demonstrated by predicting the 100-year significant sea states, H_s, and the conditional mean spectral peak period, T_p. The duration of the sea state must be chosen to define the probability level of the 100-years H_s and this duration is commonly chosen as 3-hours. The most probable extreme crest height of this sea state is smaller than the 100-year crest height determined from fully long term analysis, *i.e.* the return period is smaller then 100 years. In fact the 100-year value is approximately 10% larger than the most probable extreme crest height of the 100-year 3-hour sea state. It will be quite similar for response problems. This fault has to be accounted for if a short term concept can be consistently used for predicting long term extreme values. In order to take into account the uncertainty in the response, X, one can do one of the following *i.e.*

- One may increase the duration of the sea state artificially. But since the extremes increases rather slowly with the duration, duration has to be made rather long maybe around 24 hours. This is inconvenient if time domain simulations are to be used for establishing the short term distribution of response maxima.

- The sea state level may be increased artificially, *i.e.* blow up the contour lines using using omission sensitivity factors, Madsen (1988), to compensate for the uncertainty in the response, *e.g.* Winterstein et al. (1993). Another approach is to increase the maximum significant wave height along the contour line with about 10% and adopt the contour line through this point as a proper design contour line. Haver (1996) has applied a combination of increased duration of the sea sea states and and artificial high sea states, *i.e.* the duration was increased slightly from 3 to 6 hours and the maximum significant wave height was increased by 7%.

- One can estimate a higher fractile, α, of the extreme value distribution.

- Alternatively, a correction factor to be multiplied by the expected largest value must be found.
- Or a correction factor can be multiplied by the probable extreme value.

A disadvantage of the inflated contour line is said to be that the structures are exposed to unphysical sea states. For the last couple of years it has been recommended to use contour lines of a non-inflated type. This means that the maximum significant wave height along the contour line equals the 100-year significant wave height. Accordingly, the effects of the short term variability has to be compensated for by either increasing the sea state duration or selecting a higher fractile of the 3-hour extreme value distribution, or use the two last suggested short term characteristics and appropriate correction factors.

Herein, focus will be put on the fractile approach, but the correction factor approach will be discussed for linear response. The correction factor to be multiplied with the expected largest value or the probable extreme is believed to be more case dependent than the fractile approach. However, it is left to see which size the fractile, α, must have to get reasonable estimates of the D-year response. Naturally, the fractile will depend on the response type and possibly the degree of nonlinearity. Other factors may be forward speed, wave heading and vessel type. Return period and sea area might influence the fractile size.

Over the years, contour lines are most often determined such that they follow lines of constant probability density. A more consistent approach is probably to determine contour lines corresponding to constant exceedance probability. This can be conveniently done using methods from the field of reliability analysis. Usually the aim of a reliability analysis is to estimate the exceedance probability of a particular capacity or load level. This is very efficiently and, most often, very accurately done using the FORM-technique, see *e.g.* Madsen et al. (1986).

5.2.1 FORM and Inverse FORM

By introducing the "Inverse FORM" method, it will be shown how these contours can be directly generated.

First Order Reliability Method - FORM

The reliability measure of probability of failure is given as

$$P_F = \int_{g(\mathbf{z})\leq 0} f_{\mathbf{Z}}(\mathbf{z})d\mathbf{z} \tag{5.2}$$

where $\mathbf{Z}$ is the set of basic variables $\mathbf{Z} = (Z_1, ..., Z_n)$ and $g(\mathbf{z})$ is the failure function. The failure function is defined in terms of the basic variables as

$$g(\mathbf{z}) = \begin{cases} < 0 & \text{failure set} \\ = 0 & \text{limit state set} \\ > 0 & \text{safe set} \end{cases} \tag{5.3}$$

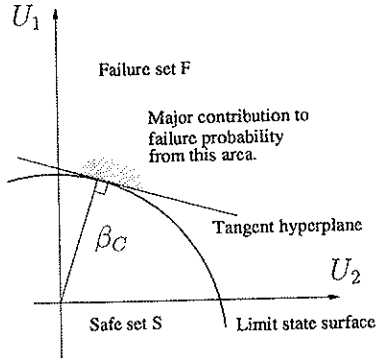

Figure 5.1: *Illustration of approximate failure probability calculation based on FORM, Madsen et al. (1986)*

If the basic variables are normally distributed and the failure surface is a hyperplane (linear), the probability of failure is simply

$$P_F = \Phi(-\beta_C) \tag{5.4}$$

β_C is called the reliability index, see Fig. 5.1.

An exact evaluation of Eq. 5.2 is rarely feasible as the basic variables are in general not normally distributed. Alternative methods such as numerical integration must be used, but they are very time consuming. In structural engineering dealing with structures of high reliability, it is usually sufficient to calculate the failure probability within a factor of $2-5$. A method satisfying this is First Order Reliability Method, FORM, *i.e.* a linearization of the failure surface.

The variable transformation of $\mathbf{Z}$ into a standardised normal u-space, independent of FORM/SORM, is given as

$$\mathbf{U} = \mathbf{T}(\mathbf{Z}) \;\Rightarrow\; \mathbf{Z} = \mathbf{T}^{-1}(\mathbf{U}) \tag{5.5}$$

where $\mathbf{Z}$ is an arbitrarily distribution and correlated, while $\mathbf{U}$ is standard, normally distributed and independent. The failure probability function in the u-space is now given in terms of the failure function in the z-space as

$$g_{\mathbf{z}}(\mathbf{Z}) = g_{\mathbf{z}}(\mathbf{T}^{-1}(\mathbf{U})) = g_{\mathbf{u}}(\mathbf{U}) \tag{5.6}$$

To find the probability of failure in the u-space one is searching for the minimum distance, β, from the origin to a point on the failure surface, see Eq. 5.3. This point is the design point $\mathbf{U}^*$ which is the solution of

$$\min|\mathbf{U}| \text{ ; subject to } g_{\mathbf{U}}(\mathbf{u}) = 0 \Rightarrow \beta = |\mathbf{U}^*| \tag{5.7}$$

FORM uses $\mathbf{U}^*$ as a linearization point, *i.e.* the failure surface $g_{\mathbf{U}}(\mathbf{u})$ is approximated by a hyperplane, or, if preferred, a quadratic approximation provided by SORM.

Inverse First Order Reliability Form - Inverse FORM

Consider a response quantity X as a function of a set of basic variables $\mathbf{Z}$. Using FORM, the basic variables in the z-space is transformed into a set of variables $\mathbf{U}$ in the u-space, *i.e.* $X = x(\mathbf{U})$. Assuming that the uncertainty in the basic variables are dominating, the response X can be treated as a deterministic variable. FORM seeks the failure probability of exceeding a known response value, x_{cap}, through

$$\text{Given } x_{cap}\text{: } \beta = \min |\mathbf{U}|\text{; when } g(\mathbf{U}) = x_{cap} - x(\mathbf{U}) = 0 \tag{5.8}$$

In probabilistic design, the capacity x_{cap} is not given but rather sought with the goal that the reliability β is achieved. Of course this can be found with the FORM technique using an iteration routine or else one can do the opposite, namely to find the capacity x_{cap} given the reliability β using the "Inverse FORM routine" as described by (Winterstein et al. 1993),

$$\text{Given } \beta\text{: } x_{cap} = \max x(\mathbf{U})\text{; when } |\mathbf{U}| = \beta \tag{5.9}$$

Solving Eq. 5.9 for a set of variables $\mathbf{U}$ in u-space one get a sphere with radius corresponding to $\beta = |\mathbf{U}|$ in the u-space. The contour lines in z-space specified to a probability of exceedance P_F are obtained by inverse transformation, $\mathbf{Z} = \mathbf{T}^{-1}(\mathbf{U})$. That means, for a desired probability level β, the environmental analyst need only to report the contour lines of critical $\mathbf{Z}$ values. Since the response is deterministic, the response x_{cap} may be found.

In general, the randomness of the response x can not be neglected. It can be included as a third variable to obtain a proper estimate. But, as already mentioned, it would be nice for the structural analyst if the contours were problem independent, *i.e.* decoupled from the response, and this will be studied in this work. Methods which can be used to account for the randomness of the variable x is mentioned in beginning of Sect. 5.2.

5.2.2 Comparison of Contour Lines of Environmental Variables

A comparison of contour lines applying constant probability density and constant probability of exceedance, established using Haver et al. (1980) and Ude and Winterstein (1996) respectively, are shown in Fig. 5.2. The two approaches will coincide in the reference point, *i.e.* 10-, 100- and 100 year significant wave height and conditional mean spectral peak period, but they may differ slightly as one moves away from this point. However, in the area where the largest responses are expected to occur, *i.e.* large wave heights, there is no significant difference in using the lines of constant probability density or constant probability of exceedance.

The latter approach is, however, more efficient. If more variables are to be included in the problem, *i.e.* 3D-contour surfaces, the IFORM approach can easily be extended to include more variables. The IFORM technique will be used in the following when the contour lines are established.

Introducing response surface for the response characteristics, the IFORM-technique can be utilised as a very fast tool for predicting response extremes corresponding to a prescribed return

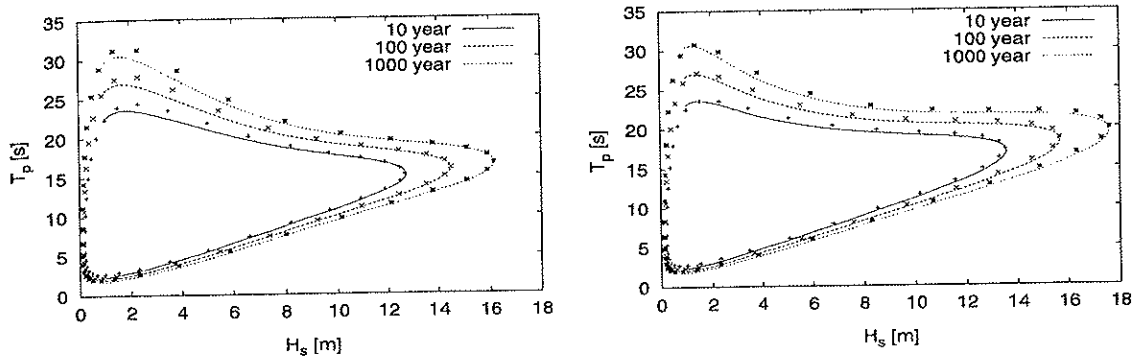

(a) Northern North Sea

(b) Aasgard

Figure 5.2: *Contour lines at the Northern North Sea and Aasgard for return periods* 10, 100 *and* 1000 *years. The lines are lines of constant probability density and the dots are lines of constant probability of exceedance (IFORM).*

period. However, this requires that the short term response characteristics are available at least for a reasonable area surrounding the design point. Such an extended version of the simulation program presented in Ude and Winterstein (1996), is described in Kumar and Winterstein (1997).

5.2.3 Classical Longterm Analysis Versus IFORM Technique

In order to verify the accuracy of the IFORM technique, the lifetime extreme values were calculated using the classical long term approach and compared to the results obtained using the mentioned IFORM technique solving Eq. 3.69, Kumar and Winterstein (1997).

The wave heights with return periods 20, 50 and 100 years were calculated using Eq. 3.69 using the classical solution method, h_D, and the IFORM technique, $h_{D,IFORM}$, at different areas along the Norwegian coast. The results are presented in Table 5.1. One may notice that the wave height using the classical technique, h_D, is always larger than the resulting wave height using the IFORM technique, $h_{D,IFORM}$. Increasing return period decrease the difference between the two solutions. However, the difference is small and in all cases less than 5%.

Long term extreme values for the linear, vertical bending moment midship for the S-175 container ship using both solution methods are also calculated. The results are shown in Table 5.2. Six different headings and four different Froude numbers are applied. The IFORM solution, $r^l_{D,IFORM}$, are in all cases smaller than the values obtained by the classical solution method, r^l_D. However, the difference is rather small and in all cases less than 3.0%.

This deviation is partly due to that formulation of the long term problem. Kumar and Winterstein (1997) uses an extreme value distribution instead of a distribution of maxima and weighting

Table 5.1: *Comparison of wave heigths corresponding to 20, 50 and 100 year return periods using classical longterm analysis, h_D, and solution found using the IFORM technique, $h_{D,IFORM}$.*

	$\frac{h_D}{h_{D,IFORM}}$		
Return period	20	50	100
Northern North Sea	1.033	1.027	1.023
Sleipner	1.040	1.031	1.028
Ekofisk	1.045	1.036	1.031
Aasgard	1.033	1.026	1.023
Statfjord	1.034	1.027	1.024

Table 5.2: *Comparison of vertical bending moment midship corresponding to 100 year return periods using classical longterm analysis, r^l_{100}, and solution found using the IFORM technique, $r^l_{100,IFORM}$. Scatter diagram is from the Northern North Sea.*

	$\frac{r^l_{100}}{r^l_{100,IFORM}}$			
Heading	$Fn = 0.0$	$Fn = 0.1$	$Fn = 0.2$	$Fn = 0.275$
0	1.006	1.006	1.004	1.006
30	1.006	1.008	1.009	1.007
60	1.018	1.014	1.015	1.014
120	1.021	1.022	1.020	1.020
150	1.008	1.006	1.010	1.011
180	1.004	1.005	1.004	1.005

function in the long term formulation which is applied in this work. Applying IFORM to solve the long term problem with an extreme value distribution for the response in a sea state, gives conservative results for the wave response, *i.e.* the failure surface is curved towards origo, see Fig. 5.3, compared to exact solution of the same formulation. Non conservative results are found for the long term extremes of the vertical bending moment midship, *i.e.* the failure surface is curved away from origo. Thus, a contribution to the deviation may be caused by the approximation of the failure surface. Deviation may also be caused by the numerical solution in the simulation program, Kumar and Winterstein (1997), and the simulation program used to solve the problem in the standard formulation.

5.3 Linear Response

The aim of design load calculation is in principle to establish responses corresponding to a prescribed return period, *e.g.* D-year. In order to predict consistent estimates of D-year responses, some sort of long term analysis must be carried out. As already mentioned, the contour line approach can be used in order to predict the D-year value without carrying out the full long term

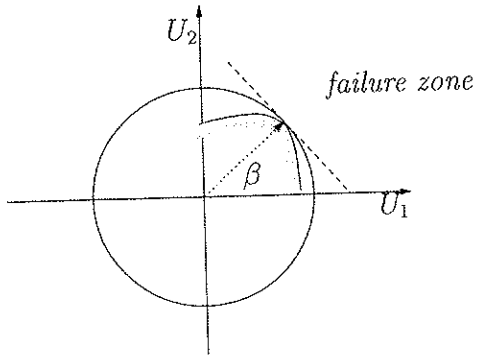

Figure 5.3: *Illustration of failure zone using IFORM.*

analysis. That is some sort of short term statistics will be applied to estimate the D-year value. The most intuitive estimate of the D-year load would be to use the median value, the expected largest or the probable extreme value. However, in general these short term extreme values will underestimate the long term extreme value due to the short term variability. Different ways to take into account the short term variability are discussed in Sect. 5.2.

In this work, both the design fractile and correction factor approach will be treated. However, the focus will be on the fractile approach as this method will be applied for both Gaussian and non Gaussian response. For Gaussian response the Rayleigh distribution is used to describe the maxima distribution. The design extreme value is given by, Eq. 3.58, *i.e.*

$$r^l_{\alpha,design} = \sqrt{2m_0 \ln \frac{N}{\hat{\alpha}}} \text{ where } \hat{\alpha} = 1 - \alpha$$

where $\hat{\alpha}$ is the probability of being exceeded, N the number of maxima and m_0 is the zeroth spectral moment.

5.3.1 Design Fractile Approach

In addition to find a good estimate of the above mentioned fractile and correction factor, one also needs knowledge about the dominant response. In our case, the vertical midship bending moment is studied. Therefore, one has to find the dimensioning load, as a function of heading and speed, which will indicate the importance of needed accurate estimate of the load. The 100-year values for the midship bending moment midship, for a given speed, as a function of the heading is shown in Fig. 5.4(a). As shown in earlier Ch. 4, the bending moment has a maximum in head sea waves. The vertical bending moment in head seas increases as the forward speed increases.

Fig. 5.4(b) shows the short term characteristic design extreme value, the expected largest value and the probable extreme value, calculated along the lines of constant probability of exceedance, together with the long term extreme value. The return period for the environmental contour line for the Northern North sea is 100 years, see Fig. 5.2(a) and the duration of the selected

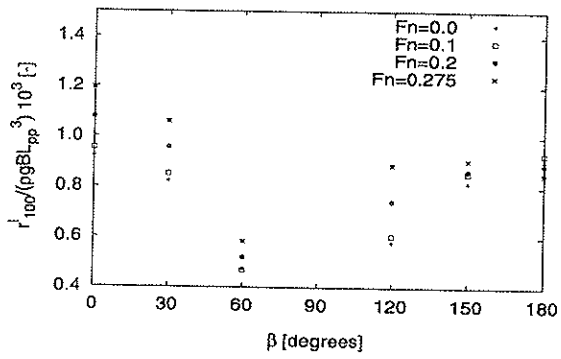

(a) Vertical bending moment midship for the S-175 container ship.

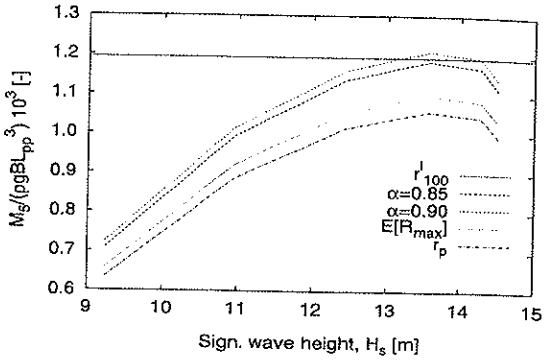

(b) Estimates of r^l_{100} for $Fn = 0.275$ in head seas.

Figure 5.4: 100-*years values and estimates of the vertical bending moment midship for the S-175 container ship.*

short term sea states are 3 hours. One may notice that the expected largest and the probable extreme values will not give good estimates of r^l_{100}. The design extreme value corresponding to a probability of exceedance $\hat{\alpha} = 0.10 - 0.15$ represents a good estimate, *i.e.* $\alpha = 85 - 90\%$.

The magnitude of the fractile needed in order to use the short term characteristic design extreme value, $r^l_{\alpha,design}$, to estimate the 100-year value, is given by the following equation;

$$F_{R_{max}}(R < r^l_{100}) = [F_R(R < r^l_{100})]^N = \alpha = 1 - \hat{\alpha} \tag{5.10}$$

giving

$$r^l_{100} = \sqrt{2m_0 \ln \frac{N}{\hat{\alpha}}} \quad \Rightarrow \quad \alpha = 1 - \hat{\alpha} = N \exp\left(-\frac{(r^l_{100})^2}{2m_0}\right) \tag{5.11}$$

where N is the number of maxima and m_0 the zeroth spectral moment. The minimum value of α, is the smallest fractile you can use in order to get $r^l_{\alpha,design} = r^l_{100}$, , *i.e.* something between $0.85 - 0.90$ for the above case. A larger value will give conservative results for the r^l_{100}-value. However, by rounding off the minimum fractile upwards to the closest multiple of five, the over-estimation will only be a few percent.

In order to find the minimum fractile needed to use the design extreme value to estimate the 100-year value of the vertical bending moment midship, Eq. 5.11 is solved for various of speed and headings for the S-175 container ship. The results are shown in Fig. 5.5. An interesting observation is that for a given heading, the fractile is decreasing as the loads are increasing, *i.e.* forward speed is increasing. For a given speed, the fractile increases from bow to beam seas, and decreases rapidly from beam to following seas. This will be discussed thouroghly in Sect. 5.3.5.

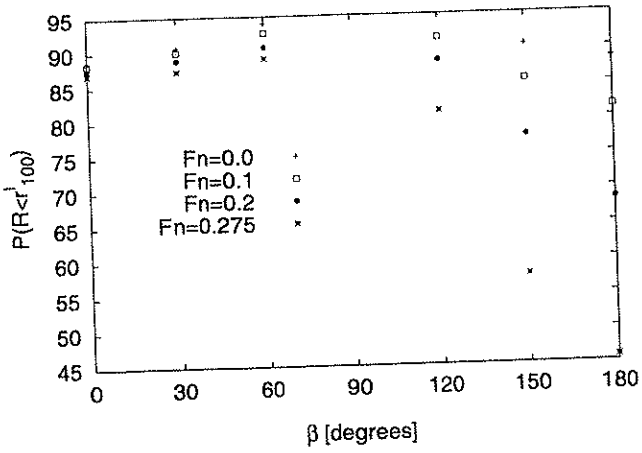

Figure 5.5: *Minimum fractile needed in order to get* $r^l_{100} = r^l_{\alpha,design}$ *for the S-175 container ship. Different heading and speeds.*

This indicates that the fractile found for head sea waves at zero forward speed can be used as a design fractile for the given ship. This design fractile will give a sufficiently accurate measure of the design load, *i.e.* 100-year value of the vertical bending moment midship, for the given ship. That means

$$\alpha_{design} = \alpha(\theta = 0.0, Fn = 0.0) \tag{5.12}$$

Taking the above observations into account, the design fractile is set to be $\alpha = 90\%$. This value is found by rounding off the minimum fractile at head sea waves at $Fn = 0.0$ upwards to the closest multiple of five, *i.e.* $87\% \approx 90\%$.

The design fractile for the S-175 container ship is found to be $\alpha = 0.90$, *i.e.* a 10% probability of exceeding $r^l_{\alpha,design}$ and correspondingly 90% chance to be below. The design fractile will overestimate r^l_{100} in most cases except for some cases at quartering seas and with low forward speed. Since one is looking for a design extreme value, the underestimation at quartering seas is less important. Since the underestimation also decrease when the forward speed is increasing, this implies that as the loads are getting larger the underestimation decrease. Taken into account that the underestimation is less than 4%, these events are less significant when one is looking for the largest vertical bending moments midship, Fig. 5.6(a). This can also be seen in Fig. 5.6(b), showing the 100-year vertical bending moment versus the design extreme value. It is evident that there is a linear relationship between the two values and also that using $r^l_{0.90,design}$ is a good estimate of r^l_{100}.

The minimum fractile to estimate the r^l_{100} is independent of the sea area. The minimum fractiles for both the Sleipner, Ekofisk, Aasgard and Statfjord fields were all equal to $\alpha = 90\%$, *i.e.* the probability that the extreme value will be below $r^l_{\alpha,design}$ is 90%. The same was concluded for 100-year crest heights for these sea areas. For h_{100} the necessary fractile is also equal to $\alpha = 90\%$.

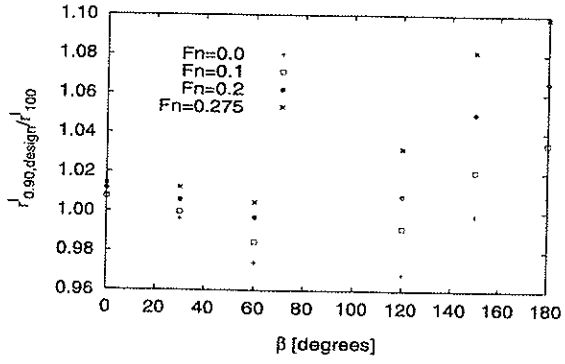

(a) The ratios between the design extreme value, $r^l_{0.90}$, and the 100-year value, r^l_{100}, as function of the wave heading, β.

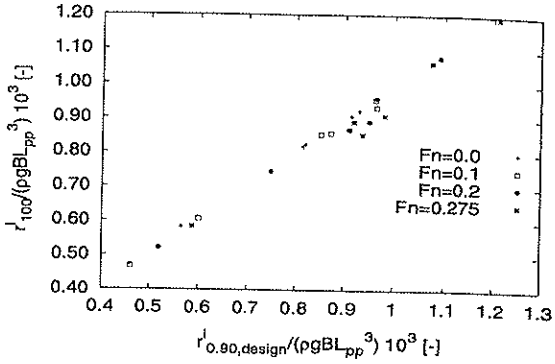

(b) 100-year value, r^l_{100}, versus the design extreme value, $r^l_{0.90}$.

Figure 5.6: *Estimation of the 100-year value, r^l_{100}, of the vertical bending moment midship using the design extreme value with a fractile $\alpha = 0.90$, $r^l_{0.90}$. Results for the S-175 container ship at different heading and speeds.*

Another issue, is the fractile's sensitivity to the return period. One could be tempted to apply the 90% fractile in order to estimate the D-year value using contour lines corresponding to a return period D for other than the 100-year problem. In general, this will not be the case. For wave heights, it seems like a 90% fractile, Fig. 5.7(a), is appropriate for most return periods even if the wave response will be slightly underestimated for the largest return periods, see Fig. 5.7(b). However, for the vertical bending moment midship the alteration for the minimum fractile is more prominent. If a 90% fractile is used to estimate the 100-year value, it will be underestimated by approximately 5% since the value of α increases as D increases. This indicates that care should be exercised, if an estimated design fractile determined for a given return period is to be applied for other than the original return period.

5.3.2 Design Correction Factor Approach

The effect of short term randomness can also be taken into account by introducing a correction factor to be multiplied with the expected largest value, Eq. 3.56, or else the most probable extreme value, Eq. 3.57. As mentioned, it is expected that this is a more case dependent than the fractile approach. However, as long as the response is Gaussian, the correction factor κ can be determined in a similar manner as the design fractile, α_{design}, in the fractile approach.

The correction factor, κ, to be multiplied with the most probable extreme value is presented in Fig. 5.8(a). One may notice that the behaviour of the correction factor is similar as for the minimum fractile. That is, for a given heading the value of the correction factor decreases as the the speed is increasing. The value of the correction factor has a maximum at quartering seas

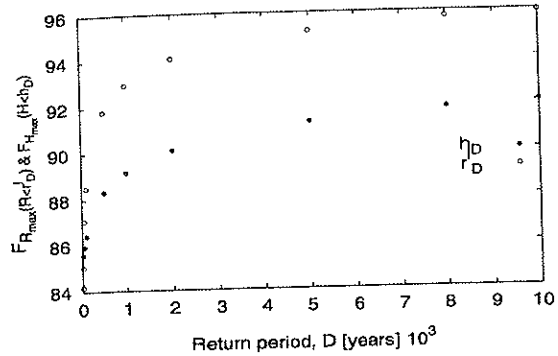

(a) The probability that the extreme vertical bending moment, R, and wave height, H, is below the long term values r^l_D and h_D respectively.

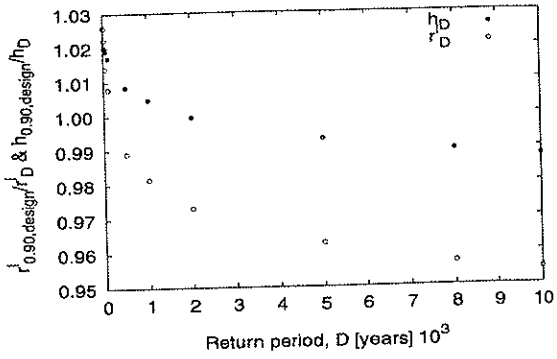

(b) Ratios between the design extreme values using $\alpha = 0.90$, $r^l_{0.90}$ and $h_{0.90}$, and long term values, r^l_D and h_D respectively.

Figure 5.7: *Fractile sensitivity to the return period, D-years, and the deviation from the long term vertical, bending moment midship, r^l_D, and wave height, h_d, value by using* 10% *probability of exceedance. That is* 90% *chance of being below $r^l_{0.90,design}$ or $h_{0.90,design}$. (*1 = 1000 *years,* 2 = 2000 *years etc.)*

and a minimum at following seas. Since the vertical bending moment is largest at head sea, it will be appropriate to use the correction factor at head sea and zero forward speed as a design value. This will be conservative for the largest loads of interest, but the loads at quartering seas will be slightly underestimated. The design correction factor to be multiplied with the most probable extreme value is given as

$$\kappa_{r^l_{p,design}} = \kappa_{r^l_p}(\theta = 0.0, Fn = 0.0) \tag{5.13}$$

The design correction factor, $\kappa_{r^l_{p,design}}$, for the S-175 container ship was found to be approximately 1.15, see Fig. 5.8(a). The estimated long term value using the 100-year contour curve and the most probable extreme value multiplied with $\kappa_{r^l_{p,design}} = 1.15$ are shown in Fig. 5.8(b). It seems that the by using $\kappa_{r^l_{p,design}} = 1.15$ adequate results are obtained for the 100-year value of the vertical bending moment midship for all speeds and headings.

Using the correction factor approach on the expected largest value, the tendencies will be similar, and reasonable estimates of the 100-years long term extreme value will be found. The value of the correction factor for S-175 ship will be approximately $\kappa_{E[R^l_{max}],design} = 1.1$, and is given by

$$\kappa_{E[R^l_{max}],design} = \kappa_{E[R^l_{max}]}(\theta = 0.0, Fn = 0.0) \tag{5.14}$$

If the underlying loading mechanism is nonlinear, the most probable extreme and the expected largest value given by Eq. 3.56 & 3.57, will be too crude since the distribution of the maxima is not Rayleigh distrbuted. An improvement, depending on the response problem, is to describe the distribution of the maxima by the Weibull distribution. That is the most probable maximum,

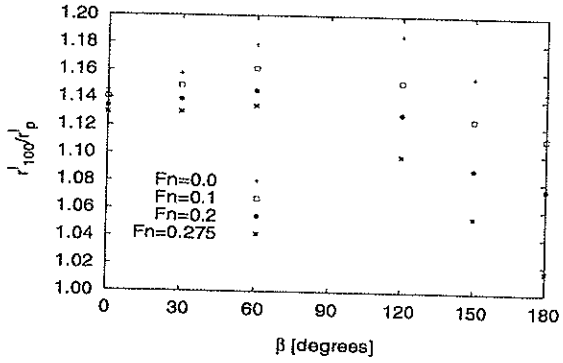

(a) The ratios between the 100-year value, r^l_{100}, and the most probable largest value, r^l_p, as function of the wave heading, β.

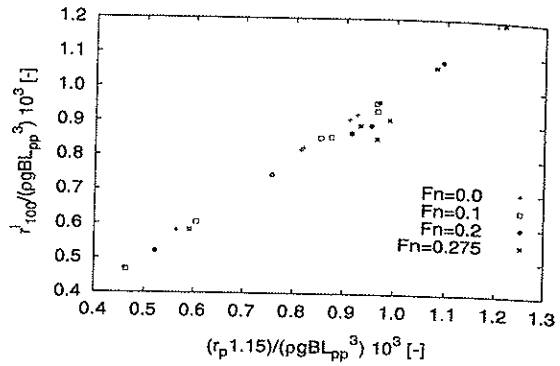

(b) 100year value, r^l_{100}, versus the most probable largest value, r^l_p, multiplied with the design correction factor 1.15.

Figure 5.8: *Correction factor to be used with the most probable largest value and estimation of the 100-year value of the vertical bending moment midship using* $\kappa_{r^l_{p,design}} = 1.15$. *Results for the S-175 container ship at different heading and speeds.*

r^{nl}_p, and the expected largest value, $\kappa_{E[R^{nl}_{max}]}$, is given by Eq. 3.59 and 3.60 respectively. The estimated correction factors for the S-175 container ship at head seas and with zero forward speed is given as $\kappa_{r^{nl}_p} = 1.19$ & $\kappa_{E[R^{nl}_{max}]} = 1.13$ and $\kappa_{r^{nl}_p} = 1.13$ & $\kappa_{E[R^{nl}_{max}]} = 1.09$ for sagging and hogging moment midship respectively. It is believed that the correction factors approach in this case will be less robust than the fractile approach since the nonlinearities affects the distribution in the tail. However, this is not studied any further in this work.

5.3.3 Estimated Design Fractiles

The minimum fractile needed to estimate the hundred year value of the vertical bending moment calculating the design extreme value along the hundred year contour lines is established for several ships using the procedure described in Sect. 5.3.1. The vessels are described in Ch. 4, except for the EuroExpress which can be found in Sagli et al. (1997). Hull forms and main dimensions[1] are given in Appendix F and the mass distributions used are given in Appendix G.

It is found that the fractile is dependent on the size of the hundred year value of the vertical bending moment midship. That means that large ships have smaller design fractiles than ships with shorter length, *i.e.* the larger load the smaller fractile.

There is a linear relationship between the hundred year value and the main dimensions of the vessels, see Fig. 5.9(a). The minimum fractile versus the value $L^3_{pp}B\rho gC_b$ is presented in Fig. 5.9(b). These dimensions are chosen since $L^3_{pp}B\rho gC_b$ has the unit $[Nm]$. C_b is included since the

[1]The hull form and massdistribution for the EuroExpress is confidential and is not included, however a *fish-view* picture of the hull is shown.

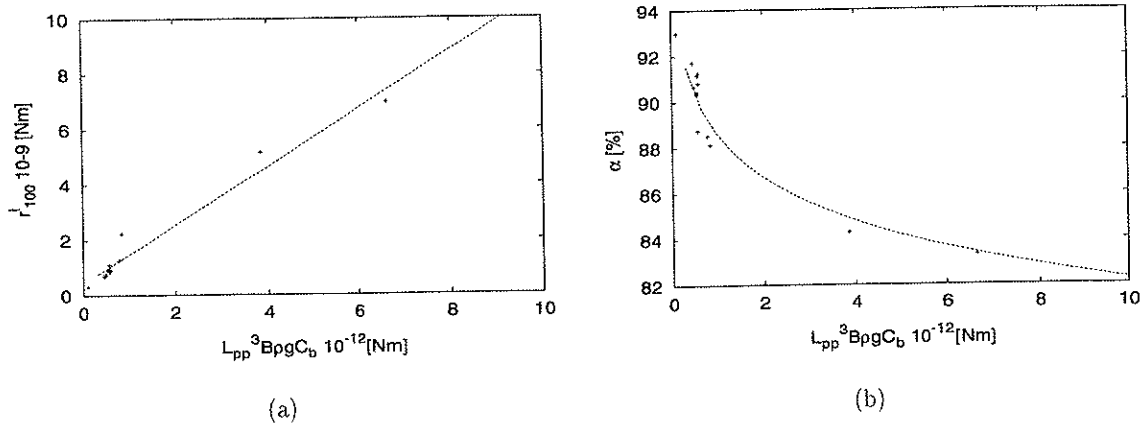

Figure 5.9: *Relation between the* 100*-year value of the vertical bending moment mid ships,* r^l_{100}*, and estimated design fractiles,* α*, versus main dimensions of the vessel.*

shape of the hull shape influences the vertical bending moment. Since the miniumum fractile needed is decaying as the value along the abscissa is increasing, an exponential decaying funcion is fitted to the data.

Vessels with equal hull form, but with different load distribution may also get different minimum fractiles. However, the difference is small. This was the case for the Mariner vessels, Wolverine State and California Bear.

The design fractile, α_{design}, for each vessel is presented in Table 5.3. The design fractiles are established on the basis of the minimum fractile found for each vessel and rounded off upwards to the closest fifth integer, *i.e.* $87\% \approx 90\%$. The last column shows the ratio between the estimate of the hundred year value, $r^l_{\alpha_{design}}$, and the hundred year value, r^l_{100}. By using the design fractiles presented in the table, the r^l_{100} value will only be overestimated by approximately 4% in the worst cases. Remembering that the design fractile will decay when the Froude number is increasing, this will give conservative estimates of the hundred year values of the vertical bending moment midships.

An estimate of the design fractile can also be found using the fitted curve in Fig. 5.9(b) for vessels with $L'_{pp}s$ ranging from $116 - 270$m. This will be a more general approach and might be used for other vessels than those presented herein.

5.3.4 Estimated Design Correction Factors

As mentioned, an alternative to the design fractile approach is the correction factor approach. The correction factor should be multiplied by the short term characteristic, expected largest or most probable extreme value, calculated along the 100 year contour line to get an estimate the 100 year value, r^l_{100}.

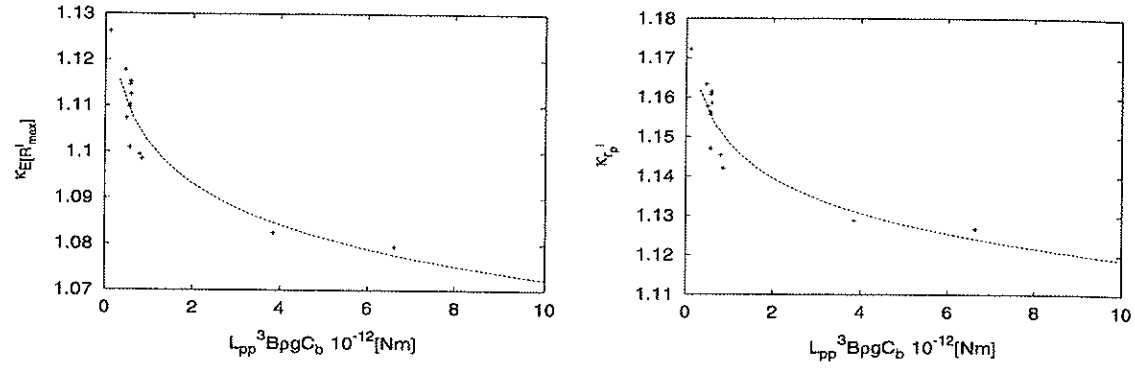

(a) (b)

Figure 5.10: *Design correction factors,* $\kappa_{E[R^l_{max}]}$ *and* $\kappa_{r^l_p}$ *as a function of the main dimension of the vessel.*

The correction factor, $\kappa_{r^l_p}$ and $\kappa_{E[R^l_{max}]}$, are found for all vessels. The behaviour of the correction factors are similar to the behaviour of the minimum fractile, *i.e.* the value of $\kappa_{r^l_p}$ and $\kappa_{E[R^l_{max}]}$ decay when the loads to be estimated increase.

The design correction factors for a range of vessels are shown in Table 5.3. The correction factor to be used together with the most probable and expected largest extreme are given in columns seven and nine respectively. In addition the relative errors using these factors are given in column eight and ten. Using these factors, the estimated 100-year value is only under- or overestimated by a few percent.

The estimated correction factors are shown in Fig. 5.10 as a function of the main dimensions, $L^3_{pp}B\rho gC_b$ for vessels with $L'_{pp}s$ ranging from $116 - 270$m. An exponential decaying function is fitted to the data and included in the figures. The fitted function can be used in order to get a measure of the value of the correction factors, $\kappa^l_{r_p}$ and $\kappa_{E[R^l_{max}]}$.

The correction factor approach will not be utilised any further in this thesis. It was merely mentioned, to emphasise that there exist other approaches than using the design fractile to estimate long term extremes using contour curves.

5.3.5 Fractile and Correction Factor Sensitivity

Intuitively, one may guess that there must be a connection between the correction factor/fractile size and the location of the maximum coefficient of contribution, $\max C_R(si)$, see Sect. 3.8. If the sea state $si = (H_s, T_p)_i$ is located in a region with large duration, see Fig. 3.6, one may expect that the correction factor/fractile will be relatively larger than if the $\max C_R(si)$ is located on a region with smaller duration.

This may be explained as follows. The number of peaks applied in the long term analysis is a function of the duration of the sea states, and naturally the return period, D. Consequently, the number of maxima in the contributing sea states, *i.e.* $C_R(si) > a$, will be larger when $\max C_R(si)$ is located at sea states with relatively large duration. When the contour line approach is applied to estimate the long term extreme response, a large number of maxima in the contributing sea states must be compensated for by either a higher correction factor or fractile. Changes in the correction factor/fractile can be related back to shift in the location of $\max C_R(si)$, and possibly the number of maxima. Factors affecting the location of $(H_s, T_p)_i$, are for instance forward speed, heading into the waves, type of vessel and nonlinear effects.

As seen previously, the correction factor/fractile tends to decrease when the forward speed is increasing and the heading is fixed. And in addition, the correction factor/fractile increases from head to beam seas. This is because the transfer function peak frequency decreases as the forward speed gets larger and the heading goes towards beam seas. Accordingly, the location of $\max C_R(si)$ will move towards larger and smaller peak periods respectively.

The dependency of the vessel size, see Fig. 5.9(b) & 5.10, can be explained by similar reasons. That is, large ships has maximum response at larger wave lengths than smaller ships. Consequently, the coefficient of contribution has maximum at increasingly larger peak periods as the vessel size increases. Thus, a smaller correction factor/fractile is necessary to get an adequate estimate of the D-year response.

As mentioned, the number of maxima included may also influence the size of the correction factor/fractile size. This can be seen in Fig. 5.7(a), where the necessary fractile size is found for several return periods. The fractile size does increase when the return period gets longer, *i.e.* more maxima is included in the analysis but the location of $\max C_R(si)$ is the same.

Care should be taken, when the maximum coefficient of contribution is located at a sea state with peak period larger than the mean spectral peak period in the reference point, *i.e.* 100-years significant wave height. In Haver et al. (1998a), Haver et al. (1998b) it is suggested to use fractiles less than 90% for systems which are sensitive to shorter periods. Looking at the transfer functions, it is probable that the coefficient of contribution has a maximum for larger peak period than the one in the reference point. Based on the experience in this work and in Haver et al. (1998a), Haver et al. (1998b), it seems like the value of the fractile is approximately symmetrical *w.r.t.* the location of the sea state with $\max C_R(si)$ and peak period in the reference point. This is also reasonable with respect to the previous argumentation. This conclusion is based on three response cases from Haver et al. (1998a), Haver et al. (1998b) and 13 from this thesis. Some scatter is experienced for the design fractile for three different models of the Mariner vessel, see Table 5.3. More cases should preferentially be tested out to get more data and be able to study the issue closer.

Table 5.3: *Ship data, design fractiles, α_{design}, and design factors, $\kappa_{r^1_{p,design}}$ & $\kappa_{E[R^1_{max}],design}$, for each vessel.(FL=Full Load, LL=Light Load, EB=East Bound, WB=West Bound)*

Ship	L_{pp} [m]	Beam [m]	C_b [-]	α_{design} [%]	$\frac{r^1_{\alpha_{design}}}{r^1_{100}}$	$\kappa_{r^1_{p,design}}$	$\frac{\kappa_{r^1_p}}{r^1_{100}}$	$\kappa_{E[R^1_{max}],design}$	$\frac{\kappa_{E[R^1_{max}]}}{r^1_{100}}$
S-175	175	25.4	0.572	90	1.008	1.15	1.004	1.10	1.001
SL-7	270	32.2	0.598	85	1.003	1.13	1.019	1.08	0.997
Wolverine State FL	151.2	21.8	0.65	95	1.033	1.16	1.002	1.11	0.998
Wolverine State LL	151.2	21.8	0.61	95	1.026	1.16	0.997	1.12	1.002
California Bear EB	160.9	23.2	0.58	95	1.030	1.16	0.999	1.11	0.995
California Bear WB	160.9	23.2	0.60	95	1.032	1.16	1.001	1.11	0.999
reefer vessel	160	24.7	0.57	95	1.029	1.16	0.999	1.12	1.004
Tanker	272.8	40.2	0.80	85	1.006	1.13	1.003	1.08	1.001
Destroyer	116.7	12.4	0.55	95	1.017	1.17	0.998	1.13	1.003
Mariner 2251A-V1	158.5	23.1	0.61	95	1.034	1.16	1.003	1.11	1.000
Mariner 2251A-V2	158.5	23.1	0.61	90	1.006	1.15	1.003	1.10	1.000
Mariner 2251B	158.5	23.1	0.61	95	1.035	1.16	1.004	1.11	1.000
EuroExpress	219.5	20.2	0.39	90	1.009	1.14	0.996	1.10	1.001

As the design fractile, the correction factor would probably be symmetrical *w.r.t.* to the location of the sea state with $\max C_R(si)$ and the peak period of the reference point, *i.e.* 100-years significant wave height. In Haver et al. (1998a), Haver et al. (1998b) it may be seen that the correction factor for the most probable extreme value for the systems presented therein decreases as the eigenperiod decreases. The explanation is as for the design fractile, Sect. 5.3.3.

The fractile and correction factor sensitivity to the locality of the sea state, si, with maximum coefficient of contribution is illustrated i Fig. 5.11. The arrows indicate the direction in which the fractile and correction factor decreases in value as si moves along the arrows. For example a small ship located with $\max C_R(si)$ at sea state $si = (10.5s, 10.5m)$ has a design fractile of 95%, while a large ship with $si = (13.5s, 13.5m)$ may have a fractile of approximately 85%. The correction factor has a similar behaviour.

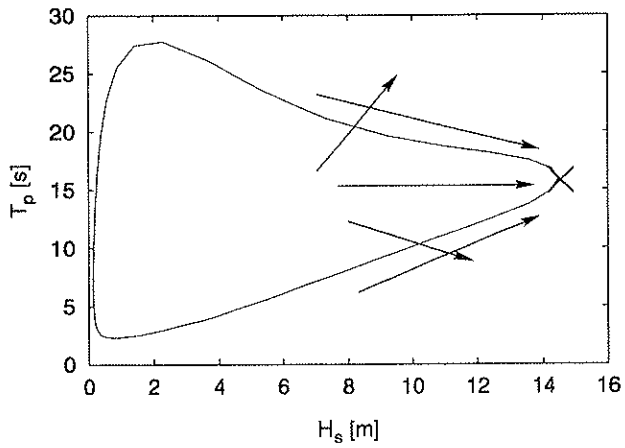

Figure 5.11: *The figure shows the direction in which the correction factor/fractile experiences an decrease in value as the locality of the sea state with* $\max C_R(si)$ *moves in the same direction. The direction is indicated by* $\rightarrow$ *and* $\times$ *is the reference point, i.e.* 100*-years significant wave height and the mean spectral peak period.*

5.4 Nonlinear Response

In this work, the nonlinear response is found by using the simulation program LANWIL, (Wu and Moan 1996), Wu et al. (1996), which is presented in details in Sect. 2.5 and Appendix A.1.2.

In order to estimate the lifetime extreme value using nonlinear response, one has to determine the short term distributions. This includes three tasks

- determine the necessary length of the simulations
- generation of the samples of maxima

- find appropriate distribution model and estimate the corresponding distribution parameters

Finally, some sort of long term analysis must be carried out. The life time extreme value for a given return period of D-year can then be determined. This issue will be described in the following sections.

5.4.1 Evaluating and Comparing Time series

The stability of the statistical moments may be investigated by comparing values calculated for portions of a long realization or from different realizations of the same initial process. The mean value and the standard deviation are normally quite stable, while the higher order moments, *i.e.* skewness and kurtosis, will vary significantly between the realizations. The mean value and the variance can be estimated from reasonable short realizations. A rather large sample is required to get reliable estimates of the skewness and kurtosis since the statistical uncertainty increases as the order of the moment increases.

This can be seen in Fig. 5.13 which shows the statistical moments calculated for different realization lengths of the initial process by using Eq. B.2. The statistical moments are calculated for the vertical bending moment midship on the S-175 container ship in head sea waves. Both linear and nonlinear simulations are included. In addition, the statistical moments obtained by conducting frequency domain analysis is included for the linear case. The 100-year sea state and the corresponding mean peak period in the Northern North Sea is applied. This sea state is indicated in Fig. 5.12 by a ♦. The shortest realizations were 15 minutes and the longest were 6 hours.

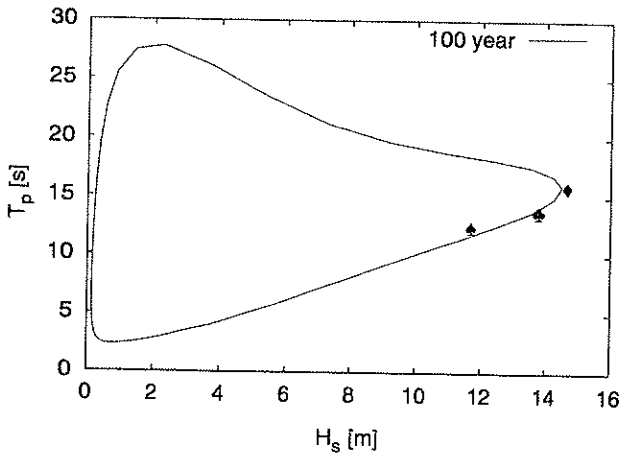

Figure 5.12: *Contour lines of the Northern North Sea for return period of 100 years.* ♣*:* $H_s = 13.56m$ *and* $T_p = 13.76s$. ♦*:* $H_s = 14.5m$ *and* $T_p = 15.9s$. ♠*:* $H_s = 11.5m$ *and* $T_p = 12.5s$.

The statistical moments are also calculated for portions of a long realization and are given in

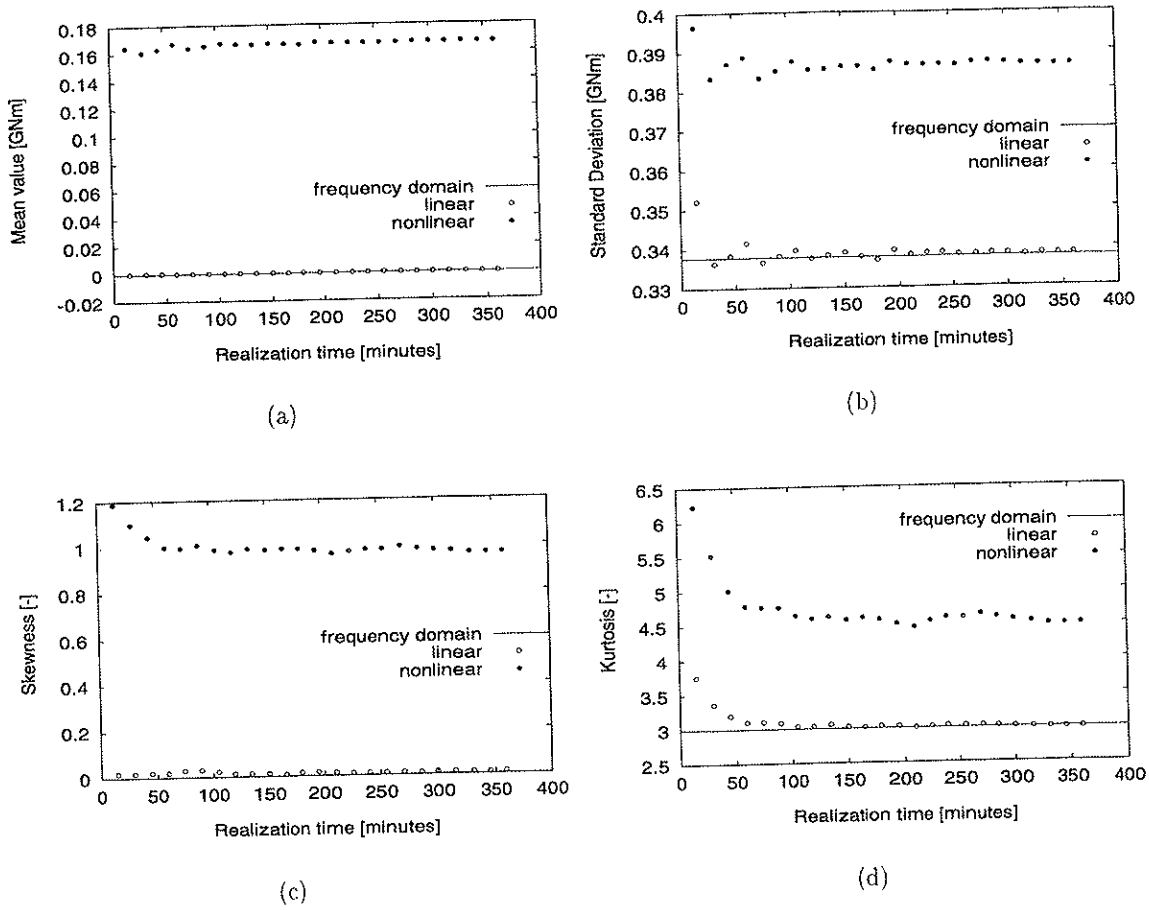

Figure 5.13: *Estimated statistical moments for realizations of the initial process of the vertical bending moment midship on the S-175 container ship in head sea waves with a forward speed at* $Fn = 0.275$. *The sea state is* $H_s = 14.5m$ *and* $T_p = 15.9s$. *The length of the realization is indicated along the abscissa.*

Table 5.4 - 5.5. The shortest are 36 realizations of 10 minutes each and the longest are 6 realizations of 60 minutes. It is seen that the standard deviations of the estimated moments are reduced as the realization lengths increases.

It seems that realizations of 3 hours are stable enough for a practical purpose for the first four moments. Therefore, 3 hours realization will be applied in the following.

5.4.2 Fitting of Distribution Models to Samples of Maxima

This section describes the methods used to fit the following models to the maxima samples:

- The Rayleigh distribution

Table 5.4: *Statistics of parameters of thirtysix 10 minutes realization of the initial process of simulated bending moment midship for the S-175 container ship.* $Fn = 0.275$. $H_s = 14.5m$ *and* $T_p = 15.9s$.

	Est. mean [GNm]	Est. stdv [GNm]	Est. skewness [-]	Est. kurtosis [-]	Est. avr. cycle frq. $[s^{-1}]$
linear response:					
Mean	0.0	0.338	0.010	2.972	0.149
Standard deviation	0.0	0.014	0.041	0.254	0.004
Coefficient of variation [-]	-	0.041	-	0.085	0.028
Max	0.0	0.367	0.095	3.593	0.158
Min	0.0	0.311	-0.069	2.489	0.140
nonlinear response:					
Mean	0.167	0.386	0.956	4.456	0.146
Standard deviation	0.009	0.013	0.133	0.832	0.004
Coefficient of variation [-]	0.054	0.034	0.139	0.187	0.030
Max	0.186	0.414	1.368	7.774	0.157
Min	0.150	0.361	0.750	3.440	0.140

Table 5.5: *Statistics of parameters of six 60 minutes realization of the initial process of simulated bending moment midship for the S-175 container ship.* $Fn = 0.275$. $H_s = 14.5m$ *and* $T_p = 15.9s$.

	Est. mean [GNm]	Est. stdv [GNm]	Est. skewness [-]	Est. kurtosis [-]	Est. avr. cycle frq. $[s^{-1}]$
linear response:					
Mean	0.0	0.338	0.009	2.994	0.149
Standard deviation	0.0	0.004	0.0	0.070	0.0
Coefficient of variation [-]	-	0.011	-	0.023	0.0
Max	0.0	0.343	0.020	3.103	0.151
Min	0.0	0.334	0.002	2.910	0.148
nonlinear response:					
Mean	0.167	0.387	0.963	4.493	0.146
Standard deviation	0.002	0.003	0.040	0.210	0.0
Coefficient of variation [-]	0.013	0.008	0.042	0.046	0.0
Max	0.170	0.390	1.008	4.785	0.149
Min	0.164	0.382	0.902	4.213	0.145

- The Weibull distribution
- The Weibull-tail distribution
- The Generalised Gamma distribution

Moment estimation is used to fit the Rayleigh, Weibull and Generalised Gamma distribution models. Moment estimators are based on the principle that the m parameters $\theta_1, \theta_2, ..., \theta_m$, are chosen so that the moments on the distribution are equal to the moments of the sample, *i.e.*

$$\mu_R^n(\theta_1, \theta_2, ..., \theta_m) = \int_{-\infty}^{\infty} r^n p_R(r; \theta_2, ..., \theta_m) dr \tag{5.15}$$

The principle is giving a set of m equations to find the m unknown estimators $\theta_1, \theta_2, ..., \theta_m$.

The parameters in the Weibull-tail distribution are found by linear regression in Gumbel scale, see page 118.

The Rayleigh Distribution

The scale parameter in the Rayleigh distribution, Eq. 3.29, is found by setting the mean value of the model equal to the mean value of the sample, see Appendix B, *i.e.*

$$\mu_R = m_R \tag{5.16}$$

For visualization, the sample of maxima may be presented graphically by a straight line by using a Rayleigh probablity paper. The value along the the abscissa is given as

$$\frac{r}{\sqrt{2}\hat{A}} \tag{5.17}$$

and the value along the ordinate as

$$\sqrt{-\ln(1 - P_R(r))} \tag{5.18}$$

The Weibull Distribution

The three parameters in the Weibull distribution is found by setting the three first statistical moments of the model equal to the corresponding measures of the sample, see Eq. 3.36. The location parameter, δ, and the scale parameter, β, are given by the estimates of the mean value and the standard deviation of the sample maxima, Eq. 3.36. In addition the shape factor, γ, is found by solving the following equation, Bury (1975);

$$\gamma_{1R} = g_{1R} \tag{5.19}$$

where the γ_{1R} is the skewness of the model given as

$$\frac{\Gamma(1 + 3/\gamma) - 3\Gamma(1 + 1/\gamma)\Gamma(1 + 2/\gamma) + 2\Gamma^3(1 + 1/\gamma)}{[\Gamma(1 + 2/\gamma) - \Gamma^2(1 + 1/\gamma)]^{3/2}} \tag{5.20}$$

and g_{1R} is the skewness of the sample, see Appendix B.

where $u_i = \ln r_i$. $\bar{u}$, s_u^2 and g_{1u} are the mean value, variance and skewness of the logarithm to the observed sample. In addition Stacy and Mihram (1965) derived the following three equations

$$-|g_{1u}| = \frac{\frac{d^3}{dm^3}\ln\Gamma(m)}{\left\{\frac{d^2}{dm^2}\ln\Gamma(m)\right\}^{3/2}} \tag{5.26}$$

$$\gamma = \pm\left\{\frac{\frac{d^2}{dm^2}\ln\Gamma(m)}{s_u^2}\right\} + \text{if } g_{1u} < 0 \tag{5.27}$$

$$\lambda = \exp\left\{-\bar{u} + \frac{\frac{d}{dm}\Gamma(m)}{\gamma}\right\} \tag{5.28}$$

The three parameters can be found directly from the graphic solution presented in Stacy and Mihram (1965). However, in this work the estimates of γ, m and λ is found by a trial and error method. That is, the solution is a combination of solving the above equations and weighted curve-fitting. The parameters are varied until the best fit is obtained. Since the tail distribution is of vital importance, a weighting function is applied during the fitting with weight factors which is gradually increasing towards the tail.

5.4.3 Selection of Samples of Maxima

The method of moments put most of its effort into making a good fit around the mean value of the distribution model. The goodness of the tail is highly dependent on the choice of the model. When one is looking for the extreme values, it is important that the model distribution agrees with the tail of the sample distribution . Methods that increase the weight of the tail is suggested below in addition to the more crude method of using all available maxima.

Using All Peaks

Both local and global maxima are included in the maxima sample, see Fig. 5.14(a). Theoretically this is wrong if slamming occur. It can be shown that the succeeding peaks, *i.e.* whipping, are dependent on the initial "slam-peaks", *i.e.* the following peaks are deterministic. This will violate the basic assumption in extreme value statistics, saying that all maxima are independent. However, if the vessel is treated as rigid, the whipping response is not taken into account. Thus, the assumption of independency is not violated. On the other hand, the local maxima are slightly correlated to the global maxima indicating that this method is not ideal with respect to independence.

Using Global Maxima

An alternative to using all local and global maxima, is to use only the global maxima. This will eliminate some of the smaller maxima occurring, and thus give more importance to the tail. As opposed the method above, *i.e.* using all peaks, the local maximum which is expected to be more correlated to the local maxima than the following global maxima, will be eliminated. Another advantage is that the number of maxima in the sample will be equal to the number of

The Weibull-tail Distribution

The Weibull-tail method has been proposed by Sødahl (1991) for nonlinear problems. The Weibull-tail distribution is fitted by requiring the Weibull model to give the same extremes as a Gumbel model fitted to the largest extremes in segments of the time serie.

The Weibull-tail method may be implemented by

- Finding the maxima given by a set of realizations of the same process generated by different sets of random phases and frequencies for the spectral components.
- Splitting long realization into segments and finding the largest maxima within the segment. This approach has been applied in this work.

The scale and shape parameters of the Weibull-tail distribution are given as estimates of the mean value and standard deviation of the set of the largest maxima, *i.e.*

$$\beta = \frac{1}{\ln \bar{n}_{max}} \left[\left(\frac{m_{Re} - \delta}{s_{Re}} \right) C_1 - C_2 \right] \tag{5.21}$$

$$\gamma = \frac{s_{Re}\beta}{C_1} [\ln(\bar{n}_{max})]^{\frac{1-\beta}{\beta}} \tag{5.22}$$

where β and γ is the scale and shape parameters in the Weibull distribution. δ is the location parameter. $\bar{n}_{max}$, m_{Re} and s_{Re} is the average number of maxima for each segment or realization, mean value and standard deviation of the set of the largest maxima. C_1 and C_2 are regression estimators and can be found in Sødahl (1991). The location parameter, δ, is found by using the standard method of moments by using all maxima in the realization, as presented in Sect. 5.4.2.

Farnes (1990) indicates that 8-10 segments are reasonable for most cases, however long realizations are needed to give accurate results.

The Generalized Gamma Distribution

To find the three parameters, γ, m and λ, the method proposed by Stacy and Mihram (1965) has been used. The method determines the parameters by equating the following three logarithmic moments to those of the model, *i.e.*

$$\bar{u} = \frac{1}{N} \sum_{i=1}^{N} u_i \tag{5.23}$$

$$s_u^2 = \frac{1}{N-1} \sum_{i=1}^{N} (u_i - \bar{u})^2 \tag{5.24}$$

$$g_{1u} = \frac{1}{(N-1)(N-2)} \frac{1}{s_u^3} \sum_{i=1}^{N} (u_i - \bar{u})^3 \tag{5.25}$$

zero-up-crossings. If the weighting function in a long term analysis is to be found, one can count the number of zero-up-crossing instead of the number of peaks.

Using Linear Response to Locate Nonlinear Maxima, the LRNM Method

Another possibility, is to use the linear response to locate the region where maxima might occur. That is , first the time step where a linear maxima occur is located. Knowing this time step, one may find a nonlinear maxima in the region close to the linear maxima.

Using a Up-crossing filter

This filter is based on the fact that the number of maxima minus the number of minima above a certain response level, ξ, corresponds to the number of up-crossings at the up-crossing-level, see Fig. 5.14(c). This filter was proposed in Farnes (1990) and later used in Videiro (1998).

The filter examines the realizations at levels below each maximum starting with the lowest maximum. If a minimum exist below the maximum considered, both the maximum and minimum are removed. The procedure is repeated until all minima above the up-crossing-level, *i.e.* mean value of the series, zero *etc.* , is removed. The filter will in general not change the tail of the distribution, but it will remove local maxima close to the chosen up-crossing-level.

Using a Filter with Time window

The last method that was tried, was a window filter. That is, by carefully keeping track of all maxima and the corresponding point in time, only the largest maxima within a certain period of time is sampled. The size of the window was set to a percentage of the zero-up-crossing period. The method is visualized in Fig. 5.14(d). Using a time window filter, the large values will be given more weight in the fitting procedures.

The use of a window filter can be justified, in the case of slam with following whipping response. As already mentioned, the peaks after a slam are deterministic. By using this filter, one picks the largest peak value and disregard the following peaks. In the case of a rigid body, the whipping does not occur and there is no particular reason for choosing this filter type.

5.4.4 Fitting the Three Parameter Weibull Distribution to the Maxima Samples

The three parameter Weibull distribution was used to fit the maxima samples. The distribution was found to be less dependent on the type of maxima sample generated above. The Generalized gamma distribution is the most sensitive distribution, which also is expected due to the large number of parameters. The Generalized gamma distribution gives a good identification of the size of the extreme response, but the estimated extreme value is rather sensitive to the filtering technique. There was no significant difference in the behavior of the Weibull-tail and the three parameter Weibull distribution. However, since the Weibull-tail is fitted by using a small number of maxima, the estimated extreme value will be burdened with more uncertainty

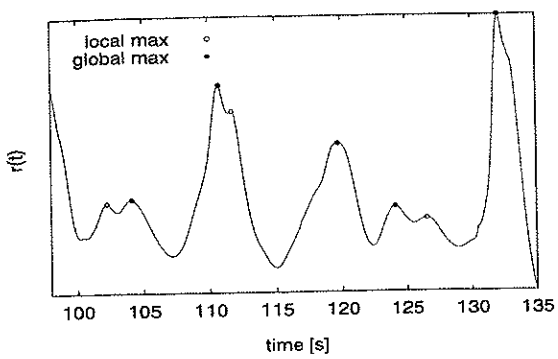

(a) Using all peaks and only global maxima.

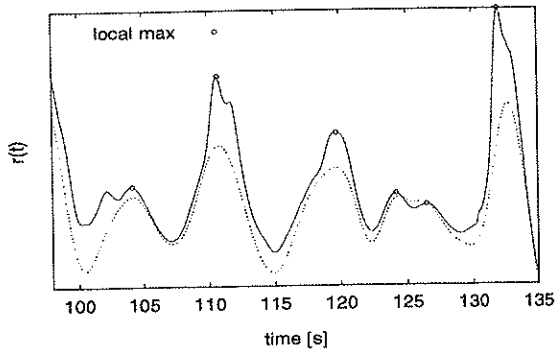

(b) Maxima using the LRNM method.

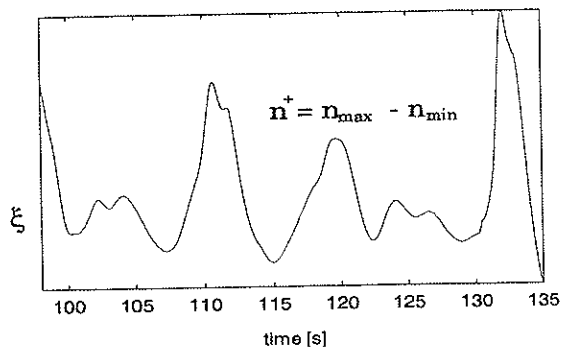

(c) Using an Up-crossing filter.

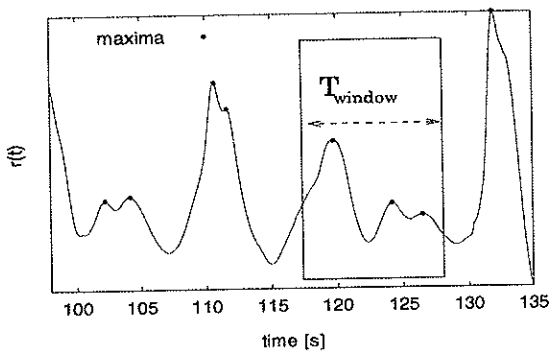

(d) Using a filter with time window.

Figure 5.14: *Filtering routines to establish maxima samples (- nonlinear response, ··· linear response).*

than the traditional Weibull distribution. The Rayleigh distribution underestimates the sagging response and overestimates the hogging response. Fig. 5.15 show the fitting of the mentioned distributions to two different maxima samples, *i.e.* using global maxima and maxima established using the LRNM method.

The samples of maxima were established by using the LRNM method, see page 120. This method makes the fitting procedure very stable. As mentioned in Sect. 2.5.4, there were numerical problems in extreme sea states when bottom slamming occurred. The bottom slamming midship caused a sudden, large hogging response when the region close to midship was out of water in sagging condition. In some cases, extremely large hogging responses occured and this caused problems when the distribution parameters were estimated. In particular this was a problem for the Weibull-tail distribution when the distribution parameters for the hogging response were estimated. The LRNM method makes the fitting procedure stable, since the method in

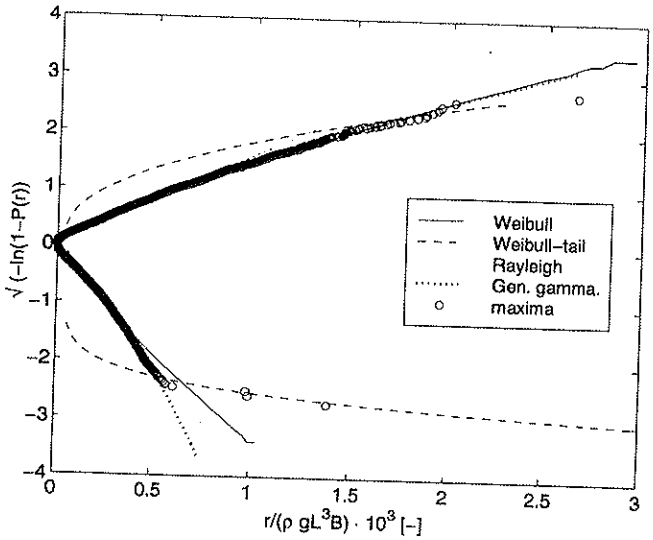

(a) Global

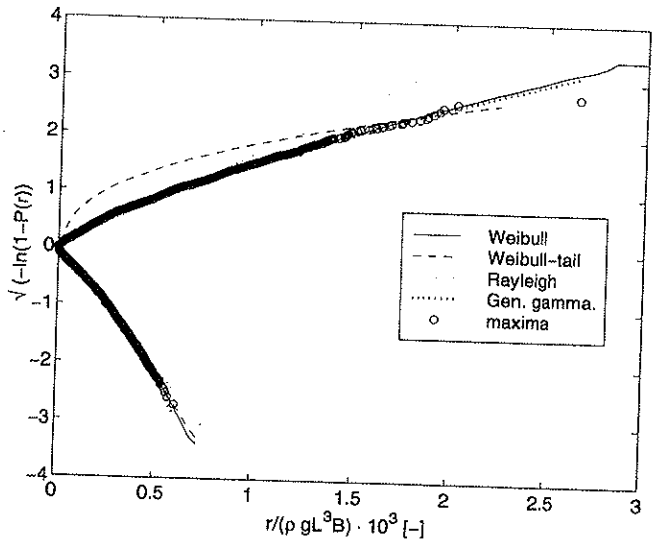

(b) LRNM

Figure 5.15: *Fitting distributions to two different maxima samples. Both are generated from the simulation of the nonlinear vertical bending moment midship in the sea state* $H_s = 13.56m$ *&* $T_p = 13.76s$ *for S-175 container ship at* $Fn = 0.275$. *The number of section is* $N = 42$. *(Sagging and hogging are the positive and negative value respectively.)*

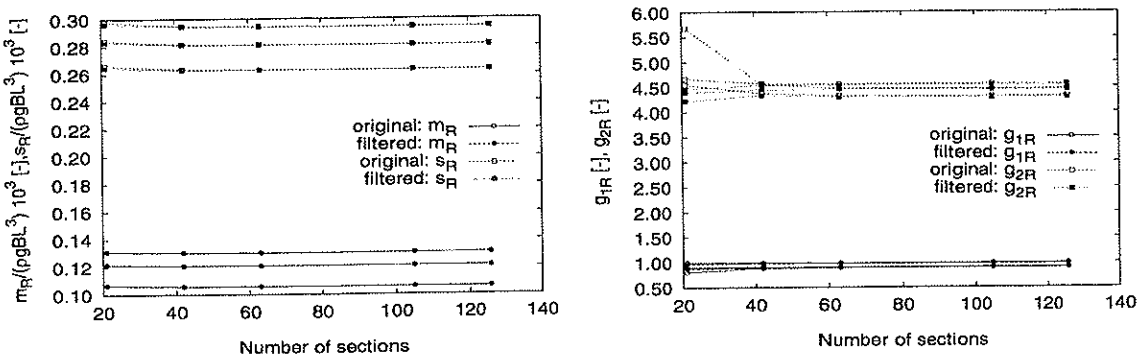

(a) m_R & s_R (b) g_{1R} & g_{2R}

Figure 5.16: *Statistical moments for original and filtered realizations of the initial process as a function of increased number of sections along the ship hull. Vertical bending moment midship for the S-175 container ship in irregular, head sea.* $Fn = 0.275$

general would not detect these peak values. This can be seen in Fig. 5.15(b) where this method is applied. In Fig. 5.15(a) a sample of global maxima is applied.

The vertical bending moment response histories for the S-175 container ship were filtered using a Matlab routine (a low pass filter called Butter, *i.e.* high frequent oscillations are avoided). This was done since the instabilities had an effect on the calculated statistical moments. However, the statistical moments were less sensitive to the numerical instability than the estimated Weibull parameters. 42 sections were appropriate and there was no significant improvement for the first four statistical moment by increasing the number of section any further. A comparison of estimated mean value, standard deviation, skewness and kurtosis is shown in Fig. 5.16 for original and filtered realizations for forward speed with $Fn = 0.275$. The three sea states applied are shown in Fig. 5.12. All data points are given in Appendix J. A comparison of the estimated design extreme values, see Eq. 3.61, for both the original and filtered realization are shown in Fig. 5.17. Two different maxima samples are represented, *i.e.* global maxima and LRNM. One may notice that beyond $N = 42$ there is small changes in the estimated extreme value. Neither filtering of the realizations nor using different maxima samples influence the sagging response significantly. However, the hogging response is highly affected by the filtering of the maxima sample. The LRNM is approximately constant and independent of the number of sections. When the number of sections is large, the results for the global maxima sample converge towards the results from the LRNM sample. Fig. 5.18 presents the estimated design extreme values for the filtered realization using global maxima and LRNM. The values are made dimensionless *w.r.t.* the design extreme value for $N = 126$. And again there is no large differences between the two maxima samples for sagging, but the hogging response is sensitive. This is due to the numerical instability indicated.

All data for the fitted three parameter Weibull distribution can be found in Appendix J. Both

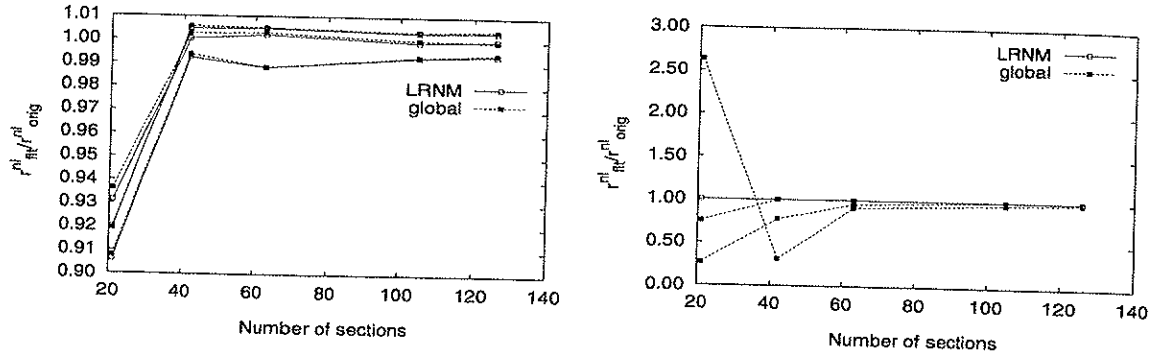

(a) sagging (b) hogging

Figure 5.17: *Comparison of the estimated design extreme values, $r_{0.90,design}$, using two different maxima samples versus increased number of sections along the ship hull. Both filtered and original realization are presented. Vertical bending moment midship for the S-175 container ship in irregular, head sea. $Fn = 0.275$*

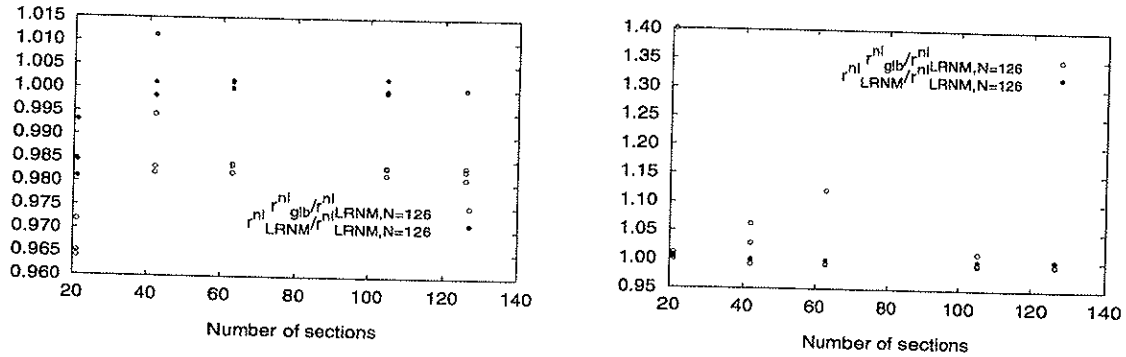

(a) sagging (b) hogging

Figure 5.18: *Comparison of the estimated design extreme values, $r_{0.90,design}$, using two different maxima samples versus increased number of sections along the ship hull. The design extreme values are normalized by the the value obtained with 126 section long the hull. Only filtered realizations are presented. Vertical bending moment midship for the S-175 container ship in irregular, head sea. $Fn = 0.275$.*

data for the original and filtered realization are shown together with results for global and LRNM maxima samples.

One should remember, that the numerical instability is dependent on the vessel type and of course the forward speed. This indicates that the response histories must be checked for each

case. As already mentioned in Sect. 2.5.4, the S-175 containership was highly influenced by these instabilities while simulations conducted on a tanker did not have such problems. The destroyer showed small irregularities which had only minor influence on the final results.

Another option is of course to increase the number of sections along the length of the hull. The numerical instability will thus decrease and the response will converge, see Fig. 2.9. The disadvantage is that the CPU-time will increase. When the number of sections is doubled, the CPU-time is also doubled. The number of necessary sections, will also be dependent on the specific vessel and its characteristics, *i.e.* main dimensions and hull form. The forward speed will also play an important role in this problem. At zero forward speed it is less likely that this problem will occur. Neither will small sea states cause a problem. In this work the realizations were checked carefully, and the necessary actions were taken if problems occured. The LRNM filtering technique was used in all cases, but the additional lowpass-filter was only used in some cases.

5.4.5 Approximate Longterm Analysis

The nonlinear lifetime extreme values are estimated by conducting an *approximate* long term analysis. The method is described in Sect. 3.8. The idea is to use a limited number of sea states in the analysis, instead of using the complete scatter diagram which is a more common approach. In order to do so, the sea states which do contribute to the life time extreme value, must be located. This can be done by using the linear, frequency domain analysis and establish the corresponding coefficients of contribution. This will be a preliminary estimate of the response and location of the maximum $C_R(si)$-value, *i.e.* the corresponding sea state.

The nonlinear simulations are conducted by the program LANWIL, (Wu and Moan 1996), Wu et al. (1996). The generated random phases and frequencies used in the irregular sea, are equivalent for all sea states, *i.e.* the seed is always the same. Ideally the seed should also be a random number, so that the random frequencies and phases would be different in each simulation. If the random frequencies and phases used in the simulations were different in each sea state, the statistical uncertainty would have been reduced. That means that in this case this is not accounted for.

The procedure applied to estimate the nonlinear, long term response can be split into two steps which is

Step I:

1. establish transfer function from linear, frequency domain analysis $\Rightarrow$ $H(\omega)$
2. find linear D-year response from classical long term analysis $\Rightarrow$ r_D^l
3. find the coefficient of contribution, $C_R(si)$, for every sea state
4. locate $\max C_R(si)$ and the corresponding sea state, $si = (H_s, T_p)_i$

Step II:

The first iteration is conducted with sea state si from **Step I**, and the steps are followed from 1 to 3, before returning back to step 1 and the inclusion of more sea states. The iteration procedure to find the nonlinear r_D^{nl} is as follows.

1. start nonlinear simulations in the sea states in the neighbourhood of si
   - find sample of maxima using the LRNM-method
   - estimate the three Weibull parameters
   - find the total number of maxima in the selected sea states, Nsi_j
2. find the nonlinear D-year response from approximate long term analysis, r^{nl}_{D,Nsi_j}
3. find the $C_R(si)_j$-values
4. if $|r^{nl}_{D,Nsi_{j-1}} - r^{nl}_{D,Nsi_j}| > \varepsilon$ check the $C_R(si)_j$ -values at the boundaries of the included sea state area to locate new sea states to be included. Return to 1.
5. else if $|r^{nl}_{D,Nsi_{j-1}} - r^{nl}_{D,Nsi_j}| < \varepsilon$ let $r^{nl}_{D,Nsi_j} = r^{nl}_{D,Nsi=\infty}$ and thus $r^{nl}_{D,Nsi=\infty} = r^{nl}_D$

The above procedure is applied to find the nonlinear vertical bending moment on three different vessels. The scatter diagram are from the Northern North Sea. The Pierson-Moskowitz spectrum is applied in all cases. The chosen return period is $D = 100$ years.

Calculations are carried out using the S-175 container ship at two forward speeds, *i.e.* $Fn = 0.0$ & $Fn = 0.275$. In addition, analysis were performed with the tanker and the destroyer at $Fn = 0.0$ & $Fn = 0.2$. These three vessels are chosen due to the diversity in main dimensions and hull forms. The S-175 container vessel is long and slender with a large bow-flare. One would expect large nonlinear effects on this vessels. The tanker has a large block coefficient and the above water hull form is wall-sided. The vessel will probably not be much influenced by nonlinearities. The destroyer is relatively small with large deadrise angle and has a smaller block coefficient than the S-175 and the tanker. It will more likely experience larger motions and therefore more bow flare slam than the other two.

The results are presented in Table 5.6 and 5.7. The estimated nonlinear, longterm vertical bending moments midship are made dimensionless with the corresponding linear value. Also presented are the sea state si with maximum $C_R(si)$-value and the value $\max C_R(si)$.

One may notice that the nonlinear, long term sagging moment is larger than the corresponding linear value for zero forward speed, $Fn = 0.0$. Largest nonlinearities are detected for the S-175 container ship, where the nonlinear value is approximately twice the linear value. As expected the tanker does not experience large nonlinear effects. The long term sagging response is increased by approximately 30% for the destroyer.

When the Froude number is increased, the nonlinear sagging moment is further increased and

becomes more than doubled for S-175 container ship. Since operability restrictions are not taken into considerations, one may experience these abnormal large response values. It is interesting to note that the nonlinear effects decrease the response with increased velocity for both the tanker and the destroyer. This tendency is also occasionally observed in regular waves , see Fig. 4.11. Also in that case the forward speed caused a reduction in the experienced vertical bending moment midships, *i.e.* nonlinear response is smaller than the corresponding linear response.

The nonlinear effects tend to decrease the hogging response. The reduction is increasing as the forward speed is increasing for all vessels. The effect is most prominent for the destroyer. The reduction is somewhat smaller for the S-175 container ship. The change in the hogging response is smallest for the tanker.

The long term sagging and hogging responses for the S-175 container ship are compared to the long term responses obtained by using the IFORM-technique, $r^{nl}_{100,IFORM}$, Kumar and Winterstein (1997). The distribution of the response applied in the long term formulation is the Hermite distribution, see Sect. 3.6. Since the Hermite-distribution has not been verified for nonlinear ship response, its applicability can not be guaranteed. The ratios between r^{nl}_{100} and $r^{nl}_{100,IFORM}$ for are close to 1, except the ratio for the hogging at $Fn = 0.0$ which shows relatively large deviation, see Table 5.8. The Hermite model probably contributes to the deviation between the estimated long term extremes. A slightly simplified formulation of the long term response was applied, see comments in Sect. 5.2.3. Problems were also encountered applying the simulation program, Kumar and Winterstein (1997). That is, the simulation program would not converge to stable results. It is of course possible that the IFORM is converged towards wrong solution. Therefore the IFORM extreme value must be subjected to additional uncertainty. Winterstein et al. (1994) verified the model through simulation for TLP's.

Table 5.6: 100-*year nonlinear vertical sagging moment midship. The values are made nondimensional w.r.t. to corresponding linear value.*

Ship	Fn	$H_{s,\max C_R(si)}$ [m]	$T_{p,\max C_R(si)}$ [s]	$\max C_R(si)$ [%]	$\frac{r^{nl}_{100}}{r^{l}_{100}}$
S-175	0.0	11.5	12.5	11.78	1.93
	0.275	10.5	12.5	10.62	2.33
Tanker	0.0	12.5	15.5	12.73	1.08
	0.2	14.5	16.5	9.18	0.93
Destroyer	0.0	8.5	9.5	38.44	1.26
	0.2	10.5	11.5	20.43	0.98

5.4.6 Importance of the Coefficient of Contribution

The coefficient of contribution can give valuable information. Firstly, it can indicate in which area of the scatter diagram one should include more sea states. If the change in $C_R(si)$ is large, *i.e.* $\frac{\partial C_R(si)}{\partial h_s}$ or $\frac{\partial C_R(si)}{\partial t_p}$, this indicates that the sea states beyond this point are less important. A

Table 5.7: 100-*year nonlinear vertical hogging moment midship. The values are made nondimensional w.r.t. to corresponding linear value.*

Ship	Fn	$H_{s,\max C_R(si)}$ [m]	$T_{p,\max C_R(si)}$ [s]	$\max C_R(si)$ [%]	$\frac{r^{nl}_{100}}{r^{l}_{100}}$
S-175	0.0	10.5	12.5	12.28	0.79
	0.275	10.5	12.5	17.88	0.61
Tanker	0.0	13.5	15.5	11.32	0.92
	0.2	12.5	16.5	12.15	0.83
Destroyer	0.0	7.5	10.5	13.91	0.52
	0.2	10.5	10.5	29.89	0.42

Table 5.8: *Comparison of approximate longterm analysis,* r^{nl}_{100}*, and solution found by using the IFORM technique,* $r^{nl}_{100,IFORM}$*. The vessel is the S-175 containership.*

	$\frac{r^{nl}_{100}}{r^{nl}_{100,IFORM}}$	
Fn	Sagging	Hogging
0.0	0.924	0.876
0.275	1.069	0.993

small gradient will indicate the contrary. Secondly, it may help to locate the most contributing sea state in the scatter diagram, *i.e.* $C_R(si)$-maxima. In linear analysis, the dominating maximum is located in the region where $T_p = \sqrt{2\pi L_{pp}/g}$, *i.e.* $\lambda = L_{pp}$. In nonlinear analysis, other maxima may occur due to large responses at other peak periods due to nonlinearities, *i.e.* for instance slamming which is expected to occur at slightly shorter and steeper waves. Inclusion of the nonlinear corrections of the hydrostatic restoring and Froude-Krylov force may also cause the second maxima. Thirdly, and maybe most important, the $C_R(si)$-value will tell us that a small number of simulations are necessary to estimate the long term response reasonable for practical purposes as long as the most important sea states are included in the analysis. To exemplify this, the long term response analysis performed with the S-175 container ship at $Fn = 0.275$ will be applied. The $C_R(si)$-distribution is shown in Fig. 5.19 as a function of the significant wave height, H_s, and the peak period, T_p. The $C_R(si)$-values are plotted as contour lines ranging from 0-17%.

Both sagging and hogging have two distinct peaks where $C_R(si)$ reaches a maximum. The maxima in sagging are almost equivalent in value, whereas the second peak in hogging is relatively small. The maxima are close, and they are easily detected by studying the $C_R(si)$-gradient.

As long as the sea state with maximum $C_R(si)$-value, see Table 5.6 and 5.7, is captured there is no need to perform a large number of simulations. By using Fig. 5.19 one may select a number of sea states and thereafter find the total sum of the contributing sea states, *i.e.*

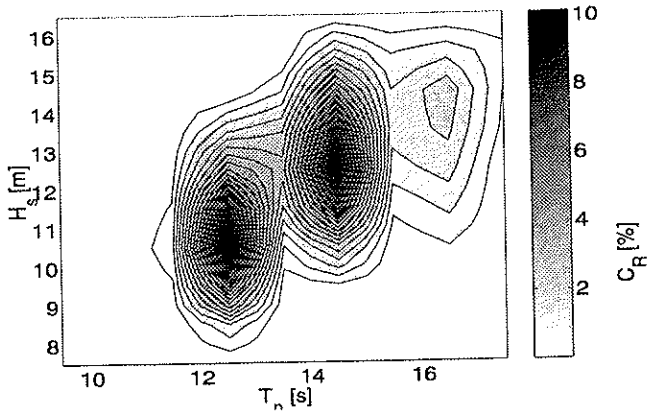

(a) Sagging

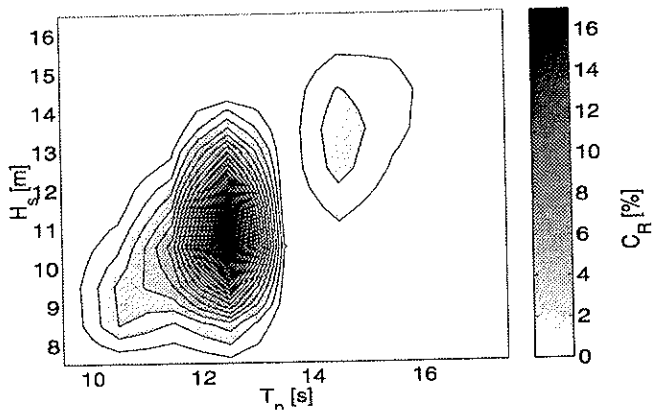

(b) Hogging

Figure 5.19: *Coefficient of contribution, $C_R(si)$, for the nonlinear vertical bending moment midship. S-175 container ship at $Fn = 0.275$.*

$$\text{total contribution} = \sum_{Nsi} C_R(si) \tag{5.29}$$

The chosen sea states can then be applied to estimate the desired nonlinear longterm bending moment, $r^{nl}_{D,Nsi}$. The deviation from the *true* answer with $Nsi = \infty$, can be expressed as the ratio $\frac{r^{nl}_{D,Nsi}}{r^{nl}_{D}}$. The ratio $\frac{r^{nl}_{D,Nsi}}{r^{nl}_{D}}$ versus $\sum_{Nsi} C_R(si)$ is shown in Fig. 5.20 for the S-175 container ship, the tanker and the destroyer. Both zero forward speed and forward speed are represented.

Since the distribution of the $C_R(si)$-values for the S-175 at $Fn = 0.275$ has two maxima, one could wonder if both maxima must be located to get a reasonable long term estimate. For the

sagging, both maxima-regions have $\sum_{Nsi} C_R(si) \approx 50\%$. Looking at Fig. 5.20(a), this will only cause a reduction in the response of about 5%. Including only the sea state with maximum $C_R(si)$-value, enclosed by a circle in Fig. 5.20, causes a reduction of approximately 8% and 14% for hogging and sagging respectively. The small maxima in hogging, has very little effect on the long term response. Excluding this maxima region, causes a reduction of less than 0.5%. For both the tanker and the destroyer inclusion of 50% of the $C_R(si)$-vales cause reduction of approximately 5%.

The degree of nonlinearity is reflected in these figures, see Fig. 5.20(a)-5.20(c). The ratios $\frac{R^{nl}_{D,Nsi}}{R^{nl}_{D}}$ are gathered along one line both for the tankers sagging and hogging response This is probably due to the fact that the response is only slightly nonlinear. The ratios $\frac{R^{nl}_{D,Nsi}}{R^{nl}_{D}}$ for the S-175 container ship and the destroyer show more scatter. This is probably caused by nonlinear effects.

Even if the *approximate* long term analysis and knowledge about the $C_R(si)$-coefficient, will reduce the man hours and computing time, it is still rather time consuming to estimate the long term design value. A further simplification of the long term problem, is to use the contour line approach. This will be studied in the next chapter.

5.4.7 Design Fractile Approach

The contour line approach can be used to predict the D-year response without carrying out a full or an *approximate* long term analysis. As for Gaussian response, the design extreme value will be applied to estimate the D-year value and to account for the randomness in the response. Since the Weibull distribution has been found appropriate for the nonlinear sagging and hogging moment, the design extreme value is found by using Eq.3.61, *i.e.*

$$r^{nl}_{\alpha,design} = \beta\{\ln(\frac{N}{\hat{\alpha}})\}^{1/\gamma} + \delta$$

The design fractiles, α_{design}, are found from linear analysis using contour line approach given in Table 5.3. The design fractiles for the S-175 container ship, the tanker and the destroyer are 90%, 85% and 95% respectively. The duration of the short term sea states are 3 hours and the contour line for the Northern North Sea is shown in Fig. 5.12. The design extreme value is calculated along this contour line and the largest one is chosen as the, design value, $r^{nl}_{\alpha_{design}}$, according to Eq. 5.1. The sea state giving maximum short term response along the 100-year contour line, $H_{s,design}$ & $T_{p,design}$, and the corresponding ratio $r^{nl}_{\alpha_{design}}/r^{nl}_{100}$ are presented in Table 5.9 & 5.10.

The contour line combined with the design extreme value seems to give reasonable estimates of the nonlinear lifetime extreme value. In particular, the results for the tanker are satisfying. This is because the response is only slightly affected by the nonlinearities. The sea state with $\max C_R(si)$ is therefore located close to the $\max C_R(si)$ for linear response. The used design fractile will therefore be accurately determined,, Sect. 5.3.5. The estimated design values for the S-175 container ship and the destroyer is somewhat underestimated. This is because the the nonlinear response has $\max C_R(si)$ at smaller and steeper sea states requiring a higher fractile to

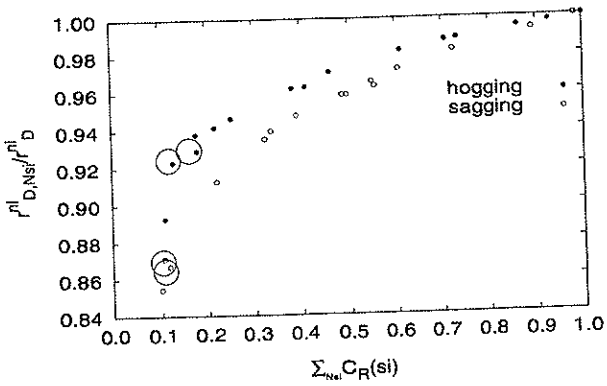

(a) S-175

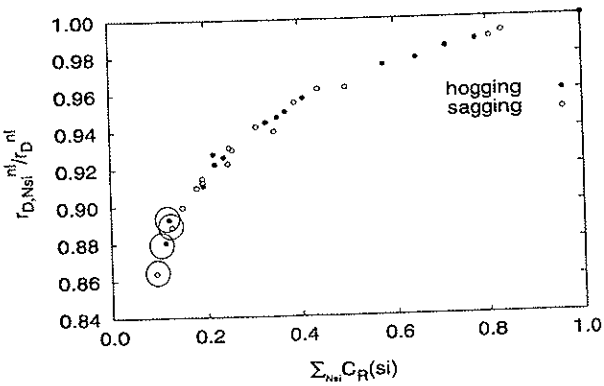

(b) Tanker

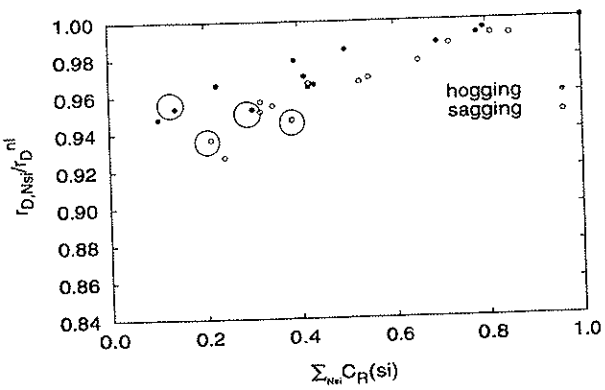

(c) Destroyer

Figure 5.20: *Influence on the estimated* 100*-year value of the vertical bending moment midship due to a reduced number of included sea states. All speeds included. Result using only the sea state with maximum coefficient of contribution is enclosed by a circle.*

Table 5.9: *Ratios between short term extreme values using the design fractile approach and the long term response,* $\frac{r^{nl}_{\alpha_{design}}}{r^{nl}_{100}}$. *Nonlinear sagging response.*

Ship	Fn	α_{design}[%]	$H_{s,design}$ [m]	$T_{p,design}$ [s]	$\frac{r^{nl}_{\alpha_{design}}}{r^{nl}_{100}}$
S-175	0.0	90	13.559	13.761	0.9713
	0.275	90	14.261	14.901	0.9739
Tanker	0.0	85	14.500	15.917	0.9953
	0.2	85	14.500	15.917	1.0303
Destroyer	0.0	95	9.230	9.344	0.9913
	0.2	95	12.437	12.488	0.9754

get $r^{nl}_{\alpha_{design}}/r^{nl}_{100} > 1.0$. One may observe that the underestimation is less than 3% in most cases. One particular result is the estimated life time hogging moment for the destroyer at $Fn = 0.0$. The underestimation is approximately 7%. In the author's opinion, this is due to a combination of a highly nonlinear hogging response and that the $\max C_R(si)$ is far off the corresponding linear location. The fractile, $\alpha_{design} = 0.95$, is therefore too small to estimate this value properly.

However, in design one is looking for the dominant loads. Since the sagging response is satisfactorily estimated by using the design fractiles from linear analysis, the method seems to be useful in order to estimate the lifetime extreme values for nonlinear bending moment midships.

According to the experience in this work, it seems to be reasonable to apply the fractile determined by linear response analysis also for the nonlinear response analysis. A 85% fractile is appropriate for the tanker, but increasing the fractile to 90% will give conservative estimates of the long term extreme value. For the S-175 container ship a 90% fractile is suitable and a 95% fractile is needed for the destroyer.

Table 5.10: *Ratios between short term extreme values using the design fractile approach and the long term response,* $\frac{r^{nl}_{\alpha_{design}}}{r^{nl}_{100}}$. *Nonlinear hogging response.*

Ship	Fn	α_{design}[%]	$H_{s,design}$ [m]	$T_{p,design}$ [s]	$\frac{r^{nl}_{\alpha_{design}}}{r^{nl}_{100}}$
S-175	0.0	90	12.437	12.488	0.9752
	0.275	90	12.437	12.488	0.9746
Tanker	0.0	85	14.500	15.917	1.0059
	0.2	85	14.500	15.917	0.9917
Destroyer	0.0	95	12.437	12.488	0.9297
	0.2	95	12.437	12.488	0.9957

Chapter 6

Effect of Varying Forward Speed on Linear Response

6.1 Introduction

In this chapter, the applicability of the contour line concept for varying forward speed will be studied. The aim is to obtain a reasonable estimate of the 100-year value by a proper choice of stochastic characteristics, *i.e.* to see which short term characteristic is most suitable when the speed is dependent on the significant wave height.

A moving ship will typically reduce speed as the significant wave height increases. The amount of speed reduction will depend on the severity of the sea and the ship master's interpretation of the situation. Therefore, the ship speed can be modelled as a random variable with parameters (mean and standard deviation) depending on the significant wave height, H_s. In such cases, the forward speed should possibly be included as the third dimension in the contour problem, *i.e.* the contour line should be generalised to a contour surface. Herein, the application of contour lines will also be studied in a somewhat simplified manner. The adequacy of $H_s - T_p$ contour lines for various choices of forward speed will be investigated, and the use of $H_s - U$ contour lines for given spectral periods will be studied.

6.2 Long Term Results

To study the adequacy of the contour line concept in the forward speed case, the contour line concept is applied to the ITTC container vessel, S-175. The data and the hull form is presented in Appendix F. Mass distribution is given in Appendix G. The information is taken from 15th & 16th ITTC Seakeeping Committee (1983).

The long term wave climate in the Northern North Sea is used, see Sect. 3.8.2. It is assumed that the short term distribution of the surface elevation is Gaussian.

Assuming the response is linear, the transfer functions can be calculated by using ordinary strip theory, Salvesen et al. (1970) as implemented in VERES, Fathi (1997). Since the sea elevation is Gaussian, the short term distribution of the response maxima is described by the Rayleigh distribution. In this example, the vertical bending moment midship was chosen. The calculation was performed for three different Froude numbers namely $Fn = 0.1$, 0.2 and 0.3, i.e $U = 4.14$, 8.29 and 11.39m/s respectively. The resulting transfer functions are presented in Fig. 6.2.

The long term distribution of the response is calculated by using Eq. 3.67. To simplify the calculation, the vessel is assumed to run in long crested, head sea waves. It is assumed that the heading angle is independent of the significant wave height, *i.e.* β can be removed from Eq. 3.67. Further, the velocity profile for the S-175 container ship is obtained by using the vertical acceleration criteria in Sect. 3.9.3. That is, the limiting significant wave height for a given speed is found by using Eq. 3.91. The limiting wave height is taken to be the minimum value along the operability limiting curve, implying that the vessel can operate in all sea states with significant wave height below the limiting value. A RMS-value of $0.15g$ in the centre of gravity allows for heavy manual work, NORDFORSK (1987). It assumed that there is a deterministic relation between the significant wave height and the forward speed. The resulting "stair case" velocity profile is shown in Fig. 6.1. It must be emphasised that the velocity profile is just an illustrative example, for most practical cases the forward speed is much less than indicated by the present velocity profile.

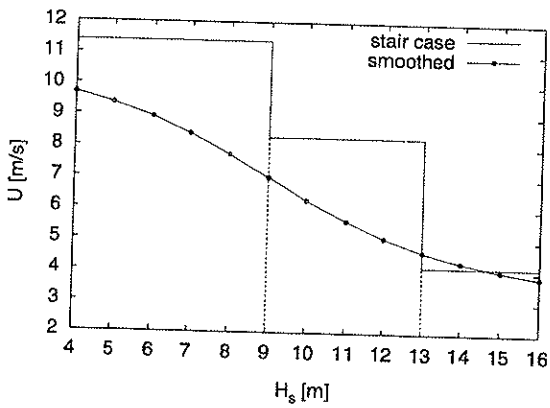

Figure 6.1: *"Stair case" and smoothed velocity profile for the S-175 container ship. Established by use of the acceleration criteria* $0.15g$ *in the centre of gravity.*

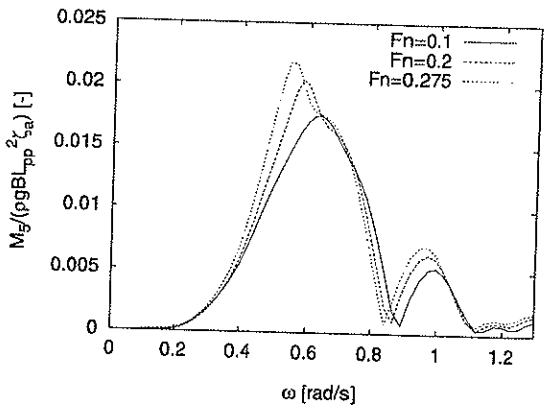

Figure 6.2: *The transfer functions for the vertical bending moment midship in head sea waves for the S-175 at three different forward speeds.*

The lifetime extreme value is first calculated by using the complete long term description of the

Table 6.1: *Lifetime extreme values calculated by using complete long term analysis to selected "areas" of the scatter diagram.*

	Life time extreme value		
Profile	All H_s	$H_s > 8.5$	$H_s > 10.5$
"staircase" profile	1.437	-	-
$Fn = 0.1$	1.314	1.314	1.313
$Fn = 0.2$	1.487	1.487	1.486
$Fn = 0.275$	1.642	1.642	1.641

response. The return period used is 100 years and the Pierson Moskowitz spectrum is used. In order to study the effect of using a velocity profile compared to a fixed speed for all significant wave heights, both a forward speed independent on H_s and "staircase" profile were used. As can be seen from Table 6.1 and Fig. 6.3 the life time extreme value is not significantly affected by the lower sea states. The largest contribution is from sea states with significant wave height ranging from $H_s = 12.5m - 13.5m$. As concerns the "stair case" velocity profile, the corresponding life time extreme value does not differ too much from the values obtained by using constant forward speeds. This is probably due to the fact that the life time extreme values in this case, are in general mainly affected by the velocities in the higher sea states and sea states with a significant wave height at about $11 - 15$ meters, see Table 6.1.

As already mentioned, the environmental contour line for the Northern North Sea will be adopted. Both the contour lines following constant probability density and constant exceedance probability are presented in Fig. 5.2(a). As may be noticed, the contour lines are almost identical in areas with large significant wave height, while the accuracy deceases as one moves towards smaller wave heights. This indicates that in the area of concern, there is no significant difference in using either the lines of constant probability or constant probability of exceedance. However, the latter is used in order to calculate the short term characteristics since the computer code is available and could easily be modified.

6.3 Short Term Results

The 85% fractile for the design extreme value, the expected largest and the characteristic extreme value, see Eq. 3.56-3.58, are calculated along the lines of constant probability of exceedance. The return period for the environmental contour line for the Northern North Sea is 100 years and the duration of the selected sea states are set equal to 3 hours.

The three first figures, Fig. 6.4(a) - 6.4(c) , show the short term characteristics together together with the life time extreme value obtained by using the complete long term analysis with the "stair case" velocity profile given in Fig. 6.1. It is clear that, except for the forward speed $Fn = 0.275$ (U=11.39m/s) in the short term characteristic, neither the expected largest value nor the characteristic extreme value represents proper estimates of the 100-year bending moment. When the highest forward speed is used for all sea states along the 100-year contour line,

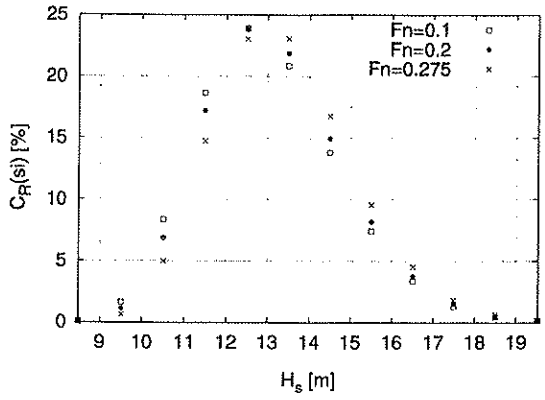

Figure 6.3: *Coefficient of contribution for sea states with $H_s > 8.5m$. Only constant forward speeds were used.*

it is seen from Fig. 6.4(a) that the expected largest value slightly exceeds the 100-year value, while Fig. 6.4(b) shows that the probable extreme value is rather close to the target value. The reason for this is that as $Fn = 0.275$ is used for the most extreme sea states (for which a much lower speed is used in the long term analysis, see Fig. 6.1), it represents "artificial high speed". This means that the fact that the short term variability is omitted by selecting a deterministic short term characteristic is compensated for by using a "too large" forward speed, *i.e.* an inflated forward speed when using the terminology as applied before.

The short term extreme value obtained by adopting the 85% fractile of the extreme value distribution, estimates the 100-year value with good accuracy if a Froude number of $Fn = 0.2$, *i.e.* $U = 8.29m/s$ is chosen, see Fig. 6.4(c). It is seen that the adequacy of the various fractiles depends on the selected speed for the contour line analysis. In Fig. 6.4(d) - 6.4(f) results for various fractiles are shown for three choices of the forward speed. In the figures, the 100-year values as obtained from a long term analysis are also given, both for the "stair case" velocity profile in Fig. 6.1 and for a constant speed. By applying a constant speed in the long term analysis, the 90% fractiles is adequate for all speeds. For the "stair case" profile, the appropriate fractile is dependent on the speed applied to estimate the design extreme value. It seems that the best choice of speed, is the speed in the area of the most influencing sea states, see Fig. 6.1 and 6.3, *i.e.* $Fn \approx 2.0$. Using speeds corresponding to $Fn = 0.1$ and $Fn = 0.275$, the design extreme value will underpredict or overpredict the 100-year value using the "stair case" profile, respectively. To get reasonable results, abnormal fractiles must be applied. However, using the design extreme value at $Fn = 0.2$, reasonable values are obtained for a fractile between $75 - 80\%$. The largest design extremes along the curves in Fig. 6.4(d) - 6.4(f) are also identified and presented in Table 6.2. The design extreme values are normalised both with the life time extreme values from the complete long term analysis using "star case" profile and constant speed. The best fractile should be the one with a normalised value closest to 1.0.

It can be seen from the figures and the table that in case of constant profiles the best fractile seems to vary between $85 - 90\%$. If the "staircase" profile is used, the best fractile seem to be

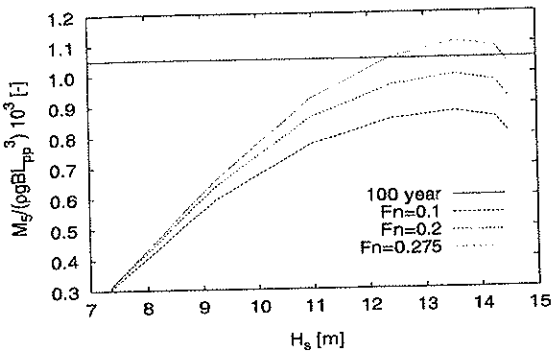

(a) Expected largest value

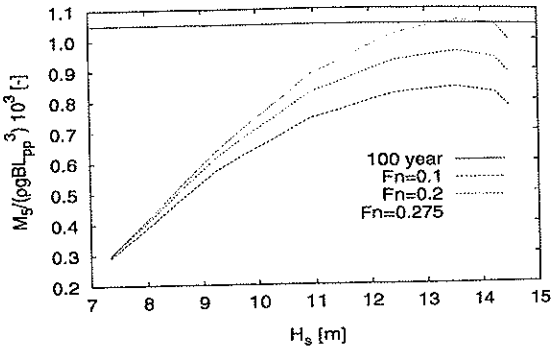

(b) Characteristic extreme value

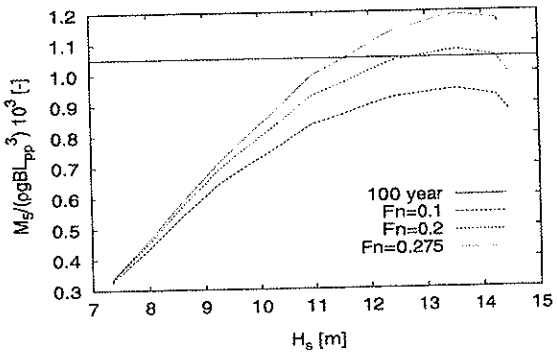

(c) Design extreme value, 85%

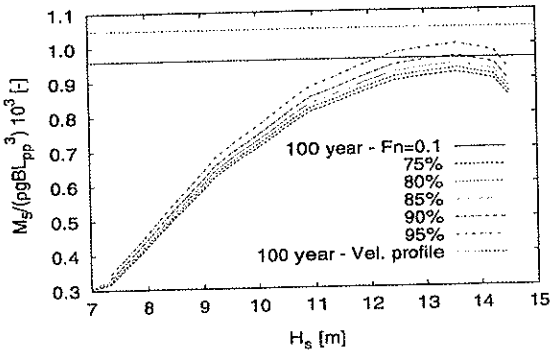

(d) Design Extreme value at $Fn = 0.1$

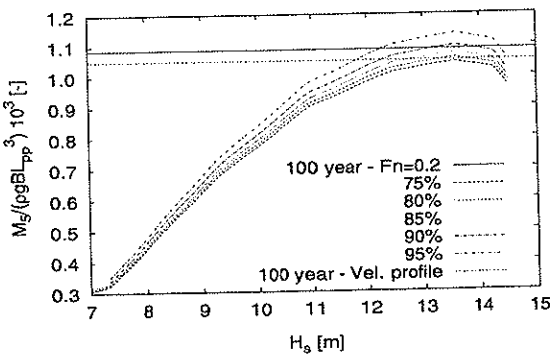

(e) Design Extreme value at $Fn = 0.2$

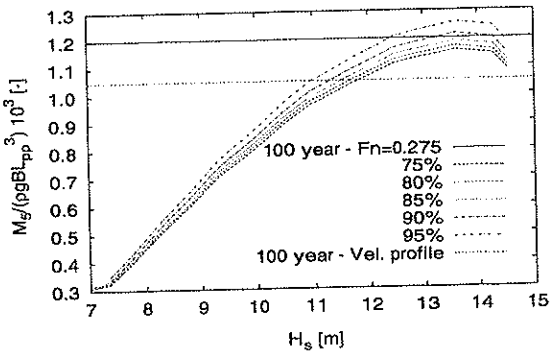

(f) Design Extreme value at $Fn = 0.275$

Figure 6.4: *Fig. 6.4(a) - 6.4(f) show short term characteristics for the vertical bending moment midship at head sea waves for the S-175 container ship.*

Table 6.2: *Design extreme values using different fractiles and forwards speeds. The design extreme values are normalised by the life time extreme value obtained by using the "staircase" profile and constant forward speeds indicated by "stairc." and const. respectively.*

Fractile	75%		80%		85%		90%		95%	
Profile	Stairc.	Const.	Stairc.	Const.	Stairc.	Const.	Stairc.	Const.	Stairc.	Const.
$Fn = 0.1$	0.876	0.957	0.887	0.967	0.901	0.986	0.921	1.007	0.954	1.043
$Fn = 0.2$	0.995	0.961	1.007	0.973	1.023	0.989	1.045	1.010	1.082	1.046
$Fn = 0.275$	1.102	0.964	1.116	0.967	1.134	0.992	01.158	1.013	1.199	1.048

between $75 - 80\%$ for the $Fn = 0.2$. However, a 90% fractile will estimate the design extreme value within an error of 5% in this case. Of course, this is case dependent and other results may be obtained for other heading angles, speeds and vessels.

6.4 Significant Wave Height - Speed Contour Lines

In order to study the use of $H_s - U$ contour lines, the distribution

$$f_{H_sU}(h,u) = f_{H_s}(h) f_{U|H_s}(u|h) \tag{6.1}$$

must be established. The randomness of U given H_s is assumed to be well described by a log-normal distribution. The functional form of this model is given in Eq. 3.82, while the parameters have to be estimated as shown below. The distribution for H_s is assumed to be described by Eq. 3.81.

A smoothed mean velocity versus significant wave height, H_s, is, in view of the illustrative purpose of this study, assumed to be given by

$$\mu_U = -3.0 \arctan\left[\frac{(h-9)}{4}\right] + 7 \tag{6.2}$$

An illustration of the smoothed velocity profile is shown in Fig. 6.1. The coefficient of variation is set constant to 20% for all wave heights. The expected value and the standard deviation of $\ln U$ in terms of μ_U can be found in Bury (1975). The contour lines are generated by the use of the IFORM technique, Ude and Winterstein (1996). The resulting lines for return periods of 10, 100 and 1000 years are shown in Fig. 6.5(a). Looking at Fig. 6.5(a) one may notice that seems to be two forward speed for every significant wave height. This is a result of using the log-normal to describe the randomness given U given H_s, and is not physical. If the exponential distribution is applied instead, the lower region which indicates that U is almost independent of H_s will not occur. The same will occur in Sect. 6.5 where the log-normal distribution is applied to create contour surfaces.

The design extreme values are calculated along the lines of constant probability of exceedance for given values of the peak period for a return period of 100 years. As before, the Pierson

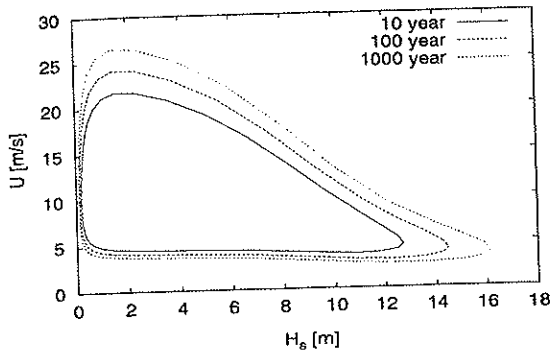

(a) $H_s - U$ contour lines

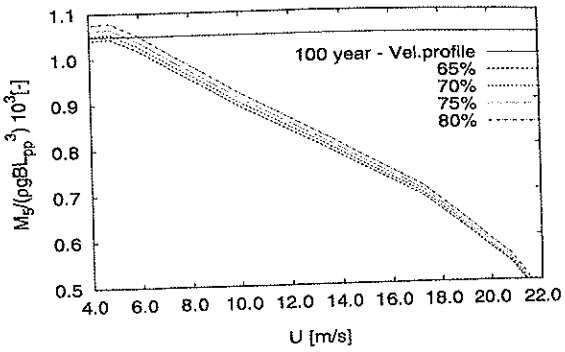

(b) Design extreme value, $T_p = \sqrt{\frac{2\pi L_{pp}}{g}}$

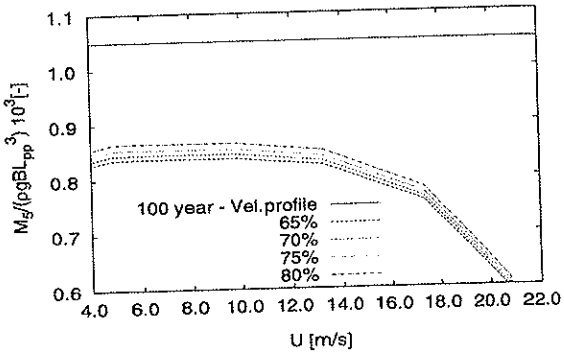

(c) Design extreme value, $T_p|H_s$

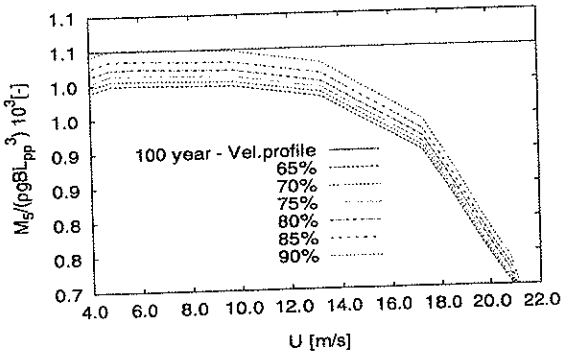

(d) Design Extreme value, $T_p|H_s$

Figure 6.5: *Fig 6.5(a) shows the contour lines for the Northern North sea using the IFORM technique. The design extreme value for different fractiles. The sea state duration is equal to 3 hours in Fig. 6.5(b) and 6.5(c), while 100 hours is applied in Fig. 6.5(d).*

Moskowitz spectrum is applied. Two cases are presented. First the peak period was kept constant such that $T_p = \sqrt{2\pi L_{pp}/g}$, *i.e.* $\lambda = L_{pp}$. Thus the peak of the transfer function will approximately (the peak is somewhat influenced by the forward speed) coincide with the peak of the wave energy spectrum. In the second case, the peak period is equal to the conditional mean value given by Eq. 3.86 indicated by $T_p|H_s$ in the figures. The first and second case are presented in Fig. 6.5(b) - 6.5(d) together with the 100 year life time extreme value obtained by using the complete long term analysis, *i.e.* with a velocity profile given in Fig. 6.1.

Looking at Fig. 6.5(b), it seems like the 70% fractile yield a good estimate of the life time extreme value when T_p is kept constant and selected such that the corresponding wave length coincides with the ship length. One may also notice that it is not the cases with small velocities that give large forces. The cases governing the extremes are situated in the area of large

significant wave height, H_s, and it is of major importance to adopt proper speed to use for these events, see Fig. 6.5(a). This is as expected since the forward speed does not influence the transfer function in any great extent. On the other hand, the response is proportional to the wave height as long as the problem is linear.

When the peak period is set equal to the conditional mean value, a different situation occur. Fig. 6.5(c) shows that in this case, a 3 hour duration is not long enough to estimate the life time extreme value if not very, very high fractiles are adopted. If the mean period is used, a duration of 100 hours must be adopted if a proper short term value shall be obtained at a reasonable fractile level, see Fig. 6.5(d). This suggests that short term variability can be accounted for by selecting a more unfavourable period, T_p, but more strongly it suggests that a full three dimensional contour surface should be recommended for the purpose of estimating the 100-year value by means of short term analysis.

6.5 Three Dimensional Contour Lines

It is seen from the previous pages that for the forward speed case, all three slowly varying parameters, significant wave height, spectral peak period and forward speed, are of importance. Accordingly, a three dimensional contour surface should have been established. It is not possible to read proper subset of parameter combinations of the figure of such a surface, so in practice it has to be given as a set of two dimensional strips of the body. Alternatively, one may provide numerical number for the contour surface in a three dimensional matrix. Although, problem independent contour can be given in any dimension, it is not very attractive to do so for more than three dimensional problems regarding the slowly varying parameters. However, for three dimensional problem it can be done and this will be illustrated below. For higher dimensions one should rather solve the complete long term problem and include the fast process as a random parameter, and further solve the problem by the conventional way or applying IFORM technique.

The three dimensional density function of the three slowly varying parameters are given by

$$f_{H_sT_pU}(h,t,u) = f_{H_s}(h) f_{T_p|H_s}(t|h) f_{U|H_s}(u|h) \tag{6.3}$$

where the models for $f_{H_s}(h)$ and $f_{T_p|H_s}(t|h)$ are given by Eq. 3.81 and 3.82, Haver and Nyhus (1986). The conditional density function for the forward speed, $f_{U|H_s}(u|h)$ is modelled by a log-normal model with a conditional mean forward speed given by Eq. 6.2, and a coefficient of variation equal to 0.2 for all wave heights. It is assumed that the forward speed is independent of the peak period, T_p. The expressions for the parameters of the log-normal model can be found in Bury (1975).

A full long term analysis using the IFORM, Ude and Winterstein (1996), technique is carried out. Based on this analysis, the 100-year bending moment is found to be $1.43 \cdot 10^9 Nm$. This is a result very close to the result, presented in Table 6.1, obtained using a straight forward long term analysis using the simulation program LOSSY, Farnes and Passano (1989). The slowly varying characteristics which together with this extreme value of the fast process defines the design point which are $11.3m$, $13.3s$ and $6.1m/s$. The question now is how well could this

value be predicted by short term analysis if using short term sea state combinations located on the surface corresponding to FORM probability of exceedance $3.42 \cdot 10^{-6}$, *i.e.* the 100-year probability of exceedance for an arbitrary 3-hour sea state. The contour surface is shown in Fig. 6.6.

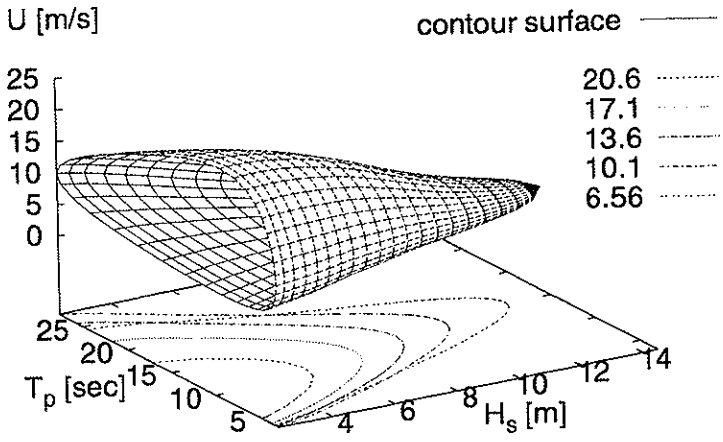

Figure 6.6: *Three dimensional 100-year contour surface for significant wave height, H_s, spectral peak period, T_p, and forward speed, U.*

As short term characteristics, the median and the 90% fractile is adopted. Using the median, the estimated "100-year value" is found to be $1.26 \cdot 10^9$, while the 90% fractile yields $1.41 \cdot 10^9$. This means that the median under predicts the 100-year value with approximately $10 - 15\%$, while adoption of the 90% fractile results is a rather accurate prediction. The sea state parameters and speed corresponding to the 90% fractile results are $13.2m$, $13.6s$ and $5.4m/s$ respectively.

6.6 Conclusion

As forward speed is introduced into the contour problem, it is more complicated to recommend adequate fractiles to be used in connection with two-parameter contour lines (*i.e.* significant wave height, H_s, - spectral peak period, T_p, or significant wave height, H_s, - forward speed, U). If the forward speed is independent of the wave height, proper results are obtained for the 90% fractile. A 90% fractile is suitable, if the change of speed is carried out at the smaller sea states where the coefficient of contribution is low. That is, the speed is constant in and close to the sea state with $\max C_R(si)$ or the design sea state on the contour line.

For varying speed the choice of fractile becomes very dependent on the chosen speed for the

short term sea state on the contour line. When a contour line based on speed and wave height is used, the optimum fractile becomes very dependent on the spectral peak period. It is therefore concluded that for the forward speed case, both significant wave height, spectral peak period and forward speed should be included in the contour problem, *i.e.* a contour surface should be established.

As a three dimensional contour is introduced for the forward speed case, the 90% fractile seems to give adequate results.

A more extensive discussion is given in Sect. 7.7.

CHAPTER 7

Effect of Restricted Service on Linear and Nonlinear Response

7.1 Introduction

A ship master may avoid severe weather by manoeuvre the vessel into calmer sea areas or simply keep the vessel anchored in harbour until the weather has calmed down. In this chapter, the operational restrictions, see Sect. 3.9 and Fig. 3.7, will be used to study the latter,- namely the effect on the response due to restricted service.

The aim is to study the effect of restricted service on the linear and nonlinear long term responses and how the model weather restrictions can be accounted for in the long term analysis. It is further the purpose, to find a model which can be used in combination with the contour line approach based on the fractiles determined in Ch. 5. Different methods to model the restricted service will be presented and the use of contour line concepts applicability will verified. The effect of varying forward speed is not included.

Prediction of transfer functions and nonlinear, time domain simulations of the vertical bending moment midship are conducted using the simulation program LANWIL, see Appendix A.1.2. The estimated transfer functions will be similar to the transfer functions obtained by using the simulation program VERES, Fathi (1997), since they are both based on linear, strip theory.

7.2 Linear, Long Term Response Due to Restricted Service

To study the effect of restricted service on the long term vertical bending moment midship, the ITTC container ship S-175 is chosen. The data and hull form is given in Appendix F. Mass

distribution is given in Appendix G. The Northern North Sea is chosen as sea environment, see Eq. 3.80 - 3.82 and Haver and Nyhus (1986). The vessel is running in long crested, head sea waves with constant forward speed.

The operability limiting boundaries are established on basis of the sea keeping criteria presented in Sect. 3.9, *i.e.*

- Vertical acceleration at CG
- Vertical acceleration at FP
- Green water on deck
- Slamming at FP

A RMS-value of $0.15g$ in the centre of gravity, CG, allows for heavy manual work. $0.15g$ is also applied for vertical acceleration at the fore perpendicular, FP. Green water on deck has been calculated for a probability of 7%. The slamming criteria is found by calculating the k-factor using Slam2d, Heggelund et al. (1998), and defining a critical pressure, P_{crit}. The critical pressure is set to be 60% of the hydrostatic pressure, Hoff (1999). The probability of slam is 3%. For more information see Sect. 3.9.

The linear, long term extreme response is calculated by using Eq. 3.92. That is the upper limit of the significant wave height is changing as the peak period increases. Since the vessel is only present in selected parts of the scatter digram limited by the operability limiting curves, see Fig. 3.7, this represents long term responses due to restricted service when the ship master seeks shelter in a harbour. As shown in Sect. 5.4.6 there is only a few sea states which do contribute to the long term response. Therefor one may approximate the limiting boundary by the minimum value of $H_s^{lim}(T_p)$ and still expect that a reasonable estimate of the long term response due to restricted service should be obtained. The operability limiting curve is approximated as

$$\tilde{H}_s = \min H_s^{lim}(T_p) \tag{7.1}$$

The ratios between the linear, long term vertical bending moment using $H_s^{lim}(T_p)$ and $\tilde{H}_s$ as upper limits respectively are presented in Table 7.1. It seems that there is a small difference in the estimated moments using the two methods except for two cases. That is the sea keeping criteria "Vertical acceleration at FP" at $Fn = 0.2$ and $Fn = 0.275$. The value $\tilde{H}_s$ is small, *i.e.* $\min H_s^{lim}(T_P) < 4m$, for these two speeds. This may indicate the approximate operability limit should be applied with care for small limiting significant wave heights.

7.3 Modification of the Scatter Diagram

Restricted service may also be modelled by creating a scatter diagram which takes into account the fact that the ship master prefers the calmer sea state. The modification of the original, simultaneous distribution $F_{H_s,T_p}(h,t) = F_{H_s}(h)F_{T_p}(t|h)$ into $\hat{F}_{H_s,T_p}(h,t) = \hat{F}_{H_s}(h)F_{T_p}(t|h)$ will be discussed in the following.

Table 7.1: *Ratios between the linear, long term vertical bending moment midship using $H_s^{lim}(T_p)$ and the result by using $\tilde{H}_s$ as the upper limit. S-175 at four different foward speed in head sea waves in the Northen North Sea. Return period is 100-years.*

	Limiting criteria			
Fn	Vertical acceleration at CG	Vertical acceleration at FP	Green water on deck	Slamming at FP
0.0	1.0	1.038	1.009	1.048
0.1	1.0	1.040	1.006	1.008
0.2	1.004	1.166	1.005	1.070
0.275	1.002	1.157	1.051	1.050

Scatter diagram which takes into account the effect of restricted service may be modelled in different ways. Three different methods are applied herein. The first method is to truncate the distribution. Physically, truncation may be compared to a situation where the ship master is never present in sea states with significant wave height larger than $\tilde{H}_s$. In reality, some variability should be allowed for. The truncated area above in the distribution function should have been added the distribution somewhere between $H_s = 0 - \tilde{H}_s$ depending on how the bad weather is avoided. Most likely, the area should have been added just below the limit $\tilde{H}_s$, since the ship master will in general only manoeuvre into slightly better weather. In this work it assumed that the probability density above the truncation limit can be divided uniformly between $H_s = 0 - \tilde{H}_s$. A truncated distribution with upper limit H_s^{lim} is given as, Bury (1975);

$$\hat{F}_{H_s}(h) = \frac{F_{H_s}(h)}{F_{H_s}(\tilde{h}_s)} \tag{7.2}$$

Truncation of the Weibull distribution is illustrated in Fig. 7.1 where the continues line is the original Weibull distribution. The truncation limit is set to be $5m$ due to illustrative purposes. In order to establish the contour lines, IFORM transformation is applied, see Appendix I. The significant wave height using the truncated Weibull distribution is simply given by

$$h = \beta[-\ln(1 - \hat{\Phi}(U_1))]^{1/\gamma} \tag{7.3}$$

where $\hat{\Phi}(U_1) = \Phi(U_1)F_{H_s}(\tilde{h}_s)$. However, the ship master will in general also be in larger sea states. This encourages establishment of distribution with tail. In this work, the second and third method are modifications the Weibull-distribution describing the behaviour of the significant wave height, H_s by

- Rescaling of the Weibull distribution
- Reshaping of the Weibull distribution

Rescaled and reshaped Weibull distribution describes the situation where the ship master manoeuvre into calmer areas and some variability around the limiting value, $\tilde{H}_s$, is allowed for. The rescaling of the of Weibull distribution is done by finding a new scale parameter β^*. The scale

parameter $\beta^\star$ will be applied in the Weibull distribution instead of β which is the original scale parameter from Sect. 3.8.2. The scale parameter might be determined by letting $\tilde{H}_s$ represent the D-year sea state. Meaning that in the modified scatter diagram, the significant wave height will only exceed $\tilde{H}_s$ once every D-year. This method is chosen since the classical contour lines are determined in this manner. The new scale parameter is given as

$$\beta^\star = \frac{\tilde{h}_s}{[-\ln(\frac{1}{DN_s})]^{1/\gamma}} \tag{7.4}$$

where N_s is the number of sea states within a year. Thus DN_s is the number of sea states in D-years. The IFORM transformation gives

$$h = \beta^\star[-\ln(1-\hat{\Phi}(U_1))]^{1/\gamma} \tag{7.5}$$

The third method applied in this work, was to reshape the Weibull distribution to take into account restricted service. The procedure is similar to the one above. That is $\tilde{H}_s$ represent the D-year sea state This will give us

$$\gamma^\star = \frac{\ln(-\ln(\frac{1}{DN_s})}{\ln(\frac{\tilde{h}_s}{\beta})} \tag{7.6}$$

where $\gamma^\star$ is the new shape parameter. Accordingly, the IFORM transformation is written as

$$h = \beta[-\ln(1-\hat{\Phi}(U_1))]^{1/\gamma^\star} \tag{7.7}$$

The distribution of the significant wave height consists of both the log-normal and the Weibull distribution. Since the Weibull distribution is changed so that restricted service is taken in to account, also the log-normal distribution must be changed. That is since the cumulative distribution should be equal to one when h is large. In this work this is approximately done by setting the value of the cumulative log normal distribution equal to the cumulative *new* Weibull distribution at the shift point $h = \eta$, see Eq. 3.81. The procedure will be equivalent for all three modifications of the Weibull distribution. That is

$$\Phi(\frac{\ln\eta - \mu_{\ln H_s}}{\sigma^\star_{\ln H_s}}) = \hat{F}_{H_s}(\eta) \tag{7.8}$$

The new scale parameter in the log-normal distribution valid for $h \leq \eta$ is estimated as

$$\sigma^\star_{\ln H_s} = \frac{\ln\eta - \mu_{\ln H_s}}{\Phi^{-1}(\frac{\ln\eta - \mu_{\ln H_s}}{\sigma^\star_{\ln H_s}})} \tag{7.9}$$

The IFORM transformation for the log-normal distribution will be given as

$$h = \exp\{\mu_{\ln H_s} + \sigma^\star_{\ln H_s} U_1\} \tag{7.10}$$

It seems that the part of the scatter diagram which is described by the log-normal distribution, does not affect the estimated long term response significantly, except for cases where the limiting significant wave height is close to the shift value η. How the log-normal distribution is modified is therefore of no importance for the final result. The contour lines for the Northern North sea

by applying the Weibull distribution which is either truncated at $\tilde{H}_s$ or rescaled or reshaped by letting $\tilde{H}_s = H_D$ are given in Fig. 7.2. H_D is the D-year significant wave height. The log-normal distribution is rescaled depending on the modification on the Weibull distribution.

A comparison of the two different modifications are shown in Fig. 7.1 together with the truncated distribution and the original Weibull distribution. The new scale and shape parameters, $\beta^\star$ and $\gamma^\star$ is found by letting $\tilde{H}_s$ represent the 100-year significant wave height. $\tilde{H}_s = 5$ is chosen for the purpose of illustration. The figure shows that a rescaled distribution has smaller density in the tail then the reshaped distribution. Which implies that the reshaped distribution allows for more severe sea states. Accordingly, larger long term responses are expected.

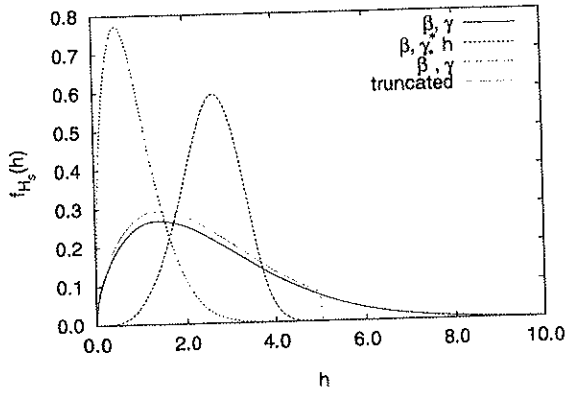

Figure 7.1: *The original Weibull density distribution with scale and shape parameters β and γ. Rescaled and reshaped Weibull distributions with scale and shape parameters $\beta^\star$ and $\gamma^\star$ respectively and truncated Weibull distribution. The operability limit is equal to $\tilde{H}_s = 5.0m$.*

7.4 Linear and Nonlinear Long Term Response Using the Modified Scatter Diagram

The linear, long term vertical bending moment midship using the modified scatter diagram $\hat{F}_{H_s,T_p}(h,t)$ of the Northern North Sea is calculated for the S-175 container ship, see Eq. 3.93. It is assumed that the short term maxima distribution is well described by the Rayleigh distribution. The vessel is running in long crested, head sea waves. The forward speed is constant. Results are presented in Fig. 7.3 as a function of the limiting significant wave height $\tilde{H}_s$. For the truncated scatter diagram this represents an upper limit and the vessel is never present in higher sea states. The rescaling and reshaping allows for some variability around the limiting value.

It is interesting to note that the r^l_{100} values for the vertical bending moment midship obtained by a truncated scatter diagram, are very close to the long term results obtained using the operability limit given by $\tilde{H}_s$. The difference is in the range $0.01 - 0.1\%$ and therefore negligible. This is because the value $\frac{1.0}{F_{H_s}(\tilde{h}_s)}$ is close to 1.0, even for wave heights close to the shift parameter

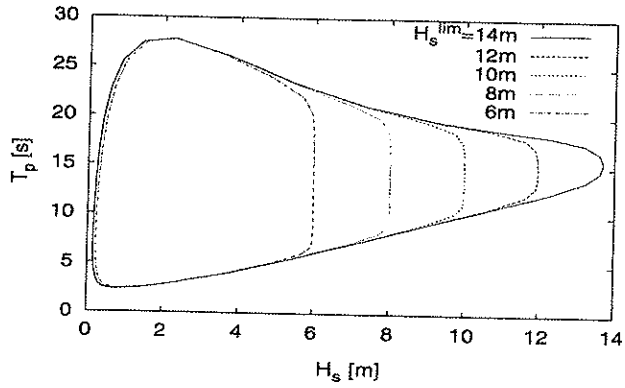

(a) Truncation

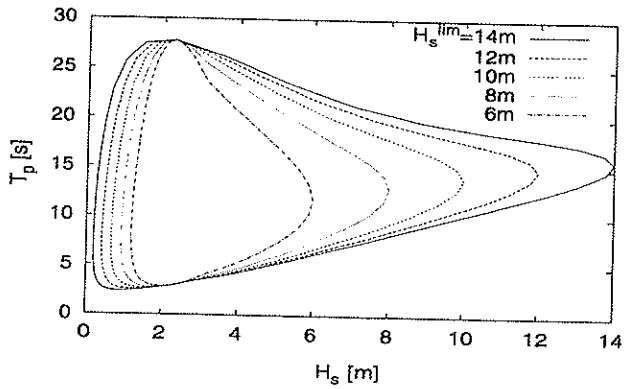

(b) Rescaled, β^*

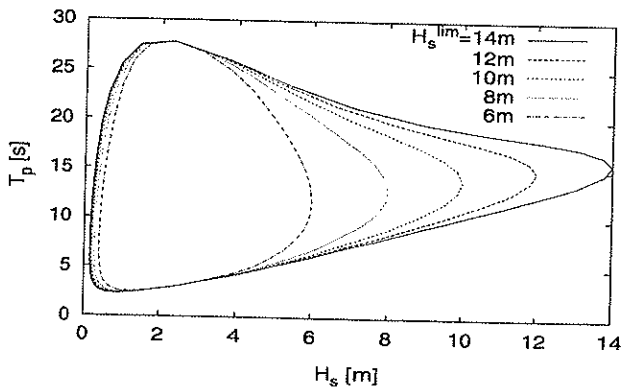

(c) Reshaped, γ^*

Figure 7.2: *Contour lines of the Northern North Sea for a return period $D = 100$ years for limiting significant wave height, $\tilde{H}_s$.*

η. That is why there will not be a large difference between these two methods. If the truncated distribution is found appropriate to model the restricted service, it is simpler to do long term analysis using the operability limit $\tilde{H}_s$ as discussed in Sect. 7.2. The final results will be almost equivalent.

All three models of $\hat{f}_{H_s,T_p}(h,t)$, show that the linear, long term vertical bending moment midship decreases rapidly as the limiting significant wave height decreases, see Fig. 7.3. As expected, the truncated distribution will give larger response values than the other two methods. This is also expected since the vessel spends more time in rough weather than using the two other models of $\hat{f}_{H_s,T_p}(h,t)$. The rescaling gives the smallest 100-years values when compared to using truncation and reshaping of the scatter diagram. This is because rescaling will give a model where the vessel spends more and more time in the smaller sea states as $\tilde{H}_s$ decreases. This is not the case for the reshaping, see Fig. 7.1. Accordingly the results will be somewhere between the long term results using the rescaled and truncated distribution.

Also the nonlinear, long term vertical bending moment midship, r^{nl}_{100}, is calculated. The Weibull distribution is applied to describe the distribution of the maxima , see Sect. 5.4.4. The LRNM method is used to create the maxima samples, Sect. 5.4.3. The simulation time was set to three hours according to experience made previously. In order to limit the number of simulation, the procedure given in Sect. 5.4.5 was applied. The effect of restricted service is modelled by applying the rescaled scatter diagram with limiting significant wave height equal to $10m$. The 100-year long term sagging and hogging moments are given in Table 7.2 . Also the most contributing sea states are given together with the coefficient of contribution, $C_R(si)$. The ratios $\frac{r^{nl}_{100}}{r^{l}_{100}}$ for sagging are smaller than the corresponding values given in Table 5.6, when the original scatter diagram was applied. That is simply because the degree of nonlinearity decreases when the included sea states are less severe. This argument can also be used to explain why the ratios are larger than the corresponding values in Table 5.7 for the hogging response. A comparison between the nonlinear long term value in restricted versus unrestricted service are given in the last column in Table 7.2. A 30% reduction of the sagging moment is experienced when severe sea states above $10m$ are avoided. The restricted service has an effect of $15-20\%$ on the hogging moment.

Table 7.2: *100-year nonlinear vertical sagging and hogging moment midship for the S-175 container ship, r^{nl}_{100} Effect due to restricted service is taken into account by applying a rescaled scatterdiagram for an operability limit at $\tilde{H}_s = 10m$, see Fig. 7.2(b). The values are made nondimensional w.r.t. to corresponding linear value, r^{l}_{100}, and nonlinear value $r^{nl,unrest}_{100}$, in unrestricted service.*

	Fn	$H_{s,\max C_R(si)}$ [m]	$T_{p,\max C_R(si)}$ [s]	$\max C_R(si)$ [%]	$\frac{r^{nl}_{100}}{r^{l}_{100}}$	$\frac{r^{nl}_{100}}{r^{nl,unrest}_{100}}$
sagging	0.0	9.5	12.5	19.34	1.81	0.71
	0.275	8.5	12.5	23.76	2.21	0.71
hogging	0.0	8.5	11.5	17.64	0.86	0.82
	0.275	8.5	12.5	14.87	0.69	0.85

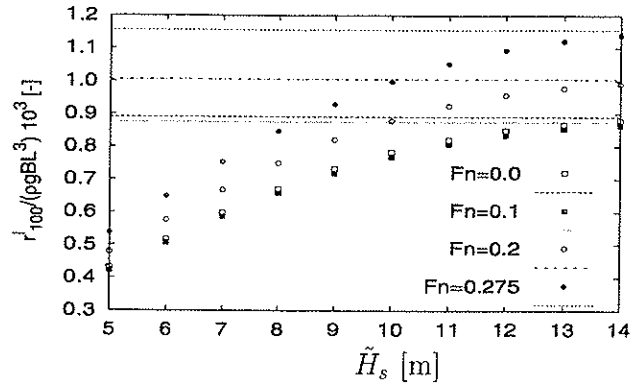

(a) Truncation

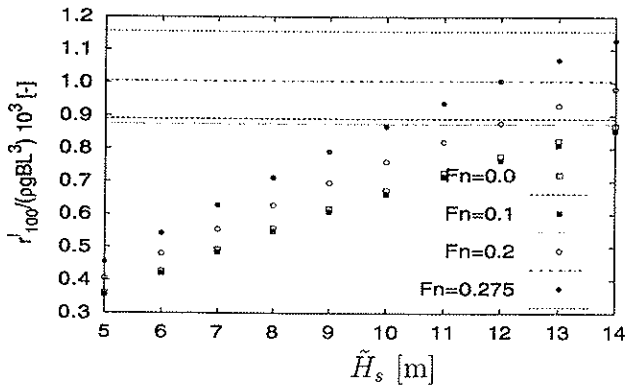

(b) Rescaled, β^*

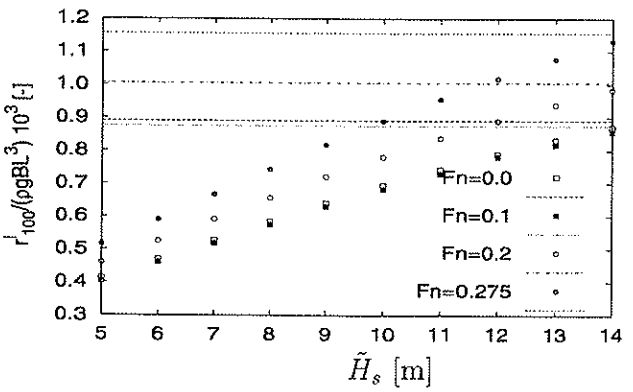

(c) Reshaped, γ^*

Figure 7.3: *Long term* 100*-year linear, vertical bending moment midship for the S-175 container ship in head sea waves. Scatter diagrams which are modified for restricted service are applied. Weather restrictions are indicated by the value* $\tilde{H}_s$*. The long term values in unrestricted service are included lines.*

7.5 Linear and Nonlinear Long Term Response Using Modified Contour Lines

The long term response is obtained by using the the scatter diagram with contour line as shown in Fig. 7.2(b). The return period for the environmental contour line for the Northern North Sea is 100 years and the duration of the sea states along the line is three hours. The design extreme value with an appropriate fractile has in this work shown to be adequate for unrestricted service, Ch. 5. Based on the linear term results in Ch. 5, the fractile $\alpha_{design} = 90\%$ is chosen for the S-175 container ship, see Table 5.3. This is done because the fractile must be known on beforehand. If the fractile from linear analysis applicable also in restricted service it is convenient.

The linear design value is given by Eq. 3.58. All three modifications of the scatter diagram are applied in the analysis. Fig. 7.4 shows the estimated 100-year values of the linear, vertical bending moment midship using the contour line approach. The results using the truncated scatter diagram are given in Fig. 7.4(a), while Fig. 7.4(b) and 7.4(c) show the obtained results using the rescaled and reshaped scatter diagram respectively. The 100-year values conducting a complete long term analysis given on the ordinate are equivalent to those presented in Fig. 7.3.

Truncating the scatter diagram, will underestimate the long term response in most cases if the contour line approach is applied. One could suggest to solve the problem by increasing the fractile. However, the fractile will be dependent on the value $\tilde{H}_s$ since the underestimation increases as the value $\tilde{H}_s$ decreases, see Fig. 7.4(a). This indicates that a truncated distribution is not particularly applicable combined with the contour method. However, if restricted service is modelled by rescaling of the scatter diagram, the contour line approach gives acceptable results even for the smallest limiting wave heights, *i.e.* $r^l_{100} \approx r^l_{0.90}$. This is because the modified scatter diagram has got a new form, while the truncation only "adds" probability without changing the form of the distribution. Changing the form will move the location of the sea state with $\max C_R(si)$ relatively, while in a truncated distribution the sea state $si = (H_s, T_P)_i$ will be located at the truncation point as long as $H_{s,i} \leq \tilde{H}_s$. Reshaping the scatter diagram will give reasonable good estimates of the long term response using the contour approach for the largest long term values. Some scatter is observed at the lower long term values. This implies that using the contour line, rescaling of the scatter diagram will be most applicable combined with the contour line approach since the long term maxima can estimated accurately.

The 100-year values for the nonlinear, vertical bending moment midship are estimated using the contour lines of the rescaled scatter diagram with limiting, significant wave height $\tilde{H}_s = 10m$. The design extreme values are calculated using Eq. 3.61, since the Weibull distribution has shown to be appropriate to describe the maxima distribution. The simulation time is set to three hours. According earlier experience, a 90% fractile is applied for this vessel. The dimensionless values are given in Table 7.3 together with the design point on the contour line. A 90% fractile seems to produce long term values close to the target value since the dimensionless values are close to unity for both sagging and hogging at $Fn = 0.0$ and $Fn = 0.275$.

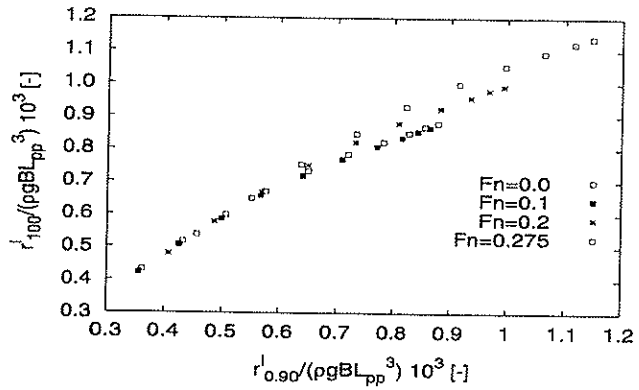

(a) Truncation

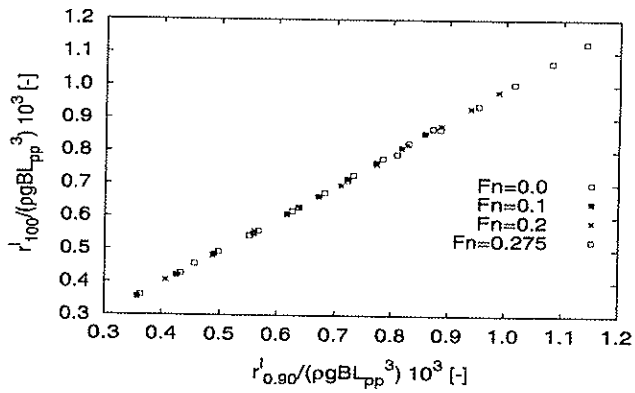

(b) Rescaled, β^*

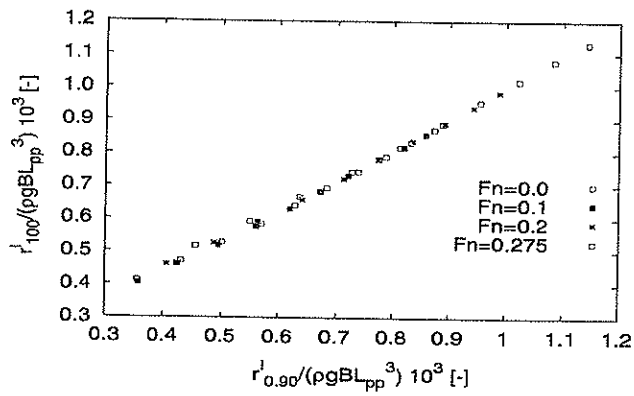

(c) Reshaped, γ^*

Figure 7.4: *Comparison of linear, long term maxima, r^l_{100}, with the design value, $r^l_{0.90}$, determined by the contour method. Results for the S-175 container ship at different speeds and limiting significant wave heights, $\tilde{H}_s$, see Fig. 7.3.*

Table 7.3: *Comparison of nonlinear, long term maxima, r^{nl}_{100}, with the design value, $r^{nl}_{0.90}$, determined by the contour method based on operability restriction with rescaled scatter diagram. Nonlinear sagging and hogging response for the S-175 container ship with a limiting significant wave height $\tilde{H}_s = 10m$, see Fig. 7.3.*

	Fn	$H_{s,design}$ [m]	$T_{p,design}$ [s]	$\frac{r^{nl}_{a_{design}}}{r^{nl}_{100}}$
sagging	0.0	9.832	12.789	1.0270
	0.275	9.832	12.789	1.0145
hogging	0.0	9.348	11.548	1.0043
	0.275	9.832	12.789	0.9854

7.6 Conclusion

The limiting operability limits, $H_s^{lim}(T_P)$, can be approximated by setting the limiting significant wave height for all period equal to the minimum value along the operability limiting curve, *i.e.* $\tilde{H}_s = \min H_s^{lim}(T_p)$. The estimated long term extreme value will not be significantly affected by this approximation.

Effects due to restricted service might be modelled by truncation of the simultaneous distribution $F_{H_s,T_p}(h,t) = F_{H_s}(h)F_{T_p}(t|h)$ into $\hat{F}_{H_s,T_p}(h,t)$. A truncated distribution does not allow for any variability around the operability limit, *i.e.* the vessel is never present in sea states with significant wave heights larger than $\tilde{H}_s$. The two other modifications of the scatter diagram allow for some variability at $\tilde{H}_s$. Probably the reality should be modelled as something between a truncated distribution and a rescaled or reshaped distribution.

Long term analysis using a truncated model, will give approximately the same long term responses as performing long term analysis with an approximate operability limit $\tilde{H}_s = \min H_s^{lim}(T_p)$ as upper limit.

All three modification of the scatter diagram show that the linear, long term response decreases rapidly as the limiting significant value, $\tilde{H}_s$, decreases. Rescaling yields the lowest long term values, while the reshaping gives somewhat larger long term extremes and truncation gives the largest values. The maximum difference between the long term values using truncated and rescaled distribution is as much as 20%. The nonlinear, long term value is found based on operability restriction with rescaled scatter diagram using $\tilde{H}_s = 10m$ as upper limit. The long term vertical sagging is reduced by 30%, while hogging moment is reduced by approximately $15-20\%$ compared to values obtained in unrestricted service.

It seems that if restricted service should be modelled, rescaling of the scatter diagram is preferred if the contour line approach should be applied in order to find the lifetime extreme value. Using the contour line approach in combination with truncated and reshaped scatter diagram, will in most cases underestimate the long term extreme value.

The contour line approach is able to reproduce the 100-year long term extreme values. Proper results are obtained using a 90% fractile for both linear and nonlinear response independent on the forward speed. One should remember, that the speed is kept constant in these analysis. If however, the speed is dependent on the wave height, the forward speed should probably be included as a third variable, *i.e.* a contour surface should be established. When restricted service is considered, the most contributing sea states, *i.e.* $\max C_R(si)$, are more likely concentrated in areas where the vessel experiences speed changes.

7.7 Conclusive Remarks to the Contour Line Approach

As mentioned in Ch. 1 one of the objectives of the thesis, was to contribute to develop a simplified method for calculating design loads on modern ships. Both probabilistic and nonlinear character of the load should be accounted for. It is important to know how the simplifications affect the accuracy of the estimated design loads in view of saved man efforts and computation time. This is in particular important if the response is nonlinear and simulation in the time domain must be performed. The conventional long term analysis will become both complicated and time consuming. The accuracy will be discussed assuming that error less than approximately 5% is negligible. It is also important to note that the response mentioned herein refers to the vertical bending moment midship.

If the response is linear, conventional long term analysis is rather straight forward. The analysis is neither complicated nor time consuming, and operability restrictions can easily be accounted for. The contour line approach, *i.e.* design extreme values together with an appropriate fractile in selected sea states given by the contour line, can be a good alternative if contour curves are readily available and statistical tools for conventional long term analysis are not in hand. If the contour curves must be established, a complete long term analysis can be equally considered. In this work, the linear response analysis has been applied to verify the contour line methods applicability for later use in connection with nonlinear, long term response analysis. In the case studies different response cases have been studied in connection with the contour line approach. That is

- linear and nonlinear response
- unrestricted and restricted service

where restricted service can further be divided into

- varying forward speed and manoevring in order to avoid severe sea states

For linear response in unrestricted service a fractile of 90% seems reasonable for most ships, but for vessels with length smaller than $160m$ the fractile can advantageously be increased to 95%. This fractiles yield reasonable results at all headings.

For nonlinear response, the fractile obtained using linear response analysis gave reasonable estimated for the nonlinear vertical bending moment midship for the S-175 container ship, tanker

and the mariner. For these vessels 90%, 85% and 95% fractiles were applied respectively. Using the fractile to 90% for the tanker will give conservative results. In particular good results were obtained for sagging response. At one occasion, the hogging response was underestimated by as much as 7%.

For linear response and varying forward speed the following is observed for the S-175 container ship:

- A 90% fractile is suitable when change of forward speed is performed at wave heights lower than the sea sates which yields maximum contribution to the long term extreme value. That is, the speed which should be applied in the sea states given by the contour line is constant in and close to the region containing the sea state with $\max C_R(si)$ or the design sea state on the contour line.

- If change of speed is conducted close to the sea state which yields maximum response, care should be exercised in choosing the appropriate speed to be applied in the contour line approach. A possibility is to chose the largest speed. A 90% fractile will yield a conservative estimate of the long term extreme value.

- Application of $H_s - U$ contour is questionable since the fractile will be highly dependent on the peak period applied in the short term analysis.

- Introducing the forward speed as a third variable, a $H_s - T_p - U$ contour surface can be established. A 90% fractile gives tolerable results of the long term extreme value using the contour surface.

Operability restrictions such as manoevring in order to avoid severe sea states, can be modelled by modifying the scatter diagram. Truncation, rescaling and and reshaping of the scatter diagram are used in this work. A truncated distribution does not allow for any variability around the operability limit, while this is allowed for using reshaping or rescaling of the scatter diagram. The best picture of the reality is most likely a combination of the former and one of the two latter modifications of the scatter diagram.

For linear response for the S-175 container ship accounting for manoevring in order to avoid severe sea states, all three modifications above are applied. The following is experienced:

- A truncated distribution is fairly easy to establish, but can not be applied in combination with the contour line approach since the fractile will be dependent on the operability limit, *i.e.* the fractile must be increased as the limit decreases.

- A reshaped scatter diagram will in general underestimate the long term extreme value using the contour line approach. The underestimation increases as the limiting significant wave height decreases.

- Rescaling of the scatter diagram gives reasonable estimates of the long term extreme value using 90% fractile for the S-175 container ship.

For nonlinear response only rescaling of the scatter diagram is used to take into account the effect of manoevring. A 90% fractile is suitable to estimate the long term extreme sagging and hogging values for the S-175 container ship.

The linear and nonlinear long term extremes will be reduced when the effect of manoevring in order to avoid severe sea states is taken in to account.

In this work the attention has been put on the contour line approach as an efficient tool to estimate the long term extreme values which is in particular important for the nonlinear response. Compared to estimation of the nonlinear, long term extreme value using approximate long term analysis, Sect. 5.4.5, the latter involves search for the most contributing sea states to be be applied in the long term analysis. The method is dependent on experience and is somewhat more elaborate than the contour line approach. The contour line method is more specific and easy to apply. For the cases used in this work, approximately 5-6 simulations are performed to estimate the nonlinear, long term extreme value. It is in the authors opinion that at least 9 simulations must be performed for the approximate long term analysis. This is to ensure that the sea state with maximum contribution to the long term value is captured which is required to get an acceptable estimate.

Nonlinear response taken into account such as varying forward speed and restricted manoevring using the truncated model or the reshaped model is not considered in this work. It is in the authors opinion, that nonlinear response can be treated as the linear response if the speed is dependent on the significant wave height. Regarding the restricted manoevring, it is emphasised that the main purpose was to apply the contour line approach and none of the two modifications mentioned here was promising. However, modelling the restricted service due to manoevring using a truncated scatter diagram is probably easy to use together with the approximate long term analysis which procedure is described in Sect. 5.4.5.The sea state with maximum coefficient of contributions is always located close to the truncation limit. The requirement is that the significant wave height where the truncation is conducted is smaller than the original significant wave height with maximum coefficient of contribution. The sea state is easy to locate and a long term estimate can be obtained with a small number of simulations. However, this kind of analysis is not performed in this work.

A large number of linear response analysis and a significantly smaller number of nonlinear analysis have been performed. The purpose is to apply the fractile from linear analysis, to estimate the nonlinear, long term extreme values. It seems that fractiles to be applied for both linear and nonlinear analysis, can be determined for linear response in unrestricted service in head sea with zero forward speed. It is reason to believe that the fractiles can be applied when the effect of operability restrictions should be accounted for, in accordance with the work presented in this thesis, for both linear and nonlinear response. More nonlinear simulations are required to fully confirm the the contour method's accuracy. It is in the authors opinion that both the linear and nonlinear response analysis give a good impression of the applicability of the contour line approach.

Chapter 8

Conclusions and Suggestions for Further Work

The intention of this study has been to investigate the uncertainty in the hydrodynamic models applied to estimate the vertical bending moment midship. In addition, efficient long term analysis and a simplified method to estimate the long term extreme value based on the contour line concept are presented and verified for both linear and nonlinear response applying different vessels, forward speeds and operational restrictions.

The main conclusions are presented in the following chapters assuming that error less than approximately 5% is negligible. It is important to note that the response mentioned to herein refers to the vertical bending moment midship.

8.1 Uncertainty Analysis

The uncertainty of the theoretical models used to estimate linear, Salvesen et al. (1970), and nonlinear response, Wu and Moan (1996), Wu et al. (1996), are studied. The hydrodynamic theories are incorporated into the simulation programs VERES, Fathi (1997), and LANWIL respectively, see Appendix A. The conclusions drawn from this work are presented in the next two sections.

8.1.1 Modelling of Uncertainty in Linear Strip Theory

The model error of the transfer function is given as a function of the wave frequency. Different types of errors were tested. The transfer function uncertainty was modelled by the difference between the measured and predicted transfer function value. Due to lack of experimental data, it is concluded that the model error could be modelled using cubic splines. This is the most well behaved model error. However, one should remember that with limited experimental data

points, no approach is ideal.

The uncertainty in the transfer function is characterised by calculating the corresponding long term extreme value. The uncertainty in the long term extreme values is found by quantifying the ratio between the true and the predicted long term extreme value, *i.e.* the ratio between the measured and predicted value respectively. The return period has no significantly influence on the relative error. Meaning, the values found in this work for a return period of hundred years can be applied also for other return periods.

Sensitivity analysis shows that there is a limited region of the transfer function that contributes to the long term extreme values. The study justifies that only the model error of the main peak of transfer function need to be modelled.

A significant scatter is observed comparing estimated, relative error for a given wave heading for the different vessels. In particular, one should notice that there is a discrepancy between the relative error for a given vessel when experimental data submitted by different organisations are used. The results provided by a given organisation always tend to either overestimate or underestimate the response.

A linear tendency between the relative error and the dimensionless model error at the frequency giving a decomposed wave length equal to the ship length, is discovered. This information is applied to find an estimate of the relative error within a band.

The long term extreme response is highly influenced by the model uncertainty. The relative error band varies somewhat with the heading angle. In particular, the band is large for quartering sea at sixty degrees. This may be caused by coupling to roll motion.

8.1.2 Model Uncertainty of Nonlinear, Strip Theory

The uncertainty associated with the error in nonlinear theory is expressed as the ratio between the measured and simulated regular response amplitude.

For some response cases, there seems to be a relation between model error and the wave steepness. However, it can not be concluded to be a general trend for all vessels and response cases.

A relation between the degree of nonlinearity in the response and the model error, is also investigated. As for the previous case, no clear tendencies are observed even if in some cases the model error seems to have a linear relation to the degree of nonlinearity. Since the model error of the nonlinear, strip theory seems to be independent of wave steepness and degree of nonlinearity in the response, this implies that the theory is able to account for even large nonlinearities and that no systematic errors, which can easily be corrected for, are present. Since no general trend is observed, an average value for the model error for a given wave length is found.

The average value of the model error is found to be independent of the wave length. The tendency is that the value varies around a mean value. Therefore, a model error with mean

value and standard deviation is established for each of the response cases. The model error for the sagging response are in most cases less than one, *i.e.* the response is overestimated. Hogging response is more likely to be underestimated. However, model error for hogging response seems to be more case dependent than sagging response.

A relation between the mean value of the model error and the block coefficient is examined. It is believed that the number of data is too small to ascertain that the relation is linear. If more data where available, one could naturally be study this more carefully.

The nonlinear model error herein is determined for each vessel and might be used for similar vessel types.

8.2 Simplified Estimates of Long Term Extreme Response

The inverse First Order Reliability Method, IFORM, has been preferred to establish the contour lines of the environmental parameters, significant wave height and peak period. A computer code based on IFORM was readily available and could easily be modified. This method is also particular efficient if more parameters are to be included, *i.e.* if a contour surface should be established. However, contour curves on lines of the environmental parameter might also be establish using the lines with a constant probability density. The contour curves using the two different methods will be approximately equivalent.

The scatter diagram for the Northern North Sea and the Pierson Moskowitz spectrum are applied in all analysis. The sea surface elevation is assumed to be Gaussian.

8.2.1 Linear Response

The contour line approach has been found useful in order to estimate the D-year life time extreme value for ships with and without forward speed, given that suitable short term characteristics are chosen for the purpose. In this work, the focus has been put on the design extreme value. The design extreme value and a fractile have been applied in selected, three-hour sea states given by the D-year contour line. This will give a reasonable estimate of the D-year long term extreme value given that the appropriate fractile is applied.

The necessary fractile, α, seems to be independent of the sea environment in consideration. The chosen return period will influence the size of the fractile. The necessary fractile for $D = 100$ will underestimate the $D = 10.000$ years response. However, the underestimation is small.

The design fractiles found are in the range from $0.95 - 0.85$. A fractile of 90% seems reasonable for most ships, but for vessels with length smaller than $160m$ the fractile can be advantageously be increased to 95%.

The use of correction factors have been briefly discussed. The design correction factor to be

multiplied with the expected largest and most probable extreme value are 1.1 and 1.15 respectively.

This presented fractiles and correction factors are valid for ships with lengths ranging from $116 - 270$m.

8.2.2 Nonlinear Response

In order to estimate the nonlinear, lifetime extreme value, the short term distribution must be determined. This includes three tasks, - namely determination of simulation length, generation of maxima sample and finding an appropriate distribution. The results are respectively

- 3 hours simulations
- Using linear response series to locate the nonlinear maxima, *i.e.* LRNM-method
- Three parameter Weibull-distribution

The long term extreme values are found using

- *approximate* long term analysis
- contour line approach

The *approximate* long term analysis is convenient since it includes only a limited number of sea states. These sea states are located by establishing the coefficient of contribution for the corresponding linear response. The maximum value of $C_R(si)$ is used as a starting point, and an increasing number of sea states are included until the coefficient of contribution for the nonlinear response is located and the nonlinear, long term extreme value has converged. If approximately 50% of the $C_R(si)$-values are included less then 5% underestimation is experienced for the S-175 container ship, the tanker and the destroyer. Including only the sea state with $\max C_R(si)$, the underestimation is still smaller then 15%. It is concluded that, if the $\max C_R(si)$ is included in the analysis, only a limited number of sea states is necessary to get an acceptable estimate of the D-year value of the nonlinear vertical bending moment midship, *i.e.* sagging and hogging.

The nonlinear lifetime extremes are also estimated by using the contour line approach which is a special way to select the few sea states included in the long term analysis. The approach is based on the results from the linear analysis. That is, the design extreme value, $r^{nl}_{\alpha,design}$, is calculated along the contour using the design fractile found in the linear analysis. The sagging response is satisfactorily estimated for all three vessels at both zero and non-zero forward speed. Applying the contour line generally makes a too low estimate of the long term extreme sagging response. However, the underestimation is small in all cases. The nonlinear bending moment for the tanker is accurately determined for both sagging and hogging. The long term hogging response is also underestimated in most cases. In particular, the hogging response for the destroyer at $Fn = 0.0$ is conspicuous. The ratio between $r^{nl}_{\alpha_{design}}/r^{nl}_{100}$ is as small as 0.92. This is due to the fact that the sea state with $\max C_R(si)$ for the nonlinear response is far apart from the corresponding sea

state in linear analysis. Accordingly the fractile determined using linear analysis is to small.

In this work, this underestimation is believed to be connected with location of the maximum contributing sea state. As concluded for linear response, the design fractile is dependent on the size of the vessel. There is a connection between the period giving wave length equal to the ship length and the value of the design fractile. That is, the smaller vessel the higher fractile. Since nonlinear response will most likely be larger for somewhat smaller wave lengths, one would expect that the fractile found from the linear analysis would slightly underestimate the long term nonlinear bending moment.

However, the conclusion is that the contour line approach is able to predict the nonlinear, long term vertical bending moment accurately enough for practical purposes using the fractiles estimated by linear response analysis. For the vessels with length larger than $160m$, a 90% fractile can be used. For smaller vessels a 95% fractile is suggested. In particular, the sagging moment is well estimated. This is uplifting, since the sagging response is larger than hogging response, and will therefore be the dimensioning load.

8.3 Case studies

Two case studies of the applicability of the contour line approach have been carried out when operability limitations were taken into account. The S-175 container ship was applied in both cases. The aim was to check if contour line approach were able to predict the life time extreme values when restricted service is taken into account, *i.e.* varying forward speed and when manoeuvring were performed in order to avoid severe sea states. The main conclusions from the case studies can be summarised as follows.

8.3.1 Effect of Varying Forward Speed on Linear Response

Inclusion of forward speed into the contour problem makes the analysis more complex. In this thesis three different alternatives have been applied to study the effect of varying forward speed on linear response. That is

- H_s-T_p contour with forward speed, U, as a function of H_s
- H_s-U contour with selected peak period, T_p
- H_s-T_p-U contour surface

Using H_s-T_p contour line with a forward speed which is independent of the wave height, proper results are obtained using a design fractile equal to 0.90 for the S-175 container ship. In addition, if the long term extreme value is independent of the speed change, *i.e.* change of speed is carried out in areas where coefficient of contribution is low, a 90% is applicable. That is, the speed is constant in and close to the sea state with $\max C_R(si)$ or the design sea state on the contour line. The analysis can then be carried out using the forward speed for this area.

If change of speed is conducted in area where $C_R(si)$ reaches its maximum or close to the design sea state on the contour line, the design fractile is dependent on the chosen speed applied in the short term sea states along the contour line. If the $H_s - U$ contour lines are chosen, the fractile is very sensitive to the chosen peak period used in the short term sea states. Application of $H_s - U$ contour lines are therefore not recommended. It is suggested that all three parameters should be introduced into the contour problem. That is, a contour surface should be established for the significant wave height, peak period and forward speed, *i.e.* $H_s - T_p - U$ contour line.

If the $H_s - T_p - U$ contour surface is applied, $\alpha_{design} = 0.90$ seems to give tolerable results.

8.3.2 Effect of Restricted Service on Linear and Nonlinear Response

Effect of restricted service on linear and nonlinear response can be accounted for by remodelling the smoothed scatter diagram. In this work three different models are applied based on:

- truncation
- rescaling
- reshaping

A truncated distribution does not allow for any variability around the operability limit, *i.e.* the vessel is never present in sea states with significant wave heights larger than the limiting significant wave height. The two other modifications of the scatter diagram allow for some variability at the limit. The a combination of the truncated and one of the two other models is most likely the best picture of the reality.

Application of all three modifications are applied in linear response analysis. The truncated model is easy to establish, but can not be used in combination with the contour line approach as the fractile will be dependent on the truncation limit. Using the contour line approach with a reshaped scatter diagram will in general underestimate the long term extreme values. The underestimation increases as the limiting significant wave height decreases. If the contour line approach is to be used, rescaling of the scatter diagram can be applied. Accordingly, a 90% fractile is adequate for linear response for the S-175 container ship.

The rescaled scatter diagram is applied to estimate the nonlinear, vertical bending moment midship, *i.e.* sagging and hogging, using the contour line approach. A 90% fractile gives reasonable estimates of the long term sagging and hogging extreme values.

The linear and nonlinear long term extremes will be reduced when the effect of restricted service is taken in to account.

In this case study, the speed is constant and independent of the significant wave height. Thus, linear and nonlinear long term extremes will be adequately estimated using an 90% fractile for zero and nonzero forward speed. However, if the speed is varying over the included significant

wave height range, application of a contour surface should be considered. Since the service is restricted it is more likely that the speed will change in the areas where the coefficient of contribution is reaching its maximum value.

8.3.3 Conclusive Remarks to the Contour Line Approach

In the case studies different response cases have been studied in connection with the contour line approach. Five combinations of the following are studied

- linear and nonlinear response
- unrestricted and restricted service

where restricted service is divided into

- varying forward speed and manoeuvring in order to avoid severe sea states

Effect of varying forward speed on the nonlinear long term response is not considered in this work.

A large number of linear response analysis and a significantly smaller number of nonlinear analysis have been performed. The purpose is to apply the fractile from linear analysis, to estimate the nonlinear, long term extreme values. It seems that fractiles determined for linear response in unrestricted service in head sea with zero forward speed, can be applied for both linear and nonlinear analysis. It is reason to believe that these fractiles are suitable when the effect of operability restrictions should be accounted for, in accordance with the work presented in this thesis, for both linear and nonlinear response. More nonlinear simulations are required to fully confirm the the contour method's accuracy. It is in the authors opinion that both the linear and nonlinear response analysis give a good impression of the applicability of the contour line approach.

8.4 Suggestions for Further Work

The suggested further work related to the topic described in this thesis may be grouped into

- Improvement of the model uncertainty analysis
- Refinement of the simplified method

Regarding the first point, the lack of experimental data is assumed to constitute the main limitation of the present formulation. In particular, when uncertainty in the transfer function is modelled. If unlimited number of data point were available, one would be able to apply for instance regression analysis to account for the frequency dependence. A polynomial formulation which would be simpler to apply than the present spline formulation. In addition estimates of the uncertainty of the coefficients in the applied polynomial could be found.

However, as shown in this work detailed experimental analysis could be done for the frequency

region close to the peak frequency of the transfer function. An approximate solution of the model error of the transfer function could be applied for the other frequency region, *i.e.* at the tail of the transfer function.

Concerning the nonlinear response, laboratory experiments could give information of the response in irregular seas. Model uncertainty could then be modelled on fractile level as against wave-by-wave approach, Winterstein and Sweetman (1999). That is the distribution function used in the analysis, should be in close agreement with the distribution function from measurements if they were available. This uncertainty measure could be useful in combination with estimation of long term extreme values using the contour line approach.

In this study, the vertical bending moment midship has been studied. It is left to study the model uncertainty for other loads and load combinations, *e.g.* torsional moment and horizontal bending as well as combined local and global loads. Effect of short crested sea is not touched, and could be a topic for further study. In addition, effect of routing could be taken into account.

It is shown that long term extremes can be obtained by considering only a few sea states, it remains to justify this approach for combined loads that may have their maxima in different sea states.

The robustness of the contour line approach should be further examined. In particular combination of nonlinear response and varying forward speed. Analysis with other vessel types should be carried out and other response cases should be tested. The applicability of the contour line approach for estimating the long term extreme values for combination of horizontal and vertical bending as well as torsional moment due to steady state and transient loading and combination of global hull girder bending and local pressures due to steady state loading. Effects due to short crested seas and routing should also be considered.

In particular, more extensive analysis should be carried out for the nonlinear vertical bending moment midship. It could be interesting to include statistical uncertainty in the nonlinear simulation of the vertical bending moment midship. The effect on the design fractile approach and the *approximate* long term analysis could be taken into account.

The contour method should also be checked for nonlinear response on ship with an arbitrary orientation with respect to the wave pattern. In this work, the vessel is treated as rigid. Therefore, the effect of hydroelasticity should be taken into account. The applicability of the contour line method for multihull vessels should also be a topic for further research.

References

15TH & 16TH ITTC SEAKEEPING COMMITTEE (1983, March). Summary of results obtained with computer programs to predict ship motions in six degree of freedom and related responses (1976-1981).

21TH ITTC (1996, September). 21st international towing tank conference.

ADEGEEST, L., A. BRAATHEN, AND T. VADA (1998). Evaluation of methods for estimation of extreme nonlinear ship responses based on numerical simulations and model tests. In *Proc. of the 21th Symposium on Naval Hydrodynamics*, Washington DC, USA. Preprints.

ANDERSEN, O. J., P. E. BJERKE, AND P. STRASS (1996). Environmental design basis: Aasgard. Technical Report 96S18223, STATOIL, Stavanger, Norway.

ANDERSEN, O. J., E. FORLAND, S. K. HAVER, AND P. STRASS (1987a). Design criteria for the Troms I area. Technical report, STATOIL, Stavanger, Norway.

ANDERSEN, O. J., E. FORLAND, S. K. HAVER, AND P. STRASS (1987b). Environmental design basis: Statfjord. Technical report, STATOIL, Stavanger, Norway.

BECK, R. F. AND O. FALTINSEN (1999). Contribution to chapter 2 on Non-linear ship hydrodynamics. ISSC'2000, Comm. VI.1.

BINGHAM, H. B., F. T. KORSMEYER, J. N. NEWMAN, AND G. E. OSBORNE (1993). The simulation of ship motions. In V. C. PATEL AND F. STERN (Eds.), *Proc. of the 6th Int. Conf. on Numerical Ship Hydrodynamics*, Washington, D. C., pp. 561–579. National Academy Press.

BISHOP, R. E. D. AND W. G. PRICE (1979). *Hydroelasticity of ships*. Cambridge, U.S.A: Cambridge University Press.

BJERKE, P. E., O. J. ANDERSEN, S. K. HAVER, AND P. STRASS (1991, December). Europipe pipeline environmental design basis for the detailed engineering phase. Technical Report IGT-KOB-91009, STATOIL, Stavanger, Norway.

BØRRESEN, R. AND F. TELLSGÅRD (1980). Time history simulation of vertical motions and loads on ships in regular, head waves of large amplitudes. Technical Report 91-0134, Det Norske Veritas, Oslo, Norway.

BURY, K. V. (1975). *Statistical Models in Applied Science.* New York, U.S.A: John Wiley & Sons.

CHANG, M.-S. (1977). Computations of three-dimensional ship-motions with forward speed. In J. V. WEHAUSEN AND N. SALVESEN (Eds.), *Proc. of the 2th Int. Conf. on Numerical Ship Hydrodynamics*, Berkeley, California, pp. 124–136. University of California.

CHEYNEY, W. AND D. KINCAID (1985). *Numerical Mathematics and Computing.* Pacific Grove, California: Brooks/Cole Publishing Company.

CHICCO, M. J. AND E. NUMATA (1969, September). Midship wave bending moments in a model of the cargo ship "Wolverine state" running at oblique headings in regular waves. Technical Report SSC-201, Ship Structure Committee, Washington, D.C.

DALZELL, J. F. (1962a, November). An investigation of midship bending moments experienced in extreme regular waves by models of a tanker and a destroyer, appendix. Technical Report DL-927, Davidson Laboratory, New Jersey.

DALZELL, J. F. (1962b, November). An investigation of midship bending moments experienced in extreme regular waves by models of the mariner type ship and three variants Appendix, vol. I. Technical Report DL-926, Davidson Laboratory, New Jersey.

DALZELL, J. F. (1962c, November). An investigation of midship bending moments experienced in extreme regular waves by models of the mariner type ship and three variants Appendix, vol.II. Technical Report DL-926, Davidson Laboratory, New Jersey.

DALZELL, J. F. (1964a, February). An investigation of midship bending moments experienced in extreme regular waves by models of a tanker and a destroyer. Technical Report SSC-156, Ship Structure Committee, Washington, D.C.

DALZELL, J. F. (1964b, January). An investigation of midship bending moments experienced in extreme regular waves by models of the mariner type ship and three variants. Technical Report SSC-155, Ship Structure Committee, Washington, D.C.

DASS (1995-1999). Dynamic analysis and system support project.

DNV (1987). Column stabilized units. In *Classification Notes.* Høvik, Norway: DNV. Note no. 31.4.

DNV (1995). Hull structural design: Ships with length 100 metres and above. In *Rules for Classification of Ships*, Chapter 1, pp. 12– Pt.3 Sec.3. Høvik, Norway: DNV.

FALTINSEN, O. (1979). Theoretical seakeeping, a state-of-the art survey. In *Int. Symposium on Advances in Marine Technology*, Trondheim, Norway, pp. 229–225.

FALTINSEN, O. AND T. SVENSEN (1990). Incorporation of seakeeping theories in CAD. In G. VAN OORTMERSSEN (Ed.), *CFD and CAD in Ship Design*, pp. 146–164. Elsevier Science Publichers B.V.

FALTINSEN, O. M. (1990). *Sea Loads on Ships and Offshore Structures.* Cambridge, England: Cambridge University Press.

FALTINSEN, O. M. AND R. ZHAO (1991). Numerical predictions of ship motions at high forward speed. *Phil. Trans. R. Soc. Lond. A. 334*, 241–252.

FARNES, K. A. (1990). *Long-term Statistics of Response in Non-linear Marine Structures.* Ph. D. thesis, Norwegian Institute of Technology, Trondheim, Norway.

FARNES, K. A. AND E. PASSANO (1989, August). *LOSSTA User's Manual.* Trondheim, Norway: SINTEF.

FATHI, D. (1997, January). *DASS Project: VERES Version 3.0 - User's Manual.* (3.0 ed.). Trondheim, Norway: MARINTEK, Sintef Group.

FUJINO, M. AND B. S. YOON (1986, September). A practical method of estimating ship motions and wave loads in large amplitude waves. *Int. Shipbuilding Progress 33*(385), 159–172.

GIE, T. S. (1972, December). Wave load measurements on a model of large container ship. Technical Report 173 S, Netherlands Ship Research Centre TNO.

GREENHOW, M. (1988). Water-entry and -exit of a horizontal cylinder. (Computational Mechanics).

GREENHOW, M. AND W.-M. LIN (1983, September). Nonlinear free surface effcets: Experiments and theory. Technical Report 83-19, MIT.

GUMBEL, E. J. (1958). *Statistics of Extremes.* New York: Colombia University Press.

HAVER, S. (1980). *Analysis of Uncertainties Related to the Stochastic Modelling of Ocean Waves.* Ph. D. thesis, Norwegian Institue of Technology, NTH, Trondheim, Norway.

HAVER, S. (1987). On the joint distribution of heights and periods of sea waves. *Ocean Engineering 14*(5), 359–376.

HAVER, S. (1993). Extreme wave conditions for the ekofisk area. Technical Report BKON207, STATOIL, Stavanger, Norway.

HAVER, S. (1995, November). Uncertainties in force and response estimates. In *E& P Forum*, London, England.

HAVER, S. (1996, December). Environmental contour lines. Note.

HAVER, S. AND K. A. NYHUS (1986, April). A wave climate description for long term response calculation. In *Proc. of OMAE'86*, Tokyo, Japan, pp. 27–34.

HAVER, S., G. SAGLI, AND T. M. GRAN (1998a, May–April). Long term response analysis of fixed and floating structures. In *Proc. of Wave'98-Ocean Wave Kinematics, Dynamics and Loads on Structures*, Houston, USA. Int. OTRC Symp.

HAVER, S., G. SAGLI, AND T. M. GRAN (1998b, April). Long term response analysis of fixed and floating structures. Technical Report 98s97*4715, STATOIL, Stavanger, Norway.

HAVER, S., R. SIGBJØRNSEN, AND M. MØRCH (1980). Pht version 3 - A computer program for estimation of the long term joint probability density of significant wave height and average period. Technical Report STF71 A80009, SINTEF, Trondheim, Norway.

HEGGELUND, S., H. HASLUM, J. A. NILSEN, AND R. ZHAO (1998). *Slam2d 2.0 - User's Manual.* (2.0 ed.). Trondheim, Norway: MARINTEK, Sintef Group.

HERMUNDSTAD, O. A. (1995). *Theoretical and Experimental Hydroelastic Analysis of High Speed Vessels.* Ph. D. thesis, Norwegian Institue of Technology, NTH, Trondheim, Norway.

HERMUNDSTAD, O. A., J. V. AARSNES, AND T. MOAN (1999, March). Linear hydroelastic analysis of high-speed catamarans and monohulls. *J. of Ship Research 43*(1), 48–63.

HOFF, J. R. (1994). Private notes.

HOFF, J. R. (1999). Private conversation.

HOGBEN, N., N. M. DACUNCHA, AND C. F. OLLIVER (1986). *Global Wave Statistics.* Feltham, England: British Maritime Technology Limited.

HOGBEN, N. AND F. E. LUMB (1967). *Ocean Wave Statistics.* London: Her Majesty's Stationary Office.

JENSEN, J. J. AND P. T. PEDERSEN (1979). Wave-induced bending moments in ships - a quadratic theory. *Royal Inst. of Naval Architects 121*, 151–165.

JONATHAN, P. AND P. H. TAYLOR (1996). Wave-induced loads on fixed offshore structures. In *Proc. of OMAE'96*, New York. ASME.

KAPLAN, P., M. BENATAR, J. BENTSON, AND T. A. ACHTARIDES (1984). Analysis and assessment of major uncertainty associated with ship hull ultimate failure. Technical Report SSC-322, Ship Structure Committee, Washington, D.C.

KAPLAN, P. AND A. I. RAFF (1972). Evaluation and verification of computer calculations of wave-induced ship structural loads. Technical Report SSC-229, Ship Structure Committee, Washington, D.C.

KORBIJN, F. (1991, January). Analysis of the sag to hog regular wave model test results and comparisons with results from available nonlinear theory. Technical Report 91-0134, Det Norske Veritas, Oslo, Norway.

KORBIJN, F. (1992, October). Analysis of the phase II sag to hog model test results in regular and irregular waves and comparison with results from available non-linear theory. Technical Report 92-0193, Det Norske Veritas, Oslo, Norway.

KORBIJN, F. (1998). Private conversation.

KRING, D., Y. F. HUANG, P. D. SCLAVOUNOS, T. VADA, AND A. BRAATHEN (1996). Nonlinear ship motions and wave induced-loads by a Rankine method. In *Proc. of the 21st Symposium on Naval Hydrodynamics*, Trondheim, Norway, pp. 16–33.

KRING, D. AND P. D. SCLAVOUNOS (1995). Numerical stability analysis for time-domain ship motion simulation. *J. of Ship Research 39*(4), 313–288.

KUMAR, S. AND S. R. WINTERSTEIN (1997, June). SURFIT: Using moment surfaces to estimate extreme response from wave, wind and current. Technical Note No. RMS-28, Stanford University, California, U.S.A.

LANGEN, I. (1981). *On Dynamic Analysis of Floating Bridges.* Ph. D. thesis, Norwegian Institute of Technology, Trondheim, Norway.

LANGEN, I. AND R. SIGBJÖRNSEN (1979). *Dynamisk Analyse av Konstruksjoner.* Trondheim, Norway: Tapir.

LARSEN, C. M. AND E. PASSANO (1990). extreme response estimation for marine risers. In *Proc. of OMAE'90*, pp. 361–369. ASME.

LIN, W. M., M. MEINHOLD, N. SALVESEN, AND D. YUE (1994). Large-ampltitude motions and wave loads for shi design. In *Proc. of the 20th Symposium on Naval Hydrodynamics*, Trondheim, Norway, pp. 192–213.

LIN, W. M., M. J. MEINHOLD, K. M. WEEMS, S. ZHANG, AND M. H. C. WEEMS (1996, July). *User's Guide to the LAMP System: LAMP theory and Implementation.* Maryland, USA: SAIC, Science Applications International Corporation.

LLOYD, A. R. J. M., J. C. BROWN, AND J. F. W. ANSLOW (1980). Motions and loads on ship models in regular oblique waves. *Royal Inst. of Naval Architects 122*, 20–33.

LOUNGUET-HIGGINS, M. S. (1963). The effect of non-linearities on statistical distribution in the theory of sea waves. *J. of Fluid and Structures 17*(3), 459–480.

MADSEN, H. O. (1988, January). Omission sensitivity factors. *Structural Safety 5*(1), 35–45.

MADSEN, H. O., S. KRENK, AND N. C. LIND (1986). *Methods of Structural Safety.* New Jersey: Prentice-Hall International, Inc.

MYRHAUG, D. (1992, August). 81524 hydrodynamikk og havmiljø: Havmiljø. Trondheim,Norway. In Norwegian.

MYRHAUG, D. (1993, August). 81538 probabilistic theory of sealoads. Trondheim,Norway.

NAKOS, D., D. KRING, AND P. D. SCLAVOUNOS (1993). Rankine panel methods for transient free-surface flows. In V. C. PATEL AND F. STERN (Eds.), *Proc. of the 6th Int. Conf. on Numerical Ship Hydrodynamics*, Washington, D. C., pp. 613–632. National Academy Press.

NAKOS, D. AND P. D. SCLAVOUNOS (1990a). Ships motions by a three dimensional rankine panel method. In *Proc. of the 18th Symposium on Naval Hydrodynamics*, Ann Arbor, Michigan.

NAKOS, D. E. (1990). *Ship Wave Patterns and Motions by a Three Dimensional Rankine Panel Method.* Ph. D. thesis, Massachusetts Institute of Technology, MIT, Cambridge, USA.

NAKOS, D. E. AND P. D. SCLAVOUNOS (1990b). On steady and unsteady ship wave patterns. *J. of Fluid Mechanics 215*, 263–288.

NETHERCOTE, W. C. E. (1981). Motions and bending moments of a warship design. *Trans. of Royal Inst. of Naval Architects 123*, 353–375.

NEWLAND, D. E. (1984). *Random Vibrations and Spectral Analysis.* New York: John Wiley & Sons, Inc.

NEWMAN, J. N. (1977). *Marine Hydrodynamics.* Cambridge, USA: Massachusetts Institute of Technology, MIT.

NIKOLAIDES, E. AND P. KAPLAN (1991). Uncertainties in stress analysis of marine structures. Technical Report SSC-363, Ship Structure Committee, Washington, D.C.

NITTA, A., H. ARAI, AND A. MAGAINO (1992). Basis of IACS unified longitudinal strength standard. *Marine Structures 5*, 1–21.

NUMATA, E. AND W. F. YONKERS (1969, November). Midship wave bending moments in a model of the mariner-class cargo ship "California bear" running at oblique headings in regular waves. Technical Report SSC-202, Ship Structure Committee, Washington, D.C.

NORDFORSK (1987). *Assessment of Ship Performance in a Seaway.* Copenhagen, Denmark: NORDFORSK, Nordic Co-operative.

NORSOK STANDARD (1999). Actions and action effects. N-003, Rev. 1.

OCHI, M. (1964). Prediction of occurrence and severity of ship slamming at sea. In *Proc. of the 5th Symposium on Naval Hydrodynamics*, Bergen, Norway, pp. 545–589.

OCHI, M. (1978, December). Generalization of the rayleigh probability distribution and its application. *J. of Ship Research 22*(4), 259–265.

OCHI, M. K. (1990). *Applied Probability and Stochastic Processes.* New York, U.S.A: John Wiley & Sons.

OLUFSEN, A., C. M. LARSEN, B. J. LEIRA, AND E. PASSANO (1991, February). Extreme response estimation of flexible risers. Technical Report Report 2.1-17, SINTEF, Trondheim, Norway.

PETERSEN, J. B. (1992). *Non-linear strip theories for ship response in waves.* Ph. D. thesis, The Technocal University of Denmark.

PRESS, W. H., S. A. TEUKOLSKY, W. T. VETTERLING, AND B. P. FLANNERY (1992). *Numerical Recipes in FORTRAN.* USA: Camdridge University Press.

SAGLI, G., M.-K. WU, AND T. MOAN (1997). Nonlinear wave load effects for design of slender monohull vessels. In *Proc. of NAV'97*, Naples, Italy, pp. 8.3–8.16. Tipolitografica G. Giglio.

SALVESEN, N. (1981, December). Five years of numerical naval ship hydrodynamics at dtnsrdc. *J. of Ship Research 25*(4), 219–235.

SALVESEN, N., E. O. TUCK, AND O. M. FALTINSEN (1970). Ship motions and sea loads. *Trans. SNAME 78*, 250–287.

SCHELLIN, T. E., C. OSTERGAARD, AND C. G. SOARES (1996). Uncertainty assessment of low frequency load effects for containerships. *Marine Structures 9*, 313–332.

SOARES, C. G. (1984). *Probabilistic Models for Load Effects in Ship Structures.* Ph. D. thesis, Norwegian Institue of Technology, NTH, Trondheim, Norway.

SOARES, C. G. (1986). Calibration of visual observations of wave period. *Ocean Engineering 13*(6), 539–547.

SOARES, C. G. (1991). Effect of transfer function uncertainty on short-term ship response. *Ocean Engineering 18*(4), 329–362.

SOARES, C. G. (1995). Effect of wave directionality on long-term wave-induced load effects in ships. *J. of Ship Research 39*(2), 150–159.

SOARES, C. G. AND T. MOAN (1987). Model uncertainty in wave induced bending moments for fatigue design of ship structures. Technical Report MK/R99/87, Department of Marine Structures, Norwegian Institute of Technology, Trondheim, Norway.

SOARES, C. G. AND T. MOAN (1991). Model uncertainty in the long-term distribution of wave induced bending moments for fatigue design of ship structures. *Marine Structures 4*, 295–315.

SOARES, C. G. AND M. F. S. TROVÃO (1991). Influence of wave climate modelling on the long-term prediction of wave induced response of ship structures. In W. G. PRICE, P. TEMAREL, AND A. J. KEANE (Eds.), *Dynamics of Marine Vehicles and Structures in Waves*, pp. 1–362. Elsevier Science Publishers B.V.

SOARES, C. G. AND P. C. VIANA (1988). Sensitivity of the response of marine structures to wave climatology. In B. A. SCHREFLER AND O. C. ZIENKIEWICZ (Eds.), *Int. Conf. on Computer Modelling in Ocean Engineering*, Rotterdam, Netherlands, pp. 487–492. Balkema.

SØDAHL, N. R. (1991). *Methods for Design and Analysis of Flexible Risers*. Ph. D. thesis, Norwegian University of Science and Technology, Trondheim, Norway.

STACY, E. W. AND G. A. MIHRAM (1965, August). Parameter estimation for a generalized gamma distribution. *Technometrics 7*(3), 349–358.

STRANG, G. (1988). *Linear Algebra and its Applications*. San Diego, California: Harcourt Brace Jovanovich.

TIKKA, K. K. (1989). *Prediction of critical conditions for extreme vessel response in random seas*. Ph. D. thesis, University of California, Berkeley, California, USA.

TORHAUG, R. A. (1996). *Extreme Response of Nonlinear Ocean Structures: Identification of Minimal Stochastic Wave Input for Time Domain Simulation*. Ph. D. thesis, Stanford University, USA.

TORSETHAUGEN, K. (1987, May). Gyldighetsområdet for Jonswap-spekteret. Technical Report 02.0788.00/01/87, SINTEF, Trondheim, Norway.

TORSETHAUGEN, K. (1993). A two peaked spectrum model. In *Proc. of OMAE'93*, pp. 175–180. ASME.

TUCKER, M. J., P. G. CHALLENOR, AND J. T. CARTER (1984). Numerical simulation of a random sea: a common error and its effect upon wave group statistics. *Applied Ocean Research 6*(2), 118–122.

UDE, T. C. AND S. R. WINTERSTEIN (1996, June). IFORM: An inverse-form routine to estimate response levels with specified return periods. Technical Note No. TN-3, Stanford University, California, U.S.A.

UENO, M. AND I. WATANABE (1987). On the asymmetry of vertical bending moment on ships. *J. of The Society of Naval Architects of Japan 162*, 175–182. In Japanese.

VADA, T. AND J. B. HELMERS (1992, August). Non-linear ship hydrodynamics. state-of-art review. Technical Report 92-2039, Det Norske Veritas, Oslo, Norway.

VIDEIRO, P. M. (1998). *Reliability based design of marine structures*. Ph. D. thesis, Norwegian University of Science and Technology, Trondheim, Norway.

VON KÁRMÁN, T. AND F. L. WATTENDORF (1929). The impact on seaplane floats during landing. In *National Advisory Committee for Aeronautics, NACA*, pp. 309–313. Technical Note.

WAGNER, H. (1932). Über Stoß- und Gleitvorgänge and der Oberfläche von Flüssigkeiten. *Zeitschr. für angewandte Mathematik und Mechanik 12*(4), 193–214.

WALDEN, H. (1967). The characteristics of sea waves in the north atlantic. Technical Report No. 41, Deutscher Wetterdienst Seewetteramt, Hamburg, Germany. In German.

WANG, L. (1999). Private notes.

WANG, Z., J. J. JENSEN, AND J. XIA (1998). On the effect of green water on deck of the bending moment. In M. C. W. OOSTERVELD AND S. G. TAN (Eds.), *Proc. PRADS'98*, Amsterdam, Netherlands, pp. 239–245. Elsevier Science B. V.

WATANABE, H. AND H. OHTSUBO (1998). Analysis of the accident of the MV Nakhodka. Part I. Estimation of loads. *J. of Marine Science and Technology 3*, 171–180.

WINTERSTEIN, S. R. (1988, October). Nonlinear vibration models for extremes and fatigue. *J. of Engineering Mechanics 114*(10), 1772–1790.

WINTERSTEIN, S. R. AND B. SWEETMAN (1999, July). Air gap response of floating structures: statistical predictions vs observed behaviour. In *Proc. of OMAE'99*.

WINTERSTEIN, S. R., T. C. UDE, C. A. CORNELL, P. BJERAGER, AND S. HAVER (1993). Environmental parameters for extreme response: Inverse form with omission factors. In G. I. SCHUËLLER, M. SHINOZUKA, AND J. T. P. YAO (Eds.), *Proc. of IOSSAR'93*, Rotterdam, pp. 77–84. A. A. Balkema.

WINTERSTEIN, S. R., T. C. UDE, AND G. KLEIVEN (1994). Springing and slow-drift responses: Predicted extremes and fatigue vs. simulation. In C. CHRYSSOSTOMIDIS, M. S. TRIANTAFYLLOU, A. J. WHITTLE, AND M. S. H. FATT (Eds.), *Proc. of BOSS'94*, pp. 1–15. PERGAMON.

WU, M.-K., J. V. AARSNES, O. A. HERMUNDSTAD, AND T. MOAN (1996). A practical prediction of wave-induced structural responses in ships with large amplitude motion. In *Proc. of the 21st Symposium on Naval Hydrodynamics*, Trondheim, Norway.

WU, M.-K. AND T. MOAN (1996, June). Linear and nonlinear hydroelastic analysis of high-speed vessels. *J. of Ship Research 40*(2), 149–163.

XIA, J., Z. WANG, X. GU, J. SHEN, AND Y. WU (1995). Numerical simulation of the wave induced non-linear bending moment of ships. In *Proc. of OMAE'95*, pp. 147–153. ASME.

ZHAO, R., O. FALTINSEN, AND J. AARSNES (1996). Water entry of arbitrary two-dimensional sections with and without flow separation. In *Proc. of the 21st Symposium on Naval Hydrodynamics*, Trondheim, Norway, pp. 118–133.

Appendix A

Existing Programs

A.1 Linear and Nonlinear Strip Theories

Traditionally, the ship motion problem is formulated in the frequency domain and linearised by assuming that the motions and incident wave amplitude are small relative to the draft of the ship, e.g. Salvesen et al. (1970). When ship forward speed gets higher, it is no longer reasonable to use the conventional strip theory since the fluid near the ship hull can not be sufficiently described by two-dimensional flow. A high-speed formulation was presented by Faltinsen and Zhao (1991). These two theories are incorporated in VERES, Fathi (1997), a simulation program developed at MARINTEK AS.

Due to limitations of the linear strip theories, many investigators have extended the frequency domain strip theories to large amplitude time domain strip theory approaches. In these approaches, the hydrostatic restoring force and the Froude-Krylov forces are accurately included while the hydrodynamic restoring forces and the diffraction forces are approximately included. Such an approach has been utilised in the simulation program LANWIL developed by Wu and Moan (1996), Wu et al. (1996).

A.1.1 VERES

The VERES (VEssel RESponse), Fathi (1997), program is a linear strip theory program that calculates ship motions and loads in the frequency domain. The first version of VERES treated only cases for mono hulls with low to moderate speed. A problem solved by the traditional strip theory developed by Salvesen et al. (1970). Later the program was extended to include the high-speed formulation, Faltinsen and Zhao (1991). This version can also be applied on twin-hulls, however the interaction between the hull is not accounted for.

VERES has been developed as a part of the DASS, DASS (1999), project at MARINTEK AS.

Applications

The program calculates

- Motion transfer functions in six degrees of freedom
- Relative motion [1] transfer functions (relative motion between the ship and the wave)
- Motions at specified points
- Unsteady global loads [2] (forces and moments)
- May take into account viscous effects by empirical formulas
- Short term and long term statistics of the above mentioned response quantities
- Operational restrictions and profiles

Valid for slender mono- and twin hull at low to high speed.

A.1.2 LANWIL

LANWIL, Linear And Nonlinear Wave Loads, is a strip theory program that calculates linear- and nonlinear wave induced motions and loads. The nonlinear approach include the hydrostatic restoring force and the Froude-Krylov forces accurately, while the hydrodynamic forces are approximately included. Effect of Green water on deck is taken into account. The flexibility of the ship has been taken into account by employing a number of dry eigenmodes in addition to the six rigid-body modes.The linear theory applies to mono hulls and catamarans at all wave headings, but the nonlinear theory is so far restricted to head and following sea.

Theoretical background may be found in Wu and Moan (1996), Wu et al. (1996).

Applications

LANWIL calculates

- Motion transfer functions for heave and pitch
- Sectional transfer function for shear forces and bending moment
- Sectional linear and nonlinear time series for heave and pitch, shear force and bending moments
- Two approaches to calculate the sectional loads, *i.e.* assuming rigid body and elastic body

[1] *Motions* includes both displacements, velocities and accelerations

[2] With *unsteady*, they are referring to the wave induced dynamic part of the global loads, as opposed to the steady loads, which also are present in calm water

A.1.3 NV1418

NV1418 is a two dimensional, nonlinear strip theory program which calculates the motion and loads in the time domain. A simplified second order theory has been implemented in order to take into account the effects from flare and bottom slamming. Another second order effect is green water on deck and this has been regarded as a "quasi static" effect. The ship hull is rigid, *i.e.* the flexibility of the hull is not included. The theory is only applicable to ship in head sea waves travelling with a constant forward speed. The theory behind the program is given in Børresen and Tellsgård (1980).

Applications

NV1418 determine

- Heave and pitch motions
- Sectional shear forces and bending moment

A.2 Three Dimensional Programs

Three dimensional programs may be divided in two groups: Rankine source methods and methods based on Green's functions. Compared to the methods which are based on Green's function, the Rankine source methods have the following advantages and disadvantages:

- Advantages
  - the evaluation of the influence matrix is simple
  - extension to nonlinear free surface condition is a possibility
- Disadvantages
  - large equation system due to panelling of the free surface cause increase in the computing time

A.2.1 Rankine Source Methods

In the Rankine source methods, the velocity potential is described by a distribution of Rankine sources over the wetted surface of the body and the free surface. The panelling of the free surface is necessary since the Rankine sources do not fulfil the free surface conditions. The linear frequency domain problem has been solved by this method by Nakos (1990), Nakos and Sclavounos (1990b), Nakos and Sclavounos (1990a). The linear time domain problem was later solved by Kring and Sclavounos (1995), Nakos, Kring, and Sclavounos (1993). An extension to the nonlinear problem was presented by Kring et al. (1996). The Rankine source methods are implemented in the simulation program SWAN (Ship Wave ANalysis) as a cooperation between Massachusetts Institute of Technology, MIT, and Det Norske Veritas Research AS, DNV.

A.2.2 Green Function Methods

In the Green function methods, the velocity potential is described by a distribution of Green functions over the wetted surface of the body. The panelling of the free surface is no longer needed as the Green function satisfies the free surface condition. The theory behind the linear time domain program TiMIT developed at MIT is presented in *e.g.* Bingham et al. (1993). The Green functions method is also applied in the LAMP (Large Amplitude Motion Program), Lin et al. (1996), system of codes which have been developed by Lin et al. (1994) for calculations of motions and loads in large amplitude waves.

A.2.3 SWAN

SWAN is a complete three dimensional motion program. The program models the complex ship-wave interaction. Early versions of the SWAN treated the linear steady and sea keeping problems in the frequency domain. More recently the method was extended to also include the time domain. The last work has been dedicated to the treatment of the nonlinear see keeping problem. The first extension to the linear problem was to include the nonlinear hydrostatic restoring and Froude-Krylov forces. The final version is a fully nonlinear problem where the complete hydrodynamic problem is solved at each time step. The ship-wave interaction is treated according the weak scatterer hypothesis where it is postulated that the ship wave disturbance is small compared to the ambient waves, see Kring et al. (1996).

The program is developed as a cooperation between Massachusetts Institute of Technology, MIT, and Det Norske Veritas Research AS, DNV. SWAN includes a multitude of numerical techniques to provide the user with the most appropriate solution tool for analysis of ship motions.

Applications

- Calculation of added mass, damping coefficients and exciting forces and moments. These are integrated effects of the hydrodynamic pressure over the hull.
- Prediction of the motion of a steady freely floating ship. The motion is defined by both amplitude and phase relative to the incoming wave.
- Calculation of shear forces and bending moments at arbitrary section of the ship (Calculation of the global loads is performed with linear and nonlinear extension of the hydrostatic restoring forces and Froude-Krylov. Computation of the global loads with use of the weak scatterer hypothesis is not yet included, but will be incorporated, Kring et al. (1996).)
- Prediction of quadratic mean forces and moments due to waves. These include the added resistance, the steady side force and the mean yaw moment.
- Calculation of pressure on the hull and in the fluid, the fluid velocities on the hull and in the fluid and the wave elevation on the sea surface.
- Simulation of the steady turbulent boundary layer along the ship hull and the viscous wake behind the ship for prediction of total drag on the ship.

- Valid for full-shaped ships at low to moderate speeds and for fine-shaped ships from low to high speeds.

A.2.4 LAMP

The LAMP system of codes have been developed to calculate motion and loads in large amplitude waves. LAMP is based on a multi level approach which is a system of codes with different level of sophistication. In general, the physics underlying the ship-wave interaction is best understood using comparisons generated by incremental increase in complexity. This means that the lower level codes act as a filtering mechanism for the selection of more accurate but more complex and computationally intensive codes. The computation methods and hardware requirements for the LAMP code is presented in Table A.1.

Table A.1: *Computation methods and hardware requirements for the LAMP code.($\mathcal{Z} = 0$ and $\mathcal{F}(t)$ are still water surface and incident wave surface respectively),Lin et al. (1994).*

Method:	Hydrodynamic, Restoring and Froude-Krylov Forces	Hardware
LAMP - 4	Free Surface Boundary Conditions on $\mathcal{F}(t)$ 3-D Large-Amplitude Hydrodynamics Nonlinear Restoring and Froude-Krylov	Supercomputer
LAMP - 3	Free Surface Boundary Conditions on $\mathcal{F}(t)$ $2\frac{1}{2}$-D Large-Amplitude Hydrodynamics Nonlinear Restoring and Froude-Krylov	Workstation
LAMP - 2	Free Surface Boundary Conditions on $\mathcal{Z} = 0$ 3-D Linear Hydrodynamics Nonlinear Restoring and Froude-Krylov	Workstation
LAMP - 1	Free Surface Boundary Conditions on $\mathcal{Z} = 0$ 3-D Linear Hydrodynamics Linear Restoring and Froude-Krylov	Workstation

Applications

- Calculation of shear forces, bending- and torsional moment at arbitrary section of the ship.
- Prediction of motions of a ship in seaway
- Two approaches to calculate the sectional loads, one assuming rigid body and and the other one assuming elastic body
- Added- and wave resistance can be calculated
- In oblique or beam sea, forces due to lift- and viscous effect can be included (In oblique sea and beam sea, forces due to lift- and viscous effects will have a significant effect on motions and loads)

- Calculation of the hydrodynamic pressure distribution over the hull
- Normally a run is conducted with a constant forward speed at a given heading angle, but any path or speed may be specified

Appendix B

Evaluating and Comparing Time Series

Deviations from the Gaussian distribution can be expressed by four statistical moments. The mean, the variance, the skewness and the kurtosis may be calculated from the distributions of the process

$$\begin{aligned} \mu_X &= \int f(x)dx \\ \sigma_X^2 &= \int (x-\mu_X)^2 f_X(x)dx \\ \gamma_{1X} &= \frac{\int (x-\mu_X)^3 f_X(x)dx}{\sigma_X^3} \\ \gamma_{2X} &= \frac{\int (x-\mu_X)^4 f_X(x)dx}{\sigma_X^4} \end{aligned} \tag{B.1}$$

The variance, σ^2, is a measure of the variation about the mean value and is equal to the square of the standard deviation.The skewness, γ_{1X}, is a measure of the asymmetry of the distribution and the kurtosis, γ_{2X}, is a measure of the density in the tails of the distribution, *i.e.* the probability of extremes. The mean value and skewness will be zero for a Gaussian process while the kurtosis have the value three.

If the process is ergodic, the above values may be estimated from the time series peak values as

$$\begin{aligned} m_X &= \frac{1}{N}\sum_{j=1}^{N} x_j \\ s_X^2 &= \frac{1}{N-1}\sum_{j=1}^{N}(x_j - m_X)^2 \end{aligned}$$

$$g_{1X} = \frac{1}{N}\sum_{j=1}^{N}\frac{(x_j - m_X)^3}{s_x^3} \qquad (B.2)$$

$$g_{2X} = \frac{1}{N}\sum_{j=1}^{N}\frac{(x_j - m_X)^4}{s_x^4}$$

where N is the number of peak values. The stability of the last four parameters may be investigated by comparing the parameters for portions of a long realization or for many realizations of a process. The mean and the variance will normally be quite stable and can be calculated for rather short realizations. The last two parameters, the skewness and the kurtosis, are more unstable and larger realizations are needed to get stable results. This is because extreme behaviour in portions of the realizations tend to dominate these two higher moments.

Appendix C

Approximation by Spline Functions

Sometimes the value of a function$f(x)$ is known at a given set of data $[x_1, .., x_n]$, but no analytical expression for $f(x)$ is available. Therefore its value can not be calculated at an arbitrary value in the interval.

Therefore one which to to draw a curve/fit a function through or by the points x_i. There are number of ways of doing this. The most common approach among functional form are the polynomials. The function values can also be established by means of the method of least squares. The former is more suitable if you have a smaller number of data whereas the latter are used when the amount of data is large. Another possibility is to use the so-called spline function. A spline is a function consisting of of polynomial pieces joined together with a certain smoothness conditions. The cubic splines consisting of third degree polynomial are the most popular ones. They produce interpolated functions which is continuous through the second derivative. Compared to ordinary polynomials, a spline is much "stiffer", *i.e.* in the sense that polynomials may go berserk and exhibit wild oscillations between the tabulated points.

C.1 Natural Cubic Splines

The first and second degree of splines are useful in certain applications, but they both suffer and obvious imperfection. The first degree spline has abrupt changes in all derivatives. The lack of smoothness for the quadratic spline is not so obvious, but the curvature is discontinuous at the knots $[x_1, x_2, .., x_n]$.

The general definition of a spline of degree k is

- The domain of S is $[a, b]$
- $S, S', S'', .., S^{k-1}$ are continuous in the domain $[a, b]$

- The domain $[a, b]$ is divided into subintervals $[a = x_1, x_2, .., x_{n-1}, x_n = b]$ and S is a polynomial of degree k

The goal of cubic spline is to establish a spline which is continuous throughout the second derivative, *i.e.* slope and curvature, in the domain $[a, b]$. The cubic spline is constructed so that

$$S(x) = \begin{cases} S_1(x) & ; x_1 < x < x_2 \\ S_2(x) & ; x_2 < x < x_3 \\ \vdots & \\ S_{n-1}(x) & ; x_{n-1} < x < x_n \end{cases} \tag{C.1}$$

where $S_i = a_i + b_i x + c_i x^2 + d_i x^3$. In each subinterval the polynomial goes through two knots , *i.e.* x_{i-1} and x_i, giving us $2(n-1)$ equations. Requiring continuous slope and curvature gives another $2(n-2)$ equations. For a unique solution two other conditions must be specified at the end knots x_1 and x_n. One way of doing so, is to set $S''(x_1)$ and/or $S''(x_n)$ equal to zero, *i.e.* a natural cubic spline. The values $S''(x_1)$ and/or $S''(x_n)$ can also be calculated so that the first derivative have a specified value at one or both ends, Press et al. (1992).

Cheyney and Kincaid (1985) claims that natural cubic splines are the best functions to apply for curve fitting. This statement is based on the cubic spline property saying that if S is a natural cubic spline interpolating the twice-continuous function f at knots $[a = x_1, x_2, .., x_{n-1}, x_n = b]$ then the integral of the square $S''(x)$ is less then equal to the integral of the square of $f''(x)$.

Appendix D

Least Square Method

Given a set of data points $(x_1, y_1), ...(x_n, y_n)$, the Least Square Method finds a solution for a desired model $\mathbf{X}$ by minimising

$$\mathbf{E}^2 = ||\mathbf{Y} - \mathbf{X}\beta|| \tag{D.1}$$

where $\mathbf{Y}$ is the matrix containing the y-values, $\mathbf{X}$ is the chosen model and β is the coefficient matrix. The least squares solution of the inconsistent[1] system $\mathbf{Y} = \mathbf{X}\beta + \epsilon$ of m equations and n unknowns is given as, Strang (1988)

$$\mathbf{X}^\mathbf{T}\mathbf{X}\hat{\beta} = \mathbf{X}^\mathbf{T}\mathbf{Y} \tag{D.2}$$

If the columns of $\mathbf{X}$ are linearly independent, then $\mathbf{X}^\mathbf{T}\mathbf{Y}$ is invertible and

$$\hat{\beta} = (\mathbf{X}^\mathbf{T}\mathbf{X})^{-1}\mathbf{X}^\mathbf{T}\mathbf{Y} \tag{D.3}$$

$(\mathbf{X}^\mathbf{T}\mathbf{X})^{-1}\mathbf{X}^\mathbf{T}$ is called a *pseudoinverse* and is applied to the system since $\mathbf{X}$ is a rectangular matrix and cannot be inverted, Strang (1988). Using the Least Square Method $\hat{\beta}$ is always unbiased, *i.e.* $E(\hat{\beta}) = \beta$.

Proof:

$$\begin{aligned} E(\hat{\beta}) &= E\left((\mathbf{X}^\mathbf{T}\mathbf{X})^{-1}\mathbf{X}^\mathbf{T}\mathbf{Y}\right) \\ &= (\mathbf{X}^\mathbf{T}\mathbf{X})^{-1}\mathbf{X}^\mathbf{T}E(\mathbf{Y}) \\ &= (\mathbf{X}^\mathbf{T}\mathbf{X})^{-1}\mathbf{X}^\mathbf{T}E(\mathbf{X}\beta + \epsilon) \\ &= (\mathbf{X}^\mathbf{T}\mathbf{X})^{-1}\mathbf{X}^\mathbf{T}\mathbf{X}\beta + (\mathbf{X}^\mathbf{T}\mathbf{X})^{-1}\mathbf{X}^\mathbf{T}E(\epsilon) \\ &= \mathbf{I}\beta = \beta \end{aligned} \tag{D.4}$$

[1]There more equations than unknowns. A solution which is optimal for all data points can be found by minimising Eq. D.1

Appendix E

Relative difference

Table E.1: *The ratios* $\frac{r^l_{100}}{r^l_{50}}$ *and* $\frac{r^l_{100}}{r^l_{20}}$. *The Pierson Mosckowitz spectrum is used in the analysis.*

The ratio $\frac{r^l_{100}}{r^l_{50}}$ using the Pierson-Moskowitz spectrum										
Heading	0		30		60	120	150		180	
	SHI	SRI	SHI	SRI	SRI	SRI	SHI	SRI	SHI	NKK
$H(\omega)$	1.035	1.035	1.034	1.034	1.033	1.033	1.036	1.036	1.037	1.037
$H(\omega)\phi_{cubic}(\omega)$	1.033	–	1.034	1.034	1.033	1.033	1.037	1.037	1.038	1.039
$H(\omega)+\phi(\omega)_{cubic}$	1.033	–	1.033	–	1.035	1.034	–	–	–	–
$H(\omega)\phi(\omega)_{linear}$	1.033	–	1.033	1.034	1.032	1.034	1.037	1.037	1.038	1.039
$H(\omega)+\phi(\omega)_{linear}$	1.033	–	1.033	–	1.034	1.033	–	–	–	–
$H(\omega)\frac{\sum_i \hat{H}_i H_i}{\sum_i H_i^2}$	1.035	1.034	1.034	1.034	1.033	1.033	1.036	1.036	1.037	1.037

The ratio $\frac{r^l_{100}}{r^l_{20}}$ using the Pierson-Moskowitz spectrum										
Heading	0		30		60	120	150		180	
	SHI	SRI	SHI	SRI	SRI	SRI	SHI	SRI	SHI	NKK
$H(\omega)$	1.084	1.084	1.083	1.083	1.079	1.080	1.087	1.087	1.091	1.091
$H(\omega)\phi_{cubic}(\omega)$	1.080	–	1.080	1.083	1.080	1.081	1.090	1.092	1.093	1.095
$H(\omega)+\phi(\omega)_{cubic}$	1.081	–	1.081	–	1.086	1.082	–	–	–	–
$H(\omega)\phi(\omega)_{linear}$	1.081	–	1.081	1.083	1.080	1.081	1.090	1.091	1.092	1.095
$H(\omega)+\phi(\omega)_{linear}$	1.081	–	1.080	–	1.082	1.081	–	–	–	–
$H(\omega)\frac{\sum_i \hat{H}_i H_i}{\sum_i H_i^2}$	1.084	1.084	1.083	1.082	1.080	1.081	1.087	1.087	1.091	1.091

Table E.2: *The ratios* $\frac{r^I_{100}}{r^I_{50}}$ *and* $\frac{r^I_{100}}{r^I_{20}}$. *The Jonswap spectrum is used in the analysis.*

The ratio $\frac{r^I_{100}}{r^I_{50}}$ using the Jonswap spectrum										
Heading	0		30		60	120	150		180	
	SHI	SRI	SHI	SRI	SRI	SRI	SHI	SRI	SHI	NKK
$H(\omega)$	1.035	1.035	1.034	1.034	1.033	1.035	1.034	1.034	1.035	1.035
$H(\omega)\phi_{cubic}(\omega)$	1.032	–	1.033	1.034	1.032	1.033	1.035	1.037	1.036	1.037
$H(\omega)+\phi(\omega)_{cubic}$	1.033	–	1.033	–	1.035	1.032	–	–	–	–
$H(\omega)\phi(\omega)_{linear}$	1.033	–	1.033	1.035	1.031	1.032	1.035	1.037	1.036	1.037
$H(\omega)+\phi(\omega)_{linear}$	1.033	–	1.033	–	1.031	1.032	–	–	–	–
$H(\omega)\frac{\sum_i \hat{H}_i H_i}{\sum_i H_i^2}$	1.035	1.035	1.035	1.034	1.033	1.035	1.034	1.034	1.035	1.035

The ratio $\frac{r^I_{100}}{r^I_{20}}$ using the Jonswap spectrum										
Heading	0		30		60	120	150		180	
	SHI	SRI	SHI	SRI	SRI	SRI	SHI	SRI	SHI	NKK
$H(\omega)$	1.085	1.085	1.083	1.083	1.080	1.085	1.082	1.082	1.086	1.086
$H(\omega)\phi_{cubic}(\omega)$	1.080	–	1.081	1.083	1.078	1.080	1.087	1.089	1.089	1.092
$H(\omega)+\phi(\omega)_{cubic}$	1.080	–	1.081	–	1.086	1.079	–	–	–	–
$H(\omega)\phi(\omega)_{linear}$	1.080	–	1.081	1.083	1.076	1.079	1.087	1.089	1.089	1.092
$H(\omega)+\phi(\omega)_{linear}$	1.081	–	1.081	–	1.077	1.079	–	–	–	–
$H(\omega)\frac{\sum_i \hat{H}_i H_i}{\sum_i H_i^2}$	1.085	1.085	1.083	1.083	1.081	1.085	1.083	1.082	1.086	1.086

Appendix F

Hull forms

Table F.1: *Ship data.*

Ship	L_{pp} [m]	B [m]	D [m]	C_b [-]	VCG [m]	LCG [m]
S-175	175	25.4	9.5	0.572	9.55	2.55
SL-7	270	32.2	10.85	0.598	13.49	10.12
Wolverine State - full load	151.2	21.8	9.14	0.65	7.77	-0.98
Wolverine State - light load	151.2	21.8	5.95	0.61	6.86	-0.23
California Bear - east bound	160.9	23.2	6.4	0.58	7.32	3.02
California Bear - west bound	160.9	23.2	7.5	0.60	8.23	2.68
Reefer vessel	160	24.7	8.93	0.57	10.4	4.12
Tanker	272.8	40.2	14.91	0.80	11.91	-0.91
Destroyer	116.7	12.4	4.27	0.55	2.10	3.95
Mariner 2251A-V1	158.5	23.1	8.45	0.61	8.82	2.24
Mariner 2251A-V2	158.5	23.1	8.45	0.61	8.29	2.21
Mariner 2251B	158.5	23.1	8.45	0.61	8.96	2.25
EuroExpress	219.5	20.2	7.25	0.39	-	-

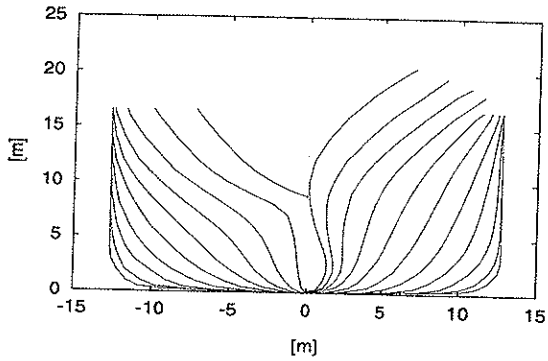

(a) S-175

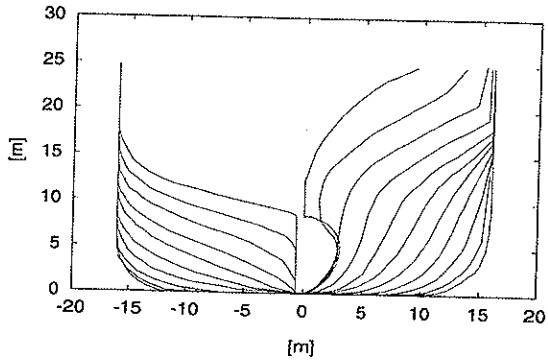

(b) SL-7

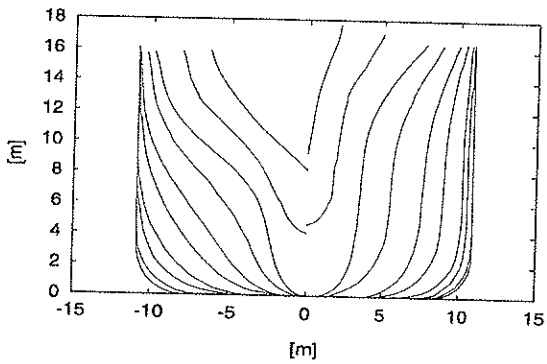

(c) Wolverine State

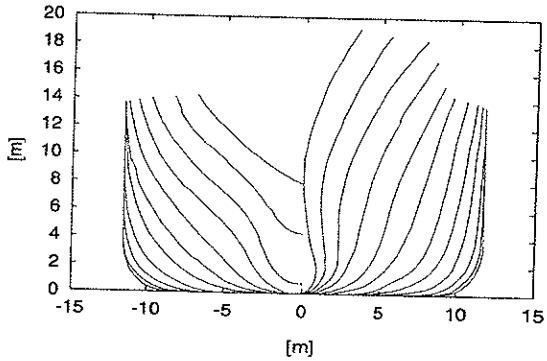

(d) California Bear

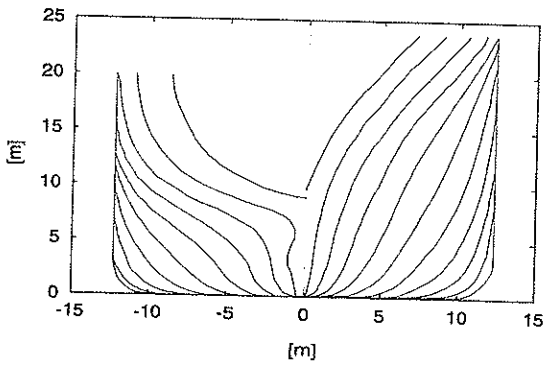

(e) Reefer vessel

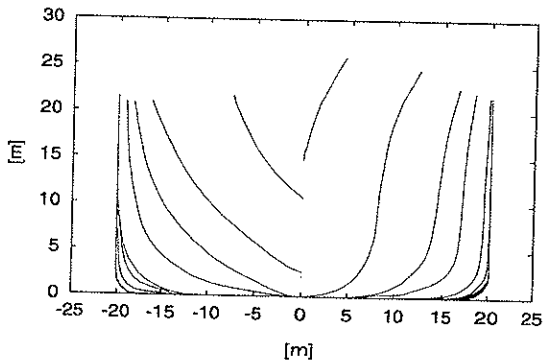

(f) Tanker

Figure F.1: *Hull forms.*

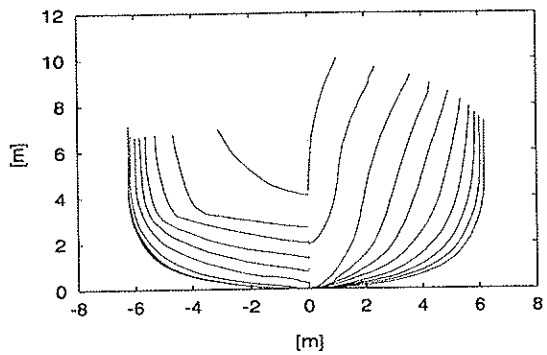

(a) Destroyer

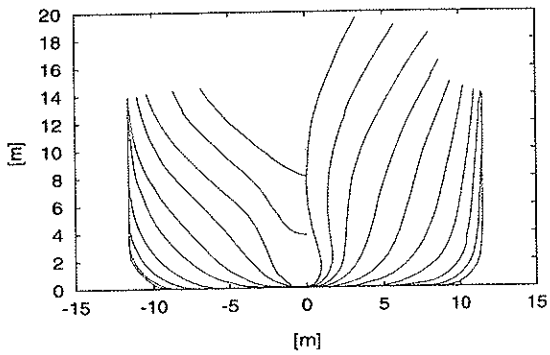

(b) Mariner 2251A-V1 & 2251A-V2

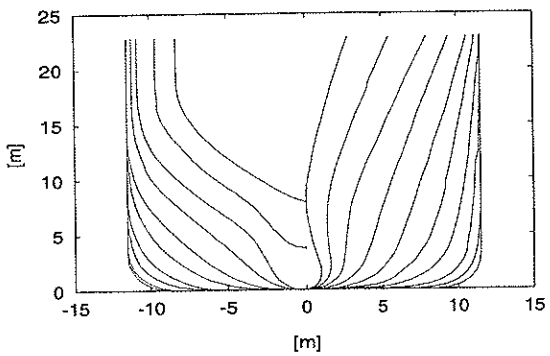

(c) Mariner 2251B

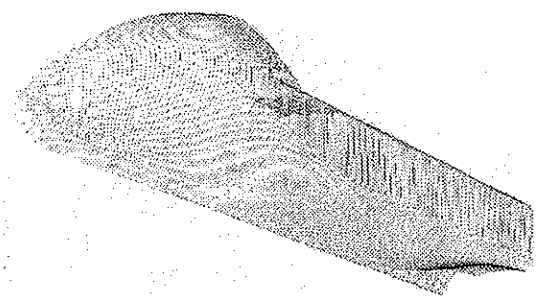

(d) EuroExpress

Figure F.2: *Hull forms.*

Appendix G

Mass distributions

Table G.1: *Mass distribution for the S-175 container ship, 15th & 16th ITTC Seakeeping Committee (1983).*

Segment no. i	$(\frac{x}{L_{pp}})_{1i}$	$(\frac{x}{L_{pp}})_{2i}$	m_i [ton]
1 (F.P.)	-87.50	-78.75	519.42
2	-78.75	-70.00	711.12
3	-70.00	-61.25	850.25
4	-61.25	-52.50	1020.30
5	-52.50	-43.75	1190.35
6	-43.75	-35.00	1314.02
7	-35.00	-26.25	1406.77
8	-26.25	-17.50	1530.45
9	-17.50	-87.50	1654.12
10	-87.50	0.00	1700.50
11	0.00	87.50	1654.12
12	87.50	17.50	1570.64
13	17.50	26.25	1484.07
14	26.25	35.00	1397.50
15	35.00	43.75	1360.40
16	43.75	52.50	1360.40
17	52.50	61.25	1267.64
18	61.25	70.00	1051.22
19	70.00	78.75	850.25
20 (A.P.)	78.75	87.50	680.20

Table G.2: *Mass distribution for Wolverine State - full load, Chicco and Numata (1969) & Kaplan and Raff (1972).*

Segment no. i	$(\frac{x}{L_{pp}})_{1i}$	$(\frac{x}{L_{pp}})_{2i}$	m_i [ton]
1 (F.P.)	-75.59	-71.81	103.19
2	-71.81	-64.25	303.62
3	-64.25	-56.69	527.86
4	-56.69	-49.13	855.29
5	-49.13	-41.57	105.17
6	-41.57	-34.02	1191.65
7	-34.02	-26.46	1299.80
8	-26.46	-18.90	1388.10
9	-18.90	-11.34	1406.96
10	-11.34	-3.78	1416.88
11	-3.78	3.78	1430.77
12	3.78	11.34	1434.74
13	11.34	18.90	1384.13
14	18.90	26.46	1285.91
15	26.46	34.02	1070.59
16	34.02	41.57	784.84
17	41.57	49.13	710.42
18	49.13	56.69	765.99
19	56.69	64.25	588.38
20	64.25	71.81	509.00
21	71.81	75.59	210.349

Table G.3: *Mass distribution for Wolverine State - light load, Chicco and Numata (1969) & Kaplan and Raff (1972).*

Segment no. i	$(\frac{x}{L_{pp}})_{1i}$	$(\frac{x}{L_{pp}})_{2i}$	m_i [ton]
1 (F.P.)	-75.59	-60.47	547.78
2	-60.47	-43.35	818.19
3	-43.35	-30.24	1660.23
4	-30.24	-15.12	1958.47
5	-15.12	0.0	1060.75
6	0.0	15.12	1590.64
7	15.12	30.24	1381.86
8	30.24	43.35	1248.66
9	43.35	60.47	1070.69
10 (A.P.)	60.47	75.59	680.99

Table G.4: *Mass distribution for California Bear - eastbound route, Numata and Yonkers (1969).*

Segment no. i	$(\frac{x}{L_{pp}})_{1i}$	$(\frac{x}{L_{pp}})_{2i}$	m_i [ton]
1 (F.P.)	-79.05	-70.76	213.88
2	-70.76	-55.62	730.54
3	-55.62	-39.24	1237.03
4	-39.24	-20.08	1861.45
5	-20.08	-1.85	1747.13
6	-2.47	3.09	971.65
7	3.09	8.34	919.42
8	8.34	13.90	932.78
9	13.90	19.47	669.98
10	19.47	39.24	2105.75
11	39.24	57.78	1641.01
12	57.78	72.61	760.04
13 (A.P.)	72.61	81.88	277.61

Table G.5: *Mass distribution for California Bear - eastbound route, Numata and Yonkers (1969).*

Segment no. i	$(\frac{x}{L_{pp}})_{1i}$	$(\frac{x}{L_{pp}})_{2i}$	m_i [ton]
1 (F.P.)	-79.10	-70.45	217.91
2	-70.45	-55.62	747.11
3	-55.62	-39.55	132.05
4	-39.55	-21.01	233.47
5	-21.01	-2.47	307.20
6	-2.47	7.72	1811.24
7	7.72	13.29	954.78
8	13.29	18.54	584.91
9	18.54	38.62	2289.65
10	38.62	56.86	1933.30
11	56.86	72.61	1269.04
12 (A.P.)	72.61	81.88	276.48

Table G.6: *Mass distribution for the reefer vessel, Korbijn (1992).*

Segment no. i	$(\frac{x}{L_{pp}})_{1i}$	$(\frac{x}{L_{pp}})_{2i}$	m_i [ton]
1 (F.P.)	-80.0	-70.0	454.45
2	-70.0	-60.0	454.45
3	-60.0	-50.0	454.45
4	-50.0	-40.0	454.45
5	-40.0	-30.0	1715.93
6	-30.0	-20.0	1715.93
7	-20.0	-10.0	1715.93
8	-10.0	0.0	1715.93
9	0.0	10.0	1476.25
10	10.0	20.0	1476.25
11	20.0	30.0	1476.25
12	30.0	40.0	1476.25
13	40.0	50.0	1476.25
14	50.0	60.0	1476.25
15	60.0	70.0	1476.25
16 (A.P.)	70.0	80.0	1476.25

Table G.7: *Mass distribution for the tanker, Dalzell (1964a).*

Segment no. i	$(\frac{x}{L_{pp}})_{1i}$	$(\frac{x}{L_{pp}})_{2i}$	m_i [ton]
1 (F.P.)	-136.40	-122.71	1006.13
2	-122.71	-109.37	1293.43
3	-109.37	-95.48	4979.96
4	-95.48	-81.95	7551.09
5	-81.95	-68.30	8450.91
6	-68.30	-54.64	8795.88
7	-54.64	-37.63	8899.19
8	-37.63	-3.73	18612.20
9	-3.73	40.60	45792.40
10	40.60	68.01	8692.38
11	68.01	81.76	7864.56
12	81.76	95.52	3570.06
13	95.52	109.37	2173.08
14	109.37	123.12	4200.92
15 (A.P.)	123.12	136.40	2345.55

Table G.8: *Mass distribution for the destroyer, Dalzell (1964a).*

Segment no. i	$(\frac{x}{L_{pp}})_{1i}$	$(\frac{x}{L_{pp}})_{2i}$	m_i [ton]
1 (F.P.)	-58.37	-52.65	30.18
2	-52.65	-46.80	57.483
3	-46.80	-39.92	107.86
4	-39.92	-35.15	89.33
5	-35.15	-29.39	147.59
6	-29.39	-23.46	219.72
7	-23.46	-17.50	282.53
8	-17.50	-11.77	196.20
9	-11.77	-6.09	181.10
10	-6.09	-0.20	229.93
11	-0.20	5.68	263.66
12	5.68	12.92	190.32
13	12.92	21.58	425.46
14	21.58	28.86	275.76
15	28.86	34.79	250.46
16	34.79	40.79	191.76
17	40.79	46.80	156.03
18	46.80	52.65	81.56
19 (A.P.)	52.65	58.37	77.68

Table G.9: *Mass distribution for the Mariner 2251A-V1 & 2251B, Dalzell (1964b).*

Segment no. i	$(\frac{x}{L_{pp}})_{1i}$	$(\frac{x}{L_{pp}})_{2i}$	m_i [ton]
1 (F.P.)	-79.25	-75.02	109.80
2	-75.02	-67.27	477.17
3	-67.27	-58.59	963.27
4	-58.59	-51.31	778.25
5	-51.31	-43.32	658.41
6	-43.32	-35.34	844.81
7	-35.34	-27.59	916.23
8	-27.59	-19.84	1107.70
9	-19.84	-11.86	1185.95
10	-11.86	-3.87	1219.75
11	-3.87	4.34	1604.62
12	4.34	12.09	1312.98
13	12.09	20.08	1168.54
14	20.08	27.83	1092.90
15	27.83	35.81	1094.41
16	35.81	44.03	1520.47
17	44.03	52.01	1205.64
18	52.01	59.76	938.47
19	59.76	67.51	675.02
20	67.51	75.26	379.82
21 (A.P.)	75.26	79.25	130.53

Table G.10: *Mass distribution for the Mariner 2251A-V2, Dalzell (1964b).*

Segment no. i	$(\frac{x}{L_{pp}})_{1i}$	$(\frac{x}{L_{pp}})_{2i}$	m_i [ton]
1 (F.P.)	-79.25	-71.27	311.72
2	-71.27	-63.52	301.25
3	-63.52	-55.77	299.96
4	-55.77	-47.78	307.70
5	-47.78	-39.80	306.33
6	-39.80	-32.05	296.01
7	-32.05	-24.30	294.72
8	-24.30	-16.32	309.10
9	-16.32	-13.27	120.42
10	-13.27	-10.92	983.37
11	-10.92	-8.57	987.25
12	-8.57	-4.58	1671.25
13	-4.58	-2.23	986.93
14	-2.23	4.11	4131.06
15	4.11	11.86	5047.90
16	11.86	15.38	160.77
17	15.38	22.89	342.08
18	22.89	31.11	372.76
19	31.11	38.86	350.13
20	38.86	47.08	369.94
21	47.08	54.59	336.96
22	54.59	62.58	356.70
23	62.58	70.80	365.76
24 (A.P.)	70.80	79.25	374.70

Appendix H

Applied transfer functions

Table H.1: *Overview over applied transfer functions.*

Ship	Fn	Headings
S-175	0.275	0, 30, 60, 120, 150, 180
SL-7	0.220	0, 45
	0.245	0, 25, 45, 65, 115, 135, 155
	0.270	0, 45
Wolverine State - full load	0.214	0, 30, 60, 120, 150, 180
Wolverine State - light load	0.214	0, 30, 60, 120, 150, 180
California Bear - east bound	0.258	0, 30, 60, 120, 150, 180
California Bear - west bound	0.258	0, 30, 60, 120, 150, 180
Reefer vessel	0	0
	0.145	0

APPENDIX I

IFORM - transformation

The IFORM - technique may be used to establish the the lines of constant probability of exceedance. A detailed derivation of the contour lines for the distribution $f_{H_s,T_p}(h,t)$, see Eq. 3.81 & 3.82, is given herein.

The probability of exceedance is given by

$$p_e = \frac{1}{DN_s} \tag{I.1}$$

where D is the return period and N_s is number of sea states within one year. The duration of the sea states are in this work set to be three hours.

The transformation is given as

$$\bar{\Phi}(\bar{U}) = \Phi(U_1)\Phi(U_2) = F_{H_s}(h)F_{T_p}(t|h) \tag{I.2}$$

$\Phi()$ and $\bar{\Phi}()$ are standard, normal distributions. Then

$$\bar{\Phi}(-\beta_C) = p_e \;\Rightarrow\; \beta_C = -\bar{\Phi}^{-1}(p_e) \tag{I.3}$$

The contour lines in U-space will be circles with radius equal to β_C, Fig. I.1. The values of U_1 and U_2 are therefore given by

$$U_1 = \beta_C \cos(\theta) \tag{I.4}$$
$$U_2 = \beta_C \sin(\theta) \tag{I.5}$$

The corresponding values of H_s and T_p must be found, so that

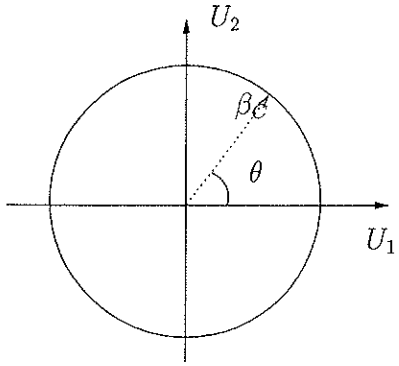

Figure I.1: *Definition of U-space*

$$\Phi(U_1) = F_{H_s}(h) \tag{I.6}$$
$$\Phi(U_2) = F_{T_p}(t|h) \tag{I.7}$$

When $h \leq \eta$ the density function for the significant wave height is given by the log-normal distribution. That is

$$\Phi(U_1) = \Phi\left(\frac{\ln h - \mu_{\ln H_s}}{\sigma_{\ln H_s}}\right) \Rightarrow h = \exp\{\mu_{\ln H_s} + \sigma_{\ln H_s} U_1\} \tag{I.8}$$

and when $h > \eta$, the significant wave height is described by the Weibull-distribution. Thus

$$1 - \exp\{-(\frac{h}{\beta})^{\gamma}\} = \Phi(U_1) \Rightarrow h = \beta[-\ln(1 - \Phi(U_1))]^{\gamma} \tag{I.9}$$

The peak period, T_P, is given by the log-normal distribution giving

$$\Phi(U_2) = \Phi\left(\frac{\ln t - \mu_{\ln T_p}}{\sigma_{\ln T_p}}\right) \Rightarrow t = \exp\{\mu_{\ln T_p} + \sigma_{\ln T_p} U_2\} \tag{I.10}$$

Appendix J

Analysis of the nonlinear responses

Table J.1: *Statistical moments for the sea state* $H_s = 11.5m$ *&* $T_p = 12.5s$

No. of sections	realization type	$m_R \cdot [10^9 Nm]$	$s_R \cdot [10^9 Nm]$	$\gamma_{1R}[-]$	$g_{2R}[-]$	$\omega^+[s^{-1}]$
21	orig	0.14595	0.36429	0.80870	5.68013	0.16056
	filtered	0.14595	0.36220	0.87368	4.39236	0.15537
42	orig	0.14488	0.36061	0.88034	4.55064	0.15759
	filtered	0.14488	0.35994	0.89498	4.44889	0.15472
63	orig	0.14489	0.36001	0.89366	4.47326	0.15528
	filtered	0.14489	0.35976	0.89188	4.45462	0.15500
105	orig	0.14480	0.35997	0.89569	4.45767	0.15574
	filtered	0.14480	0.35975	0.89383	4.44348	0.15500
126	orig	0.14484	0.35996	0.89681	4.45712	0.15481
	filtered	0.14484	0.35978	0.89396	4.44426	0.15500

Table J.2: *Statistical moments for the sea state* $H_s = 13.56m$ *&* $T_p = 13.76s$

No. of sections	realization type	$m_R \cdot [10^9 Nm]$	$s_R \cdot [10^9 Nm]$	$\gamma_{1R}[-]$	$g_{2R}[-]$	$\omega^+[s^{-1}]$
21	orig	0.17494	0.40771	0.89903	4.54693	0.15741
	filtered	0.17949	0.40549	0.88262	4.22309	0.15111
42	orig	0.17844	0.40365	0.90205	4.37080	0.15287
	filtered	0.17844	0.40306	0.89798	4.33247	0.15130
63	orig	0.17841	0.40309	0.90116	4.31928	0.15194
	filtered	0.17841	0.40266	0.89566	4.29012	0.15083
105	orig	0.17841	0.40282	0.89902	4.30667	0.15120
	filtered	0.17841	0.40247	0.89307	4.28078	0.15074
126	orig	0.17849	0.40295	0.90015	4.31357	0.15074
	filtered	0.17850	0.40261	0.89423	4.28797	0.15046

Table J.3: *Statistical moments for the sea state* $H_s = 14.5m$ *&* $T_p = 15.9s$

No. of sections	realization type	$m_R \cdot [10^9 Nm]$	$s_R \cdot [10^9 Nm]$	$\gamma_{1R}[-]$	$g_{2R}[-]$	$\omega^+[s^{-1}]$
21	orig	0.16642	0.38903	0.99769	4.66647	0.14889
	filtered	0.16642	0.38752	0.96668	4.46623	0.14639
42	orig	0.16544	0.38534	0.98644	4.56872	0.14639
	filtered	0.16544	0.38491	0.97868	4.53771	0.14385
63	orig	0.16540	0.38490	0.98329	4.55967	0.14639
	filtered	0.16540	0.38454	0.97690	4.53459	0.14583
105	orig	0.16536	0.38484	0.98121	4.55586	0.14583
	filtered	0.16536	0.38451	0.97508	4.53116	0.14574
126	orig	0.16543	0.38490	0.98138	4.55328	0.14593
	filtered	0.16534	0.38547	0.97532	4.52980	0.14574

Table J.4: *Weibull parameters for original realizations of the sagging response in the sea state* $H_s = 11.5m$ *&* $T_p = 12.5s$

No. of sections	type of maxima	$\gamma[-]$	$\beta \cdot [10^9 Nm]$	$\delta \cdot [10^8 Nm]$	$r^{nl}_{0.90,design} \cdot [10^9 Nm]$
21	global	1.4358	0.6758	0.2949	3.3326
	LRNM	1.3622	0.6275	0.5716	3.4095
42	global	1.4267	0.6308	0.6394	3.1745
	LRNM	1.3773	0.6036	0.6479	3.2303
63	global	1.4184	0.6237	0.7442	3.1754
	LRNM	1.3709	0.5984	0.6780	3.2302
105	global	1.4158	0.6237	0.7215	3.1829
	LRNM	1.3667	0.5966	0.6893	3.2381
126	global	1.4114	0.6199	0.7809	3.1844
	LRNM	1.3666	0.5962	0.6897	3.2364

Table J.5: *Weibull parameters for original realizations of the hogging response in the sea state* $H_s = 11.5m$ *&* $T_p = 12.5s$

No. of sections	type of maxima	$\gamma[-]$	$\beta \cdot [10^9 Nm]$	$\delta \cdot [10^8 Nm]$	$r^{nl}_{0.90,design} \cdot [10^9 Nm]$
21	global	$4.172 \cdot 10^6$	$8.901 \cdot 10^4$	$8.901 \cdot 10^5$	0.4865
	LRNM	2.5021	0.4015	-0.7831	0.9186
42	global	0.6748	0.9737	1.5964	3.0010
	LRNM	2.4975	0.39803	-0.7702	0.9130
63	global	1.7235	0.2958	-0.1669	1.1239
	LRNM	2.4928	0.3968	-0.7473	0.9130
105	global	2.2788	0.3718	-0.4994	0.9591
	LRNM	2.4926	0.3969	-0.7532	0.9135
126	global	2.4345	0.3906	-0.6706	0.9272
	LRNM	2.4933	0.3971	-0.7570	0.9135

Table J.6: *Weibull parameters for original realizations of the sagging response in the sea state* $H_s = 13.56m$ *&* $T_p = 13.76s$

No. of sections	type of maxima	$\gamma[-]$	$\beta \cdot [10^9 Nm]$	$\delta \cdot [10^8 Nm]$	$r^{nl}_{0.90,design} \cdot [10^9 Nm]$
21	global	1.5087	0.8173	0.2626	3.7215
	LRNM	1.4452	0.7766	0.4129	3.8021
42	global	1.5453	0.7954	0.3900	3.5023
	LRNM	1.4946	0.7698	0.2969	3.5669
63	global	1.5508	0.7962	0.3756	3.4849
	LRNM	1.4984	0.7688	0.2881	3.5478
105	global	1.5642	0.8014	0.3514	3.4605
	LRNM	1.5118	0.7749	0.2366	3.5232
126	global	1.5660	0.8028	0.3506	3.4597
	LRNM	1.5130	0.7757	0.2343	3.5221

Table J.7: *Weibull parameters for original realizations of the hogging response in the sea state* $H_s = 13.56m$ *&* $T_p = 13.76s$

No. of sections	type of maxima	$\gamma[-]$	$\beta \cdot [10^9 Nm]$	$\delta \cdot [10^8 Nm]$	$r^{nl}_{0.90,design} \cdot [10^9 Nm]$
21	global	0.6280	0.0872	1.8267	3.4542
	LRNM	2.8031	0.4556	-1.0569	0.9192
42	global	1.5601	0.2803	0.4804	1.2516
	LRNM	2.7945	0.4523	-1.0565	0.9144
63	global	2.5692	0.4268	-0.7927	0.9545
	LRNM	2.7928	0.4520	-1.0548	0.9144
105	global	2.8481	0.4598	-1.1124	0.9098
	LRNM	2.7994	0.4533	-1.0635	0.9144
126	global	2.8324	0.4567	-1.0764	0.9108
	LRNM	2.7948	0.4528	-1.0600	0.9150

Table J.8: *Weibull parameters for original realizations of the sagging response in the sea state* $H_s = 14.5m$ *&* $T_p = 15.9s$

No. of sections	type of maxima	$\gamma[-]$	$\beta \cdot [10^9 Nm]$	$\delta \cdot [10^8 Nm]$	$r^{nl}_{0.90,design} \cdot [10^9 Nm]$
21	global	1.4758	0.7965	-0.0325	3.7066
	LRNM	1.4031	0.7442	0.1573	3.7845
42	global	1.5328	0.7784	0.0397	3.4239
	LRNM	1.4705	0.7425	0.0537	3.4938
63	global	1.5225	0.7700	0.0843	3.4255
	LRNM	1.4596	0.7326	0.1074	3.4941
105	global	1.5182	0.7683	0.1164	3.4347
	LRNM	1.4557	0.7308	0.1358	3.5023
126	global	1.5233	0.7704	0.0978	3.4252
	LRNM	1.4603	0.7328	0.1220	3.4932

Table J.9: *Weibull parameters for original realizations of the hogging response in the sea state* $H_s = 14.5m$ *&* $T_p = 15.9s$

No. of sections	type of maxima	$\gamma[-]$	$\beta \cdot [10^9 Nm]$	$\delta \cdot [10^8 Nm]$	$r^{nl}_{0.90,design} \cdot [10^9 Nm]$
21	global	1.6500	0.2858	0.2918	1.1609
	LRNM	2.7340	0.4233	-0.9333	0.8775
42	global	2.7812	0.4247	-0.9483	0.8652
	LRNM	2.7333	0.4203	-0.9281	0.8712
63	global	2.7911	0.4263	-0.9682	0.8642
	LRNM	2.7250	0.4182	-0.9131	0.8707
105	global	2.7699	0.4222	-0.9206	0.8655
	LRNM	2.7227	0.4178	-0.9042	0.8712
126	global	2.7789	0.4239	-0.9382	0.8651
	LRNM	2.7222	0.4175	-0.9001	0.8711

Table J.10: *Weibull parameters for filtered realizations of the sagging response in the sea state* $H_s = 11.5m$ *&* $T_p = 12.5s$

No. of sections	type of maxima	$\gamma[-]$	$\beta \cdot [10^9 Nm]$	$\delta \cdot [10^8 Nm]$	$r^{nl}_{0.90,design} \cdot [10^9 Nm]$
21	global	1.4523	0.6381	0.6461	3.1210
	LRNM	1.4024	0.6124	0.5820	3.1758
42	global	1.4073	0.6163	0.8049	3.1831
	LRNM	1.3663	0.5911	0.6915	3.2317
63	global	1.4087	0.6180	0.7782	3.1839
	LRNM	1.3629	0.5934	0.7020	3.2371
105	global	1.4082	0.6173	0.7874	3.1835
	LRNM	1.3637	0.5939	0.7007	3.2360
126	global	1.4096	0.6186	0.7717	3.1835
	LRNM	1.3633	0.5938	0.6985	3.2371

Table J.11: *Weibull parameters for filtered realizations of the hogging response in the sea state* $H_s = 11.5m$ *&* $T_p = 12.5s$

No. of sections	type of maxima	$\gamma[-]$	$\beta \cdot [10^9 Nm]$	$\delta \cdot [10^8 Nm]$	$r^{nl}_{0.90,design} \cdot [10^9 Nm]$
21	global	1.4476	0.2552	0.5067	1.2794
	LRNM	2.5025	0.4020	-0.7882	0.9193
42	global	2.3707	0.3832	-0.6004	0.9402
	LRNM	2.4962	0.3976	-0.7623	0.9131
63	global	2.0017	0.3340	-0.1647	1.0242
	LRNM	2.4905	0.3965	-0.7508	0.9135
105	global	2.4402	0.3917	-0.6854	0.9263
	LRNM	2.4913	0.3966	-0.7479	0.9138
126	global	2.5032	0.3993	-0.7562	0.9152
	LRNM	2.4898	0.3963	-0.7453	0.9139

Table J.12: *Weibull parameters for filtered realizations of the sagging response in the sea state* $H_s = 13.56m$ *&* $T_p = 13.76s$

No. of sections	type of maxima	$\gamma[-]$	$\beta \cdot [10^9 Nm]$	$\delta \cdot [10^8 Nm]$	$r^{nl}_{0.90,design} \cdot [10^9 Nm]$
21	global	1.6116	0.8201	0.1997	3.3783
	LRNM	1.5492	0.7884	0.1185	3.4458
42	global	1.5395	0.7855	0.4419	3.4806
	LRNM	1.4918	0.7613	0.3205	3.5398
63	global	1.5609	0.7945	0.3824	3.4440
	LRNM	1.5100	0.7695	0.2475	3.5058
105	global	1.5647	0.7959	0.3674	3.4362
	LRNM	1.5130	0.7701	0.2424	3.4976
126	global	1.5616	0.7940	0.3935	3.4400
	LRNM	1.5118	0.7697	0.2432	3.5002

Table J.13: *Weibull parameters for filtered realizations of the hogging response in the sea state* $H_s = 13.56m$ *&* $T_p = 13.76s$

No. of sections	type of maxima	$\gamma[-]$	$\beta \cdot [10^9 Nm]$	$\delta \cdot [10^8 Nm]$	$r^{nl}_{0.90,design} \cdot [10^9 Nm]$
21	global	2.7933	0.4567	-1.0506	0.9252
	LRNM	2.8003	0.4552	-1.0507	0.9196
42	global	2.4459	0.4091	-0.6386	0.9719
	LRNM	2.7905	0.4520	-1.0522	0.9154
63	global	2.8297	0.4553	-1.0643	0.9098
	LRNM	2.7948	0.4521	-1.0520	0.9142
105	global	2.8323	0.4566	-1.0777	0.9105
	LRNM	2.7961	0.4527	-1.0579	0.9148
126	global	2.8311	0.4558	-1.0649	0.9103
	LRNM	2.7963	0.4528	-1.0574	0.9149

Table J.14: *Weibull parameters for filtered realizations of the sagging response in the sea state* $H_s = 14.5m$ *&* $T_p = 15.9s$

No. of sections	type of maxima	$\gamma[-]$	$\beta \cdot [10^9 Nm]$	$\delta \cdot [10^8 Nm]$	$r^{nl}_{0.90,design} \cdot [10^9 Nm]$
21	global	1.5388	0.7802	-0.0040	3.4078
	LRNM	1.4670	0.7365	0.0739	3.4822
42	global	1.4986	0.7538	0.1862	3.4435
	LRNM	1.4380	0.7172	0.2044	3.5106
63	global	1.4958	0.7512	0.2058	3.4434
	LRNM	1.4353	0.7150	0.2099	3.5112
105	global	1.4944	0.7510	0.2096	3.4475
	LRNM	1.4346	0.7149	0.2212	3.5140
126	global	1.4980	0.7523	0.1991	3.4400
	LRNM	1.4379	0.7161	0.2107	3.5064

Table J.15: *Weibull parameters for filtered realizations of the hogging response in the sea state* $H_s = 14.5m$ *&* $T_p = 15.9s$

No. of sections	type of maxima	$\gamma[-]$	$\beta \cdot [10^9 Nm]$	$\delta \cdot [10^8 Nm]$	$r^{nl}_{0.90,design} \cdot [10^9 Nm]$
21	global	2.8088	0.4342	-1.0183	0.8721
	LRNM	2.7278	0.4224	-0.9234	0.8783
42	global	2.7836	0.4249	-0.9475	0.8651
	LRNM	2.7212	0.4179	-0.9059	0.8716
63	global	2.7746	0.4232	-0.9328	0.8653
	LRNM	2.7151	0.4164	-0.8928	0.8715
105	global	2.7736	0.4232	-0.9288	0.8659
	LRNM	2.7186	0.4172	-0.8960	0.8717
126	global	2.7755	0.4235	-0.9320	0.8657
	LRNM	2.7187	0.4172	-0.8961	0.8717

Previous Dr. ing Thesis at the Department of Marine Structures

Kavlie, Dag	:	Optimization of Plane Elastic Grillages. 1967.
Hansen, Hans R.	:	Man-Machine Communication and Data-Storage Methods in Ship Structural Design. 1971.
Gisvold, Kaare M.	:	A Method for Non-Linear Mixed -Integer Programming and its Application to Design Problems.
Lund, Sverre	:	Tanker Frame Optimalization by Means of SUMT-Transformation and Behaviour Models. 1971.
Vinje, Tor	:	On Vibration of Spherical Shells Interacting with Fluid. 1972.
Lorentz, Jan D.	:	Tank Arrangement for Crude Oil Carriers in Accordance with the New Anti-Pollution Regulations. 1975.
Carlsen, Carl A.	:	Computer-Aided Design of Tanker Structures. 1975.
Larsen, Carl M.	:	Static and Dynamic Analysis of Offshore Pipelines during Installation. 1976.
Hatlestad, Brigt	:	The Finite Element Method Used in a Fatigue Evaluation of Fixed Offshore Platforms. 1979.
Valsgård, Sverre	:	Finite Difference and Finite Element Method Applied to Non-Linear Analysis of Plated Structures. 1979.
Pettersen, Erik	:	Analysis and Design of Cellular Structures. 1979.
Nordsve, Nils T.	:	Finite Element Collapse Analysis of structural Members Considering Imperfections and Stresses due to Fabrication. 1980.
Fylling, Ivar J.	:	Analysis of Towline Forces in Ocean towing Systems. 1980.
Haver, Sverre	:	Analysis of Uncertainties Related to the Stochastic Modelling of Ocean Waves. 1980.
Odland, Jonas	:	On the Strength of Welded Ring Stiffened Cylindrical Shells Primarily Subjected to Axial Compression. 1981.
Engesvik, Knut	:	Analysis of Uncertainties in the Fatigue Capacity of Welded Joints. 1982.

Eide, Oddvar Inge	:	On Cumulative Fatigue Damage in Steel Welded Joints. 1983.
Mo, Olav	:	Stochastic Time Domain Analysis of Slender Offshore Structures. 1983.
Amdahl, Jrrgen	:	Energy Absorption in Ship-Platform Impacts. 1983.
Czujko, Jerzy	:	Collapse Analysis of Plates subjected to Biaxial Compression and Lateral Load. 1983.
Soares, C. Guedes	:	Probabilistic Models for Load Effects in Ship Structures. 1984.
Mørch, Morten	:	Motions and Mooring Forces of Semi Submersibles as Determined by Full-Scale Measurements and Theoretical Analysis. 1984.
Engseth, Alf G.	:	Finite Element Collapse Analysis of Tubular Steel Offshore Structures. 1985.
Baadshaug, Ola	:	Systems Reliability Analysis of Jacket Platforms. 1985. (Confidential)
Hessen, Gunnar	:	Fracture Mechanics Analysis of Stiffened Tubular Members. 1986.
Taby, Jon	:	Ultimate and Post-Ultimate Strength of Dented Tubular Members. 1986.
Wessel, Heinz-J.	:	Fracture Mechanics Analysis of Crack Growth in Plate Girders. 1986.
Leira, Bernt Johan	:	Gaussian Vector-Processes for Reliability Analysis Involving Wave-Induced Load Effects. 1987.
Xu Jun	:	Non-linear Dynamic Analysis of Space-framed Offshore Structures. 1988.
Guoyang Jiao	:	Reliability Analysis of Crack Growth under Random Loading Considering Model Updating. 1989.
Olufsen, Arnt	:	Uncertainty and Reliability Analysis of Fixed Offshore Structures. 1989.
Wu Yu-Lin	:	System Reliability Analyses of Offshore Structures Using Improved Truss and Beam Models. 1989.

Farnes, Knut-Aril	:	Long-Term Statistics of Response in Non-linear Marine Structures. 1990.
Sotberg, Torbjørn	:	Application of Reliability Methods for Safety Assessment of Submarine Pipelines. 1990.
Hoen, Christopher	:	System Identification of Structures Excited by Stochastic Load Processes. 1991.
Sødahl, Nils	:	Methods for Design and Analysis of Flexible Risers. 1991.
Haugen, Stein	:	Probabilistic Evaluation of Frequency of Collision between Ships and Offshore Platforms. 1991.
Ormberg, Harald	:	Non-linear Response Analysis of Floating Fish Farm Systems. 1991.
Marley, Mark J.	:	Time Variant Reliability under Fatigue Degradation. 1991.
Bessason, Bjarni	:	Assessment of Earthquake Loading and Response of Seismically Isolated Bridges. 1992.
Sævik, Svein	:	On Stresses and Fatigue in Flexible Pipes. 1992.
Dalane, Jan Inge	:	System Reliability in Design and Maintenance of Fixed Offshore Structures. 1993.
Karunakaran, Daniel	:	Nonlinear Dynamic Response and Reliability Analysis of Drag-Dominated Offshore Platforms. 1993.
Passano, Elizabeth	:	Efficient Analysis of Nonlinear Slender Marine Structures. 1994.
Bech, Sidsel M.	:	Experimental and Numerical Determination of Stiffness and Strength of GRP/PVC Sandwich Structures. 1994.
Hovde, Geir Olav	:	Fatigue and Overload Reliability of Offshore Structural Systems, Considering the Effect of Inspection and Repair. 1995.
Wang, Xiaozhi	:	Reliability Analysis of Production Ships with Emphasis on Load Combination and Ultimate Strength. 1995.
Hellan, Øyvind	:	Nonlinear Pushover and Cyclic Analyses in Ultimate Limit State Design and Reassessment of Tubular Steel Offshore Structures. 1995.

Hermundstad, Ole A.	:	Theoretical and Experimental Hydroelastic Analysis of High Speed Vessels. 1995.
Eknes, Monika Løland	:	Escalation Scenarios Initiated by Gas Explosions on Offshore Installations. 1996.
Halse, Karl Henning	:	On Vortex Shedding and Prediction of Vortex-Induced Vibrations of Circular Cylinders. 1997.
Igland, Ragnar Torvanger	:	Reliability Analysis of Pipelines during Laying, Considering Ultimate Strength under Combined Loads. 1997.
Vikestad, Kyrre	:	Multi-Frequency Response of a Cylinder Subjected to Vortex Shedding and Support Motions. 1998.
Azadi, Mohammad R.E.	:	Analysis of Static and Dynamic Pile-Soil-Jacked Behaviour. 1998.
Videiro, Paulo Mauricio	:	Reliability Based Design of Marine Structures. 1998.
Mainçon, Philippe	:	Fatigue Reliability of Long Welds Application to Titanium Risers. 1999.
Langhelle, Nina Kristin	:	Experimental Validation and Calibration of Nonlinear Finite Element Models for Use in Design of Aluminium Structures Exposed to Fire. 1999.
Berstad, Are Johan	:	Calculation of Fatigue Damage in Ship Structures. 1999.
Tveiten, Bård Wathne	:	Fatigue Assessment of Welded Aluminium Ship Details. 1999.